UNIVERSIDAD DE CASTILLA-LA MANCHA

DEPARTAMENTO DE INGENIERÍA ELÉCTRICA,
ELECTRÓNICA, AUTOMÁTICA Y COMUNICACIONES

OPTIMAL POWER FLOW WITH STABILITY CONSTRAINTS

TESIS DOCTORAL

AUTOR: RAFAEL ZÁRATE MIÑANO

DIRECTORES:

ANTONIO J. CONEJO NAVARRO

FEDERICO MILANO

Ciudad Real, Junio de 2010

UNIVERSIDAD DE CASTILLA-LA MANCHA

DEPARTMENT OF ELECTRICAL ENGINEERING

OPTIMAL POWER FLOW WITH STABILITY CONSTRAINTS

PhD THESIS

AUTHOR: RAFAEL ZÁRATE MIÑANO

SUPERVISORS:

ANTONIO J. CONEJO NAVARRO

FEDERICO MILANO

Ciudad Real, June 2010

Contents

List of Figures

List of Tables

Notation

The notation used throughout this thesis is stated below for quick reference. Note that if a superscript "s" is added, the resulting symbol indicates stressed operating condition.

Functions

$I_k(\cdot)$ Current magnitude through branch k as a function of the problem variables.

$I_{nm}(\cdot)$ Current magnitude from bus n to bus m as a function of the problem variables.

$P_k(\cdot)$ Active power flow through branch k as a function of the problem variables.

$P_{nm}(\cdot)$ Active power flow from bus n to bus m as a function of the problem variables.

$Q_k(\cdot)$ Reactive power flow through branch k as a function of the problem variables.

$Q_{nm}(\cdot)$ Reactive power flow from bus n to bus m as a function of the problem variables.

$S_{\mathrm{e}j}(\cdot)$	Ceiling function of the Automatic Voltage Regulator (AVR) connected to generator j.
z	Total cost function.
z_{D}	Cost function of load active power adjustments.
z_{G}	Cost function of generator active power adjustments.
z_{LTC}	Cost function of set point adjustments for on-Load Tap-Changing (LTC) transformers.
z_{PHS}	Cost function of set point adjustments for PHase-Shifting (PHS) transformers.
z_{SVC}	Cost function of set point adjustments for Static Var Compensator (SVC) devices.
z_{TCSC}	Cost function of set point adjustments for Thyristor-Controlled Series Compensator (TCSC) devices.
z_{V}	Cost function of voltage magnitude adjustments.

Variables

$b_{\mathrm{SVC},n}$	Susceptance of the SVC device at bus n.
E'_j	Electromotive force magnitude of generator j.
$E'_{\mathrm{d}j}$	d-axis transient voltage of generator j.
$E'_{\mathrm{q}j}$	q-axis transient voltage of generator j.
$I_{\mathrm{d}j}$	d-axis current of generator j.

$I_{\mathrm{q}j}$	q-axis current of generator j.
$P_{\mathrm{D}i}$	Active power consumption of demand i.
$P_{\mathrm{D}n}$	Total active power consumption in bus n.
$P_{\mathrm{e}j}$	Electrical power of generator j.
$P_{\mathrm{G}j}$	Active power production of generator j.
$P_{\mathrm{G}n}$	Total active power production in bus n.
$Q_{\mathrm{D}n}$	Total reactive power consumption in bus n.
$Q_{\mathrm{G}j}$	Reactive power production of generator j.
$Q_{\mathrm{G}n}$	Total reactive power production in bus n.
$Q_{\mathrm{SVC}n}$	Reactive power injected by the SVC device at bus n.
T_k	Tap ratio of LTC transformer k.
V_n	Voltage magnitude at bus n.
$V_{\mathrm{d}j}$	d-axis voltage of generator j.
$V_{\mathrm{q}j}$	q-axis voltage of generator j.
$x_{\mathrm{TCSC},k}$	Reactance of the TCSC device of branch k.
$\Delta P_k^{\mathrm{down}}$	Active power flow decrease through branch k for security purposes.
ΔP_k^{up}	Active power flow increase through branch k for security purposes.
$\Delta P_{\mathrm{D}i}^{\mathrm{down}}$	Active power decrease in demand i for security purposes.

$\Delta P_{\mathrm{D}i}^{\mathrm{up}}$ Active power increase in demand i for security purposes.

$\Delta P_{\mathrm{D}n}^{\mathrm{down}}$ Total active power demand decrease at bus n for security purposes.

$\Delta P_{\mathrm{D}n}^{\mathrm{up}}$ Total active power demand increase at bus n for security purposes.

$\Delta P_{\mathrm{G}j}^{\mathrm{down}}$ Active power decrease in generator j for security purposes.

$\Delta P_{\mathrm{G}j}^{\mathrm{up}}$ Active power increase in generator j for security purposes.

$\Delta P_{\mathrm{G}n}^{\mathrm{down}}$ Total active power generation decrease at bus n for security purposes.

$\Delta P_{\mathrm{G}n}^{\mathrm{up}}$ Total active power generation increase at bus n for security purposes.

$\Delta V_{n}^{\mathrm{down}}$ Voltage magnitude decrease at bus n for security purposes.

$\Delta V_{n}^{\mathrm{up}}$ Voltage magnitude increase at bus n for security purposes.

δ Rotor angle of the One-Machine Infinite-Bus (OMIB) equivalent.

δ_j Rotor angle of generator j.

θ_n Voltage angle at bus n.

λ Loading parameter.

λ^* Loading margin resulting from the OPF problem described in Appendix B.

ϕ_k Phase of the PHS transformer k.

ω Rotor speed of the OMIB equivalent.

ω_j Rotor speed of generator j.

Constants

$b^{\max}_{\mathrm{SVC},n}$ Maximum susceptance of the SVC at bus n.

$b^{\min}_{\mathrm{SVC},n}$ Minimum susceptance of the SVC at bus n.

$c^{\mathrm{down}}_{\mathrm{D}i}$ Cost of decreasing load i.

$c^{\mathrm{down}}_{\mathrm{G}j}$ Offering cost of generator j to decrease its dispatched power for security purposes.

$c^{\mathrm{up}}_{\mathrm{G}j}$ Offering cost of generator j to increase its dispatched power for security purposes.

$c^{\mathrm{down}}_{\mathrm{LTC},n}$ Penalty for decreasing voltage magnitude at bus n controlled by a LTC transformer.

$c^{\mathrm{up}}_{\mathrm{LTC},n}$ Penalty for increasing voltage magnitude at bus n controlled by a LTC transformer.

$c^{\mathrm{down}}_{\mathrm{PHS},k}$ Penalty for decreasing power flow through branch k controlled by a PHS transformer.

$c^{\mathrm{up}}_{\mathrm{PHS},k}$ Penalty for increasing power flow through branch k controlled by a PHS transformer.

$c^{\mathrm{down}}_{\mathrm{SVC},n}$ Penalty for decreasing voltage magnitude at bus n controlled by a SVC device.

$c^{\mathrm{up}}_{\mathrm{SVC},n}$ Penalty for increasing voltage magnitude at bus n controlled by a SVC device.

$c^{\text{down}}_{\text{TCSC},k}$ Penalty for decreasing power flow through branch k controlled by a TCSC device.

$c^{\text{up}}_{\text{TCSC},k}$ Penalty for increasing power flow through branch k controlled by a TCSC device.

$c^{\text{down}}_{\text{V}n}$ Penalty for decreasing voltage magnitude at bus n.

$c^{\text{up}}_{\text{V}n}$ Penalty for increasing voltage magnitude at bus n.

$I^{\max}_{k}$ Maximum current magnitude through branch k.

$P^{\text{A}}_{\text{D}i}$ Base-case active power consumption of demand i.

$P^{\text{M}}_{\text{D}i}$ Active power consumption of demand i as determined by the market dispatching procedure.

$P^{\text{A}}_{\text{G}j}$ Base-case active power production of generator j.

$P^{\text{M}}_{\text{G}j}$ Active power production of generator j as determined by the market dispatching procedure.

$P^{\max}_{\text{G}j}$ Capacity (maximum power output) of generator j.

$P^{\min}_{\text{G}j}$ Minimum power output of generator j.

$P_{\text{m}j}$ Mechanical power of generator j.

$Q^{\text{A}}_{\text{D}i}$ Base-case reactive power consumption of demand i.

$Q^{\text{A}}_{\text{G}j}$ Base-case reactive power production of generator j.

$Q^{\max}_{\text{G}j}$ Maximum reactive power limit of generator j.

$Q^{\min}_{\text{G}j}$ Minimum reactive power limit of generator j.

$R_{\mathrm{G}j}^{\mathrm{up}}$	Active power ramp-up limit of generator j.
$R_{\mathrm{G}j}^{\mathrm{down}}$	Active power ramp-down limit of generator j.
$R_{\mathrm{T}_k}^{\mathrm{up}}$	Ramp-up limit of LTC transformer k.
$R_{\mathrm{T}_k}^{\mathrm{down}}$	Ramp-down limit of LTC transformer k.
$R_{\phi_k}^{\mathrm{up}}$	Ramp-up limit of PHS transformer k.
$R_{\phi_k}^{\mathrm{down}}$	Ramp-down limit of PHS transformer k.
$T_k^{\max}$	Maximum tap ratio of LTC transformer k.
$T_k^{\min}$	Minimum tap ratio of LTC transformer k.
V_n^{A}	Base-case voltage magnitude at bus n.
$V_n^{\max}$	Maximum voltage magnitude at bus n.
$V_n^{\min}$	Minimum voltage magnitude at bus n.
$x_{\mathrm{TCSC},k}^{\max}$	Maximum reactance of the TCSC device of branch k.
$x_{\mathrm{TCSC},k}^{\min}$	Minimum reactance of the TCSC device of branch k.
$\delta^{\max}$	Rotor angle limit of the OMIB equivalent.
θ_n^{A}	Base-case voltage angle at bus n.
$\phi_k^{\max}$	Maximum phase-shifter tap of PHS transformer k.
$\phi_k^{\min}$	Minimum phase-shifter tap of PHS transformer k.
$\psi_{\mathrm{D}i}$	Power factor angle of demand i.

Parameters

$A_{\mathrm{e}j}$	First ceiling coefficient of the AVR connected to generator j.
$B_{\mathrm{e}j}$	Second ceiling coefficient of the AVR connected to generator j.
$B_{j\ell}$	Element $j\ell$ of the reduced susceptance matrix.
b_k	Series susceptance of element k.
$b_{\mathrm{p}k}$	Shunt susceptance of element k.
$G_{j\ell}$	Element $j\ell$ of the reduced conductance matrix.
g_k	Conductance of element k.
$K_{\mathrm{a}j}$	Amplifier gain of the AVR connected to generator j.
$K_{\mathrm{e}j}$	Field circuit gain of the AVR connected to generator j.
$K_{\mathrm{f}j}$	Stabilizer gain of the AVR connected to generator j.
M_{C}	Total inertia coefficient of the critical machine group.
M_j	Inertia coefficient of generator j.
M_{NC}	Total inertia coefficient of the non-critical machine group.
r_k	Resistance of element k.
$T_{\mathrm{a}j}$	Amplifier time constant of the AVR connected to generator j.
$T_{\mathrm{e}j}$	Field circuit time constant of the AVR connected to generator j.
$T_{\mathrm{f}j}$	Stabilizer time constant of the AVR connected to generator j.

$T'_{\mathrm{d}0j}$	d-axis open circuit transient time constant of generator j.
$T'_{\mathrm{q}0j}$	q-axis open circuit transient time constant of generator j.
$V_{\mathrm{ref}j}$	Reference voltage of the AVR connected to generator j.
t_{step}	Integration time step.
$V_{\mathrm{r}j}^{\max}$	Maximum regulator voltage of the AVR connected to generator j.
$V_{\mathrm{r}j}^{\min}$	Minimum regulator voltage of the AVR connected to generator j.
x_k	Reactance of element k.
$x_{\mathrm{d}j}$	d-axis synchronous reactance of generator j.
$x'_{\mathrm{d}j}$	d-axis transient reactance of generator j.
$x_{\mathrm{q}j}$	q-axis synchronous reactance of generator j.
$x'_{\mathrm{q}j}$	q-axis transient reactance of generator j.
$\boldsymbol{Y}_k$	Series admittance of element k.
$\mathbf{Y}_{\mathrm{bus}}$	Reduced admittance matrix.
$\boldsymbol{Y}_{\mathrm{D}i}$	Equivalent admittance for load i.
$\boldsymbol{Y}_{\mathrm{D}n}$	Equivalent load admittance in bus n.
$\boldsymbol{Z}_k$	Series impedance of element k.
Δt	Time interval considered.
δ_{r}	Return angle of the OMIB equivalent.

δ_{u}	Unstable angle of the OMIB equivalent.
λ^{SM}	Security margin.
μ	Probability of the considered operating condition. For the stressed cases, μ^s is the probability of occurrence of the contingency considered in the stressed operating condition s.
σ_j	Sensitivity of the critical eigenvalue real part with respect to active power generation j.
ω_{b}	Base synchronous frequency.

Sets

$\mathcal{D}$	Set of demands.
$\mathcal{D}_{\mathrm{n}}$	Set of demands located at bus n.
$\mathcal{G}$	Set of on-line generators.
$\mathcal{G}_{\mathrm{C}}$	Set of critical machines.
$\mathcal{G}_{\mathrm{n}}$	Set of on-line generators located at bus n.
$\mathcal{G}_{\mathrm{NC}}$	Set of non-critical machines.
$\mathcal{N}$	Set of buses.
$\mathcal{N}_{\mathrm{G}}$	Set of generator buses.
$\mathcal{N}_{\mathrm{SVC}}$	Set of buses with SVC devices.
$\mathcal{S}$	Set of all stressed operating conditions.

$\mathcal{S}_{\mathrm{u}}$	Subset of stressed operating conditions relevant for small-signal stability analysis ($\mathcal{S}_{\mathrm{u}} \subset \mathcal{S}$).
$\mathcal{T}$	Set of time steps.
Θ_n	Set of buses connected to bus n through a branch.
Ω	Set of network branches.
Ω_{FT}	Set of fixed-tap transformers ($\Omega_{\mathrm{FT}} \subset \Omega$).
Ω_{L}	Set of transmission lines ($\Omega_{\mathrm{L}} \subset \Omega$).
Ω_{LTC}	Set of LTC transformers ($\Omega_{\mathrm{LTC}} \subset \Omega$).
Ω_{PHS}	Set of PHS transformers ($\Omega_{\mathrm{PHS}} \subset \Omega$).
Ω_{TCSC}	Set of lines with TCSC devices ($\Omega_{\mathrm{TCSC}} \subset \Omega$).

Numbers

$\mathrm{n_p}$	Dimension of control variables.
$\mathrm{n_x}$	Dimension of state variables.
$\mathrm{n_y}$	Dimension of algebraic variables.

Indices

i	Index of demands.
j, ℓ	Indices of generators.
k	Index of network branches.
n, m	Indices of buses.

Chapter 1

Introduction

This thesis is devoted to the development of procedures that ensure power system security in the context of real-time operation. The proposed procedures are intended to assist system operators in guaranteeing an appropriate security level both optimally and economically.

Power system security refers to the ability of a power system to reach acceptable steady-state operating conditions after being subjected to sudden disturbances, such as short circuits or unexpected system component failures, without uncontrolled cascading outages that potentially lead to blackouts. Blackouts have a pronounced negative impact on the economy and on society. However, within a market environment and for economic reasons, power systems are exposed to increasing stress because they are usually operated close their stability limits. Under these circumstances, the blackout risk may increase.

To reduce the risk of blackouts, the power system should be operated such that no equipment is overloaded, all bus voltage magnitudes are within appropriate limits, and acceptable steady-state operating conditions can be reached after the transient phenomena induced by a plausible contingency [9]. Although security is taken into account in the planning and operations planning stages of a power system, security assessment and control procedures are key tasks during real-time operation. In this context, the system operator must respond within a very limited time frame, usually from a few minutes to some

hours, to ensure security.

1.1 Motivation

Most existing electricity markets provide dispatch solutions that are based on economic grounds and, generally, do not explicitly consider security issues. As a result, during real-time operation, the system operator must ensure system security and implement control actions as necessary. Control actions may involve adjustments to the market solution through alterations made to the generator power outputs (generating unit redispatching), adjustments to the voltage set points and power flow control devices, and adjustments to load consumption (load shedding). Real-time operation of the power system includes three primary tasks: security assessment, contingency filtering, and security control.

Security assessment involves a number of studies in which the state of the network for each one of a pre-specified set of contingencies is determined. The method used to select the contingencies that should be included in this set continues to be a topic for discussion [102]. Although diverse criteria can be used, one commonly accepted criterion is to consider the single outage of any system element, whether or not it is preceded by a single-, double-, or three-phase fault. This is known as the $N-1$ security criterion.

Contingency filtering identifies contingencies from within a pre-specified set that can lead to system instability. The filtering criteria are such that all the critical contingencies are selected. The contingencies of interest are those that threaten the integrity of the system. Accordingly, the stability of the post-contingency state of the power system is an important characteristic.

Security control consists in deciding whether preventive or corrective control actions (or a combination of both) are suitable countermeasures against potential stability problems, and in designing the corresponding set of control actions that improve the overall system security level. Security control tools should help the system operator make appropriate decisions. In this context, the Optimal Power Flow (OPF) is an appropriate and well-established tool to identify the control actions that are needed to ensure the desired security level.

In addition, market participants expect that the security control modifies as little as possible the market dispatch solution. In order to ensure that the security adjustments minimally impact the original market solution, it is necessary to model the behavior of the system and the security constraints in detail. As a consequence, the system operator typically has to deal with a nonlinear model and advanced stability analysis concepts, such as bifurcation theory.

Furthermore, to study the transient stability under a major disturbance generally requires cumbersome time-domain simulations. Incorporating transient stability constraints within an OPF model poses the challenge of marrying time-domain simulation and optimization. Consequently, the security-targeted redispatching step is a complex and not fully solved task.

The use of a security constrained OPF is increasingly necessary in today's stressed electric energy systems, which operate under market rules. Thus, there exists a significant need to develop OPF models that incorporate diverse security constraints to guarantee an appropriate security level.

1.2 Thesis Objectives

The general objective of this thesis is to develop a security-redispatching OPF-based control tool to assist the system operator in avoiding problems related to voltage, small-signal, and transient instabilities.

Specific objectives are stated below:

1. Objectives pertaining to voltage stability:

    1.1. To formulate an OPF problem that yields an estimate of the voltage stability margin for the power system.

    1.2. To establish a criterion for contingency filtering with regard to voltage stability.

    1.3. To design a security-redispatching OPF-based control tool that explicitly considers voltage stability constraints through several system operating states. Specifically, these system states include a pre-

contingency operating condition and a set of stressed post-contingency operating conditions.

1.4. To formulate these operating conditions using an ac model of the network, as well as detailed static models of its different components, including regulating transformers and Flexible AC Transmission System (FACTS) devices.

1.5. To formulate coupling constraints between pre- and post-contingency states that represent the physical limitations of different system control components in terms of set point adjustments.

2. Objectives pertaining to small-signal stability:

2.1. To extend the security-redispatching OPF-based control tool developed in item 1 above to take into account small-signal stability problems.

2.2. To incorporate small-signal stability criteria into the contingency filtering procedure.

2.3. To formulate small-signal stability constraints based on sensitivities.

3. Objectives pertaining to transient stability:

3.1. To design a security-redispatching OPF-based control tool that explicitly considers transient stability constraints using a discretized dynamic model of the power system.

3.2. To establish an objective criterion to determine the transient stability limit.

3.3. To incorporate this transient stability limit into the security-redispatching OPF-based control tool.

1.3 Literature Review

This section reviews the technical literature related to the topics dealt with in this dissertation.

1.3.1 Voltage Stability Analysis

Several voltage stability analysis methods are described in references [13, 40, 118]. These methods can be classified under two main categories: static and dynamic methods.

In the static analysis, the power system is usually modeled by means of the power flow equations. Static methods determine the system conditions at which the equilibrium points of the power flow equations disappear. Voltage instability phenomena (e.g., voltage collapse) are associated with the appearance of certain bifurcations, specifically saddle-node and limit-induced bifurcations, in the power flow equations of the system [118]. The goal of this analysis is to determine the proximity of a given power system operating condition to the bifurcation point, i.e., to the voltage collapse point.

The most basic and widely accepted index to assess the proximity to voltage collapse is the loading margin. This index is defined as the amount of additional load, following a specific load increase pattern, that may cause voltage collapse [118]. The loading margin can be calculated in principle by starting at a given operating condition, increasing the load with small increments, and recomputing load flows at each increment until the voltage collapse point is reached. The loading margin is then the total additional load. Following this idea, the Continuation Power Flow (CPF) method is proposed in [2, 18, 19]. This method determines the loading margin by computing the solution path. Alternatively, OPF-based methods, [8, 38, 99], compute the loading margin directly, without determining the solution path between the current and the critical operating condition.

Other indices and methods have been proposed to estimate the proximity to the voltage collapse point. These indices include the minimum singular value criterion [80], the minimum eigenvalue criterion [62], the second order performance index [12], the voltage instability proximity index [120], test functions [30], the reduced determinant criterion [20], and the tangent vector index [45], as well as indices based on sensitivities [11, 56], and energy functions [46, 103]. Most of these methods are described and analyzed in [118].

Dynamic methods are intended to analyze how different devices and con-

trols affect voltage stability. With this information, emergency controls can be designed in order to stop a developing voltage collapse, for instance. In dynamic analysis, the power system is modeled by a set of differential-algebraic equations, and time-domain simulations are performed [39, 121]. These methods generally require substantial computational resources. To speed up the calculations, quasi-steady-state (QSS) methods, which combine static and dynamic approaches have been proposed in [41–43, 76]. QSS methods are also used to accurately compute the system loading margin, [41, 42]. Finally, a voltage stability analysis framework that combines bifurcation theory and time-domain simulation has also been reported in [125].

In this thesis, voltage stability analysis is addressed from a static viewpoint. The voltage stability assessment of a given operating condition is carried out using the loading margin, which is a voltage stability measurement with a physical meaning. In this thesis, loading margins are computed with an OPF-based method. The CPF method is not used since it can be shown to be a particular case of OPF approaches [8].

1.3.2 Small-Signal Stability Analysis

Small-signal stability analysis establishes that the stability of a system equilibrium point under small disturbances can be studied by linearizing the nonlinear system equations around the system equilibrium point. Then, the system stability can be determined by inspecting the eigenvalues of the system state matrix [82]. Because each eigenvalue corresponds to an oscillation mode of the system, small-signal stability analysis is also referred to as modal analysis [73, 114]. Small-signal instability is characterized by one or more eigenvalues whose real part becomes positive. As a pair of complex eigenvalues crosses the imaginary axis, it is known as Hopf bifurcation [118], and has been widely studied in recent years [21, 77, 128, 132].

Together with eigenvalues, small-signal stability analysis outputs the associated right and left eigenvectors. For a particular eigenvalue, the associated right eigenvector represents a measure of the effect of the state variables on the corresponding oscillation mode whereas the associated left eigenvector

measures the control effect on this mode. The participation factors can be obtained by appropriately combining the right and left eigenvectors, [108, 127]. A participation factor is a dimensionless magnitude that provides information about the influence of a particular state variable in a given oscillation mode. This information is used to design and place damping control devices, as for example, in [37, 58, 72, 74, 143].

The computation of all eigenvalues and eigenvectors entails a high computational burden for large-scale electric energy systems. Several "reduction" techniques have been reported in the literature to compute only the subset of eigenvalues associated with the oscillation modes of interest. These techniques include the selective modal analysis [111], the modified Arnoldi's iteration [113] and the dominant pole spectrum eigensolver [84]. Each of these techniques has special features that make it suitable for particular applications. In [75], the use of several complementary techniques has been proposed.

Since the efficient computation of eigenvalues is outside the scope of this thesis, reduction techniques are not applied, and all system eigenvalues are computed during small-signal stability assessment.

1.3.3 Transient Stability Analysis

In transient stability analysis, the focus is on the transient phenomena that follow a sudden and large disturbance in a power system. Due to the highly non-linear dynamic nature of the transient phenomena, the static analysis, such as bifurcation analysis, fails and linearization around a system equilibrium point is of no use. Typically, transient stability analysis is carried out using one of the following techniques:

- Time-domain simulation
- Direct method
- Hybrid method

These methods are briefly described in the following subsections. Alternatively, other approaches for transient stability analysis based on automatic learning methods have been proposed. Most of these methods are described in [131].

1.3.3.1 Time-domain simulation

The time-domain method consists in the numerical integration of the differential-algebraic equations that model the power system. Such calculations have always been considered to analyze the behavior of a power system when subjected to a large disturbance. Typically, implicit numerical integration methods are used to solve the transient stability model (e.g., the trapezoidal rule) [6, 73, 114]. In transient stability studies, time-domain simulations are carried out for a maximum simulation period that depends on the complexity of the system model, which is typically set to 3 s for the most simplified model and up to 15 s for highly detailed models [106].

The time-domain simulations provide the evolution of the system variables over time. A common practice to detect a loss of synchronism is to check whether or not the inter-machine rotor angle deviations lie within a specific range of values during the simulation. Unfortunately, this range is system, if not operating-point, dependent and is typically established using heuristic criteria. For instance, Table 1.1 lists some of such values that have been proposed in the literature.

Table 1.1: Rotor angle deviation limits for transient stability analysis used in the literature

Reference	Rotor angle deviation limit [degrees]
[61], [138], [78], [27]	100
[135]	120
[28]	144
[98]	180
[53]	270

1.3.3.2 Direct methods

Direct methods assess transient stability by partially or completely avoiding solving the set of differential-algebraic equations that describe the dynamics of the system. Two common direct methods are described below.

Methods based on the Lyapunov functions. These methods rely on applying the Lyapunov second criterion [82], i.e., on the construction of Lyapunov functions. A Lyapunov function is a scalar function of the system state vector with a specific mathematical characterization [67]. In short, this function must be positive definite, and its time derivative must be negative semi-definite along the solutions of the system equations. The procedure involves computing the value of the Lyapunov function for the system state corresponding to the instant when the disturbance is cleared. Stability is determined by comparing this value of the Lyapunov function with a given limit value.

The direct methods based on Lyapunov functions have two main limitations: (i) it is difficult to construct a suitable Lyapunov function for a multi-machine power system unless highly simplified models are used, and (ii) it is difficult to define a practical stability domain due to the fact that the Lyapunov criterion is only sufficient for multi-machine power systems.

The Lyapunov functions used in transient stability studies are functions of the energy type. The best-known is the transient energy function [7, 104]. With respect to the definition of the stability domain, several methods have been proposed; e.g., the closest unstable equilibrium point method [79], the method based on the boundary of the stability region to find the controlling unstable equilibrium point (BCU method) [31], and the Potential Energy Boundary Surface (PEBS) method [104].

If the transient energy function is applied to a one-machine infinite bus system modeled in the classical simplified way, the transient stability assessment is equivalent to that provided by the equal area criterion [107]. Therefore, the equal area criterion may be viewed as an application of the Lyapunov functions to simple systems.

Equal area criterion. The Equal Area Criterion (EAC) is a well-known technique used to study the transient stability of systems that comprise either

one machine and an infinite bus or two machines. A detailed description of the EAC can be found in almost any book on power system analysis, e.g., in [114] or [73]. The EAC relies on energy transfers and analyzes transient stability without solving the power system differential-algebraic equations. This technique establishes that the stability of a one-machine plus infinite bus system, or a two-machine system, is guaranteed as long as the kinetic energy stored in the system during the fault period (accelerating area) does not exceed the energy that the system can dissipate (decelerating area). The application of the EAC to multi-machine power systems is based on the empirical observation that, if synchronism is lost, the system machines divide into two groups. Then, each group can be replaced by an equivalent machine, which forms an equivalent two-machine system to which the EAC can be applied. However, the task of identifying in advance the correct groups into which the system splits makes the direct application of EAC to a multi-machine system difficult.

1.3.3.3 Hybrid methods

Hybrid methods overcome the two limitations of the Lyapunov functions based on the following two observations [106]:

1. The problem of stability estimation may be tackled by considering a two-machine or a one-machine equivalent of the multi-machine system.

2. The modeling problem may be solved by including the Lyapunov function computation within time-domain simulations.

The first observation stems from the fact that the stability condition of the Lyapunov criterion becomes both sufficient and necessary for the particular case of a two-machine or a one-machine equivalent system that is described with a simplified model. The second observation is based on the idea of constructing a Lyapunov function for the simplified power system model and evaluating this function step-by-step with the value of the system states provided by a time-domain simulation of the detailed power system model. The resulting Lyapunov function is path-dependent and is called the pseudo-Lyapunov function.

Two different hybrid approaches exist. The first considers a Lyapunov function that is constructed for the multi-machine system and computed along the multi-machine trajectory [83]. However, establishing an appropriate stability limit remains a difficult task. The second approach, the named SIngle Machine Equivalent (SIME) method [106], considers the one-machine equivalent of the multi-machine system and analyzes its stability using the EAC, which considerably simplifies the stability limit determination process.

The SIME method provides stability limits based on objective stability criteria and is used in this thesis for transient stability analysis.

1.3.4 Optimal Power Flow

The Optimal Power Flow (OPF) problem was introduced in the sixties [26, 49], and it is currently considered one of the most useful tools for power system operations and planning. In general, the OPF is a nonlinear programming (NLP) problem that determines the optimal control set points of the system to minimize a desired objective function, subject to certain system constraints [71].

The most common objective functions include the minimum operation cost, minimum active power losses, the minimum deviation from a specific operating condition. The objective function usually depends on variables with a direct economical impact (e.g., power generation or load shedding) and variables without a direct cost impact (e.g., bus voltage magnitudes).

The constraints that an OPF problem incorporates can be divided into equality and inequality constraints. The equality constraint set typically consists of both active and reactive power balance equations at each bus of the network. In general, inequality constraints represent the technical limits of the system, e.g., generator power capacity and voltage magnitude limits.

This basic OPF formulation was first extended to include security criteria in [3]. The resulting optimization problem, known as Security-Constrained Optimal Power Flow (SC-OPF), includes additional constraints related to the system operating conditions in case of contingencies. The goal of the SC-OPF problem is to guarantee that the system operates properly under both the

pre-contingency and post-contingency conditions [65].

The SC-OPF problem is generally used as a preventive control tool in the sense that it does not address the possibility of adjusting controls in the post-contingency operating conditions [24]. However, together with preventive control actions, the SC-OPF can provide corrective control actions if these adjustments are taken into account. To this end, a set of coupling constraints is added to the SC-OPF problem. These constraints recognize that the adjustment range of certain controls is determined by their set points in the pre-contingency operating condition [93].

In this thesis, a SC-OPF formulation that includes coupling constraints is proposed to address voltage and small-signal stability issues. The objective is to minimize the redispatching control actions needed to achieve a prespecified security level. Although the proposed SC-OPF problem is employed throughout the thesis as a preventive control tool, it can also be used to derive corrective control actions if required.

Many different mathematical techniques have been applied to solve the OPF problem. Their description can be found, for instance, in [10, 35, 81, 134]. The main drawback of mathematical programming solvers for NLP problems is that obtaining the global optimum cannot be guaranteed if the considered OPF formulation is not convex. However, current commercial solvers (e.g., CONOPT [50] and MINOS [95]) can be started from different initial points such that local minima are avoided. In this thesis CONOPT is employed to solve diverse OPF formulations. Alternatively, heuristic procedures, such as those proposed in [15, 17, 139, 142], can be used at the cost of not being able to precisely characterize the quality of the solution attained.

1.3.5 Optimal Power Flow with Voltage Stability Constraints

Many of the procedures proposed in the literature to address voltage problems enforce transmission capacity limits that are computed off-line to ensure voltage stability conditions, e.g., [14, 64, 136, 140]. The use of these "artificial" stability limits may result in economic inefficiencies due to sub-optimal

solutions. Stability conditions based on the power flow equations have been included along with thermal line capacity constraints in [18, 36, 87–89, 110, 124]. Security constraints in the form of post-contingency operating conditions are added to not only guarantee a stable operating condition but also a given distance to the maximum loading condition associated with bus voltage limits, equipment thermal limits and/or the system voltage stability limits. With this aim, in [22, 55, 130], voltage stability constraints based on the loading margin sensitivities with respect to control variables have been proposed. Methods for computing such sensitivities can be found in [23, 66, 90].

However, in all the approaches above, control actions are applied to a single system condition, i.e., either to the pre-contingency condition (preventive control) or to the post-contingency condition (corrective control). An OPF formulation that combines both the preventive and the corrective control was first proposed in [93]. The goal is to provide a centralized solution for the optimal pre- and post-contingency dispatches. The optimization problem includes static constraints on both the pre-contingency and post-contingency system conditions. The post-contingency system conditions are linked to the pre-contingency condition by coupling equations in the form of ramping constraints. Recently, some OPF problems with this structure have been proposed in [25, 34, 141].

In this thesis, an OPF problem for voltage stability control is proposed. The proposed OPF formulation has the structure described above, i.e., the OPF problem includes static constraints on pre and post-contingency system conditions. The novel contribution with respect to [25, 34, 93] is that the post-contingency system conditions are further stressed by a loading parameter. This parameter is used to define a security margin. The coupling constraints ensure that the system can reach the stressed conditions such that the security margin is guaranteed.

1.3.6 Optimal Power Flow with Small-Signal Stability Constraints

The main cause of small-signal rotor angle instability is directly related to an insufficient damping torque that leads to power system oscillations. Therefore, to prevent small-signal instability, most solutions proposed in the literature add damping torque devices to the systems.

Power System Stabilizers (PSS) are widely used as appropriate devices for damping control because of their relative low cost and general effectiveness. These devices add additional stabilizing control signals to the input of generator exciters. The optimal placement and design of PSS devices has been the object of considerable research effort [37, 58, 72, 74, 143].

High Voltage Direct Current (HVDC) and Flexible AC Transmission System (FACTS) devices with supplementary control signals have been proposed as an alternative way to damp power system oscillations in [54, 92].

All these devices lead to effective solutions and are used in practice. However, from the system operation point of view, the use of damping controllers may not always be sufficient to solve the small-signal security problem. Some reasons for the limited effectiveness of damping controllers include the following [32]:

1. Implementation of damping controllers usually requires lengthy design, manufacture, installation, and commission procedures. Therefore, it is difficult to meet the short-term solution requirements for operation problems.

2. Appropriate damping controller design requires full knowledge of the technical characteristics of the system. Nowadays, this is increasingly difficult due to the electric power industry restructuring.

3. Frequently, the possibility that a power transfer is limited by the small-signal stability problem occurs only for a short period of time. Adding new controllers may not be the most efficient way to mitigate such a problem.

4. Even if appropriate damping controllers are installed, there are always situations in which specific operating conditions fall beyond what the controllers are designed for. Additional remedial measures are necessary to accommodate these operating conditions.

Therefore, some researchers have proposed OPF methods to deal with small-signal instability issues during the power system operation.

In [32], two sensitivity-based methods are proposed. The objective is to minimize generation rescheduling to maximize power transfer between two areas subject to small-signal stability constraints under a set of selected contingencies. Both methods use a linear optimization problem where the amount of active power generation rescheduled in one area is balanced by rescheduling the same amount of active power generation in the other area. The small-signal stability constraint is formulated in terms of the sensitivities of the damping ratio of the least stable rotor angle mode in the system [129] with respect to the active power generation that corresponds to a previously selected set of generators.

In [33] small-signal stability constraints are included in an OPF problem in which the expected security cost, first proposed in [34], is minimized. The OPF problem includes the pre-contingency operating conditions and the post-contingency operating conditions for an entire set of credible contingencies. The small-signal stability constraints are formulated in terms of the first-order and second-order sensitivities of a set of critical eigenvalues with respect to the OPF decision variables.

As in [33], the OPF problem proposed in this thesis for small-signal stability control also considers several operating conditions. However, the post-contingency conditions are stressed operating conditions characterized by both a contingency and a fictitious loading level that defines a distance to instability, in terms of the load power. The formulation of the small-signal stability constraints is based on the first-order Taylor series expansion of the real part of the critical eigenvalue. Thus, first-order sensitivities of the real part of the critical eigenvalue with respect to generator powers are used.

1.3.7 Optimal Power Flow with Transient Stability Constraints

The Transient Stability Constrained OPF (TSC-OPF) is a non-linear optimization problem that includes algebraic constraints and differential equations. Consequently, standard mathematical programming techniques cannot be directly applied and a variety of *ad hoc* algorithms have been proposed. A critical review of several approaches proposed for solving the TSC-OPF problem can be found in [137].

Different methods have been proposed to embed transient stability constraints in an OPF problem. In [28, 119, 135], the original TSC-OPF is converted into an optimization problem via a constraint transcription based on functional transformation techniques.

In [115] and [61], the power system transient stability model is transformed into an algebraic set of equations for each time step of the time domain simulation. This set of algebraic equations is introduced in the OPF as transient stability constraints. The size of the resulting problem is typically large. Also, in [138], this model is extended to consider multiple contingencies. The number of constraints is significantly reduced by using a reduced admittance matrix in [138] and [78].

In [53, 98, 112], the transient stability assessment is solved separately, and the results are used to determine a bound on the active power generation of a group of selected machines within a standard OPF problem. The main advantages of this approach are its compatibility with any dynamic model of the system and its relatively low computational burden. The main disadvantage is that obtaining an optimal solution cannot be guaranteed because the stability limits are approximated by bounds on active power generation.

A notable drawback of all the TSC-OPF models mentioned above, except the one proposed in [112], is the criterion used to define the stability limits. In [27, 28, 53, 61, 78, 98, 135, 138], transient stability is characterized in terms of the inter-machine rotor angle deviation. The limits imposed are arbitrarily established and their values differ from one reference to another (see Table 1.1). This fact suggests that these TSC-OPF methods cannot guarantee an

optimal solution.

On the other hand, the stability criteria used in [115, 119] are based on Lyapunov functions. Since these criteria ensure stability but are not able to ensure instability, the solutions provided may ultimately be conservative.

Finally, in [112], the SIME method is used for transient stability assessment. This method provides an objective stability criterion. However, this criterion had not been previously used directly in a TSC-OPF. The TSC-OPF problem proposed in this thesis includes discretized equations of the system transient stability model together with transient stability bounds on the angle of the one-machine equivalent system defined by the SIME method. Transient stability bounds are computed by the SIME method as well, thus avoiding arbitrary criteria.

1.4 Models and Tools

Once the market dispatching results are available, and prior to actual power delivery, the system operator must have a set of appropriate procedures with which to check system security and implement redispatching actions on the dispatching solution, if needed.

The procedures proposed in this thesis are mainly of three types: security assessment, contingency filtering, and security control procedures. The characteristics of the security assessment and contingency filtering procedures depend on the instability phenomenon of interest. The security control procedure is based on an OPF model. The objective is to minimize the cost of the control actions on the base-case operating condition (market dispatching adjusted by losses) that achieve a secure operation. This OPF problem basically includes constraints that represent the operating condition of the system that results from adjusting the base case for security purposes. If security problems are detected in the security assessment procedures, additional constraints are added to the OPF problem. The form of these additional constraints depends on the instability phenomenon that limits system operation.

1.4.1 Base Case

The starting point of the analysis in this thesis is a base-case operating condition that is established through a market dispatching solution adjusted by losses. Note, however, that other criteria can be used, e.g., the base case could be the actual system state provided by the state estimator. The input data is the solution provided by a market clearing algorithm. It is assumed that this dispatching solution does not take into account any estimate of transmission losses. Then, a non-linear OPF problem is solved to achieve the system power balance. The objective of this OPF problem is to minimize the cost of generating the power system losses. The equality constraints are the power flow equations in which voltage magnitudes at generator buses and the set point of transmission control devices are treated as variables. The inequality constraints represent voltage magnitude limits at generator buses and operating limits of transmission control devices. Other technical limits, such as the voltage magnitude limits at load buses or the current flow limits of the elements of the network, are not included when calculating the base-case solution. These limits are handled later in the security control procedures. Therefore, together with the balanced power system condition, the solution of this OPF provides the optimal set points of control devices and voltage magnitudes at generator buses to minimize the cost of generating the system losses.

1.4.2 Security Assessment and Contingency Filtering

Once the system base-case operating condition is known, security assessment procedures are carried out. These are two types of procedures: static and dynamic. The static security assessment procedures include post-contingency loading margin computation and eigenvalue analysis at the post-contingency maximum loading condition. Dynamic security assessment is a time-domain simulation of a given contingency using the SIME method. The contingencies analyzed in the security assessment procedures are those of the $N-1$ security criterion. The results of the security assessment procedures are used to select the contingencies that should be taken into account in the security control procedure.

1.4.2.1 Loading Margin Determination

For a given contingency, the post-contingency loading margin of the power system is computed using a non-linear OPF problem. The objective is to evaluate the maximum additional load that the system can provide without exceeding a technical limit or a voltage stability limit, in a given period of time. Thus, the objective function to maximize represents the load power increase with respect to the base-case load; equality constraints are the power flow equations; and inequality constraints represents technical limits, such as bus voltage magnitude limits and current flow limits through the branches of the network. In addition, inequality constraints include a set of ramping constraints that model the generator capacities within a given period of time to increase/decrease their active power outputs with respect to their base-case power outputs. Similarly, ramping constraints are used to model the capacity of some control devices, such as on-load tap-changing and phase-shifting transformers, to adjust their set points.

Each post-contingency loading margin is compared with a pre-specified value. This value is fixed by the ISO and represents the required security margin. If the post-contingency loading margin is lower than the required security margin, the contingency is included in the security control procedure because of the risk of voltage instability issues.

1.4.2.2 Eigenvalue Analysis at the Maximum Loading Condition

Eigenvalue analysis is performed for each post-contingency maximum loading condition. For this maximum loading condition, the system state matrix is evaluated and its eigenvalues are computed. If the post-contingency maximum loading condition presents one or more eigenvalues with a positive real part, then the contingency is included in the security control procedure due to the risk of small-signal instability issues.

1.4.2.3 Time-Domain Simulation and SIME Method

A time-domain simulation is carried out for each contingency. In this case, the contingency is composed of a fault and the subsequent line tripping. Time-

domain simulation solves the differential-algebraic equations of the system for a given period of time. During the time-domain simulation, the SIME method is used to identify transient instabilities. For each time step of the time domain simulation, the SIME method reduces the original multi-machine system to a two-machine system. This two-machine system is further reduced to a one-machine infinite-bus (OMIB) equivalent whose transient stability is analyzed according to the equal area criterion.

If transient instability is identified at the first-swing of the system, the SIME method provides information about the set of machines that lose synchronism (critical machines) and the value of the OMIB equivalent rotor angle at the instant at which synchronism is lost. If the instability occurs after the first swing (multi-swing instability), besides the above information, the SIME method also calculates the maximum value of the OMIB equivalent rotor angle during the first swing of the system. If the system experiences either first-swing instability or multi-swing instability, the contingency is included in the security control procedure because of potential transient instability.

1.4.3 Security Control Procedure

The proposed security control procedure is a redispatching procedure. This redispatching procedure uses an OPF problem whose objective is to minimize the cost of the adjustments with respect to the base-case operating condition needed to achieve a secure operation. The objective function includes the costs of generation power adjustments, penalties for adjustments to the voltage magnitude at generator buses and to the set point of transmission control devices, and the costs of load power adjustments. The OPF problem contains several sets of constraints. The basic constraints are related to the operating condition that results from adjusting the base case. This operating condition is hereinafter called adjusted operating condition. Equality constraints are the power flow equations of the adjusted operating condition, whereas inequality constraints represent the system technical limits. This basic formulation is extended to include security constraints as required.

1.4.3.1 Voltage Stability Constraints

Security constraints related to voltage stability are modeled by system stressed operating conditions. Each stressed operating condition is a post-contingency operating condition in which the system load is increased with respect to the base-case load. This load increase represents the security margin required by the ISO. Together with the power flow equations and technical limits of the stressed conditions, ramping constraints are added. These constraints couple the adjusted operating condition with stressed operating conditions and model the capacity of different system components to adjust their set points in a given time period. Ramping constraints guarantee that the system is able to reach the considered stressed operating conditions, thus guaranteeing the security margin.

The generation powers, voltage magnitudes at generator buses, and control device set points at the stressed operating conditions are defined in terms of adjustments to the adjusted operating condition. To ensure economic operation in the stressed systems, the costs and penalties for these adjustments are included in the objective function. To this end, the cost of operating at the adjusted condition and the cost of operating at each stressed condition are weighted. The weighting factors are defined in terms of the probabilities of occurrence of the contingencies considered for the stressed operating conditions.

1.4.3.2 Small-Signal Stability Constraints

With regard to small-signal stability, the OPF problem has a similar structure to that of the voltage stability problem, i.e., security constraints are added to the OPF in the form of stressed operating conditions. In addition, each stressed operating condition includes small-signal stability constraints. First, for each stressed operating condition, eigenvalue analysis is performed and critical eigenvalues are identified. Then, small-signal stability constraints are formulated based on the first-order Taylor series expansion of the real part of the critical eigenvalue. Thus, first-order sensitivities of the real part of the critical eigenvalue with respect to generation powers are used.

The small-signal stability constraints force the generation powers of the

stressed conditions to change such that the real part of the critical eigenvalues becomes negative. These changes eventually translate into changes in the adjusted operating condition. The size of the changes in the generation powers should be small due to the linear nature of the first-order Taylor approximation. With this goal, the size of these changes is controlled, and the OPF problem is solved iteratively.

1.4.3.3 Transient Stability Constraints

Security constraints related to transient stability are modeled with discrete-time equations that describe the multi-machine system. For each contingency considered, a set of these equations are added to the problem along with the equation of the OMIB equivalent that characterizes the contingency. Transient stability limits are introduced in the form of bounds on the OMIB equivalent rotor angle. These bounds, together with the OMIB equivalent, are formulated using the information provided by the SIME method.

Transient stability constraints and limits are defined for a particular operating condition. After solving the OPF problem, this operating condition varies, and the transient behavior of the system differs from the previous one. Therefore, transient stability of the new operating condition should be assessed. If instability is detected, transient stability constraints and limits are updated, and the OPF problem is solved again. The procedure stops when transient stability is guaranteed for all considered contingencies.

1.4.4 Additional Remarks

The security control procedures proposed in this thesis are mainly preventive control tools, i.e., the objective is to obtain the optimal control actions that should be applied here-and-now to ensure that the system operates properly if any single contingency occurs. However, security control procedures related to voltage and small-signal stability can also provide corrective control actions if the security margins in the stressed systems are reduced to zero. In such a case, the stressed operating conditions are simply the post-contingency operating conditions. If these procedures are used as preventive/corrective control

tools, the solutions are generally more economical than those provided by pure preventive control tools because the security constraints (stressed operating conditions) are less restrictive. However, the post-contingency operating conditions are only acceptable if corrective control actions are applied immediately after the contingency, and this may not be feasible in practice. The proposed preventive control tools impose a feasible post-contingency operating condition on the system with a higher loading level than the actual one. Therefore, at a cost, a greater manoeuvering margin is expected if the contingency occurs.

On the other hand, the existence of an acceptable post-contingency operating condition does not guarantee that the system can reach it. Instability phenomena can appear during the evolution of the system after contingency. In this sense, this thesis also considers transient instability phenomena.

For simplicity, the proposed procedures related to voltage and small-signal stability are designed to impose identical security margins for the considered contingencies. However, security margins can be particularized for each contingency. For example, it can be of interest to establish a security margin for a contingency leading to system collapse higher than that required for a contingency only inducing congestion in a single transmission line. In this manner, security margins can be defined in terms of the impact of contingencies on the power system or, in other words, in terms of the risk that each contingency entails for the power system.

Although the procedures related to voltage, small-signal and transient stability are presented separately throughout the thesis, they belong to a unified procedure. This unified procedure is as follows:

1. Security assessment and contingency filtering procedures related to both voltage and small-signal stability are carried out. If security criteria are violated, the corresponding OPF problem is formulated and solved until the security criteria are satisfied.

2. The transient stability assessment procedure is applied to the solution of the previous step. If transient instability phenomena are found, transient stability constraints are embedded in the OPF problem formulated in the previous step.

1.4.5 Hardware and Software

All simulations presented throughout this thesis were performed using Matlab 7.6 [123] and GAMS 22.7 [16], on a Sun Fire X4140, RoHS-5, with two 2.3-GHz processors with 8 GB of RAM. To solve power flows, compute eigenvalues, and perform time-domain simulations, PSAT [86] was used. With regard to transient stability analysis, PSAT was modified to include an embedded SIME algorithm. Finally, all OPF problems were solved using CONOPT [50] under GAMS.

1.5 Thesis Organization

This document is organized as follows.

Chapter 1 introduces the security problem and states the motivation for this thesis. Next, the main objectives pursued in this thesis are listed. Subsequently, a review of the state of the art of several topics relevant to this thesis is provided. The chapter continues by describing the proposed models and the tools used to solve the problems tackled in this dissertation. Finally, the organization of the thesis is presented.

Chapter 2 begins with an overview of voltage stability and establishes the criteria and methods for voltage stability assessment. The chapter continues with a description of the procedure used to select contingencies that threaten the system voltage stability. Next, the proposed redispatching procedure to solve security issues pertaining to voltage stability is described. Finally, the proposed procedure is illustrated using a 6-bus system. Moreover, the effect of several control devices on the redispatching procedure is analyzed and discussed in detail using a 24-bus system.

Chapter 3 begins with an overview of small-signal stability and establishes the criteria and methods for small-signal stability assessment. Subsequently, the procedure used to select contingencies that threaten the system small-signal stability is described. Then, the proposed redispatching procedure to solve security issues pertaining to small-signal stability is described. This procedure uses an OPF problem with a similar structure as that described in Chapter

2. The proposed procedure is illustrated using the WECC 9-bus, 3-machine system and tested on the New England 39-bus, 10-machine system and the IEEE 145-bus, 50-machine system. The results are analyzed and discussed.

Chapter 4 begins with an overview of transient stability analysis and describes the SIME method. Then, the proposed redispatching procedure to solve security issues pertaining to transient stability is provided. Next, the performance of the proposed procedure is illustrated using the WECC 9-bus, 3-machine system. Finally, the proposed procedure is tested on the New England 39-bus, 10-machine system and on a 1228-bus, real-world power system.

Chapter 5 provides a summary of the dissertation as well as a set of relevant conclusions and contributions related to the procedures proposed in this thesis. In addition, possible future research work is suggested.

Additionally, this document includes four appendices. Appendix A describes the OPF problem used to obtain a base-case operating condition, which constitutes the starting point of the analysis carried out throughout the thesis. Appendix B formulates the OPF problem used to compute the loading margin and the maximum loading condition of a power system. Appendix C describes the mathematical model of the power system components used throughout the thesis. Finally, Appendix D provides the data from the power systems analyzed in the examples and the case studies considered in the thesis.

Chapter 2

Optimal Power Flow with Voltage Stability Constraints

This chapter provides a security redispatching procedure that achieves an appropriate security level in terms of voltage stability. The procedure uses a Voltage Stability Constrained Optimal Power Flow (VSC-OPF) that explicitly considers security limits using stressed loading conditions. The solution of this VSC-OPF corresponds to the optimal preventive control actions that have to be taken to ensure the required security level. Furthermore, a variety of control devices are incorporated in the VSC-OPF problem to enhance system security.

The chapter begins with an overview of voltage stability. Section 2.2 presents the contingency filtering procedure used to select the contingencies that compromise a given security level. In Section 2.3, the VSC-OPF problem is formulated and the steps of the redispatching procedure are described. In Sections 2.4 and 2.5, the performance of the proposed procedure is tested on a 6-bus system and on a 24-bus system, respectively. The results are analyzed and discussed. Finally, Section 2.6 reviews the main conclusions of this chapter.

2.1 Voltage Stability

Voltage stability refers to the ability of a power system to maintain steady voltages at all buses throughout the system after suffering a disturbance from a given initial operating condition [102]. Voltage instability occurs if the power system is not able to maintain or restore the voltage profile at network buses. Typically, voltage instability is a consequence of the inability of the combined generation and transmission system to deliver the power requested by loads [44]. In particular, voltage collapse is the process by which the sequence of events accompanying voltage instability leads to a blackout or to abnormally low voltages in a significant part of the power system, [73, 122]. Voltage stability is threatened if a disturbance increases the power demand beyond the capacity of the combined transmission and generation system. After the disturbance, system devices, such as voltage regulators or on-load tap-changers, try to restore the power consumed by the loads. The restored loads increase the stress on the network, which limits its capability for power transfer and voltage support. This situation is aggravated if some generators reach their reactive power limits. The result is a run-down situation that drives the power system to collapse [40, 44, 70, 73, 122].

In this chapter, a static voltage stability analysis is presented. This analysis is computationally less intensive than other analyses based on dynamic models and is suitable to estimate voltage stability margins, identify factors that influence voltage stability and examine power system performance under a large number of operating conditions, [2, 63, 80, 94]. However, if the stability study were to involve issues such as coordination of controls and protections, the static analysis should be complemented with quasi-steady-state time-domain simulations [40, 44].

2.1.1 System Model

Regarding voltage stability studies, the model of the power system can be represented by the power flow equations in the form:

$$\boldsymbol{g}(\boldsymbol{y}, \boldsymbol{p}, \lambda) = \mathbf{0}, \tag{2.1}$$

where vector $\boldsymbol{y}$ ($\boldsymbol{y} \in \mathbb{R}^{n_y}$) contains the algebraic variables (e.g., voltage magnitude at load buses), $\boldsymbol{p}$ ($\boldsymbol{p} \in \mathbb{R}^{n_p}$) includes the control variables (e.g., active power output of generators), and λ ($\lambda \in \mathbb{R}$) is a loading parameter that is typically used to represent a parametric load change that moves the system from one equilibrium point to another. In this model, the function $\boldsymbol{g}$ ($\boldsymbol{g} : \mathbb{R}^{n_y} \times \mathbb{R}^{n_p} \times \mathbb{R} \longmapsto \mathbb{R}^{n_y}$) represents the standard power flow equations.

Power flow equations are commonly used for voltage stability studies since these equations properly define steady-state system operating conditions [118]. The use of power flow equations implies some assumptions, namely [40]: (i) generator voltages are constant under the action of automatic voltage regulators, (ii) generator reactive power limits are updated according to the operation of over-excitation limiters, and (iii) loads are constant powers (for instance, under the action of LTC transformers working in between limits, and neglecting their deadbands).

2.1.2 Bifurcation Analysis

Bifurcation theory is a widely used analytical tool for analyzing voltage instability and collapse phenomena. This theory provides general mathematical tools to classify instabilities and to study the behavior of non-linear systems in the neighborhood of bifurcation or critical equilibrium points. Moreover, this theory provides quantitative information on remedial actions to avoid critical conditions [116]. A typical assumption of bifurcation theory is that the system equations depend on a set of parameters and variables. Then, stability/instability properties are assessed by varying the parameters. Bifurcation theory makes use of the steady-state approximation, i.e., the system parameters change slowly. The system can thus be assumed to "move" smoothly from one equilibrium point to another following these changes.

Bifurcation theory identifies power system instability conditions with the appearance of Saddle-Node Bifurcations (SNBs), Limit-Induced Bifurcations (LIBs), and Hopf Bifurcations (HFs) in the system equations. The former two bifurcations are directly associated with voltage collapse, and they are presented below. The latter is associated with the lack of sufficient damping

torque, in particular under the influence of automatic voltage regulators, and it is presented in Chapter 3.

2.1.2.1 Saddle-Node Bifurcation

Figure 2.1 depicts a typical PV curve that presents a SNB. Subscript o represents the actual operating condition, whereas subscript c indicates the critical solution at the bifurcation point. This kind of bifurcation has the following properties [47, 116, 118]:

1. Two equilibria, one stable and one unstable, coalesce.
2. The sensitivity of a system variable with respect to λ is infinite.
3. The Jacobian matrix $\boldsymbol{D_y g}(\boldsymbol{y}, \boldsymbol{p}_o, \lambda)|_c$ has a simple zero eigenvalue, i.e., the Jacobian matrix is singular.
4. The dynamic of the collapse in the proximity of the bifurcation point is characterized by a monotonic change of system variables. The change is initially slow, and then it becomes fast and results in a voltage collapse.

In mathematical terms, SNB conditions are as follows:

$$\begin{aligned} \boldsymbol{g}(\boldsymbol{y}_c, \boldsymbol{p}_o, \lambda_c) &= \boldsymbol{0} \\ \boldsymbol{D_y g}(\boldsymbol{y}, \boldsymbol{p}_o, \lambda)|_c \hat{\boldsymbol{v}} = \hat{\boldsymbol{w}}^{\boldsymbol{T}} \boldsymbol{D_y g}(\boldsymbol{y}, \boldsymbol{p}_o, \lambda)|_c &= \boldsymbol{0} \\ \|\hat{\boldsymbol{v}}\| = \|\hat{\boldsymbol{w}}\| &= 1 \end{aligned}$$

where $\hat{\boldsymbol{v}}$ and $\hat{\boldsymbol{w}}$ are, respectively, the right and the left eigenvectors corresponding to the zero eigenvalue, and the operator $\|\cdot\|$ is the Euclidean norm.

A SNB is basically characterized by two power flow solutions that coalesce and disappear as certain system parameters (particularly the system load) change slowly. In practical terms, a SNB typically lead to voltage collapse.

2.1.2.2 Limit-Induced Bifurcation

In the power system context, this type of bifurcation was first studied in detail in [48]. LIBs originate from a change in system equations: a system device

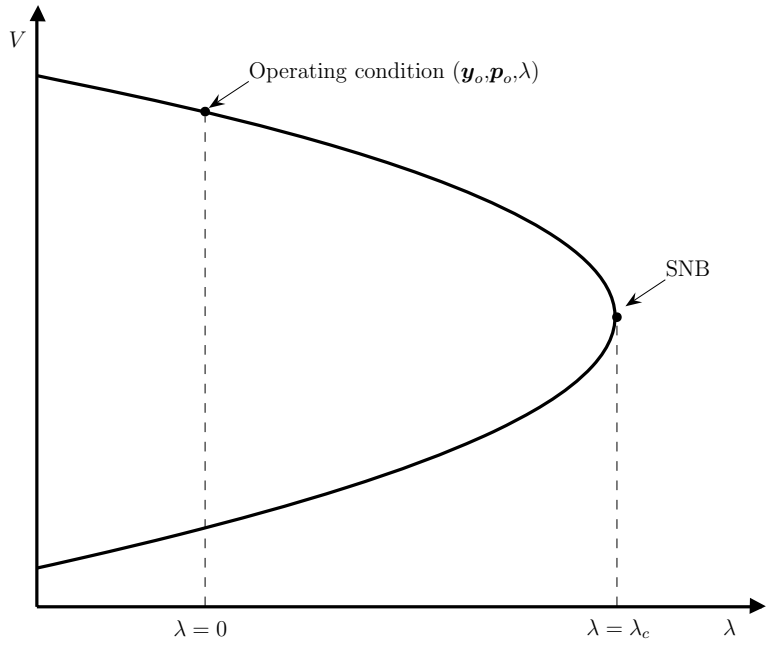

Figure 2.1: Saddle-node bifurcation.

reaches an operating limit as λ increases. This causes a "breaking point" in the system. A typical example of breaking point is the case in which one of the reactive power limits of a generator is reached. In this situation, generator j loses control over the voltage of its associated bus $V_n = V_n^{\text{ref}}$ when any of its reactive power limits is reached, i.e., $Q_{\text{G}j} = Q_{\text{G}j}^{\max}$ or $Q_{\text{G}j} = Q_{\text{G}j}^{\min}$. Therefore, the equation that fixes the voltage magnitude is substituted for the equation that fixes the reactive power output.

A breaking point can be viewed as the solution of the following system:

$$\begin{aligned} \boldsymbol{g}(\boldsymbol{y}_c, \boldsymbol{p}_o, \lambda_c) &= \mathbf{0}, \\ \tilde{g}(\boldsymbol{y}_c, \boldsymbol{p}_o, \lambda_c) &= \mathbf{0}, \end{aligned}$$

where vector function $\boldsymbol{g}$ ($\boldsymbol{g} : \mathbb{R}^{\text{n}_\text{y}} \times \mathbb{R}^{\text{n}_\text{p}} \times \mathbb{R} \longmapsto \mathbb{R}^{\text{n}_\text{y}}$) represents the initial system equations and function $\tilde{g}$ ($\tilde{g} : \mathbb{R}^{\text{n}_\text{y}} \times \mathbb{R}^{\text{n}_\text{p}} \times \mathbb{R} \longmapsto \mathbb{R}$) represents the new equation related to the reached limit. A breaking point must satisfy the

resulting set of equations. If at a breaking point two system equilibria coalesce and disappear, a LIB occurs. Mathematically, in contrast with a SNB, a LIB associated with the power flow equations is an equilibrium point $(\boldsymbol{y}_c, \boldsymbol{p}_o, \lambda_c)$ at which the corresponding Jacobian matrix $\boldsymbol{D_y g}(\boldsymbol{y}, \boldsymbol{p}_o, \lambda)|_c$ is nonsingular [126].

Figure 2.2 depicts a PV curve with a breaking point and a LIB. Observe that a breaking point does not cause voltage collapse. Once reached, the equilibrium points continue to exist as the loading parameter λ changes. However, a LIB corresponds to a point at which two equilibria coalesce and disappear, and causes voltage collapse.

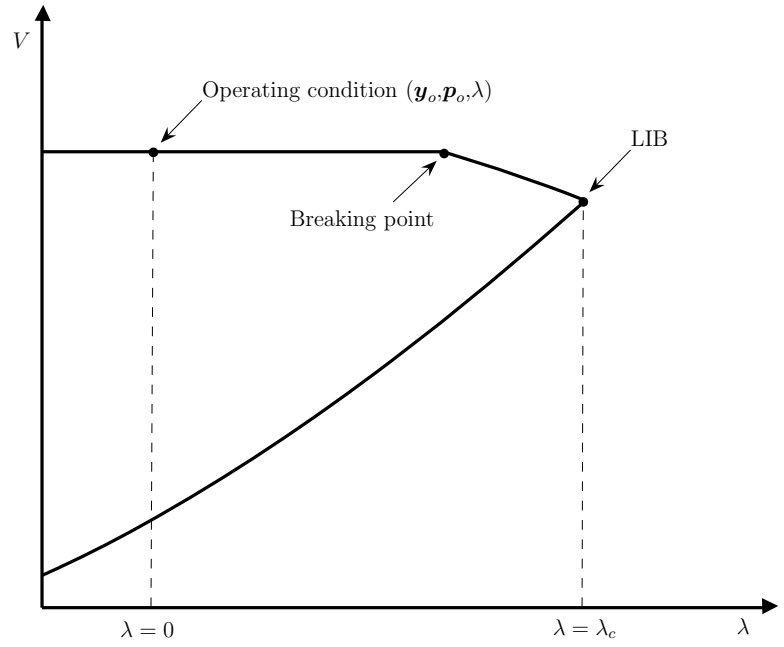

Figure 2.2: Limit-induced bifurcations.

2.1.3 Voltage Stability Assessment

Since voltage instability is often a catastrophic event, it is of interest to determine the proximity of the power system operating condition to collapse, i.e., to quantify the margin to instability. The proximity to voltage collapse can be estimated by means of several indices [118]. A very common index is the

loading margin. For a particular power system operating condition $(\boldsymbol{y}_o, \boldsymbol{p}_o)$, the loading margin is defined as the maximum amount of additional load that the system can provide until a SNB or a LIB point is reached. The value of the loading margin depends on the pattern in which the load is increased. Throughout this thesis, all system loads are increased according to the following expressions:

$$P_{\mathrm{D}i} = (1+\lambda)P^{\mathrm{A}}_{\mathrm{D}i}, \quad \forall i \in \mathcal{D} \tag{2.2}$$

$$Q_{\mathrm{D}i} = (1+\lambda)Q^{\mathrm{A}}_{\mathrm{D}i}, \quad \forall i \in \mathcal{D} \tag{2.3}$$

where $P^{\mathrm{A}}_{\mathrm{D}i}$ and $Q^{\mathrm{A}}_{\mathrm{D}i}$ are the active and reactive load powers, respectively, which correspond to the system operating condition for which the loading margin computation is required (i.e., $(P^{\mathrm{A}}_{\mathrm{D}i}, Q^{\mathrm{A}}_{\mathrm{D}i}) \in \boldsymbol{p}_o$). From expressions (2.2) and (2.3) and observing Figures 2.1 and 2.2, it follows that the loading margin is actually the value λ_c.

The loading margin associated either with a SNB or with a LIB corresponds directly to the solution of the following general optimization problem:

$$\underset{\boldsymbol{y},\,\lambda}{\text{Maximize}} \qquad \lambda \tag{2.4}$$

$$\text{subject to} \quad \boldsymbol{g}(\boldsymbol{y}, \boldsymbol{p}_o, \lambda) = \boldsymbol{0} \tag{2.5}$$

$$\boldsymbol{y}^{\min} \leq \boldsymbol{y} \leq \boldsymbol{y}^{\max} \tag{2.6}$$

where constraints (2.5) represent the power flow equations and constraints (2.6) represent system device limits, which are typically generator reactive power limits. The solution of problem (2.4)-(2.6) provides the maximum loading condition of the power system, defined by λ^* and $\boldsymbol{y}^*$, with respect to the system operating condition defined by $\boldsymbol{p}_o$.

The voltage stability assessment used in this thesis is based on the concept of loading margin. For a particular power system operating condition, the loading margin is defined as the maximum amount of additional load that the system can provide without exceeding a voltage stability limit. Voltage stabil-

ity limits lead to system collapse and correspond to a SNB or a LIB point. In this thesis, the definition of loading margin is extended to take into account technical limits, such as bus voltage limits and transmission line/transformer thermal limits. These limits do not directly cause collapse but should be avoided because they can initiate cascade line tripping phenomena. In addition, generator ramping limits are taken into account. The ramps represent the generator capacity to supply additional load within a given period of time (Δt). Similarly, ramping constraints are used to model the capacity of certain control devices, such as on-load tap-changing and phase-shifting transformers, to adjust their set points. Therefore, for a particular power system operating condition, the loading margin λ^* represents the maximum amount of additional load that the system can provide without exceeding a technical limit while ensuring that a voltage collapse does not appear within a given period of time Δt. The value of λ^* is determined according to the optimization problem described in Appendix B.

2.2 Security Assessment: Contingency Filtering

The security assessment, also known as contingency analysis [9, 65, 133], basically involves a number of studies in which the state of the network is determined for each of the selected contingencies. For the sake of simplicity, but without loss of generality, in this thesis the initial set of contingencies includes those of the $N-1$ security criterion. This initial set is reduced by means of a contingency filtering procedure in order to identify the most harmful, or critical, contingencies.

Regarding voltage stability, contingency filtering is carried out using the loading margin λ^*, which is introduced in Subsection 2.1.3, as a severity index. The selection of the critical contingencies is based on comparing the corresponding value of λ^* with a pre-defined value, the security margin (λ^{SM}). The security margin λ^{SM} is defined as the loading margin that the system should have with respect to voltage stability limits, operation limits, or physi-

cal limits, within the time interval Δt if any single contingency occurs. Thus, for a given value of λ^{SM}, the contingency filtering procedure is as follows:

1. For each of the contingencies, λ^* is calculated using the problem described in Appendix B.
2. If $\lambda^* \leq \lambda^{\mathrm{SM}}$ the contingency is selected as critical.
3. If $\lambda^* > \lambda^{\mathrm{SM}}$ the contingency is filtered out.

Other possible way to perform contingency filtering is to compute the system operating condition that corresponds to a pre-contingency system configuration where the load is increased by the amount λ^{SM}. Then, each contingency is applied and post-contingency operating conditions are computed by solving a power flow analysis. Critical contingencies are those that lead either to divergence of the post-contingency power flow calculation or to system limit violations. This methodology allows speeding up the contingency filtering procedure, but it is rather conservative, i.e., there exists the risk of labeling as critical some harmless contingencies due to the simplifying assumptions of the power flow analysis.

2.3 Security Redispatching

Once a working condition has been established through a dispatching procedure (e.g., a market clearing algorithm), but prior to actual power delivery, the independent system operator (ISO) must check system security and implement redispatching actions on the dispatching solution if needed.

This section suggests a redispatching procedure based on a Voltage Stability Constrained Optimal Power Flow (VSC-OPF) problem to assist the system operator in ensuring an appropriate security level. The starting point for the procedure is a base-case operating condition established through a dispatching solution adjusted by losses (see Appendix A).

The VSC-OPF problem considers several operating conditions: the adjusted operating condition and a set of stressed operating conditions. The adjusted operating condition results from adjusting the base-case operating

condition. Each one of the stressed operating conditions is associated with a single contingency and a fictitious loading level that enables to set a distance to instability in terms of load. Furthermore, the procedure allows control devices to be incorporated. In particular, two regulating transformers and two FACTS devices are considered: an on-Load Tap-Changing (LTC) transformer, a PHase-Shifting (PHS) transformer, a Static Var Compensator (SVC) device, and a Thyristor-Controlled Series Compensator (TCSC) device. The solution of the proposed procedure provides the preventive control actions for the base-case solution that guarantee a pre-specified security level. It is assumed that the system operator has access to the generator technical information and that the generators provide the ISO with cost offers for redispatching.

2.3.1 VSC-OPF Problem Description

This subsection describes the objective function and all constraints pertaining to the VSC-OPF problem in detail.

2.3.1.1 Objective function

The objective function is aimed at minimizing the variations with respect to the base-case solution. In particular, the objective function is composed of several terms that represent adjustment costs and penalty functions. The adjustment costs correspond to changes in the generation and load powers, while the penalty functions concern voltage magnitudes at generator buses, and set points of control devices. Thus, for the adjusted operating condition, the total cost function of generation power adjustments is

$$z_{\mathrm{G}}(\Delta P_{\mathrm{G}j}^{\mathrm{up}}, \Delta P_{\mathrm{G}j}^{\mathrm{down}}) = \sum_{j \in \mathcal{G}} c_{\mathrm{G}j}^{\mathrm{up}} \Delta P_{\mathrm{G}j}^{\mathrm{up}} + c_{\mathrm{G}j}^{\mathrm{down}} \Delta P_{\mathrm{G}j}^{\mathrm{down}}, \tag{2.7}$$

where $c_{\mathrm{G}j}^{\mathrm{up}}$ and $c_{\mathrm{G}j}^{\mathrm{down}}$ are, respectively, the offering costs of generator j to increase and decrease its power dispatch for security purposes. The total penalty

function of voltage magnitude adjustments at generator buses is

$$z_{\mathrm{V}}(\Delta V_n^{\mathrm{up}}, \Delta V_n^{\mathrm{down}}) = \sum_{n \in \mathcal{N}_{\mathrm{G}}} c_{\mathrm{V}n}^{\mathrm{up}} \Delta V_n^{\mathrm{up}} + c_{\mathrm{V}n}^{\mathrm{down}} \Delta V_n^{\mathrm{down}}. \tag{2.8}$$

The term (2.8) is included to penalize any changes to the base-case voltage magnitudes at generator buses since the voltage profile of the base case is considered to be the most suitable.

Additionally, the changes to the set point of control devices with respect to the base case are also penalized. Two types of voltage controlling devices: the LTC and the SVC; and two types of power flow controlling devices: the PHS and the TCSC, are considered in this chapter. The total penalty function of set point adjustments for the LTC is

$$z_{\mathrm{LTC}}(\Delta V_n^{\mathrm{up}}, \Delta V_n^{\mathrm{down}}) = \sum_{n \in \mathcal{N}_{\mathrm{LTC}}} c_{\mathrm{LTC},n}^{\mathrm{up}} \Delta V_n^{\mathrm{up}} + c_{\mathrm{LTC},n}^{\mathrm{down}} \Delta V_n^{\mathrm{down}}, \tag{2.9}$$

the total penalty function of set point adjustments for the PHS is

$$z_{\mathrm{PHS}}(\Delta P_k^{\mathrm{up}}, \Delta P_k^{\mathrm{down}}) = \sum_{k \in \Omega_{\mathrm{PHS}}} c_{\mathrm{PHS},k}^{\mathrm{up}} \Delta P_k^{\mathrm{up}} + c_{\mathrm{PHS},k}^{\mathrm{down}} \Delta P_k^{\mathrm{down}}, \tag{2.10}$$

the total penalty function of set point adjustments for the SVC is

$$z_{\mathrm{SVC}}(\Delta V_n^{\mathrm{up}}, \Delta V_n^{\mathrm{down}}) = \sum_{n \in \mathcal{N}_{\mathrm{SVC}}} c_{\mathrm{SVC},n}^{\mathrm{up}} \Delta V_n^{\mathrm{up}} + c_{\mathrm{SVC},n}^{\mathrm{down}} \Delta V_n^{\mathrm{down}}, \tag{2.11}$$

and the total penalty function of set point adjustments for the TCSC is

$$z_{\mathrm{TCSC}}(\Delta P_k^{\mathrm{up}}, \Delta P_k^{\mathrm{down}}) = \sum_{k \in \Omega_{\mathrm{TCSC}}} c_{\mathrm{TCSC},k}^{\mathrm{up}} \Delta P_k^{\mathrm{up}} + c_{\mathrm{TCSC},k}^{\mathrm{down}} \Delta P_k^{\mathrm{down}}. \tag{2.12}$$

Similarly, for each one of the considered stressed operating conditions, the total cost function of generation power adjustments is

$$z_{\mathrm{G}}^{s}(\Delta P_{\mathrm{G}j}^{\mathrm{up},s}, \Delta P_{\mathrm{G}j}^{\mathrm{down},s}) = \sum_{j \in \mathcal{G}} c_{\mathrm{G}j}^{\mathrm{up}} \Delta P_{\mathrm{G}j}^{\mathrm{up},s} + c_{\mathrm{G}j}^{\mathrm{down}} \Delta P_{\mathrm{G}j}^{\mathrm{down},s}, \tag{2.13}$$

the total penalty function of voltage magnitude adjustments is

$$z_{\mathrm{V}}^{s}(\Delta V_n^{\mathrm{up},s}, \Delta V_n^{\mathrm{down},s}) = \sum_{n \in \mathcal{N}_{\mathrm{G}}} c_{\mathrm{V}n}^{\mathrm{up}} \Delta V_n^{\mathrm{up},s} + c_{\mathrm{V}n}^{\mathrm{down}} \Delta V_n^{\mathrm{down},s}, \tag{2.14}$$

the total penalty function of set point adjustments for the LTC is

$$z_{\mathrm{LTC}}^{s}(\Delta V_n^{\mathrm{up},s}, \Delta V_n^{\mathrm{down},s}) = \sum_{n \in \mathcal{N}_{\mathrm{LTC}}} c_{\mathrm{LTC},n}^{\mathrm{up}} \Delta V_n^{\mathrm{up},s} + c_{\mathrm{LTC},n}^{\mathrm{down}} \Delta V_n^{\mathrm{down},s}, \tag{2.15}$$

the total penalty function of set point adjustments for the PHS is

$$z_{\mathrm{PHS}}^{s}(\Delta P_k^{\mathrm{up},s}, \Delta P_k^{\mathrm{down},s}) = \sum_{k \in \Omega_{\mathrm{PHS}}} c_{\mathrm{PHS},k}^{\mathrm{up}} \Delta P_k^{\mathrm{up},s} + c_{\mathrm{PHS},k}^{\mathrm{down}} \Delta P_k^{\mathrm{down},s}, \tag{2.16}$$

the total penalty function of set point adjustments for the SVC is

$$z_{\mathrm{SVC}}^{s}(\Delta V_n^{\mathrm{up},s}, \Delta V_n^{\mathrm{down},s}) = \sum_{n \in \mathcal{N}_{\mathrm{SVC}}} c_{\mathrm{SVC},n}^{\mathrm{up}} \Delta V_n^{\mathrm{up},s} + c_{\mathrm{SVC},n}^{\mathrm{down}} \Delta V_n^{\mathrm{down},s}, \tag{2.17}$$

and the total penalty function of set point adjustments for the TCSC is

$$z_{\mathrm{TCSC}}^{s}(\Delta P_k^{\mathrm{up},s}, \Delta P_k^{\mathrm{down},s}) = \sum_{k \in \Omega_{\mathrm{TCSC}}} c_{\mathrm{TCSC},k}^{\mathrm{up}} \Delta P_k^{\mathrm{up},s} + c_{\mathrm{TCSC},k}^{\mathrm{down}} \Delta P_k^{\mathrm{down},s}. \tag{2.18}$$

Cost function (2.13) and penalty functions 2.14-(2.18) are introduced to force all stressed systems to work economically and to minimize changes to the set points of control devices. Furthermore, a term is included to take into account the cost of adjustments to the demand power levels. These adjustments involve only demand power decrements. The total cost function of load power adjustments is

$$z_{\mathrm{D}}(\Delta P_{\mathrm{D}i}^{\mathrm{down}}) = \sum_{i \in \mathcal{D}} c_{\mathrm{D}i}^{\mathrm{down}} \Delta P_{\mathrm{D}i}^{\mathrm{down}}. \tag{2.19}$$

The cost function (2.19) is not considered explicitly for the stressed operating conditions since load powers of the stressed systems are linked to the loads of the adjusted condition (see (2.42) and (2.44)). In summary, the resulting

objective function is as follows:

$$
\begin{aligned}
z = \mu\Big(& z_{\mathrm{G}}(\Delta P_{\mathrm{G}j}^{\mathrm{up}}, \Delta P_{\mathrm{G}j}^{\mathrm{down}}) + z_{\mathrm{V}}(\Delta V_n^{\mathrm{up}}, \Delta V_n^{\mathrm{down}}) \\
& + z_{\mathrm{LTC}}(\Delta V_n^{\mathrm{up}}, \Delta V_n^{\mathrm{down}}) \\
& + z_{\mathrm{PHS}}(\Delta P_k^{\mathrm{up}}, \Delta P_k^{\mathrm{down}}) \\
& + z_{\mathrm{SVC}}(\Delta V_n^{\mathrm{up}}, \Delta V_n^{\mathrm{down}}) \\
& + z_{\mathrm{TCSC}}(\Delta P_k^{\mathrm{up}}, \Delta P_k^{\mathrm{down}})\Big) \\
& + \sum_{s\in\mathcal{S}} \mu^s \Big(z_{\mathrm{G}}^s(\Delta P_{\mathrm{G}j}^{\mathrm{up},s}, \Delta P_{\mathrm{G}j}^{\mathrm{down},s}) + z_{\mathrm{V}}^s(\Delta V_n^{\mathrm{up},s}, \Delta V_n^{\mathrm{down},s}) \\
& + z_{\mathrm{LTC}}^s(\Delta V_n^{\mathrm{up},s}, \Delta V_n^{\mathrm{down},s}) \\
& + z_{\mathrm{PHS}}^s(\Delta P_k^{\mathrm{up},s}, \Delta P_k^{\mathrm{down},s}) \\
& + z_{\mathrm{SVC}}^s(\Delta V_n^{\mathrm{up},s}, \Delta V_n^{\mathrm{down},s}) \\
& + z_{\mathrm{TCSC}}^s(\Delta P_k^{\mathrm{up},s}, \Delta P_k^{\mathrm{down},s})\Big) \\
& + z_{\mathrm{D}}(\Delta P_{\mathrm{D}i}^{\mathrm{down}}).
\end{aligned} \tag{2.20}
$$

where μ and μ^s are, respectively, the probability of operating in the adjusted operating condition and the probability of occurrence of the contingency considered in the stressed operating condition s. These probabilities satisfy:

$$
\mu + \sum_{s\in\mathcal{S}} \mu^s \;=\; 1, \tag{2.21}
$$

where $\mu^s \ll \mu$, [33].

2.3.1.2 Power flow equations for the adjusted operating condition

The adjusted operating condition is defined by the active and reactive power balance at all buses:

$$
P_{\mathrm{G}n} - P_{\mathrm{D}n} = \sum_{m\in\Theta_n} P_{nm}(\cdot), \quad \forall n \in \mathcal{N}, \tag{2.22}
$$

$$
Q_{\mathrm{G}n} - Q_{\mathrm{D}n} = \sum_{m\in\Theta_n} Q_{nm}(\cdot), \quad \forall n \in \mathcal{N}, \tag{2.23}
$$

where the powers on the left-hand side of each equation above are

$$P_{\mathrm{G}n} = \sum_{j \in \mathcal{G}_n} P_{\mathrm{G}j}, \quad \forall n \in \mathcal{N}, \tag{2.24}$$

$$P_{\mathrm{D}n} = \sum_{i \in \mathcal{D}_n} P_{\mathrm{D}i}, \quad \forall n \in \mathcal{N}, \tag{2.25}$$

$$Q_{\mathrm{G}n} = \sum_{j \in \mathcal{G}_n} Q_{\mathrm{G}j}, \quad \forall n \in \mathcal{N}, \tag{2.26}$$

$$Q_{\mathrm{D}n} = \sum_{i \in \mathcal{D}_n} P_{\mathrm{D}i} \tan(\psi_{\mathrm{D}i}), \quad \forall n \in \mathcal{N}, \tag{2.27}$$

with

$$P_{\mathrm{G}j} = P_{\mathrm{G}j}^{\mathrm{A}} + \Delta P_{\mathrm{G}j}^{\mathrm{up}} - \Delta P_{\mathrm{G}j}^{\mathrm{down}}, \quad \forall j \in \mathcal{G}, \tag{2.28}$$

$$P_{\mathrm{D}i} = P_{\mathrm{D}i}^{\mathrm{A}} - \Delta P_{\mathrm{D}i}, \quad \forall i \in \mathcal{D}, \tag{2.29}$$

and

$$\Delta P_{\mathrm{G}j}^{\mathrm{up}} \geq 0, \quad \forall j \in \mathcal{G}, \tag{2.30}$$

$$\Delta P_{\mathrm{G}j}^{\mathrm{down}} \geq 0, \quad \forall j \in \mathcal{G}, \tag{2.31}$$

$$\Delta P_{\mathrm{D}i} \geq 0, \quad \forall i \in \mathcal{D}. \tag{2.32}$$

Equation (2.27) implies that constant power factor loads are considered. The functions on the right-hand sides of (2.22) and (2.23) are the power flow equations and depend on the device connected between buses n and m. Appendix C describes these equations in detail.

The voltage magnitudes controlled by generators, LTC transformers and SVC devices are defined as

$$V_n = V_n^{\mathrm{A}} + \Delta V_n^{\mathrm{up}} - \Delta V_n^{\mathrm{down}}, \quad \forall n \in (\mathcal{N}_{\mathrm{G}} \cup \mathcal{N}_{\mathrm{LTC}} \cup \mathcal{N}_{\mathrm{SVC}}), \tag{2.33}$$

with

$$\Delta V_n^{\mathrm{up}} \geq 0, \quad \forall n \in (\mathcal{N}_{\mathrm{G}} \cup \mathcal{N}_{\mathrm{LTC}} \cup \mathcal{N}_{\mathrm{SVC}}), \tag{2.34}$$

$$\Delta V_n^{\mathrm{down}} \geq 0, \quad \forall n \in ((\mathcal{N}_{\mathrm{G}} \cup \mathcal{N}_{\mathrm{LTC}} \cup \mathcal{N}_{\mathrm{SVC}}). \tag{2.35}$$

The power flows controlled by PHS transformers and TCSC devices are defined as

$$P_k = P_k^{\mathrm{A}} + \Delta P_k^{\mathrm{up}} - \Delta P_k^{\mathrm{down}}, \quad \forall k = (n,m) \in (\Omega_{\mathrm{PHS}} \cup \Omega_{\mathrm{TCSC}}), \tag{2.36}$$

with

$$\Delta P_k^{\mathrm{up}} \geq 0, \quad \forall k = (n,m) \in (\Omega_{\mathrm{PHS}} \cup \Omega_{\mathrm{TCSC}}), \tag{2.37}$$

$$\Delta P_k^{\mathrm{down}} \geq 0, \quad \forall k = (n,m) \in (\Omega_{\mathrm{PHS}} \cup \Omega_{\mathrm{TCSC}}). \tag{2.38}$$

Finally, note that superscript "A" in (2.28), (2.29), (2.33) and (2.36) indicates the base-case solution.

2.3.1.3 Power flow equations for the stressed operating conditions

The power flow equations for the stressed operating conditions are

$$P_{\mathrm{G}n}^s - P_{\mathrm{D}n}^s = \sum_{m \in \Theta_n} P_{nm}^s(\cdot), \quad \forall n \in \mathcal{N}, \quad \forall s \in \mathcal{S}, \tag{2.39}$$

$$Q_{\mathrm{G}n}^s - Q_{\mathrm{D}n}^s = \sum_{m \in \Theta_n} Q_{nm}^s(\cdot), \quad \forall n \in \mathcal{N}, \quad \forall s \in \mathcal{S}, \tag{2.40}$$

where the powers on the left-hand side of (2.39) and (2.40) are defined as

$$P_{\mathrm{G}n}^s = \sum_{j \in \mathcal{G}_n} P_{\mathrm{G}j}^s, \quad \forall n \in \mathcal{N}, \quad \forall s \in \mathcal{S}, \tag{2.41}$$

$$P_{\mathrm{D}n}^s = \sum_{i \in \mathcal{D}_n} (1 + \lambda^{\mathrm{SM}}) P_{\mathrm{D}i}, \quad \forall n \in \mathcal{N}, \quad \forall s \in \mathcal{S}, \tag{2.42}$$

$$Q_{\mathrm{G}n}^s = \sum_{j \in \mathcal{G}_n} Q_{\mathrm{G}j}^s, \quad \forall n \in \mathcal{N}, \quad \forall s \in \mathcal{S}, \tag{2.43}$$

$$Q_{\mathrm{D}n}^s = \sum_{i \in \mathcal{D}_n} (1 + \lambda^{\mathrm{SM}}) P_{\mathrm{D}i} \tan(\psi_{\mathrm{D}i}), \quad \forall n \in \mathcal{N}, \quad \forall s \in \mathcal{S}, \tag{2.44}$$

with

$$P_{\mathrm{G}j}^s = P_{\mathrm{G}j} + \Delta P_{\mathrm{G}j}^{\mathrm{up},s} - \Delta P_{\mathrm{G}j}^{\mathrm{down},s}, \quad \forall j \in \mathcal{G}, \quad \forall s \in \mathcal{S}, \tag{2.45}$$

$$\Delta P_{\mathrm{G}j}^{\mathrm{up},s} \geq 0, \quad \forall j \in \mathcal{G}, \quad \forall s \in \mathcal{S}, \tag{2.46}$$

$$\Delta P_{\mathrm{G}j}^{\mathrm{down},s} \geq 0, \quad \forall j \in \mathcal{G}, \quad \forall s \in \mathcal{S}, \tag{2.47}$$

where $P_{\mathrm{G}j}$ is defined as in (2.28) and $P_{\mathrm{D}i}$ is defined as in (2.29).

The functions of the right-hand side of (2.39) and (2.40) have the same expressions as the power flow equations (2.22) and (2.23), respectively, except for the fact that the corresponding variables are substituted by those pertaining to the stressed operating conditions.

Equations (2.39)-(2.44) are introduced to represent the system at the loading level determined by the security margin λ^{SM}. Moreover, each set of equations (2.39)-(2.44) includes a single line outage to enforce the $N-1$ contingency criterion. Therefore, each of the stressed operating conditions is characterized by λ^{SM} and by a single contingency.

Like the adjusted operating condition, the voltage magnitudes at the generator buses and the variables controlled by regulating transformers and FACTS devices for the stressed operating conditions are defined as

$$V_n^s = V_n + \Delta V_n^{\mathrm{up},s} - \Delta V_n^{\mathrm{down},s}, \quad \forall n \in (\mathcal{N}_{\mathrm{G}} \cup \mathcal{N}_{\mathrm{LTC}} \cup \mathcal{N}_{\mathrm{SVC}}), \quad \forall s \in \mathcal{S}, \tag{2.48}$$

with

$$\Delta V_n^{\mathrm{up},s} \geq 0, \quad \forall n \in (\mathcal{N}_{\mathrm{G}} \cup \mathcal{N}_{\mathrm{LTC}} \cup \mathcal{N}_{\mathrm{SVC}}), \quad \forall s \in \mathcal{S}, \tag{2.49}$$

$$\Delta V_n^{\mathrm{down},s} \geq 0, \quad \forall n \in (\mathcal{N}_{\mathrm{G}} \cup \mathcal{N}_{\mathrm{LTC}} \cup \mathcal{N}_{\mathrm{SVC}}), \quad \forall s \in \mathcal{S}. \tag{2.50}$$

and

$$P_k^s = P_k + \Delta P_k^{\mathrm{up},s} - \Delta P_k^{\mathrm{down},s}, \quad \forall k = (n,m) \in (\Omega_{\mathrm{PHS}} \cup \Omega_{\mathrm{TCSC}}), \quad \forall s \in \mathcal{S}, \tag{2.51}$$

with

$$\Delta P_k^{\mathrm{up},s} \geq 0, \quad \forall k = (n,m) \in (\Omega_{\mathrm{PHS}} \cup \Omega_{\mathrm{TCSC}}), \quad \forall s \in \mathcal{S}, \tag{2.52}$$

$$\Delta P_k^{\text{down},s} \geq 0, \quad \forall k = (n,m) \in (\Omega_{\text{PHS}} \cup \Omega_{\text{TCSC}}), \quad \forall s \in \mathcal{S}. \tag{2.53}$$

Finally, V_n in (2.48) and P_k in (2.51) are defined as in (2.33) and (2.36), respectively.

2.3.1.4 Technical limits

The power production is limited by the capacity of the generators. Thus, under normal and stressed conditions,

$$P_{\text{G}j}^{\min} \leq P_{\text{G}j} \leq P_{\text{G}j}^{\max}, \quad \forall j \in \mathcal{G}, \tag{2.54}$$
$$P_{\text{G}j}^{\min} \leq P_{\text{G}j}^{s} \leq P_{\text{G}j}^{\max}, \quad \forall j \in \mathcal{G}, \quad \forall s \in \mathcal{S}, \tag{2.55}$$
$$Q_{\text{G}j}^{\min} \leq Q_{\text{G}j} \leq Q_{\text{G}j}^{\max}, \quad \forall j \in \mathcal{G}, \tag{2.56}$$
$$Q_{\text{G}j}^{\min} \leq Q_{\text{G}j}^{s} \leq Q_{\text{G}j}^{\max}, \quad \forall j \in \mathcal{G}, \quad \forall s \in \mathcal{S}. \tag{2.57}$$

Voltage magnitudes throughout the system under the adjusted and stressed operating conditions should be within operating limits,

$$V_n^{\min} \leq V_n \leq V_n^{\max}, \quad \forall n \in \mathcal{N}, \tag{2.58}$$
$$V_n^{\min} \leq V_n^{s} \leq V_n^{\max}, \quad \forall n \in \mathcal{N}, \quad \forall s \in \mathcal{S}. \tag{2.59}$$

The current flow through all branches of the network must be below thermal limits,

$$I_k(\cdot) \leq I_k^{\max}, \quad \forall k = (n,m) \in \Omega, \tag{2.60}$$
$$I_k^{s}(\cdot) \leq I_k^{\max}, \quad \forall k = (n,m) \in \Omega^s, \quad \forall s \in \mathcal{S}, \tag{2.61}$$

where functions $I_k(\cdot)$ depend on the device k connected between buses n and m. The expressions of these functions are defined in Appendix C. The functions $I_k^s(\cdot)$ have the same expressions as $I_k(\cdot)$ except for the fact that the corresponding variables are substituted by those pertaining to the stressed operating conditions.

Changes in the production of generators between the adjusted and the

stressed operating conditions are limited by ramping constraints,

$$P^s_{\mathrm{G}j} - P_{\mathrm{G}j} \leq R^{\mathrm{up}}_{\mathrm{G}j}\Delta t, \quad \forall j \in \mathcal{G}, \quad \forall s \in \mathcal{S}, \tag{2.62}$$

$$P_{\mathrm{G}j} - P^s_{\mathrm{G}j} \leq R^{\mathrm{down}}_{\mathrm{G}j}\Delta t, \quad \forall j \in \mathcal{G}, \quad \forall s \in \mathcal{S}. \tag{2.63}$$

The time interval Δt is the period within which generators are able to adjust their power production levels in order to reach the stressed operating conditions. Also, observe that (2.62) and (2.63) along with (2.42) and (2.44) couple the variables of the stressed systems with those pertaining to the adjusted operating condition.

Constraints (2.62) and (2.63) enforce the fact that increments and decrements to the generator power outputs can be obtained only within given rates, which in turn depend on the type and characteristics of the power plants. These constraints constitute a necessary condition to ensure that the stressed operating conditions can be reached within the considered time period.

Regarding the FACTS devices and regulating transformers considered, while the SVC and TCSC device responses to implement the required changes can be considered instantaneous for the time duration Δt, the responses of the LTC and the PHS transformers are conditioned by a mechanically driven operation, and they are not instantaneous. As for generators, these physical constraints are related to ramping limits,

$$T^s_k - T_k \leq R^{\mathrm{up}}_{\mathrm{T}_k}\Delta t, \quad \forall k = (n,m) \in \Omega_{\mathrm{LTC}}, \quad \forall s \in \mathcal{S}, \tag{2.64}$$

$$T_k - T^s_k \leq R^{\mathrm{down}}_{\mathrm{T}_k}\Delta t, \quad \forall k = (n,m) \in \Omega_{\mathrm{LTC}}, \quad \forall s \in \mathcal{S}, \tag{2.65}$$

$$\phi^s_k - \phi_k \leq R^{\mathrm{up}}_{\phi_k}\Delta t, \quad \forall k = (n,m) \in \Omega_{\mathrm{PHS}}, \quad \forall s \in \mathcal{S}, \tag{2.66}$$

$$\phi_k - \phi^s_k \leq R^{\mathrm{down}}_{\phi_k}\Delta t, \quad \forall k = (n,m) \in \Omega_{\mathrm{PHS}}, \quad \forall s \in \mathcal{S}. \tag{2.67}$$

It is implicitly assumed that the redispatching actions, such as power adjustments, and the operation of regulating transformers and FACTS devices are feasible within the time duration Δt.

Finally, any device connected to the system is allowed to vary within its

rating values. Therefore, under normal and stressed conditions, for LTC transformers:

$$T_k^{\min} \leq T_k \leq T_k^{\max}, \quad \forall k = (n,m) \in \Omega_{\text{LTC}}, \tag{2.68}$$
$$T_k^{\min} \leq T_k^s \leq T_k^{\max}, \quad \forall k = (n,m) \in \Omega_{\text{LTC}}, \quad \forall s \in \mathcal{S}, \tag{2.69}$$

for PHS transformers:

$$\phi_k^{\min} \leq \phi_k \leq \phi_k^{\max}, \quad \forall k = (n,m) \in \Omega_{\text{PHS}}, \tag{2.70}$$
$$\phi_k^{\min} \leq \phi_k^s \leq \phi_k^{\max}, \quad \forall k = (n,m) \in \Omega_{\text{PHS}}, \quad \forall s \in \mathcal{S}, \tag{2.71}$$

for TCSC devices:

$$x_{\text{TCSC},k}^{\min} \leq x_{\text{TCSC},k} \leq x_{\text{TCSC},k}^{\max}, \quad \forall k = (n,m) \in \Omega_{\text{TCSC}}, \tag{2.72}$$
$$x_{\text{TCSC},k}^{\min} \leq x_{\text{TCSC},k}^s \leq x_{\text{TCSC},k}^{\max}, \quad \forall k = (n,m) \in \Omega_{\text{TCSC}}, \quad \forall s \in \mathcal{S}, \tag{2.73}$$

and for SVC devices:

$$b_{\text{SVC},n}^{\min} \leq b_{\text{SVC},n} \leq b_{\text{SVC},n}^{\max}, \quad \forall n \in \mathcal{N}_{\text{SVC}}, \tag{2.74}$$
$$b_{\text{SVC},n}^{\min} \leq b_{\text{SVC},n}^s \leq b_{\text{SVC},n}^{\max}, \quad \forall n \in \mathcal{N}_{\text{SVC}}, \quad \forall s \in \mathcal{S}. \tag{2.75}$$

There are two kind of limits in the case of regulating transformers and FACTS devices: (i) technical operating limits, such as tap ratio and phase limits (2.68)-(2.71), and (ii) capacity limits, such as the reactance sizes of the TCSC devices (2.72)-(2.73) and susceptance sizes of the SVC devices (2.74)-(2.75).

2.3.1.5 Other constraints

The proposed VSC-OPF problem includes the following additional constraints:

$$-\pi \leq \theta_n \leq \pi, \quad \forall n \in \mathcal{N}, \tag{2.76}$$
$$-\pi \leq \theta_n^s \leq \pi, \quad \forall n \in \mathcal{N}, \quad \forall s \in \mathcal{S}, \tag{2.77}$$

$$\theta_{\text{ref}} = 0, \tag{2.78}$$

$$\theta^s_{\text{ref}} = 0, \quad \forall s \in \mathcal{S}. \tag{2.79}$$

Equations (2.76) and (2.77) are included to reduce the feasibility region, thereby causing the OPF problem to converge more rapidly in general.

2.3.1.6 VSC-OPF problem formulation

The formulation of the VSC-OPF problem is summarized below:

Minimize (2.20)

subject to

1. Power flow equations for the adjusted operating condition (2.22)-(2.23).
2. Power flow equations for all the stressed operating conditions (2.39)-(2.40).
3. Technical limits (2.54)-(2.75).
4. Other constraints (2.76)-(2.79).

2.3.2 Security Redispatching Description

The proposed security redispatching procedure is as follows.

1. *Base-Case Solution.* The base-case solution corresponds to the solution of a dispatching procedure (e.g., a market clearing procedure) adjusted by losses. Specifically, the base-case solution is obtained from the OPF problem described in Appendix A.
2. *Selection of Stressed Operating Conditions.* For a given security margin λ^{SM}, the stressed operating conditions to be included in the VSC-OPF problem (set $\mathcal{S}$) are identified by applying the procedure described in Subsection 2.2. Stressed operating conditions are defined for each one of the contingencies selected, by setting the loading parameter λ^{SM} to the desired value in equations (2.42) and (2.44).

3. *Solve the VSC-OPF problem.* The OPF problem described in Subsection 2.3.1.6 is solved. The solution corresponds to the optimal preventive control actions needed to ensure the security margin λ^{SM}.

It should be noted that the system is not expected to operate at the loading level defined by λ^{SM}. In other words, the load increase represented by λ^{SM} is not a predicted load increase. Instead, the parameter λ^{SM} is used to enforce a margin to instability, in terms of the load. A stressed operating condition is defined by a contingency and the λ^{SM} value. Accordingly, if the system at the stressed operating condition is stable, it is assumed to be stable at the adjusted operating condition as well, and it has at least a margin λ^{SM} to instability even if the contingency occurs.

A relevant case arises if $\lambda^{\mathrm{SM}} = 0$. In addition to the preventive control actions that correspond to the adjusted operating condition, the solution output by the proposed procedure defines the emergency control actions needed to maintain stability if any of the considered contingencies occurs. These emergency control actions correspond to changes to the values of the control variables under the different stressed operating conditions.

2.4 Voltage Stability - Illustrative Example

For illustration purposes, the proposed security redispatching procedure is applied to a 6-bus system (W&W 6-bus system). This system is based on the 6-bus system reported by Wood & Wollenberg in [133]. Generator data, demand data, network data and technical limits, along with the one-line diagram, for this system are provided in Appendix D. Regulating transformers and FACTS devices are not considered. For clarify, the results of each step of the proposed procedure are provided.

2.4.1 Base Case

The base-case solution is obtained from the OPF problem described in Appendix A. Table 2.1 provides this base-case solution.

Table 2.1: Voltage stability illustrative example. W&W 6-bus system: Base-case solution.

Bus #	Gen. #	Dem. #	$P^{\mathrm{A}}_{\mathrm{G}n}$ [p.u.]	$Q^{\mathrm{A}}_{\mathrm{G}n}$ [p.u.]	$P^{\mathrm{A}}_{\mathrm{D}n}$ [p.u.]	$Q^{\mathrm{A}}_{\mathrm{D}n}$ [p.u.]	V^{A}_{n} [p.u.]	θ^{A}_{n} [rad.]
1	1	-	0.4575	0.3876	0	0	1.1000	-0.0077
2	2	-	1.2441	0.5284	0	0	1.1000	0
3	3	-	0.9231	0.5640	0	0	1.1000	-0.0018
4	-	1	0	0	0.7000	0.5500	1.0466	-0.0368
5	-	2	0	0	1.0500	0.7000	1.0238	-0.0638
6	-	3	0	0	0.8000	0.6000	1.0476	-0.0444

2.4.2 Selection of the Stressed Operating Conditions

Once the base-case solution is available, contingency analysis is carried out. The analyzed contingencies correspond to the outage of each line of the system. For each one of these contingencies, the loading margin λ^* is obtained by solving the optimization problem described in Appendix B. The considered time period is set to five minutes ($\Delta t = 5$ minutes).

Table 2.2 provides the value of λ^* and the enforced limits at the maximum loading condition for each one of the analyzed contingencies.

The stressed operating conditions are selected for three different security margins: $\lambda^{\mathrm{SM}} = 0.03$, $\lambda^{\mathrm{SM}} = 0.05$, and $\lambda^{\mathrm{SM}} = 0.10$. Table 2.3 includes the results of applying the contingency filtering procedure described in Section 2.2 for the three security margins. If the required security margin is 0.03, only the stressed operating condition corresponding to the outage of line $1-5$ is taken into account in the VSC-OPF problem. If the required security margin is 0.05, three stressed operating conditions are taken into account in the VSC-OPF problem: outage of line $1-5$, outage of line $3-5$, and outage of line $3-6$. Finally, if the required security margin is 0.10, five stressed operating conditions are taken into account in the VSC-OPF problem, as indicated in Table 2.3.

Table 2.2: Voltage stability illustrative example. W&W 6-bus system: Loading margin and enforced limits.

Cont.	λ^*	Enforced Limits
1 - 2	0.1708	R_{G1}^{up}, R_{G2}^{up}, R_{G3}^{up}
1 - 4	0.1603	R_{G1}^{up}, R_{G2}^{up}, R_{G3}^{up}
1 - 5	0.0199	R_{G2}^{up}, I_{5-6}^{max}, I_{5-4}^{max}
2 - 3	0.1708	R_{G1}^{up}, R_{G2}^{up}, R_{G3}^{up}
2 - 4	0.0782	R_{G1}^{up}, R_{G3}^{up}, I_{5-6}^{max}, I_{2-1}^{max}
2 - 5	0.0862	R_{G1}^{up}, R_{G2}^{up}, I_{5-6}^{max}, I_{2-1}^{max}, I_{5-4}^{max}
2 - 6	0.1655	R_{G1}^{up}, R_{G2}^{up}, R_{G3}^{up}
3 - 5	0.0370	R_{G1}^{up}, R_{G3}^{down}, I_{5-6}^{max}, I_{5-4}^{max}
3 - 6	0.0460	R_{G1}^{up}, R_{G2}^{up}, I_{3-2}^{max}, I_{6-2}^{max}, I_{6-5}^{max}
4 - 5	0.1693	R_{G1}^{up}, R_{G2}^{up}, R_{G3}^{up}
5 - 6	0.1679	R_{G1}^{up}, R_{G2}^{up}, R_{G3}^{up}

Table 2.3: Voltage stability illustrative example. W&W 6-bus system: Stressed operating conditions for different security margins.

λ^{SM}	Contingencies Selected
0.03	Outage of line $1-5$
0.05	Outage of lines $1-5$, $3-5$ and $3-6$
0.10	Outage of lines $1-5$, $3-5$, $3-6$, $2-4$ and $2-5$

2.4.3 Solving the VSC-OPF Problem

For each of the three security margins considered, the VSC-OPF problem (2.20)-(2.79) is solved. The probability of occurrence of each selected contingency is set to 0.01. Figure 2.3 depicts the redispatching actions on the generator powers with respect to the base case for $\lambda^{SM} = 0.03$, 0.05, and 0.10, whereas Figure 2.4 depicts the redispatching actions on the demand powers

with respect to the base case for the same security margins.

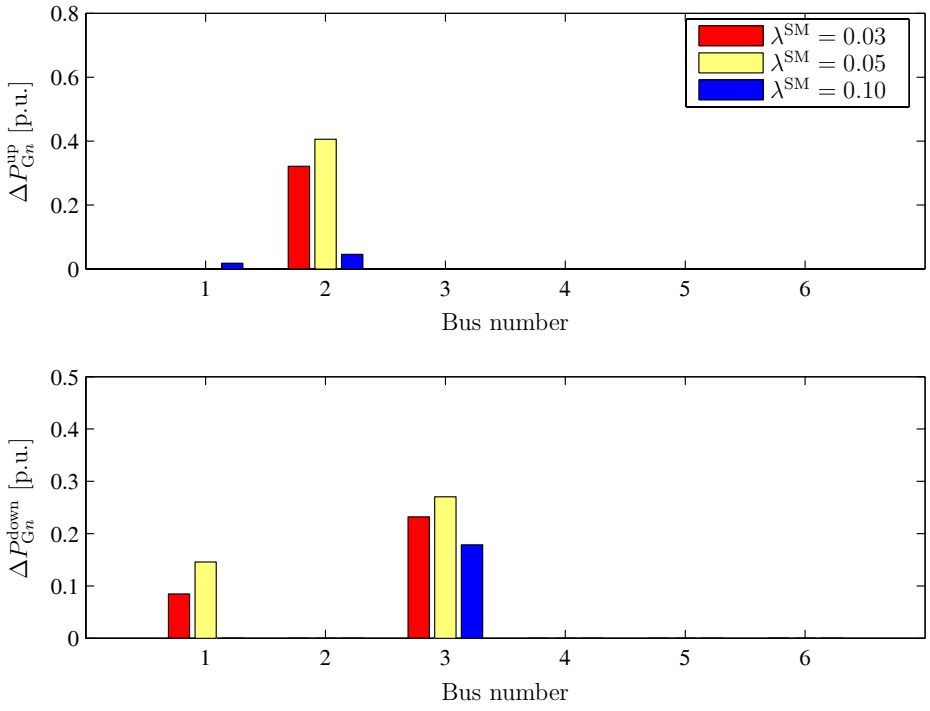

Figure 2.3: Voltage stability illustrative example. W&W 6-bus system: Redispatching actions on generator powers for $\lambda^{SM} = 0.03$, 0.05 and 0.10.

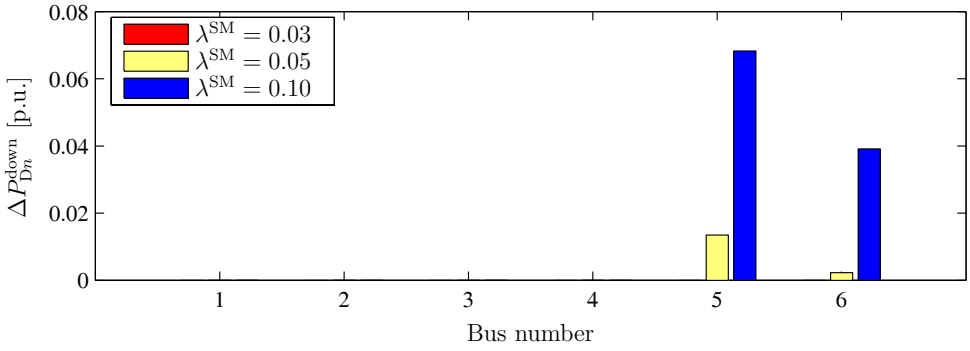

Figure 2.4: Voltage stability illustrative example. W&W 6-bus system: Redispatching actions on demand powers for $\lambda^{SM} = 0.03$, 0.05 and 0.10.

The security margin pertaining to $\lambda^{SM} = 0.03$ is achieved by redistributing

generation powers among generators, while no load power has to be shed. Due to ramping constraints, the generator of bus 2 must increase its power production in order to satisfy the single stressed operating condition. As a result, the remaining generators have to adjust their power production levels in order to supply the actual load. These are the most economical preventive control actions that satisfy the predefined security margin.

For $\lambda^{\mathrm{SM}} = 0.05$, a small amount of load has to be shed at buses 5 and 6 to satisfy the three stressed operating conditions. The generators adjust their power production levels within the range determined by their ramping constraints, to carry out the changes at minimum cost.

As expected, for $\lambda^{\mathrm{SM}} = 0.10$, the amount of power load that has to be shed is higher than in the case of $\lambda^{\mathrm{SM}} = 0.05$. With respect to generators, the power adjustments are smaller than in the previous cases as a result of the power demand reduction in the system. These are the optimal preventive control actions that ensure a system stability margin of $\lambda^{\mathrm{SM}} = 0.10$ if any of the five considered outages occurs.

2.4.4 Remarks on Penalty Factors

Penalties pertaining to generator voltage and control device adjustments are not associated with the actual cost that these adjustments involve. Actually, the cost of these adjustments can be considered negligible if compared with generation and demand power adjustments. The choice of penalty factor values is motivated by two reasons:

(i) The voltage profile and set points of control devices for the base case are considered the most suitable. From the market results, bus voltage magnitudes at generator buses and set points of control devices are calculated by solving an OPF problem that minimizes transmission losses (precisely, the cost of generating transmission losses, see Appendix A). Therefore, the base-case values for these variables are those that minimize power flows throughout the network. Bus voltages and control device settings can be also established based on other criteria. For example, by maximizing the remaining capacity of the system reactive power resources.

In any case, there is a justified interest to maintain the voltage profile and set points of control devices as close as possible to their values for the base case.

(ii) The nature of the objective function used in the proposed security control OPF problem. From the simulations performed during the work reported in this dissertation, it has been observed that if penalty factors are set to a value smaller than the generator offering costs (e.g., zero), the solution of the proposed OPF problem can be "inappropriate". For instance, solutions can be obtained that show load curtailment but no generation redispatching. This is because bus voltages are adjusted such that network losses compensate the load decrement (note that this is "cheaper" than generation redispatching). Certainly, if the load decrement is small, the adjustments in voltages could be also small, but cases are observed with a very degraded voltage profile (voltage magnitudes attaining their lower limit at several generator buses) for small load decrements, and this solution could be unsuitable from the system operation point of view. Note that if generator cost curves (operating costs) are used in the objective function, this problem does not appear because the cost of generating transmission losses is implicity considered.

A numerical example is provided in the following. For the simulations performed on the W&W 6-bus system, the offering costs of generators are $c_{\mathrm{G1}}^{\mathrm{up}} = c_{\mathrm{G1}}^{\mathrm{down}} = 12$ \$/p.u.h, $c_{\mathrm{G2}}^{\mathrm{up}} = c_{\mathrm{G2}}^{\mathrm{down}} = 10$ \$/p.u.h, and $c_{\mathrm{G3}}^{\mathrm{up}} = c_{\mathrm{G3}}^{\mathrm{down}} = 11.0$ \$/p.u.h, the costs of load curtailment are $c_{\mathrm{D}i}^{\mathrm{down}} = 1000$ \$/p.u.h for all demands, and penalty factors for voltage magnitude adjustments are $c_{\mathrm{V}n}^{\mathrm{up}} = c_{\mathrm{V}n}^{\mathrm{down}} = 100$ \$/p.u.h for all generator buses (the units of penalty factors are introduced only for compatibility with costs). Table 2.4 provides the results of applying the proposed procedure for $\lambda^{\mathrm{SM}} = 0.05$. In particular, this table shows the redispatching actions (yellow bars in Figures 2.3 and 2.4), and the resulting voltage profile for the adjusted operating condition. The total redispatching cost, i.e., $z_{\mathrm{G}}(\Delta P_{\mathrm{G}j}^{\mathrm{up}}, \Delta P_{\mathrm{G}j}^{\mathrm{down}}) + z_{\mathrm{D}}(\Delta P_{\mathrm{D}i}^{\mathrm{down}})$, is \$24.5336/h, and the network losses are 0.0801 p.u.

Table 2.4: Voltage stability illustrative example. W&W 6-bus system: Redispatching actions and voltage profile of the adjusted operating condition for $\lambda^{\mathrm{SM}} = 0.05$ using $c^{\mathrm{up}}_{\mathrm{V}n} = c^{\mathrm{down}}_{\mathrm{V}n} = 100$ \$/p.u.h.

Bus #	$\Delta P^{\mathrm{up}}_{\mathrm{G}n}$ [p.u.]	$\Delta P^{\mathrm{down}}_{\mathrm{G}n}$ [p.u.]	$\Delta P^{\mathrm{down}}_{\mathrm{D}n}$ [p.u.]	V_n [p.u.]
1	0	0.1457	0	1.1000
2	0.4059	0	0	1.1000
3	0	0.2705	0	1.1000
4	0	0	0	1.0458
5	0	0	0.0135	1.0246
6	0	0	0.0023	1.0470
Total	0.4059	0.4162	0.0158	-

Alternatively, the VSC-OPF problem is solved by using $c^{\mathrm{up}}_{\mathrm{V}n} = c^{\mathrm{down}}_{\mathrm{V}n} = 0$ \$/p.u.h. Table 2.5 provides the results. In this case, the total redispatching cost is \$24.0156/h, and the network losses are 0.1248 p.u.

Observe that, in both cases, the adjustments in system load and the amount of power that should be increased in generator 2 are equal. However, with penalty factors equal to zero, the amount of power that should be decreased in generators 1 and 3 is smaller than in the case of $c^{\mathrm{up}}_{\mathrm{V}n} = c^{\mathrm{down}}_{\mathrm{V}n} = 100$. This is possible because the solution obtained with penalty factors equal to zero corresponds to a system operating condition with low bus voltage levels and, therefore, with higher network losses. As a result, the security margin is achieved for a smaller redispatching cost but with a degraded operating condition.

In this thesis, to maintain a "good" voltage profile is preferred. Therefore, for all simulations performed throughout the dissertation, the penalties of voltage magnitude adjustments ($c^{\mathrm{up}}_{\mathrm{V}n}$,$c^{\mathrm{down}}_{\mathrm{V}n}$) and the penalties of set point adjustments of control devices ($c^{\mathrm{up}}_{\mathrm{LTC},n}$, $c^{\mathrm{down}}_{\mathrm{LTC},n}$, $c^{\mathrm{up}}_{\mathrm{PHS},k}$, $c^{\mathrm{down}}_{\mathrm{PHS},k}$, $c^{\mathrm{up}}_{\mathrm{SVC},n}$, $c^{\mathrm{down}}_{\mathrm{SVC},n}$, $c^{\mathrm{up}}_{\mathrm{TCSC},k}$, $c^{\mathrm{down}}_{\mathrm{TCSC},k}$) are set higher than the costs of generation power adjustments ($c^{\mathrm{up}}_{\mathrm{G}j}$, $c^{\mathrm{down}}_{\mathrm{G}j}$) but lower than the costs of demand decrements ($c^{\mathrm{down}}_{\mathrm{D}i}$), to avoid

Table 2.5: Voltage stability illustrative example. W&W 6-bus system: Redispatching actions and voltage profile of the adjusted operating condition for $\lambda^{\mathrm{SM}} = 0.05$ using $c_{\mathrm{V}n}^{\mathrm{up}} = c_{\mathrm{V}n}^{\mathrm{down}} = 0$ \$/p.u.h.

Bus #	$\Delta P_{\mathrm{G}n}^{\mathrm{up}}$ [p.u.]	$\Delta P_{\mathrm{G}n}^{\mathrm{down}}$ [p.u.]	$\Delta P_{\mathrm{D}n}^{\mathrm{down}}$ [p.u.]	V_n [p.u.]
1	0	0.1199	0	1.0392
2	0.4059	0	0	1.0069
3	0	0.2516	0	0.9357
4	0	0	0	0.9521
5	0	0	0.0135	0.9000
6	0	0	0.0023	0.9017
Total	0.4059	0.3715	0.0158	-

load curtailment unless it is strictly necessary to maintain system security.

2.5 Voltage Stability - Case Study

In this section, the proposed security redispatching procedure is applied to a 24-bus system (IEEE 24-bus system) based on the IEEE Reliability Test System [100]. The one-line diagram of this system is provided in Appendix D. The main purpose of the simulations is to show the effect of regulating transformers and FACTS devices on the security level of the system and the redispatching cost. The positions of these control devices have been selected based on knowledge of the network and seeking to improve the system loadability and security. FACTS device siting is outside the scope of this thesis, but the interested reader can consult [91], which suggests an efficient algorithm for FACTS device network allocation. Generator data, demand data, network data, regulating transformer data, FACTS data and technical limits are provided in Appendix D. To account for the impact of regulating transformers and FACTS devices on the redispatching procedure, the thermal limit of line

11-13 is set to 1.75 p.u. out of 5.0 p.u. Furthermore, the simulations only consider the outage of the transformer between buses 3 and 24. The probability of occurrence of this contingency is set to 0.01, and the time interval considered is $\Delta t = 5$ minutes.

In the simulations below, each regulating transformer and each FACTS device is studied separately to better illustrate its effect on the redispatching procedure. Simulation results are depicted in Figure 2.5. The curves in that figure represent the cost of the preventive control actions, i.e., $z_{\mathrm{G}}(\Delta P_{\mathrm{G}j}^{\mathrm{up}}, \Delta P_{\mathrm{G}j}^{\mathrm{down}}) + z_{\mathrm{D}}(\Delta P_{\mathrm{D}i}^{\mathrm{down}})$, as a function of the security margin λ^{SM}.

As expected, the case with no control device leads to the most expensive solutions as the value of λ^{SM} increases. For $0.04 \leq \lambda^{\mathrm{SM}} \leq 0.10$, the binding constraints are mainly voltage limits (in particular, at bus 3). For these values of the security margin, the most effective control devices are the LTC transformer and the SVC device, which is reasonable because these devices control voltage levels. On the other hand, for $0.04 \leq \lambda^{\mathrm{SM}} \leq 0.10$, the effects of the PHS transformer and the TCSC device are negligible since modifying power flows does not alleviate voltage problems.

For $\lambda^{\mathrm{SM}} > 0.10$, the binding constraints are the limits on transmission lines (in particular, on line 11-13) together with voltage limits (in particular, at bus 3). An increasing amount of load has to be shed for these security margin values and hence, the change in the slope of the redispatching cost. The most effective control devices are the PHS transformer and the TCSC device, since these devices best control power flows. For $\lambda^{\mathrm{SM}} > 0.10$ the effects of the LTC transformer and the SVC device are negligible because the operation of these devices does not alleviate the line congestions.

For illustration, two snapshots of the solutions shown in Figure 2.5 (dotted vertical lines) are further discussed: for $\lambda^{\mathrm{SM}} = 0.08$ and for $\lambda^{\mathrm{SM}} = 0.14$. Furthermore, an example that combines two control devices is also considered.

2.5.1 Solution for $\lambda^{\mathrm{SM}} = 0.08$

Figure 2.6 depicts the generation power adjustments at each bus for $\lambda^{\mathrm{SM}} = 0.08$. Power adjustments are in p.u. with respect to the base-case level. The

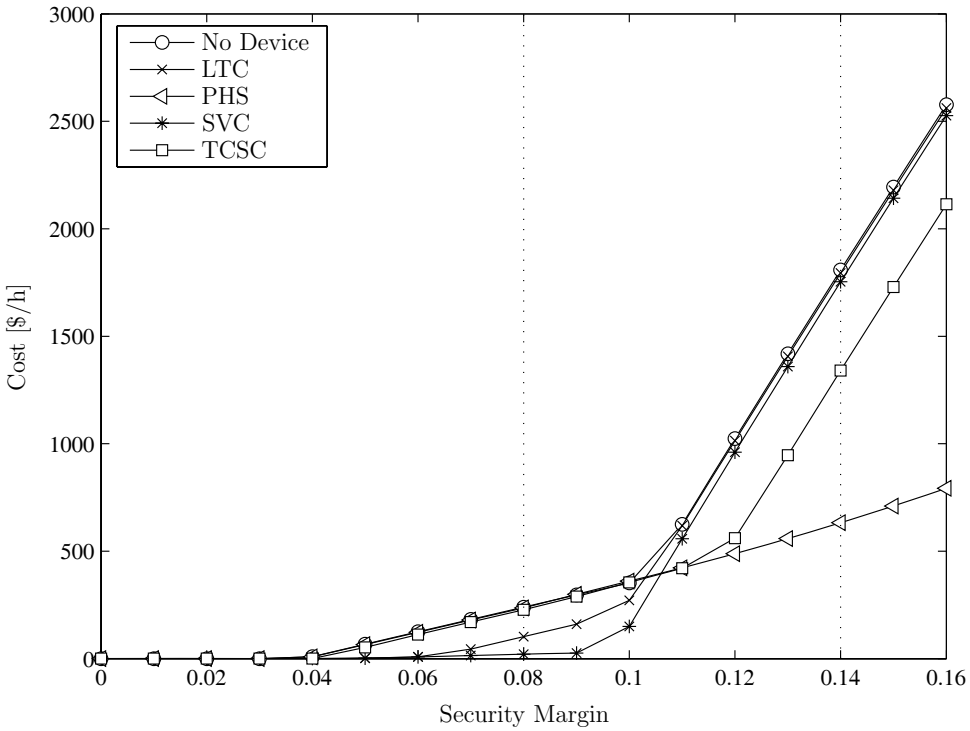

Figure 2.5: Voltage stability case study. IEEE 24-bus system: Costs of preventive control actions as a function of the security margin λ^{SM}. Effects of LTC transformer, PHS transformer, SVC device and TCSC device.

bar chart shows the solution obtained without control devices and with the LTC transformer and SVC device. Solutions with the PHS transformer and TCSC device are not depicted because these devices have a minor effect on the system for this security margin.

Figure 2.7 depicts the demand power adjustments with respect to the base case. The load to be shed is located at bus 3, whereas the power production is transferred from bus 22 to bus 13.

Table 2.6 lists the effects of regulating transformers and FACTS devices on the total generation adjustment, the total demand adjustment and the total cost of preventive control actions for the 24-bus system and $\lambda^{\mathrm{SM}} = 0.08$. Only the LTC transformer and SVC device are able to significantly reduce the cost and amount of power adjustments. However, with the SVC device, there is no need for load shedding; thus, in this case, the SVC device is more effective

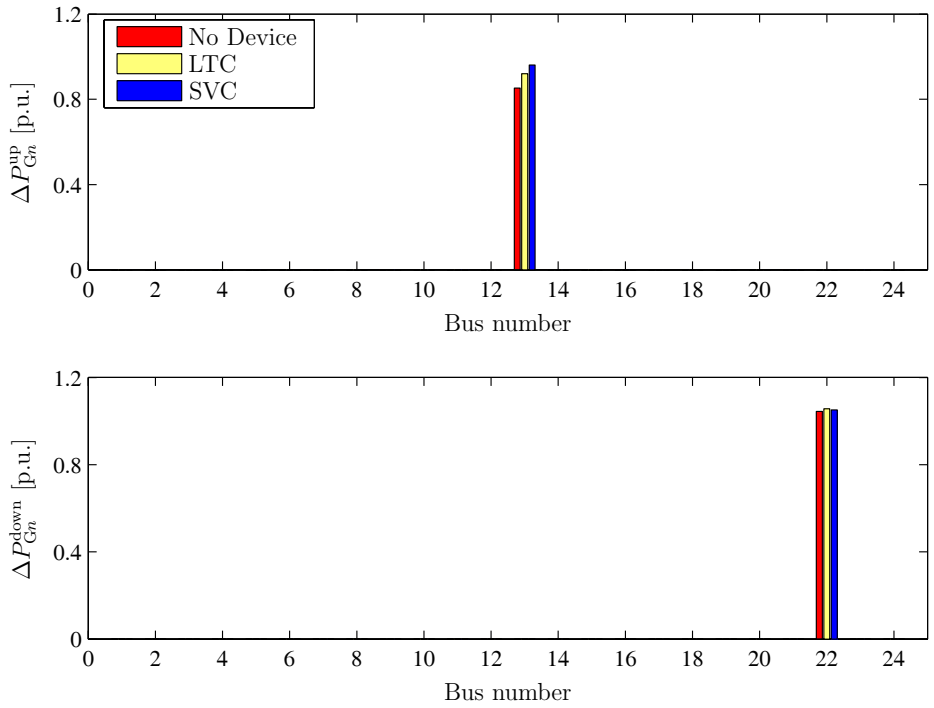

Figure 2.6: Voltage stability case study. IEEE 24-bus system: Generation power adjustments for $\lambda^{SM} = 0.08$. Effects of the LTC transformer and SVC device.

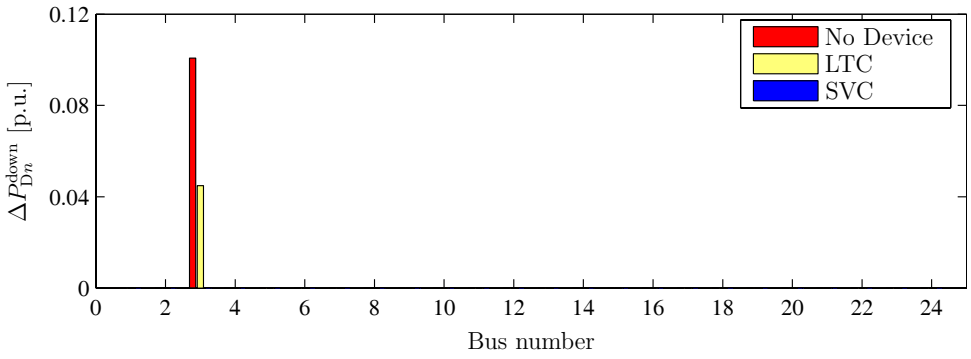

Figure 2.7: Voltage stability case study. IEEE 24-bus system: Load power adjustments for $\lambda^{SM} = 0.08$. Effects of the LTC transformer and SVC device.

than the LTC transformer. This result is mainly due to the position of the SVC device in the network.

Table 2.6: Voltage stability case study. IEEE 24-bus system: Total generation power adjustment, total demand power adjustment and total cost for $\lambda^{\mathrm{SM}} = 0.08$.

Device	$\sum_{j\in\mathcal{G}} \Delta P_{\mathrm{G}j}^{\mathrm{up}}$ [p.u.]	$\sum_{j\in\mathcal{G}} \Delta P_{\mathrm{G}j}^{\mathrm{down}}$ [p.u.]	$\sum_{i\in\mathcal{D}} \Delta P_{\mathrm{D}i}^{\mathrm{down}}$ [p.u.]	Total Cost [$/h]
No device	0.8529	1.0445	0.1008	239.77
LTC	0.9200	1.0566	0.0448	118.12
PHS	0.8561	1.0446	0.0990	236.22
SVC	0.9610	1.0510	0	20.28
TCSC	0.8630	1.0267	0.0932	227.32

2.5.2 Solution for $\lambda^{\mathrm{SM}} = 0.14$

Figure 2.8 illustrates the generation power adjustments at each bus for $\lambda^{\mathrm{SM}} = 0.14$. Once again, power adjustments are in p.u. with respect to the base-case level. The bar chart shows the solution obtained with no control device and with the PHS transformer and TCSC device. Solutions with the LTC transformer and SVC device are not depicted because these devices have a small effect on the system for this security margin. In this case, several generators are involved in the redispatching process.

Figure 2.9 depicts the demand power adjustments with respect to the base case. Due to the high loading level, the number of loads affected by shedding and the total amount of load shed are significantly higher than those in the case of $\lambda^{\mathrm{SM}} = 0.08$.

Table 2.7 provides the effects of regulating transformers and FACTS devices on the total generation adjustment, the total demand adjustment and the total cost of preventive control actions for the 24-bus system and $\lambda^{\mathrm{SM}} = 0.14$. Only the PHS transformer and TCSC device are capable of significantly reducing the cost and the amount of power adjustments. However, the PHS transformer leads to less expensive results than the TCSC device. This is basically due to the fact that the TCSC device reaches its capacity limits.

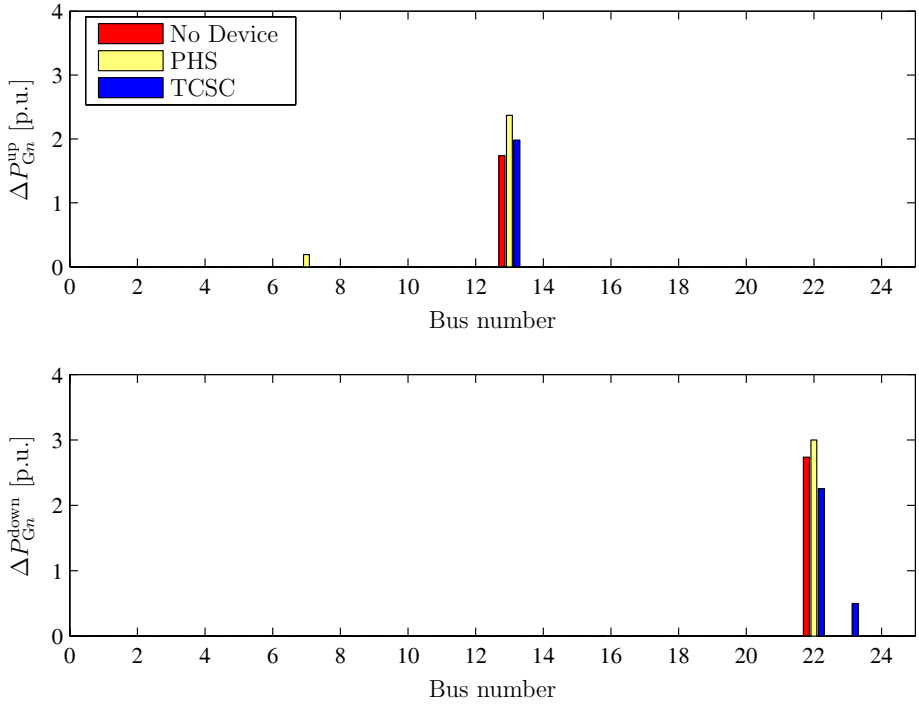

Figure 2.8: Voltage stability case study. IEEE 24-bus system: Generation power adjustments for $\lambda^{SM} = 0.14$. Effects of the PHS transformer and TCSC device.

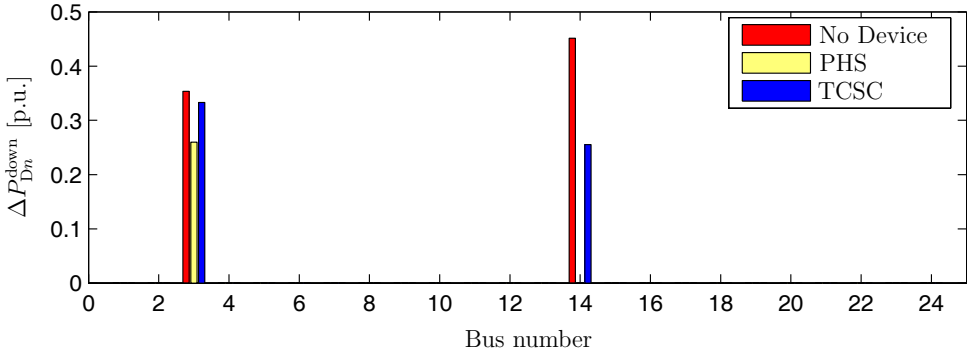

Figure 2.9: Voltage stability case study. IEEE 24-bus system: Load power adjustments for $\lambda^{SM} = 0.14$. Effects of the PHS transformer and TCSC device.

2.5.3 Effect of the FACTS Size

The capacity limits of FACTS devices define their size. Table 2.8 shows the total cost incurred using different capacity limits of SVC and TCSC devices.

Table 2.7: Voltage stability case study. IEEE 24-bus system: Total generation power adjustment, total demand power adjustment and total cost for $\lambda^{\mathrm{SM}} = 0.14$.

Device	$\sum_{j\in\mathcal{G}} \Delta P_{\mathrm{G}j}^{\mathrm{up}}$ [p.u.]	$\sum_{j\in\mathcal{G}} \Delta P_{\mathrm{G}j}^{\mathrm{down}}$ [p.u.]	$\sum_{i\in\mathcal{D}} \Delta P_{\mathrm{D}i}^{\mathrm{down}}$ [p.u.]	Total Cost [$/h]
No device	1.7413	2.7362	0.8050	1808.53
LTC	1.7509	2.7399	0.7989	1795.44
PHS	2.5601	3.0000	0.2598	625.58
SVC	1.7806	2.7464	0.7795	1753.37
TCSC	1.9836	2.7556	0.5881	1340.34

The first column indicates the factor used to reduce or increase FACTS limits. The results show that, for the considered case and with the given FACTS device positions, the size of the SVC device can be reduced by one-half without significantly affecting the total cost of redispatching actions. The results also show that an increase in the size of the TCSC device considerably reduces the total costs for $\lambda^{\mathrm{SM}} = 0.14$. In general, the proposed procedure can also be used to determine the effect of the size of FACTS devices on the security redispatch.

2.5.4 Effect of Regulating Transformer Ramping Constraints

Ramping constraints that regulate the functioning of LTC and PHS transformers affect the bus voltage levels and generator reactive power productions, as well as the transformer control variables, i.e., the tap ratio T and phase shifting angle ϕ. Table 2.9 shows the values of T and ϕ at the adjusted operating condition and the stressed operating condition for the two considered security margins, $\lambda^{\mathrm{SM}} = 0.08$ and $\lambda^{\mathrm{SM}} = 0.14$, respectively. The table also shows the values of transformer control variables without ramping constraints.

Table 2.8: Voltage stability case study. IEEE 24-bus system: Total cost with different control limits of FACTS devices.

	$\lambda^{\text{SM}} = 0.08$		$\lambda^{\text{SM}} = 0.14$	
Factor	SVC [$/h]	TCSC [$/h]	SVC [$/h]	TCSC [$/h]
0.1	101.63	242.24	1800.98	1765.43
0.5	20.41	235.91	1778.32	1576.75
1	20.28	227.32	1753.37	1340.34
2	20.22	220.27	1715.60	864.51
10	20.21	216.29	1704.72	608.89

The LTC transformer is not affected by ramps in either case. Considering the PHS transformer, the value of ϕ is conditioned by the value of ϕ^s due to ramping constraints for $\lambda^{\text{SM}} = 0.14$. Observe that if ramping constraints were not considered in the problem, the PHS transformer would not be able to reach the stressed operating condition within the considered time period. In the case without ramping constraints, the value for ϕ is -0.0022. Taking into account the capacity of the PHS transformer to adjust its tap facility ($\pi/600$ rad/min) and the considered time period ($\Delta t = 5$ min.), the value of the phase-shifter tap could only reach -0.0284, which is a value far from -0.1403. Consequently, the security margin would not be guaranteed as the system would be unable to reach the stressed operating condition within the considered time period.

2.5.5 Effect of Combining Multiple Control Devices

The effects of the LTC transformer and SVC device (voltage controlling devices) are basically decoupled from the effects of the PHS transformer and TCSC device (power flow controlling devices). This fact suggests that the combined use of one voltage controlling device and one power flow controlling device can lead to comparatively cheaper solutions than other combinations

Table 2.9: Voltage stability case study. IEEE 24-bus system: Effects of ramping constraints on LTC and PHS variables.

		$\lambda^{\mathrm{SM}} = 0.08$		$\lambda^{\mathrm{SM}} = 0.14$	
Device	Variable	No ramps	With ramps	No ramps	With ramps
LTC	T	1.0499	1.0499	1.0470	1.0470
	T^s	1.0500	1.0500	1.0500	1.0500
PHS	ϕ	0.0930	0.0930	−0.0022	−0.1141
	ϕ^s	0.0500	0.0668	−0.1403	−0.1403

across the entire range of load levels. This is confirmed by Figure 2.10. Note that combining a PHS transformer and a SVC device leads to an overall lower cost than the linear combination of each device, especially for $\lambda^{\mathrm{SM}} > 0.10$. For example, for $\lambda^{\mathrm{SM}} = 0.14$, the cost of power adjustments in the case with no devices is \$1808.5/h; in the case with the PHS transformer this cost is \$625.6/h; in the case with the SVC device this cost is \$1753.4/h; and in the case with the PHS transformer and SVC device, this cost is \$59.7/h. Therefore, operation with only the PHS transformer saves \$1182.9/h and the operation with only the SVC device saves \$55.2/h. The joint operation of the PHS transformer and SVC device saves \$1748.8/h which is noticeably higher than the sum of the savings obtained through the separate operation of these devices.

From the analysis, it is apparent that the redispatching cost resulting from the proposed procedure can be reduced if adequate regulating transformers and FACTS devices are installed in the system. This is not a surprising result; however, the proposed procedure provides a quantitative analysis of the effect of control devices on security redispatching pertaining to voltage stability.

2.5.6 Simulation Times

Table 2.10 provides the CPU times for each simulation carried out in this case study involving different control devices (rows). This table shows the CPU time to obtain the base-case solution, i.e., to solve the OPF problem described

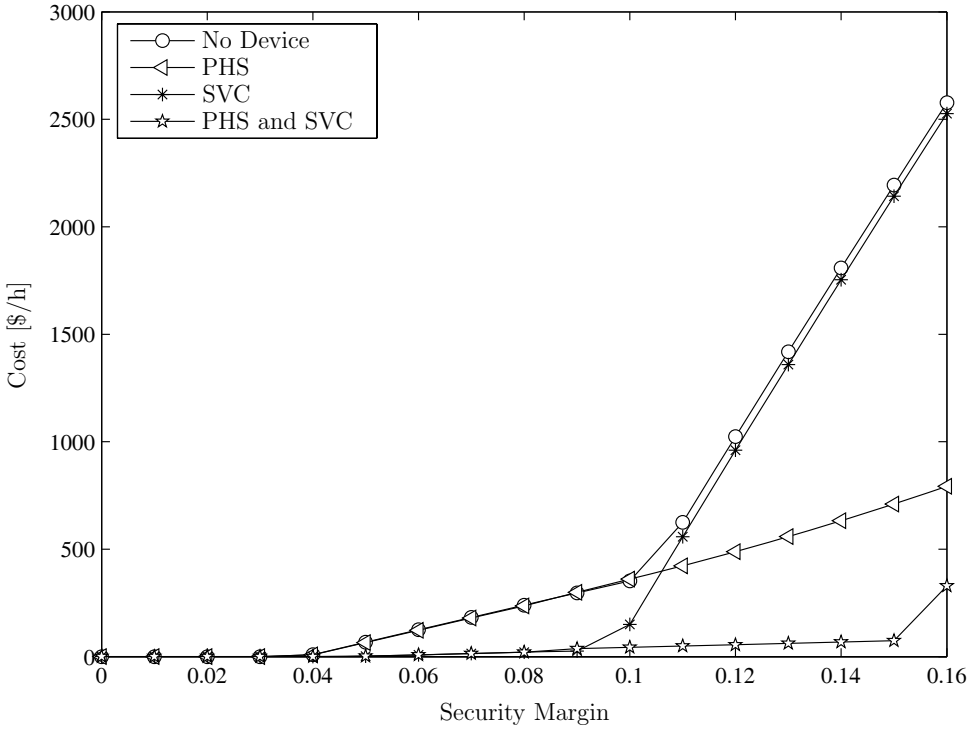

Figure 2.10: Voltage stability case study. IEEE 24-bus system: Cost of preventive control actions as a function of the security margin λ^{SM}. Simultaneous effects of the PHS transformer and SVC device.

in Appendix A for each case (second column). Table 2.10 also shows the CPU time to solve the VSC-OPF problem described in Subsection 2.3.1.6 (third column). For each case considered, this problem is solved for different values of λ^{SM}. The values provided in the third column of Table 2.10 correspond to the average CPU times required to solve the VSC-OPF problem.

2.6 Summary and Conclusions

This chapter has presented a security redispatching procedure that resolves security issues pertaining to voltage stability. It is intended to help system operators ensure an appropriate level of security. Once a base-case solution is available, contingency analysis is performed based on the concept of loading margin. For each pre-specified set of contingencies, the loading margin of the

Table 2.10: Voltage stability case study. IEEE 24-bus system: Simulation times.

Device	Base Case CPU [s]	VSC-OPF CPU [s]
No device	0.02	1.96
LTC	0.03	1.86
PHS	0.04	1.08
SVC	0.04	1.82
TCSC	0.04	1.29
PHS and SVC	0.05	1.01

system is computed and the critical contingencies are identified in terms of the desired security level. Next, the procedure uses an OPF that includes voltage stability constraints.

This OPF problem explicitly considers security limits through stressed operating conditions. The stressed operating conditions are defined by both a contingency and a pre-defined loading condition higher than that of the base case. Moreover, the proposed OPF problem may include four types of control devices: LTC transformer, PHS transformer, SVC device and TCSC device. The time delays for LTC and PHS transformers to adjust their set points are modeled as ramping limits on the tap ratios and phase angles, respectively.

A 6-bus system is used to illustrate the performance of the proposed redispatching procedure, whereas the effect of regulating transformers and FACTS devices on the proposed redispatching procedure is analyzed and discussed in detail using a 24-bus system.

Simulations results show the ability of the proposed procedure to provide a number of preventive redispatching actions for the base-case solution that achieve the desired security level with respect to voltage instability issues. This is attained at minimum cost, using the available control devices in the network.

Simulations also show that system security can be improved if appropriate control devices are installed in the system. This is confirmed by the reduction in the redispatching cost that results from the proposed procedure. Cost savings may be a key factor when deciding which device to install.

The proposed procedure is able to tackle multi-contingency cases. Thus, the VSC-OPF problem can incorporate constraints for the whole set of contingencies that correspond to the $N-1$ security criterion. However, the size of the resulting OPF problem is quite large for real-world systems, and its solution may require prohibitive computational times. Prior contingency filtering reduces the size of the VSC-OPF problem, thus incorporating only contingencies that threaten system security. Therefore, contingency filtering makes the proposed procedure appropriate from a practical point of view.

Finally, the proposed procedure solves a non-linear non-convex OPF problem. Therefore, obtaining a global optimum cannot be guaranteed. However, the non-linear programming solver can be started from different initial points in order to avoid local minima. Multi-minima have not been observed in the simulations carried out in this chapter.

Chapter 3

Optimal Power Flow with Small-Signal Stability Constraints

This chapter extends the security redispatching procedure described in Chapter 2 to take into account small-signal stability issues. The resulting security redispatching procedure achieves an appropriate system security level in terms of both voltage stability and small-signal stability. The procedure is based on an Optimal Power Flow (OPF) problem that includes both voltage stability and small-signal stability constraints. This OPF problem explicitly considers security limits through stressed loading conditions. The solution of the proposed redispatching procedure corresponds to the optimal preventive control actions required to ensure the desired security level.

The chapter begins with a brief overview of small-signal stability. In Section 3.2 the contingency filtering procedure used to select the contingencies that compromise a given security level is presented. In Section 3.3, the OPF problem is formulated and the steps of the redispatching procedure are described. In Sections 3.4 and 3.5, the performance of the proposed procedure is tested on the WECC 9-bus, 3-machine system, the New England 39-bus, 10-machine system, and the IEEE 145-bus, 50-machine system. The results are analyzed and discussed. Finally, Section 3.6 offers the main conclusions of

this chapter.

3.1 Small-Signal Stability

Small-signal stability is a general concept that can involve both voltage and rotor-angle stability. This thesis focuses on small-signal rotor-angle stability (for simplicity, hereinafter, small-signal stability). Small-signal stability is concerned with the ability of a power system to maintain synchronism under small disturbances. The disturbances are considered to be sufficiently small that the power system equations can be linearized for analysis [102].

Small-signal instability depends on the operating condition of the system and mostly appears in the form of rotor angle oscillations whose amplitude increases due to insufficient damping torque.

Small-signal instability appears in the form of local mode oscillations and/or in the form of inter-area mode oscillations. Local mode oscillations are typically rotor angle oscillations of a single generator swinging against the rest of the generators of the system. The damping of these oscillations depends on the strength of the transmission system seen by the generator, the generator excitation control system and the generator power output. Inter-area mode oscillations are related to a group of generators in one area swinging against a group of generators in another area. The characteristics of these oscillations are complex and differ significantly from those of local mode oscillations, [73], [109].

3.1.1 System Model

In small-signal stability studies the power system is represented by the following set of differential-algebraic equations (DAE):

$$\begin{bmatrix} \dot{\boldsymbol{x}} \\ \mathbf{0} \end{bmatrix} = \begin{bmatrix} \boldsymbol{f}(\boldsymbol{x}, \boldsymbol{y}, \boldsymbol{p}) \\ \boldsymbol{g}(\boldsymbol{x}, \boldsymbol{y}, \boldsymbol{p}) \end{bmatrix} \tag{3.1}$$

where vector $\boldsymbol{x}$ ($\boldsymbol{x} \in \mathbb{R}^{n_x}$) contains the state variables (e.g., δ, ω), vector $\boldsymbol{y}$ ($\boldsymbol{y} \in \mathbb{R}^{n_y}$) includes algebraic variables (e.g., V, θ, Q_G) and $\boldsymbol{p}$ ($\boldsymbol{p} \in \mathbb{R}^{n_p}$) is

the vector of control variables (e.g., P_G, P_D, Q_D). Function $\boldsymbol{f}$ ($\boldsymbol{f} : \mathbb{R}^{n_x} \times \mathbb{R}^{n_y} \times \mathbb{R}^{n_p} \longmapsto \mathbb{R}^{n_x}$) is a nonlinear vector function associated with the state variables $\boldsymbol{x}$ that usually represents the system differential equations, such as those associated with the synchronous machine dynamics, control devices, etc.; and vector function $\boldsymbol{g}$ ($\boldsymbol{g} : \mathbb{R}^{n_x} \times \mathbb{R}^{n_y} \times \mathbb{R}^{n_p} \longmapsto \mathbb{R}^{n_y}$) represents a system of algebraic equations, including the power flow equations, algebraic equations associated with the synchronous machine model, etc.

3.1.2 Small-Signal Stability Assessment

The small-signal stability of a power system depends on its operating condition. Assuming that the system is at steady-state, the power system operating condition is an equilibrium point with all the derivatives $\dot{\boldsymbol{x}}$ in (3.1) equal to zero. Then, once the control variables are known ($\boldsymbol{p} = \boldsymbol{p}_o$), the values of the remaining variables that define a system equilibrium point $(\boldsymbol{x}_o, \boldsymbol{y}_o)$ are obtained by solving the following set of equations:

$$\begin{bmatrix} \mathbf{0} \\ \mathbf{0} \end{bmatrix} = \begin{bmatrix} \boldsymbol{f}(\boldsymbol{x}_o, \boldsymbol{y}_o, \boldsymbol{p}_o) \\ \boldsymbol{g}(\boldsymbol{x}_o, \boldsymbol{y}_o, \boldsymbol{p}_o) \end{bmatrix} \tag{3.2}$$

The small-signal stability assessment is based on linearized analysis of the multi-machine power system. This analysis establishes that the stability of a system equilibrium point under small disturbances can be studied by linearizing the equations of the non-linear system around the system equilibrium point. Then, the system stability can be determined according to the roots of the characteristic equation of the linearized system. Small-signal stability assessment is also referred to as modal analysis [73, 114].

3.1.2.1 Linearization

Linearization is carried out by approximating the DAE system (3.1) by the first term of the Taylor series expansion at the system equilibrium point $(\boldsymbol{x}_o, \boldsymbol{y}_o)$.

Therefore, the linearization of (3.1) leads to the following expression:

$$\begin{bmatrix} \Delta\dot{\boldsymbol{x}} \\ \mathbf{0} \end{bmatrix} = \begin{bmatrix} \boldsymbol{D_x f} & \boldsymbol{D_y f} \\ \boldsymbol{D_x g} & \boldsymbol{D_y g} \end{bmatrix} \begin{bmatrix} \Delta\boldsymbol{x} \\ \Delta\boldsymbol{y} \end{bmatrix} \tag{3.3}$$

where $\boldsymbol{D_x f}$, $\boldsymbol{D_x g}$, $\boldsymbol{D_y f}$ and $\boldsymbol{D_y g}$ are, respectively, the Jacobian matrices of the vector functions $\boldsymbol{f}$ and $\boldsymbol{g}$ with respect to the variables $\boldsymbol{x}$ and $\boldsymbol{y}$ computed at $(\boldsymbol{x}_o, \boldsymbol{y}_o)$; and $\Delta\boldsymbol{x}$, $\Delta\boldsymbol{y}$ are small increments with respect to the equilibrium point, that is, $\Delta\boldsymbol{x} = \boldsymbol{x} - \boldsymbol{x}_o$ and $\Delta\boldsymbol{y} = \boldsymbol{y} - \boldsymbol{y}_o$.

Assuming that the Jacobian matrix $\boldsymbol{D_y g}$ is non-singular, the algebraic variables can be eliminated from (3.3) to obtain the system equation

$$\Delta\dot{\boldsymbol{x}} = \boldsymbol{A}_{\text{sys}}\, \Delta\boldsymbol{x}, \tag{3.4}$$

where $\boldsymbol{A}_{\text{sys}}$ is the system state matrix and it is computed as

$$\boldsymbol{A}_{\text{sys}} = \boldsymbol{D_x f} - \boldsymbol{D_y f}\, [\boldsymbol{D_y g}]^{-1}\, \boldsymbol{D_x g}. \tag{3.5}$$

If the Jacobian matrix $\boldsymbol{D_y g}$ is singular, a singularity induced bifurcation is said to occur. In such a case, the DAE system (3.1) should be redefined, [118]. However, since singularity induced bifurcations result from modeling issues rather than stability issues, this singularity case is not considered in this thesis.

3.1.2.2 Stability criterion

Small-signal stability can be assessed based on the eigenvalues of the system state matrix $\boldsymbol{A}_{\text{sys}}$. Lyapunov's first method, [82], establishes the following:

1. If all eigenvalues of matrix $\boldsymbol{A}_{\text{sys}}$ have negative real parts, the system equilibrium point is asymptotically stable.

2. If at least one of the eigenvalues of matrix $\boldsymbol{A}_{\text{sys}}$ has a positive real part, the system equilibrium point is unstable.

In the case of eigenvalues having real parts equal to zero, it is not possible to establish anything in general.

3.1.2.3 Bifurcation Analysis

As stated in Chapter 2, bifurcation theory assumes that the system equations depend on a set of parameters as well as on variables. Thus, stability/instability properties can be assessed by varying these parameters. Typically, the parameter used in bifurcation analysis is the system load. Bifurcation theory makes use of a quasi-static approximation, which means that the system load changes "slowly", and it can be assumed to "move" smoothly from one equilibrium point to another as a result of the load changes. Under these assumptions, modal analysis of the system equilibrium points can be performed to monitor the evolution of the eigenvalues of the system state matrix in the complex plane as the system load changes slowly.

Bifurcation theory identifies small-signal instability conditions through Hopf Bifurcations (HB). These bifurcations are characterized by a system state matrix eigenvalue, typically a pair of complex conjugated eigenvalues, whose real part becomes positive as the system load increases slowly. In other words, one pair of complex eigenvalues "moves" from the left hand side to the right hand side of the complex plane. The point where the pair of complex conjugate eigenvalues reaches (and crosses) the imaginary axis is known as the HB point [118]. Thus, the imaginary axis of the complex plane constitutes the small-signal stability frontier. Figure 3.1 illustrates a Hopf bifurcation.

3.2 Security Assessment: Contingency Filtering

In this section, the contingency filtering procedure described in Section 2.2 of Chapter 2 is enhanced to identify the harmful contingencies related to both small-signal and voltage instability. The initial set of contingencies includes all contingencies of the $N-1$ security criterion, that is, the outage of any system element. For a given security margin λ^{SM}, the proposed contingency screening procedure works as follows:

1. For each one of the initial set of contingencies, the maximum loading

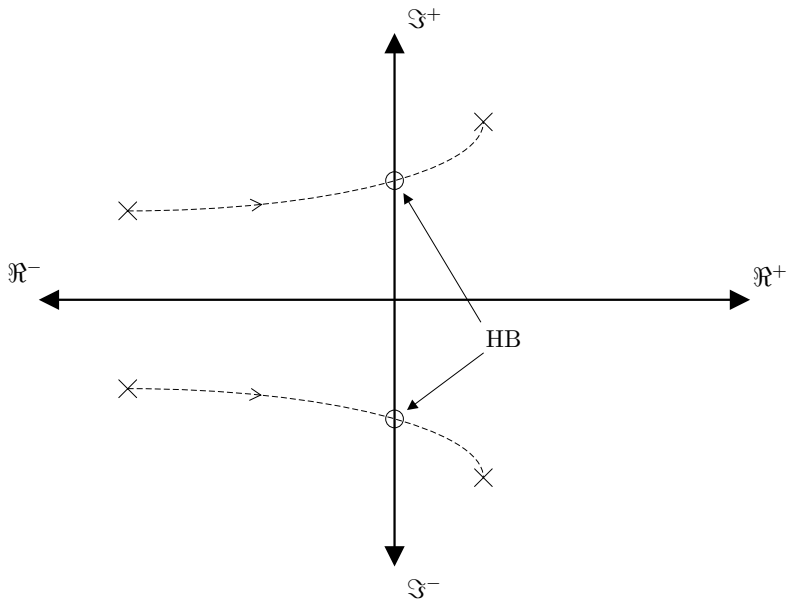

Figure 3.1: Hopf bifurcation in the complex plane.

condition and the loading margin λ^* of the system are computed using the problem described in Appendix B.

2. At the maximum loading condition, modal analysis is carried out and the eigenvalue with the largest real part α is computed.

3. If $\lambda^* \leq \lambda^{\text{SM}}$, the contingency is selected. At the loading condition defined by λ^{SM} the system exhibits potential voltage instability.

4. If $\alpha > 0$, the contingency is selected. This situation implies that a Hopf bifurcation has occurred. Thus, at the loading condition defined by λ^{SM}, the system may suffer from small-signal instability.

5. If $\lambda^* > \lambda^{\text{SM}}$ and $\alpha < 0$, the contingency is filtered out.

Note that the computation of λ^* for one contingency and the modal analysis at the corresponding maximum loading condition is independent of other contingencies. This fact can be exploited to reduce computing time by using parallel computation.

3.3 Security Redispatching

Once a working condition has been established through a dispatching procedure (e.g., a market clearing algorithm), but prior to actual power delivery, the independent system operator (ISO) must check system security and implement redispatching actions on the dispatching solution if needed.

This section suggests a redispatching procedure based on a Small-Signal Stability Constrained Optimal Power Flow (SSSC-OPF) problem to assist the system operator to ensure an appropriate security level. The starting point of the procedure is a base-case operating condition established through a dispatching solution adjusted by losses (see Appendix A).

The SSSC-OPF considers several operating conditions: the adjusted operating condition and a set of stressed operating conditions. The adjusted operating condition results from adjusting the base-case operating condition. Each of the stressed operating conditions is associated with a single contingency and a fictitious loading condition that allows setting a distance to instability in terms of load. The solution of the proposed procedure provides the preventive control actions on the base-case solution that are needed to guarantee a pre-specified security level. It is assumed that the system operator has access to the technical information of generators and that the generators provide the ISO with cost offers for redispatching.

3.3.1 SSSC-OPF Problem Description

This subsection describes the objective function and all constraints used in the SSSC-OPF problem in detail. Much of the formulation of this problem is similar to that of the VSC-OPF problem described in subsection 2.3.1 of Chapter 2. However, these equations are described again here for completeness.

3.3.1.1 Objective function

The objective function is aimed at minimizing the variations with respect to the base-case solution. In particular, the objective function is composed of several terms that represent adjustment costs and penalty functions. The

adjustment costs correspond to changes in the generation and load powers, while the penalty functions concern voltage magnitudes at generator buses. Thus, for the adjusted operating condition, the total cost function of generation power adjustments is

$$z_{\mathrm{G}}(\Delta P_{\mathrm{G}j}^{\mathrm{up}}, \Delta P_{\mathrm{G}j}^{\mathrm{down}}) = \sum_{j \in \mathcal{G}} c_{\mathrm{G}j}^{\mathrm{up}} \Delta P_{\mathrm{G}j}^{\mathrm{up}} + c_{\mathrm{G}j}^{\mathrm{down}} \Delta P_{\mathrm{G}j}^{\mathrm{down}}, \tag{3.6}$$

where $c_{\mathrm{G}j}^{\mathrm{up}}$ and $c_{\mathrm{G}j}^{\mathrm{down}}$ are, respectively, the offering costs of generator j to increase and decrease its power dispatch for security purposes. The total penalty function of voltage magnitude adjustments at generator buses is

$$z_{\mathrm{V}}(\Delta V_{n}^{\mathrm{up}}, \Delta V_{n}^{\mathrm{down}}) = \sum_{n \in \mathcal{N}_{\mathrm{G}}} c_{\mathrm{V}n}^{\mathrm{up}} \Delta V_{n}^{\mathrm{up}} + c_{\mathrm{V}n}^{\mathrm{down}} \Delta V_{n}^{\mathrm{down}}. \tag{3.7}$$

The term (3.7) is included to penalize any changes to the base-case voltage magnitudes at generator buses since the voltage profile of the base case is considered to be the most suitable. Similarly, for each one of the considered stressed operating conditions, the total cost function of generation power adjustments is

$$z_{\mathrm{G}}^{s}(\Delta P_{\mathrm{G}j}^{\mathrm{up},s}, \Delta P_{\mathrm{G}j}^{\mathrm{down},s}) = \sum_{j \in \mathcal{G}} c_{\mathrm{G}j}^{\mathrm{up}} \Delta P_{\mathrm{G}j}^{\mathrm{up},s} + c_{\mathrm{G}j}^{\mathrm{down}} \Delta P_{\mathrm{G}j}^{\mathrm{down},s}, \tag{3.8}$$

and the total penalty function of voltage magnitude adjustments is

$$z_{\mathrm{V}}^{s}(\Delta V_{n}^{\mathrm{up},s}, \Delta V_{n}^{\mathrm{down},s}) = \sum_{n \in \mathcal{N}_{\mathrm{G}}} c_{\mathrm{V}n}^{\mathrm{up}} \Delta V_{n}^{\mathrm{up},s} + c_{\mathrm{V}n}^{\mathrm{down}} \Delta V_{n}^{\mathrm{down},s}. \tag{3.9}$$

Cost function (3.8) and penalty function (3.9) are introduced to force all stressed systems to work economically and to maintain an appropriate voltage profile. Furthermore, a term is included to take into account the cost of adjustments to the demand power levels. These adjustments involve only demand power decreases. The total cost function of load power adjustments is

$$z_{\mathrm{D}}(\Delta P_{\mathrm{D}i}^{\mathrm{down}}) = \sum_{i \in \mathcal{D}} c_{\mathrm{D}i}^{\mathrm{down}} \Delta P_{\mathrm{D}i}^{\mathrm{down}}. \tag{3.10}$$

The cost function (3.10) is not considered explicitly for the stressed operating conditions since load powers of the stressed systems are linked to the loads of the adjusted condition (see (3.30) and (3.32)). In summary, the resulting objective function is as follows:

$$\begin{aligned} z = \mu\big(z_{\mathrm{G}}(\Delta P_{\mathrm{G}j}^{\mathrm{up}}, \Delta P_{\mathrm{G}j}^{\mathrm{down}}) + z_{\mathrm{V}}(\Delta V_n^{\mathrm{up}}, \Delta V_n^{\mathrm{down}})\big) \\ + \sum_{s\in\mathcal{S}} \mu^s \big(z_{\mathrm{G}}^s(\Delta P_{\mathrm{G}j}^{\mathrm{up},s}, \Delta P_{\mathrm{G}j}^{\mathrm{down},s}) + z_{\mathrm{V}}^s(\Delta V_n^{\mathrm{up},s}, \Delta V_n^{\mathrm{down},s})\big) \\ + z_{\mathrm{D}}(\Delta P_{\mathrm{D}i}^{\mathrm{down}}). \end{aligned} \tag{3.11}$$

where μ and μ^s are, respectively, the probability of operating in the adjusted operating condition and the probability of occurrence of the contingency considered in the stressed operating condition s. These probabilities satisfy:

$$\mu + \sum_{s\in\mathcal{S}} \mu^s \;=\; 1, \tag{3.12}$$

where $\mu^s \ll \mu$, [33].

3.3.1.2 Power flow equations for the adjusted operating condition

The adjusted operating condition is defined by the active and reactive power balance at all buses:

$$P_{\mathrm{G}n} - P_{\mathrm{D}n} = \sum_{m\in\Theta_n} P_{nm}(\cdot), \quad \forall n \in \mathcal{N}, \tag{3.13}$$

$$Q_{\mathrm{G}n} - Q_{\mathrm{D}n} = \sum_{m\in\Theta_n} Q_{nm}(\cdot), \quad \forall n \in \mathcal{N}, \tag{3.14}$$

where the powers on the left-hand side of each equation above are

$$P_{\mathrm{G}n} = \sum_{j\in\mathcal{G}_n} P_{\mathrm{G}j}, \quad \forall n \in \mathcal{N}, \tag{3.15}$$

$$P_{\mathrm{D}n} = \sum_{i\in\mathcal{D}_n} P_{\mathrm{D}i}, \quad \forall n \in \mathcal{N}, \tag{3.16}$$

$$Q_{\mathrm{G}n} = \sum_{j\in\mathcal{G}_n} Q_{\mathrm{G}j}, \quad \forall n \in \mathcal{N}, \tag{3.17}$$

$$Q_{\mathrm{D}n} = \sum_{i \in \mathcal{D}_n} P_{\mathrm{D}i} \tan(\psi_{\mathrm{D}i}), \quad \forall n \in \mathcal{N}, \tag{3.18}$$

with

$$P_{\mathrm{G}j} = P_{\mathrm{G}j}^{\mathrm{A}} + \Delta P_{\mathrm{G}j}^{\mathrm{up}} - \Delta P_{\mathrm{G}j}^{\mathrm{down}}, \quad \forall j \in \mathcal{G}, \tag{3.19}$$

$$P_{\mathrm{D}i} = P_{\mathrm{D}i}^{\mathrm{A}} - \Delta P_{\mathrm{D}i}^{\mathrm{down}}, \quad \forall i \in \mathcal{D}, \tag{3.20}$$

and

$$\Delta P_{\mathrm{G}j}^{\mathrm{up}} \geq 0, \quad \forall j \in \mathcal{G}, \tag{3.21}$$

$$\Delta P_{\mathrm{G}j}^{\mathrm{down}} \geq 0, \quad \forall j \in \mathcal{G}, \tag{3.22}$$

$$\Delta P_{\mathrm{D}i}^{\mathrm{down}} \geq 0, \quad \forall i \in \mathcal{D}. \tag{3.23}$$

Equation (3.18) implies that constant power factor loads are considered. The functions on the right-hand side of (3.13) and (3.14) are the power flow equations and depend on the device connected between buses n and m. Appendix C describes these equations in detail. In this chapter and for the sake of simplicity, no control devices are considered. Therefore, the power flow equations (3.13) and (3.14) only depend on the bus voltage magnitudes and angles. The voltage magnitudes at the generation buses are defined as

$$V_n = V_n^{\mathrm{A}} + \Delta V_n^{\mathrm{up}} - \Delta V_n^{\mathrm{down}}, \quad \forall n \in \mathcal{N}_{\mathrm{G}}, \tag{3.24}$$

with

$$\Delta V_n^{\mathrm{up}} \geq 0, \quad \forall n \in \mathcal{N}_{\mathrm{G}}, \tag{3.25}$$

$$\Delta V_n^{\mathrm{down}} \geq 0, \quad \forall n \in \mathcal{N}_{\mathrm{G}}. \tag{3.26}$$

Finally, note that superscript "A" in (3.19), (3.20) and (3.24) indicates base-case solution.

3.3.1.3 Power flow equations for the stressed operating conditions

The power flow equations for the stressed operating conditions are

$$P^s_{\mathrm{G}n} - P^s_{\mathrm{D}n} = \sum_{m \in \Theta_n} P^s_{nm}(\cdot), \quad \forall n \in \mathcal{N}, \quad \forall s \in \mathcal{S}, \tag{3.27}$$

$$Q^s_{\mathrm{G}n} - Q^s_{\mathrm{D}n} = \sum_{m \in \Theta_n} Q^s_{nm}(\cdot), \quad \forall n \in \mathcal{N}, \quad \forall s \in \mathcal{S}, \tag{3.28}$$

where the powers on the left-hand side of (3.27) and (3.28) are defined as

$$P^s_{\mathrm{G}n} = \sum_{j \in \mathcal{G}_n} P^s_{\mathrm{G}j}, \quad \forall n \in \mathcal{N}, \quad \forall s \in \mathcal{S}, \tag{3.29}$$

$$P^s_{\mathrm{D}n} = \sum_{i \in \mathcal{D}_n} (1 + \lambda^{\mathrm{SM}}) P_{\mathrm{D}i}, \quad \forall n \in \mathcal{N}, \quad \forall s \in \mathcal{S}, \tag{3.30}$$

$$Q^s_{\mathrm{G}n} = \sum_{j \in \mathcal{G}_n} Q^s_{\mathrm{G}j}, \quad \forall n \in \mathcal{N}, \quad \forall s \in \mathcal{S}, \tag{3.31}$$

$$Q^s_{\mathrm{D}n} = \sum_{i \in \mathcal{D}_n} (1 + \lambda^{\mathrm{SM}}) P_{\mathrm{D}i} \tan(\psi_{\mathrm{D}i}), \quad \forall n \in \mathcal{N}, \quad \forall s \in \mathcal{S}, \tag{3.32}$$

with

$$P^s_{\mathrm{G}j} = P_{\mathrm{G}j} + \Delta P^{\mathrm{up},s}_{\mathrm{G}j} - \Delta P^{\mathrm{down},s}_{\mathrm{G}j}, \quad \forall j \in \mathcal{G}, \quad \forall s \in \mathcal{S}, \tag{3.33}$$

$$\Delta P^{\mathrm{up},s}_{\mathrm{G}j} \geq 0, \quad \forall j \in \mathcal{G}, \quad \forall s \in \mathcal{S}, \tag{3.34}$$

$$\Delta P^{\mathrm{down},s}_{\mathrm{G}j} \geq 0, \quad \forall j \in \mathcal{G}, \quad \forall s \in \mathcal{S}, \tag{3.35}$$

$$\tag{3.36}$$

where $P_{\mathrm{G}j}$ is defined as in (3.19) and $P_{\mathrm{D}i}$ is defined as in (3.20).

The functions of the right-hand side of (3.27) and (3.28) have the same expressions as the power flow equations (3.13) and (3.14), respectively, except for the fact that the corresponding variables are substituted by those pertaining to the stressed operating conditions.

Equations (3.27)-(3.32) are introduced to represent the system at the loading level determined by the security margin λ^{SM}. Moreover, each set of equations (3.27)-(3.32) includes a single line outage to enforce the $N-1$ contingency criterion. Therefore, each one of the stressed operating conditions is character-

ized by λ^{SM} and by a single contingency. Like the adjusted operating condition, the voltage magnitudes at the generator buses are defined as

$$V_n^s = V_n + \Delta V_n^{\mathrm{up},s} - \Delta V_n^{\mathrm{down},s}, \quad \forall n \in \mathcal{N}_{\mathrm{G}}, \quad \forall s \in \mathcal{S}, \tag{3.37}$$

with

$$\Delta V_n^{\mathrm{up},s} \geq 0, \quad \forall n \in \mathcal{N}_{\mathrm{G}}, \quad \forall s \in \mathcal{S}, \tag{3.38}$$

$$\Delta V_n^{\mathrm{down},s} \geq 0, \quad \forall n \in \mathcal{N}_{\mathrm{G}}, \quad \forall s \in \mathcal{S}. \tag{3.39}$$

Finally, V_n in (3.37) is defined as in (3.24).

3.3.1.4 Technical limits

The power production is limited by the capacity of the generators. Hence, under adjusted and stressed operating conditions,

$$P_{\mathrm{G}j}^{\min} \leq P_{\mathrm{G}j} \leq P_{\mathrm{G}j}^{\max}, \quad \forall j \in \mathcal{G}, \tag{3.40}$$

$$P_{\mathrm{G}j}^{\min} \leq P_{\mathrm{G}j}^{s} \leq P_{\mathrm{G}j}^{\max}, \quad \forall j \in \mathcal{G}, \quad \forall s \in \mathcal{S}, \tag{3.41}$$

$$Q_{\mathrm{G}j}^{\min} \leq Q_{\mathrm{G}j} \leq Q_{\mathrm{G}j}^{\max}, \quad \forall j \in \mathcal{G}, \tag{3.42}$$

$$Q_{\mathrm{G}j}^{\min} \leq Q_{\mathrm{G}j}^{s} \leq Q_{\mathrm{G}j}^{\max}, \quad \forall j \in \mathcal{G}, \quad \forall s \in \mathcal{S}. \tag{3.43}$$

Voltage magnitudes throughout the system under the adjusted and stressed operating conditions should be within operating limits,

$$V_n^{\min} \leq V_n \leq V_n^{\max}, \quad \forall n \in \mathcal{N}, \tag{3.44}$$

$$V_n^{\min} \leq V_n^{s} \leq V_n^{\max}, \quad \forall n \in \mathcal{N}, \quad \forall s \in \mathcal{S}. \tag{3.45}$$

The current flow through all branches of the network should be below thermal limits,

$$I_k(\cdot) \leq I_k^{\max}, \quad \forall k = (n,m) \in \Omega, \tag{3.46}$$

$$I_k^{s}(\cdot) \leq I_k^{\max}, \quad \forall k = (n,m) \in \Omega^s, \quad \forall s \in \mathcal{S}, \tag{3.47}$$

where the functions $I_k(\cdot)$ depend on the device k connected between buses n and m. The expressions of these functions are provided in Appendix C. The functions $I_k^s(\cdot)$ have the same expressions as $I_k(\cdot)$ except for the fact that the corresponding variables are substituted by those pertaining to the stressed operating conditions.

Changes in the production of generators between the adjusted and the stressed operating conditions are limited by ramping constraints,

$$P_{\mathrm{G}j}^s - P_{\mathrm{G}j} \leq R_{\mathrm{G}j}^{\mathrm{up}} \Delta t, \quad \forall j \in \mathcal{G}, \quad \forall s \in \mathcal{S}, \tag{3.48}$$

$$P_{\mathrm{G}j} - P_{\mathrm{G}j}^s \leq R_{\mathrm{G}j}^{\mathrm{down}} \Delta t, \quad \forall j \in \mathcal{G}, \quad \forall s \in \mathcal{S}. \tag{3.49}$$

The time interval Δt is the period within which generators are able to adjust their power production levels in order to reach the stressed operating conditions. Also, observe that (3.48) and (3.49) along with (3.30) and (3.32) couple the variables of the stressed operating conditions with those pertaining to the adjusted operating condition.

Constraints (3.48) and (3.49) enforce the fact that increments and decrements to generator power outputs can be obtained only within given rates, which in turn depends on the type and the characteristics of the power plants. These constraints constitute a necessary condition to ensure that the stressed operating conditions can be reached within the considered time period.

3.3.1.5 Small-signal stability constraints

The eigenvalues of the system state matrix that are associated with a particular operating condition are implicit non-linear functions of the system variables and parameters. As stated in Section 3.1, small-signal instability occurs if the real part of an eigenvalue (say $\alpha \pm j\beta$) of the system state matrix "moves" from the left-hand side ($\alpha < 0$) to the right-hand side ($\alpha > 0$) of the complex plane, as a result of parameter variation. Therefore, the small-signal stability boundary is $\alpha = 0$ for all *critical* eigenvalues whose real part approaches the imaginary axis.

The goal of the proposed SSSC-OPF problem is to stabilize a set of stressed operating conditions, which in turn guarantees the stability of the adjusted

(non-stressed) operating condition with a margin. The proposed small-signal stability constraints are based on the first-order Taylor series expansion of the real part of the critical eigenvalue, assuming that α only depends on active power generation. Thus, for each of the unstable stressed operating conditions (contained in set $\mathcal{S}_{\mathrm{u}}$), the small-signal stability constraint is as follows:

$$\alpha^s + F^s \sum_{j \in \mathcal{G}} \sigma_j^s \, \delta P_{\mathrm{G}j}^s \leq \alpha^{\max}, \quad \forall s \in \mathcal{S}_{\mathrm{u}}, \tag{3.50}$$

where α^s is the real part of the critical eigenvalue that corresponds to the unstable stressed operating condition s; $\delta P_{\mathrm{G}j}^s$ is a finite variation in the form:

$$\delta P_{\mathrm{G}j}^s = P_{\mathrm{G}j}^s - P_{\mathrm{G}j}^{\mathrm{u},s}, \tag{3.51}$$

where $P_{\mathrm{G}j}^{\mathrm{u},s}$ is the active power of generator j at the unstable stressed operating condition s, and σ_j^s in (3.50) is the sensitivity of the real part α^s of the considered eigenvalue with respect to changes in the power generation $P_{\mathrm{G}j}^{\mathrm{u},s}$, i.e.,

$$\sigma_j^s = \left. \frac{\partial \alpha^s}{\partial P_{\mathrm{G}j}^s} \right|_{\mathrm{u}}. \tag{3.52}$$

Limit $\alpha^{\max}$ can be defined either in terms of the HB point ($\alpha^{\max} = 0$) or in terms of a minimal damping ratio $\zeta^{\min}$. The expression of the damping ratio for the critical eigenvalue $\alpha^s \pm j\beta^s$ is

$$\zeta = \frac{-\alpha^s}{\sqrt{(\alpha^s)^2 + (\beta^s)^2}}. \tag{3.53}$$

Thus, solving (3.53) for α^s and replacing ζ by the required damping ratio ($\zeta^{\min}$) in the resulting expression, limit $\alpha^{\max}$ is obtained as follows:

$$\alpha^{\max} = -\frac{\beta^s \zeta^{\min}}{\sqrt{1 + (\zeta^{\min})^2}}, \quad \forall s \in \mathcal{S}_{\mathrm{u}}. \tag{3.54}$$

Finally, the scaling factor F^s in (3.50) is needed because the approxima-

tion of the first-order Taylor series expansion can be inaccurate due to non-linearities if the power variations $\delta P^s_{\mathrm{G}j}$ are too large. The magnitude of these variations depends on the relative values of α^s and σ^s_j. Numerical simulations throughout the work reported in this chapter show that sensitivities (3.52) generally exhibit small values (typically absolute values less than 1), whereas the real part of an eigenvalue can, in principle, assume any value. If the difference between the α^s and σ^s_j is relatively large (e.g., a factor of 10), satisfying equation (3.50) can lead to unnecessarily large variations of $\delta P^s_{\mathrm{G}j}$. Generally, the larger the values of $\delta P^s_{\mathrm{G}j}$, the further the solution moves from the initial stressed operating condition. In some cases, the OPF problem may become infeasible. Thus, a weighting factor F^s that controls the size of $\delta P^s_{\mathrm{G}j}$ is introduced. Since all sensitivities are multiplied by the same constant F^s, the global direction of (3.50) is not modified as all power variations $\delta P^s_{\mathrm{G}j}$ are equally scaled. The following formula outputs a suitable value for the factor F^s:

$$F^s = \frac{\alpha^s - \alpha^{\max}}{\sigma^s_{\min}\overline{\delta P}} \ , \tag{3.55}$$

where

$$\sigma^s_{\min} = \min(|\sigma^s_j|), \quad \forall j \in \mathcal{G}, \quad \forall \sigma^s_j \neq 0, \tag{3.56}$$

and the parameter $\overline{\delta P}$ ($\overline{\delta P} > 0$) is the desired bound for all increments $\delta P^s_{\mathrm{G}j}$, i.e., $|\delta P^s_{\mathrm{G}j}| \leq \overline{\delta P}$. The logic behind expression (3.55) is shown below. Replacing the value of F^s provided by (3.55) in (3.50) gives

$$\alpha^s - \alpha^{\max} + \sum_{j\in\mathcal{G}}(\alpha^s - \alpha^{\max})\frac{\sigma^s_j}{\sigma^s_{\min}}\frac{\delta P^s_{\mathrm{G}j}}{\overline{\delta P}} \leq 0, \qquad \forall s \in \mathcal{S}_{\mathrm{u}}, \tag{3.57}$$

and dividing this expression by $\alpha^s - \alpha^{\max}$ renders

$$1 + \sum_{j\in\mathcal{G}} \frac{\sigma^s_j}{\sigma^s_{\min}}\frac{\delta P^s_{\mathrm{G}j}}{\overline{\delta P}} \leq 0, \quad \forall s \in \mathcal{S}_{\mathrm{u}}. \tag{3.58}$$

Equation (3.56) results in

$$\sigma^s_{\min} \leq |\sigma^s_j|, \quad \forall j \in \mathcal{G}, \quad \forall \sigma^s_j \neq 0, \tag{3.59}$$

which implies that

$$\frac{|\sigma^s_j|}{\sigma^s_{\min}} \geq 1, \quad \forall j \in \mathcal{G}, \quad \forall \sigma^s_j \neq 0. \tag{3.60}$$

Observe that to satisfy (3.58), (3.60) requires that

$$\frac{|\delta P^s_{\mathrm{G}j}|}{\overline{\delta P}} \leq 1, \quad \forall j \in \mathcal{G}, \tag{3.61}$$

and therefore

$$|\delta P^s_{\mathrm{G}j}| \leq \overline{\delta P}, \quad \forall j \in \mathcal{G}. \tag{3.62}$$

Note that the purpose of constraint (3.50) is to drive unstable eigenvalues from the right hand side to the left hand side of the imaginary axis of the complex plane. Thus, typically, as the value of $\overline{\delta P}$ decreases, the variation of α^s also decreases. Therefore, the stable operating condition is achieved through successive solutions of the proposed OPF problem.

Constraints (3.63) and (3.64) below are used along with (3.50) to ensure that the variations in the generation powers are always consistent with the signs of the sensitivities:

$$\delta P^s_{\mathrm{G}j} \geq 0 \quad \text{if} \quad \sigma^s_j < 0, \quad \forall j \in \mathcal{G}, \quad \forall s \in \mathcal{S}_{\mathrm{u}}, \tag{3.63}$$

$$\delta P^s_{\mathrm{G}j} \leq 0 \quad \text{if} \quad \sigma^s_j > 0, \quad \forall j \in \mathcal{G}, \quad \forall s \in \mathcal{S}_{\mathrm{u}}. \tag{3.64}$$

These constraints avoid cycling phenomena that can appear during the solution process. These cycling solutions are mainly due to the approximate nature of constraint (3.50).

3.3.1.6 Other constraints

The proposed SSSC-OPF problem includes the following additional constraints:

$$-\pi \leq \theta_n \leq \pi, \quad \forall n \in \mathcal{N}, \tag{3.65}$$

$$-\pi \leq \theta_n^s \leq \pi, \quad \forall n \in \mathcal{N}, \quad \forall s \in \mathcal{S}, \tag{3.66}$$

$$\theta_{\text{ref}} = 0, \tag{3.67}$$

$$\theta_{\text{ref}}^s = 0, \quad \forall s \in \mathcal{S}. \tag{3.68}$$

Equations (3.65) and (3.66) are included to reduce the feasibility region, thereby causing the OPF problem to converge more rapidly in general.

3.3.1.7 SSSC-OPF problem formulation

The formulation of the SSSC-OPF problem is summarized below:

$$\text{Minimize} \quad (3.11)$$

subject to

1. Power flow equations for the adjusted operating condition (3.13)-(3.14).
2. Power flow equations for all the stressed operating conditions (3.27)-(3.28).
3. Technical limits (3.40)-(3.49).
4. Small-signal stability constraints (3.50) and (3.63)-(3.64).
5. Other constraints (3.65)-(3.68).

3.3.2 Security Redispatching Description

The proposed security redispatching procedure based on the SSSC-OPF described in the previous subsection is as follows.

1. *Base-Case Solution.* The base-case solution corresponds to the solution of a dispatching procedure (e.g., a market clearing procedure) adjusted by losses. Specifically, the base-case solution is obtained from the OPF problem described in Appendix A.

2. *Selection of Stressed Operating Conditions.* For a given security margin λ^{SM}, the stressed operating conditions to be included in the SSSC-OPF problem (set $\mathcal{S}$) are identified by applying the procedure described in Subsection 3.2. Stressed operating conditions are defined for each of the selected contingencies by setting the loading parameter λ^{SM} in equations (3.30) and (3.32) to the desired value.

3. *Solve the SSSC-OPF Problem.* The OPF problem described in Subsection 3.3.1.7 is solved and the adjusted and the stressed operating conditions are computed. Note that the first time that this problem is solved, constraints (3.50) and (3.63)-(3.64) are not included.

4. *Solution Checking.* Modal analysis is carried out for each stressed operating condition computed in step 3. Two alternatives are possible:

   (a) The real parts of all eigenvalues associated with all stressed operating conditions are negative. Thus, all stressed operating conditions are stable and the procedure stops.

   (b) One or more stressed operating conditions result in an eigenvalue with a positive real part. Sensitivities (3.52) are computed, and the constraints (3.50) and (3.63)-(3.64) are added to the SSSC-OPF problem for each one of the unstable stressed operating conditions (set $\mathcal{S}_{\mathrm{u}}$). The procedure continues in step 3.

The flowchart in Figure 3.2 summarizes the proposed method.

It should be noted that the system is not expected to operate at the loading level defined by λ^{SM}. In other words, the load increase represented by λ^{SM} is not a predicted load increase. Instead, the parameter λ^{SM} is used to enforce a margin to instability, in terms of the load. A stressed operating condition is defined by a contingency and the λ^{SM} value. Accordingly, if the system at the

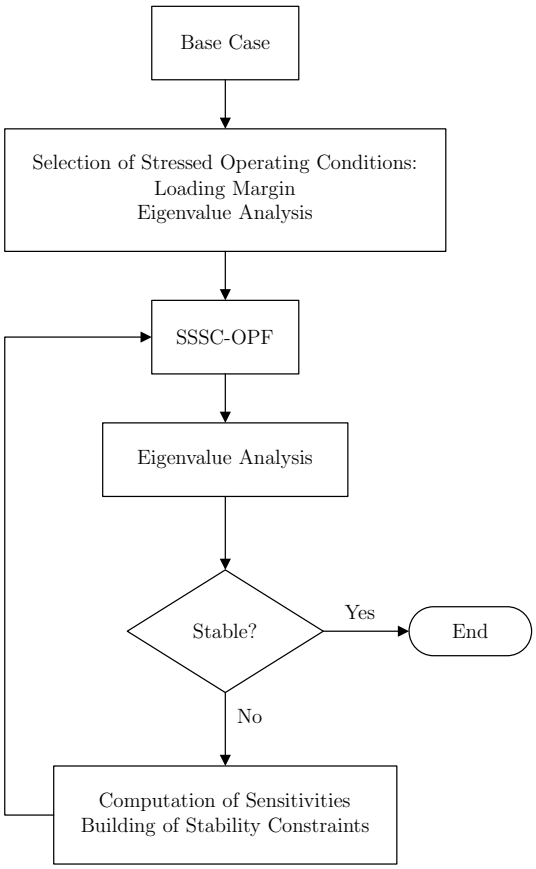

Figure 3.2: Small-signal stability. Flow chart for the proposed procedure.

stressed operating condition is stable, it is assumed to be stable at the adjusted operating condition as well, and it has at least a margin λ^{SM} to instability even if the contingency occurs.

Small-signal stability constraints are imposed on the stressed operating conditions. These constraints may cause changes in the generator powers to ensure small-signal stability for the imposed conditions. In some cases, changes in the stressed operating conditions imply changes in the adjusted operating condition because of constraints (3.30)-(3.32) and/or (3.48)-(3.49), which link the stressed operating conditions to the adjusted one. The new adjusted operating condition is the result of applying these changes to the base-case operating condition. These changes are redispatching actions, or preventive control actions,

for the base-case operating condition that are needed to ensure the desired security margin λ^{SM}.

In other cases, the changes in the stressed operating conditions do not involve any change in the adjusted operating condition. Consequently, no preventive control actions are needed to achieve the required security margin, and the adjusted operating condition remains equal to the base-case condition.

A relevant case arises if $\lambda^{\mathrm{SM}} = 0$. In addition to the preventive control actions that correspond to the adjusted operating condition, the solution output by the proposed procedure defines the emergency control actions needed to maintain stability if any of the considered contingencies occurs. These emergency control actions correspond to changes to the values of the control variables under the different stressed operating conditions.

3.3.3 Sensitivity Calculation

In this thesis, sensitivities (3.52) are computed numerically as follows:

1. As a result of the modal analysis carried out in step 4 of the proposed redispatching procedure, the real part α^s of the critical eigenvalue corresponding to a stressed operating condition s is obtained.

2. The generator power output $P^s_{\mathrm{G}j}$ is varied by a small positive quantity, ϵ, and the modal analysis is performed again. A new value of the critical eigenvalue is obtained whose real part is α^s_ϵ.

3. The sensitivity σ^s_j is computed as

$$\sigma^s_j = \frac{\partial \alpha^s}{\partial P^s_{\mathrm{G}j}} \cong \frac{\alpha^s_\epsilon - \alpha^s}{\epsilon}. \tag{3.69}$$

This procedure is repeated for all generator power outputs related to the considered stressed operating conditions.

For large systems, the numerical calculation of sensitivities may entail a significant computational burden. However, as the sensitivity computations are independent of each other, the computing time can be reduced using parallel

computation techniques. Alternatively, closed formulas for computing sensitivities significantly reduce the computational burden. These formulas can be found, for instance, in [51, 96, 97, 117].

3.4 Small-Signal Stability - Illustrative Example

For illustration purposes, the proposed security redispatching procedure is applied to the WECC 9-bus, 3-machine system. For small-signal stability analysis, the generators are modeled by a two-axis model that incorporates voltage control. These models are described in Appendix C. Moreover, the one-line diagram and complete data for this system are provided in Appendix D. For clarity, the results of each step from the proposed redispatching procedure are provided.

3.4.1 Base Case

The base-case solution is obtained from the OPF problem described in Appendix A. Table 3.1 provides this base-case solution.

3.4.2 Selection of the Stressed Operating Conditions

Once the base-case solution is available, contingency analysis is performed. For simplicity but without loss of generality, only line outages that leave the system interconnected are considered. Neither generator outages nor antenna line outages that lead to generator islanding are included in the analysis. For each contingency, the loading margin λ^* is obtained by solving the optimization problem (B.1)-(B.24) described in Subsection 2.1.3 of Chapter 2. The considered time period is set to five minutes ($\Delta t = 5$ minutes). For each one of the maximum loading conditions obtained, modal analysis is carried out. The characterization of each maximum loading condition is completed when the state variables are initialized. This initialization requires solving the set of equations (3.2), [114]. The system state matrix is built, and its eigenvalues

Table 3.1: Small-signal stability illustrative example. WECC 9-bus, 3-machine system: Base-case solution.

Bus #	Gen. #	Dem. #	$P^{\mathrm{A}}_{\mathrm{G}j}$ [p.u.]	$Q^{\mathrm{A}}_{\mathrm{G}j}$ [p.u.]	$P^{\mathrm{A}}_{\mathrm{D}i}$ [p.u.]	$Q^{\mathrm{A}}_{\mathrm{D}i}$ [p.u.]	V^{A}_{n} [p.u.]	θ^{A}_{n} [rad.]
1	1	-	1.2633	0.2510	0	0	1.1000	0
2	2	-	1.3642	0.0856	0	0	1.1000	0.0514
3	3	-	1.1955	-0.0592	0	0	1.1000	0.0476
4	-	-	0	0	0	0	1.0889	-0.0608
5	-	1	0	0	1.5000	0.6000	1.0595	-0.1164
6	-	2	0	0	1.0800	0.3600	1.0767	-0.0970
7	-	-	0	0	0	0	1.0979	-0.0193
8	-	3	0	0	1.2000	0.4200	1.0863	-0.0567
9	-	-	0	0	0	0	1.1050	-0.0101

are computed. Table 3.2 lists the calculated value of λ^*, the enforced limits and the critical eigenvalue at the maximum loading condition for each one of the contingencies analyzed.

Table 3.2: Small-signal stability illustrative example. WECC 9-bus, 3-machine system: Loading margin, enforced limits and critical eigenvalues.

Cont.	λ^*	Enforced Limits	$\alpha \pm j\beta$
6 - 4	0.1498	$R^{\mathrm{up}}_{\mathrm{G1}}$, $R^{\mathrm{up}}_{\mathrm{G2}}$, $P^{\mathrm{max}}_{\mathrm{G3}}$	-0.2413 ± j7.5584
5 - 4	0.1040	V^{min}_{5}, $R^{\mathrm{up}}_{\mathrm{G2}}$, $P^{\mathrm{max}}_{\mathrm{G3}}$	**1.4272 ± j1.8143**
7 - 5	0.1456	$R^{\mathrm{up}}_{\mathrm{G1}}$, $R^{\mathrm{up}}_{\mathrm{G2}}$, $P^{\mathrm{max}}_{\mathrm{G3}}$	-0.1349 ± j6.8823
9 - 6	0.1512	$R^{\mathrm{up}}_{\mathrm{G1}}$, $R^{\mathrm{up}}_{\mathrm{G2}}$, $P^{\mathrm{max}}_{\mathrm{G3}}$	-0.1435 ± j7.5765
7 - 8	0.1435	$R^{\mathrm{up}}_{\mathrm{G1}}$, $R^{\mathrm{up}}_{\mathrm{G2}}$, $P^{\mathrm{max}}_{\mathrm{G3}}$	-0.2147 ± j8.2791
9 - 8	0.1557	$R^{\mathrm{up}}_{\mathrm{G1}}$, $R^{\mathrm{up}}_{\mathrm{G2}}$, $P^{\mathrm{max}}_{\mathrm{G3}}$	-0.3056 ± j11.0802

The stressed operating conditions are selected for a security margin $\lambda^{\mathrm{SM}} =$

0.08. To this end, the contingency filtering procedure described in Section 3.2 is applied. Observe that no contingency needs to be selected regarding voltage stability because all loading margins are larger than the selected security margin. However, the maximum loading condition corresponding to the outage of line 5-4 exhibits a pair of complex conjugated eigenvalues with a positive real part. Therefore, the SSSC-OPF problem should include variables and constraints for the adjusted operating condition and for one stressed operating condition. The probability of occurrence of the selected contingency is set to 0.01.

3.4.3 Solving the SSSC-OPF Problem

For the security margin considered, the SSSC-OPF problem (3.11)-(3.68) is solved without constraints (3.50) and (3.63)-(3.64). Table 3.3 provides the stressed operating condition obtained.

Table 3.3: Small-signal stability illustrative example. WECC 9-bus, 3-machine system: Stressed operating condition.

Bus #	Gen. #	Dem. #	$P^s_{\mathrm{G}j}$ [p.u.]	$Q^s_{\mathrm{G}j}$ [p.u.]	$P^s_{\mathrm{D}i}$ [p.u.]	$Q^s_{\mathrm{D}i}$ [p.u.]	V^s_n [p.u.]	θ^s_n [rad.]
1	1	-	1.4424	0.1229	0	0	1.1000	0
2	2	-	1.6342	1.2266	0	0	1.1000	-0.2652
3	3	-	1.2000	0.3361	0	0	1.1000	-0.1622
4	-	-	0	0	0	0	1.0962	-0.0690
5	-	1	0	0	1.6200	0.6480	0.8212	-0.6456
6	-	2	0	0	1.1664	0.3888	1.0706	-0.1806
7	-	-	0	0	0	0	1.0345	-0.3550
8	-	3	0	0	1.2960	0.4536	1.0347	-0.3466
9	-	-	0	0	0	0	1.0840	-0.2212

The characterization of the stressed operating condition is complete once

the system state variables are initialized. Since a two-axis model incorporating voltage control is used for generators, the state variables are δ, ω, $E'_{\rm q}$, $E'_{\rm d}$, $V_{\rm m}$, $V_{\rm r1}$, $V_{\rm r2}$, and $V_{\rm f}$. The initialization of these variables is obtained from the stressed operating condition of Table 3.3 by solving the set of equations (3.2) tailored to the model used (see Appendix C). Table 3.4 lists the values calculated for these state variables.

Table 3.4: Small-signal stability illustrative example. WECC 9-bus, 3-machine system: State variables under the stressed operating condition.

State Variable	Generator 1	Generator 2	Generator 3
δ [rad]	0.1139	0.2914	0.5839
ω [p.u.]	1.0000	1.0000	1.0000
$E'_{\rm q}$ [p.u.]	1.1087	1.1414	0.9827
$E'_{\rm d}$ [p.u.]	0	0.4488	0.5983
$V_{\rm m}$ [p.u.]	1.1000	1.1000	1.1000
$V_{\rm r1}$ [p.u.]	1.1564	2.9473	2.2777
$V_{\rm r2}$ [p.u.]	-0.2036	-0.4473	-0.3733
$V_{\rm f}$ [p.u.]	1.1308	2.4852	2.0742

3.4.4 Solution Checking

Under the stressed operating condition the system state matrix is evaluated and eigenvalue analysis is carried out. Since there is a pair of complex conjugated eigenvalues with a positive real part, namely $0.3775 \pm j1.9729$ ($\lambda^{\rm SM} = 0.08$), the stressed operating condition is unstable. To establish the small-signal stability constraints (3.50) and (3.63)-(3.64), sensitivities (3.52) are computed using the procedure described in Subsection 3.3.3. The values of the sensitivities obtained are $\sigma_1^s = 0.0050$, $\sigma_2^s = 0.5230$ and $\sigma_3^s = 0.2870$. The limit $\alpha^{\max}$ is set to zero. The factor F^s is computed using $\overline{\delta P} = 1$ p.u. as

follows:

$$F^s = \frac{\alpha^s}{\sigma^s_{\min}\overline{\Delta P}} = \frac{0.3775}{0.0050 \times 1} = 75.50.$$

Taking into account the sign of the sensitivities, the small-signal stability constraints are

$$\begin{aligned} 0.3775 + 75.50(&0.0050(P^s_{\mathrm{G1}} - 1.4424) \\ &+ 0.5230(P^s_{\mathrm{G2}} - 1.6342) \\ &+ 0.2870(P^s_{\mathrm{G3}} - 1.2000)) \leq 0, \end{aligned}$$

and

$$\begin{aligned} P^s_{\mathrm{G1}} - 1.4424 &\leq 0, \\ P^s_{\mathrm{G2}} - 1.6342 &\leq 0, \\ P^s_{\mathrm{G3}} - 1.2000 &\leq 0. \end{aligned}$$

These constraints are included in the SSSC-OPF problem prior to solve it again.

3.4.5 Procedure Iterations

The procedure described in the previous subsection is repeated until the real part of the pair of complex critical eigenvalues becomes negative. This occurs after 7 iterations. Figure 3.3 depicts the eigenvalue evolution from the right-hand side to the left-hand side of the complex plane. Specifically, the critical eigenvalue moves from $0.3775 \pm j1.9729$ to $-0.0173 \pm j1.8263$.

In the first iteration, all sensitivities of the real part of the critical eigenvalue for the stressed operating condition with respect to the generator powers are positive. This result holds for all iterations, as shown in Figure 3.4.

In this situation, the only way to stabilize the stressed operating condition is to decrease the total generation. As a consequence, the total load demand must also decrease to maintain the power balance. Figure 3.5 depicts the

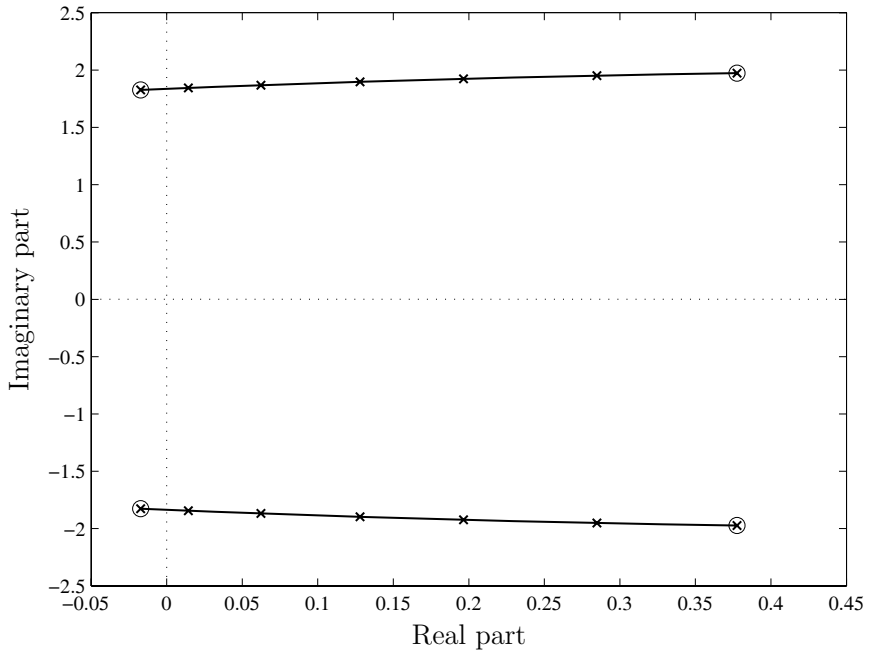

Figure 3.3: Small-signal stability illustrative example. WECC 9-bus, 3-machine system: Evolution of the pair of complex critical eigenvalues in the complex plane for $\lambda^{\mathrm{SM}} = 0.08$.

generator and load powers of the stressed operating condition that correspond to each iteration of the proposed procedure.

Due to constraints (3.30)-(3.32), which link the load of the stressed operating condition to the load of the adjusted one, the load decrease related to the stressed operating condition forces the load of the adjusted operating condition to decrease. As a consequence, the generator powers of the adjusted operating condition are modified. Figure 3.6 depicts the generator and load powers of the adjusted operating condition that correspond to each iteration of the proposed procedure.

Table 3.5 provides the generator and load powers that correspond to the final operating condition obtained after applying the proposed procedure. Table 3.5 also provides the redispatching actions with respect to the base case, namely $\Delta P_{\mathrm{G}j}^{\mathrm{up}}$, $\Delta P_{\mathrm{G}j}^{\mathrm{down}}$ and $\Delta P_{\mathrm{D}i}^{\mathrm{down}}$.

It is important to observe that $\Delta P_{\mathrm{G}j}^{\mathrm{down}}$ and $\Delta P_{\mathrm{D}i}^{\mathrm{down}}$ represent the most

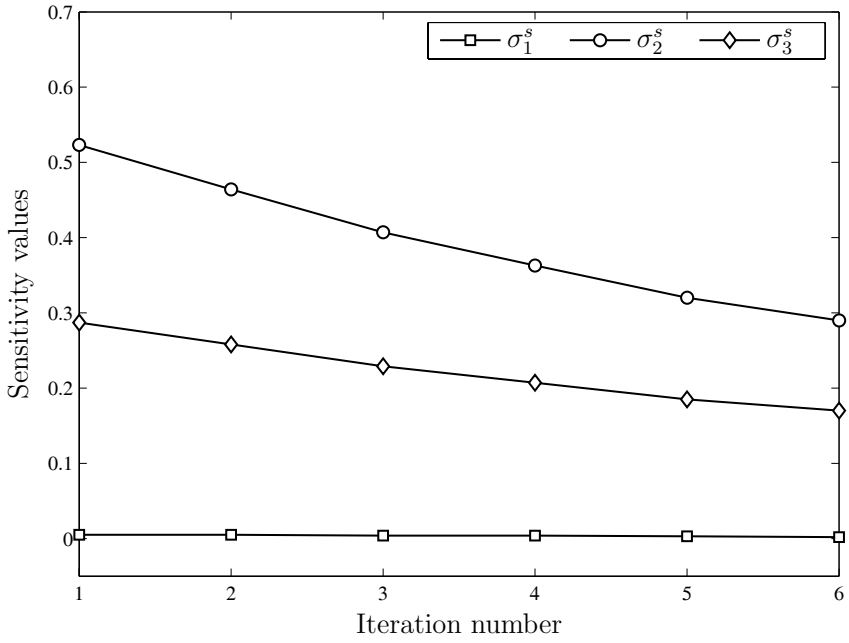

Figure 3.4: Small-signal stability illustrative example. WECC 9-bus, 3-machine system: Sensitivities of the real part of the pair of critical eigenvalues for the stressed operating condition with respect to generator powers for $\lambda^{\mathrm{SM}} = 0.08$.

economical redispatching actions that ensure the required security level.

3.5 Small-Signal Stability - Case Studies

In this section, the results of two case studies based on the New England 39-bus, 10-machine system and the IEEE 145-bus, 50-machine system are presented.

3.5.1 New England 39-Bus, 10-Machine System

In this subsection, the proposed security redispatching procedure is applied to the New England 39-bus, 10-machine system. For small-signal stability analysis, the generators are modeled using a two-axis model that incorporates a voltage controller, except for generator 10, which represents an equivalent of the New York network. These models are described in Appendix C. In order

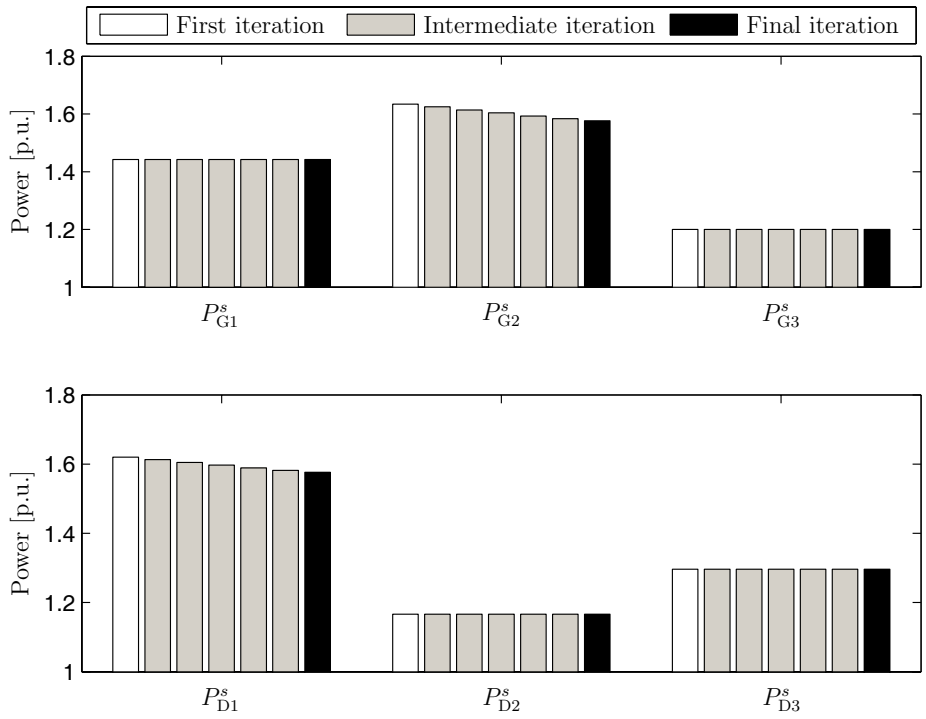

Figure 3.5: Small-signal stability illustrative example. WECC 9-bus, 3-machine system: Generator and load powers of the stressed operating condition for each iteration of the proposed procedure and for $\lambda^{\mathrm{SM}} = 0.08$.

to force small-signal instability, PSS devices are not considered. The one-line diagram and the data for this system are provided in Appendix D.

3.5.1.1 Base Case

The base-case solution is obtained from the OPF problem described in Appendix A. The result of this problem is provided in Appendix D.

3.5.1.2 Selection of the Stressed Operating Conditions

For this system, 35 possible line outages are analyzed. Tables D.20 and D.21 in Appendix D contains the network configuration of this system. The contingencies analyzed affect the first 35 branches described in these tables. None of these contingencies leads to generator islanding. For each one of these contin-

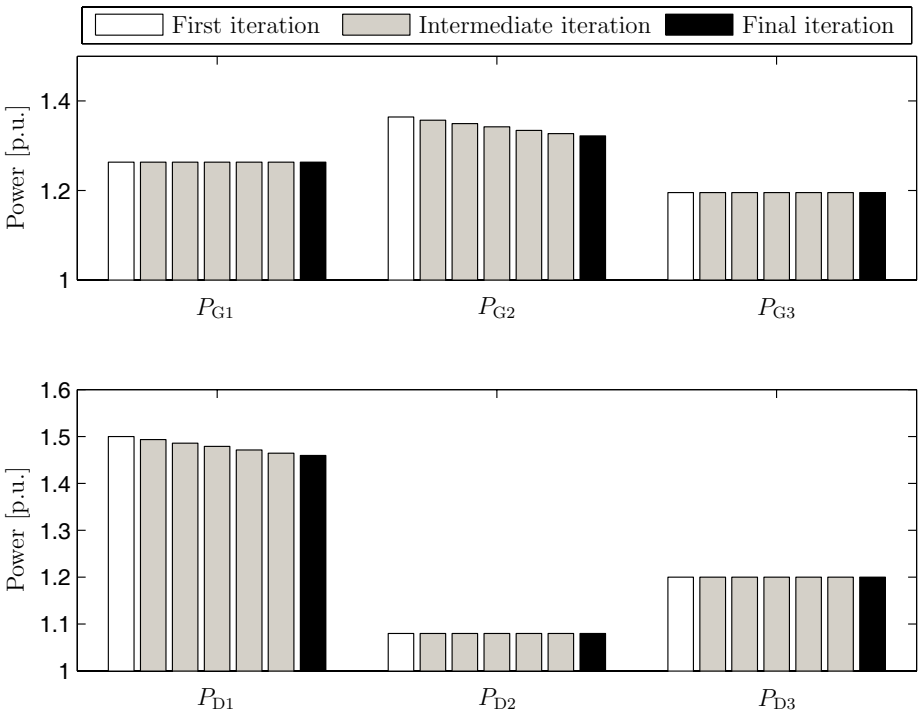

Figure 3.6: Small-signal stability illustrative example. WECC 9-bus, 3-machine system: Generator and load powers of the adjusted operating condition for each iteration of the proposed procedure and for $\lambda^{\text{SM}} = 0.08$.

gencies the loading margin λ is obtained by solving the optimization problem (B.1)-(B.24) described in Subsection 2.1.3 of Chapter 2. The time period is $\Delta t = 5$ minutes. The value of the loading margin for all considered contingencies is greater than or equal to 0.0957. At the maximum loading condition, seven contingencies induce Hopf bifurcations. Table 3.6 provides the loading margin λ and the corresponding critical eigenvalues for these seven contingencies: the outages of lines 1-2, 1-39, 2-25, 8-9, 9-39, 21-22, and 28-29.

The stressed operating conditions that must be incorporated in the SSSC-OPF problem are selected according to two security margins: $\lambda^{\text{SM}} = 0.07$ and $\lambda^{\text{SM}} = 0.09$. In these two cases, the seven contingencies from Table 3.6 are selected to conform to the stressed operating conditions. The probability of occurrence of each selected contingency is set to 0.01. In summary, the SSSC-OPF problem used in this case study embodies variables and constraints for

Table 3.5: Small-signal stability illustrative example. WECC 9-bus, 3-machine system: Adjusted operating condition and redispatching actions after applying the proposed procedure.

Bus #	Gen. #	Dem. #	$P_{\mathrm{G}j}$ [p.u.]	$\Delta P_{\mathrm{G}j}^{\mathrm{up}}$ [p.u.]	$\Delta P_{\mathrm{G}j}^{\mathrm{down}}$ [p.u.]	$P_{\mathrm{D}i}$ [p.u.]	$\Delta P_{\mathrm{D}i}^{\mathrm{down}}$ [p.u.]
1	1	-	1.2633	0	0	0	0
2	2	-	1.3220	0	0.0421	0	0
3	3	-	1.1955	0	0	0	0
4	-	-	0	0	0	0	0
5	-	1	0	0	0	1.4597	0.0403
6	-	2	0	0	0	1.0800	0
7	-	-	0	0	0	0	0
8	-	3	0	0	0	1.2000	0
9	-	-	0	0	0	0	0

the adjusted operating condition and for seven stressed operating conditions.

Table 3.6: Small-signal stability case study. New England 10-machine, 39-bus system: Loading margin and critical eigenvalues for the selected contingencies.

Cont.	λ^*	$\alpha \pm j\beta$
1 - 2	0.1004	0.1905 ± j2.5572
1 - 39	0.1004	0.2089 ± j2.5518
2 - 25	0.1002	0.2095 ± j2.7582
8 - 9	0.1006	0.0705 ± j2.6639
9 - 39	0.1007	0.0922 ± j2.6590
21 - 22	0.0957	0.7435 ± j2.4743
28 - 29	0.0976	0.4326 ± j2.9084

3.5.1.3 Solution for $\lambda^{\mathrm{SM}} = 0.07$

The initial solution (iteration 1) of the SSSC-OPF problem exhibits an unstable critical eigenvalue for two stressed operating conditions. These operating conditions are stabilized after 11 iterations of the proposed procedure using $\alpha^{\max} = 0$ and $\overline{\delta P} = 1$ p.u. for the small-signal stability constraints. Table 3.7 shows the critical eigenvalues of the considered stressed operating conditions for the initial unstable solution and for the solution after applying the proposed procedure.

Table 3.7: Small-signal stability case study. New England 39-bus, 10-machine system: Critical eigenvalues of the stressed operating conditions before and after applying the proposed procedure for $\lambda^{\mathrm{SM}} = 0.07$.

	Iteration 1	Iteration 11
Cont.	$\alpha^s \pm j\beta^s$	$\alpha^s \pm j\beta^s$
1 - 2	-0.0350 ± j2.6911	-0.1580 ± j2.7349
1 - 39	-0.0206 ± j2.6725	-0.1631 ± j2.7043
2 - 25	-0.1605 ± j2.7804	-0.3038 ± j2.5579
8 - 9	-0.1451	-0.1449
9 - 39	-0.1477	-0.1476
21 - 22	**0.3330 ± j2.6865**	**-0.0127 ± j2.5056**
28 - 29	**0.2134 ± j3.0076**	**-0.1049 ± j3.0415**

The stabilization of the stressed operating conditions affects the adjusted operating condition. Although no load curtailment is needed, redispatching actions on the generator powers of the adjusted operating condition are needed so that the power system can reach the stable stressed operating conditions. This results from the limiting effect of generator ramping constraints.

Figure 3.7 depicts the redispatching actions with respect to the base case needed to ensure the desired security margin $\lambda^{\mathrm{SM}} = 0.07$. The redispatching actions increase some generator powers, $\Delta P_{\mathrm{G}j}^{\mathrm{up}}$, and decrease some other generator powers, $\Delta P_{\mathrm{G}j}^{\mathrm{down}}$, with respect to the base-case operating condition.

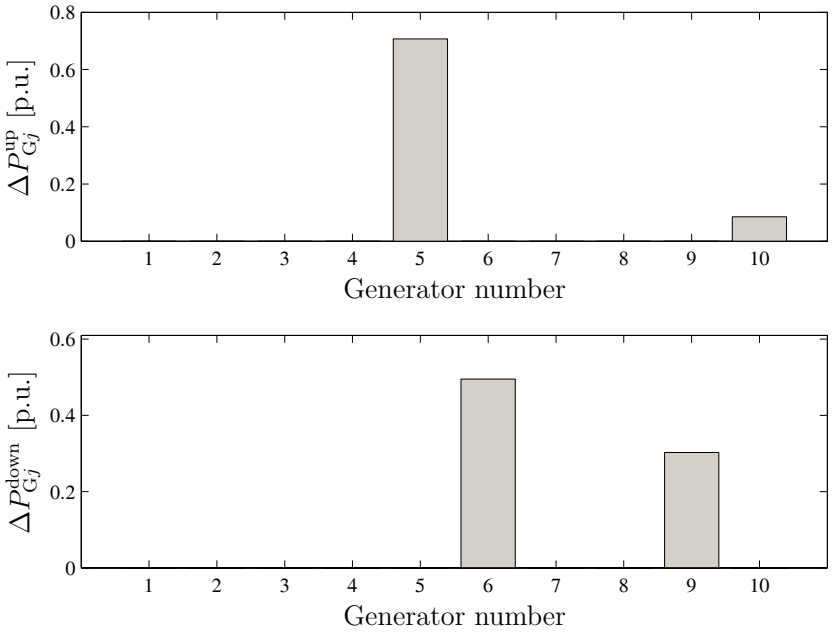

Figure 3.7: Small-signal stability case study. New England 39-bus, 10-machine system: Redispatching actions for $\lambda^{\mathrm{SM}} = 0.07$.

3.5.1.4 Solution for $\lambda^{\mathrm{SM}} = 0.09$

The initial solution (iteration 1) of the SSSC-OPF problem shows an unstable critical eigenvalue for six stressed operating conditions. These operating conditions are stabilized after 15 iterations of the proposed procedure using $\alpha^{\max} = 0$ and $\overline{\delta P} = 1$ p.u. for the small-signal stability constraints. Table 3.8 shows the critical eigenvalues of the considered stressed operating conditions for the initial unstable solution and for the solution after applying the proposed procedure.

As in the case for $\lambda^{\mathrm{SM}} = 0.07$, the stabilization of the stressed operating conditions impacts the adjusted operating condition. Figure 3.8 depicts the redispatching actions that are related to the generator powers with respect to the base case needed to ensure the desired security margin $\lambda^{\mathrm{SM}} = 0.09$. No load curtailment is needed. The redispatching actions depicted in Figure 3.8 increase some generator powers, $\Delta P_{\mathrm{G}j}^{\mathrm{up}}$, and decrease other generator powers, $\Delta P_{\mathrm{G}j}^{\mathrm{down}}$. These results show that generation redispatching can be enough to

Table 3.8: Small-signal stability case study. New England 39-bus, 10-machine system: Critical eigenvalues of the stressed operating conditions before and after applying the proposed procedure for $\lambda^{\mathrm{SM}} = 0.09$.

	Iteration 1	Iteration 15
Cont.	$\alpha^s \pm j\beta^s$	$\alpha^s \pm j\beta^s$
1 - 2	**0.1389 ± j2.5837**	**-0.1032 ± j2.7958**
1 - 39	**0.1576 ± j2.5766**	**-0.1018 ± j2.7746**
2 - 25	**0.1817 ± j2.7639**	**-0.3902 ± j2.5315**
8 - 9	-0.0088 ± j2.6779	-0.3711 ± j2.3574
9 - 39	**0.0159 ± j2.6705**	**-0.3540 ± j2.3731**
21 - 22	**0.7161 ± j2.4874**	**-0.0096 ± j2.7604**
28 - 29	**0.4228 ± j2.9157**	**-0.2930 ± j3.3282**

restore small-signal stability.

3.5.1.5 Simulation Times

This subsection discusses the computational requirements of the proposed procedure for the New England 39-bus, 10-machine system. The starting point of the procedure is the base-case operating condition obtained from the OPF problem described in Appendix A. This step requires 0.14 s. In the contingency filtering procedure, 35 contingencies are analyzed. This step involves loading margin computation and eigenvalue analysis at the maximum loading condition for each considered contingency. Table 3.9 shows the CPU times for this step. The selection of stressed operating conditions requires 10.4510 s.

Constraints and variables related to seven stressed operating conditions are included in the SSSC-OPF problem. The initial solution to this problem (i.e., without small-signal stability constraints) takes 0.38 s for $\lambda^{\mathrm{SM}} = 0.07$ and 0.39 s for $\lambda^{\mathrm{SM}} = 0.09$.

The procedure requires several iterations to reach the solution. Each iteration involves eigenvalue analysis, computing sensitivities and solving the

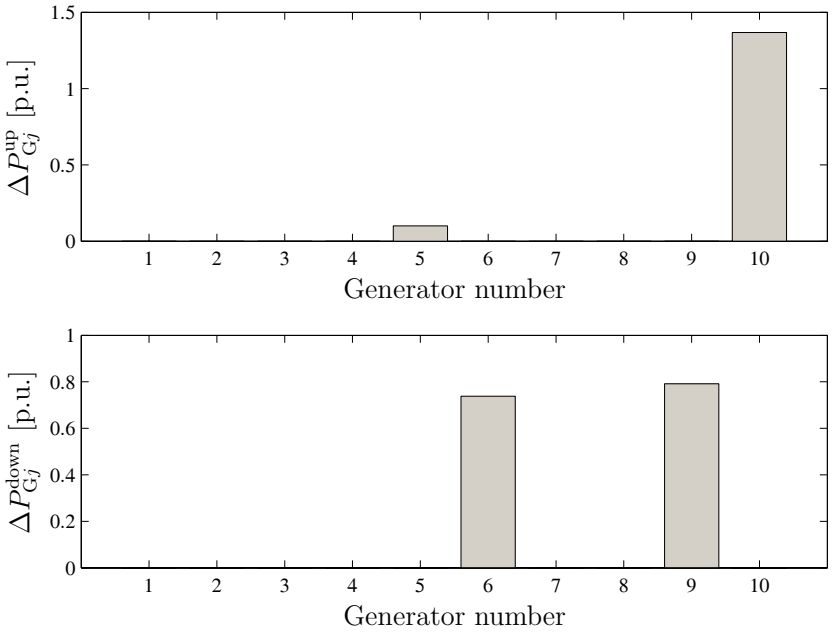

Figure 3.8: Small-signal stability case study. New England 39-bus, 10-machine system: Redispatching actions for $\lambda^{\mathrm{SM}} = 0.09$.

Table 3.9: Small-signal stability case study. New England 39-bus, 10-machine system: Computational requirements of the contingency filtering procedure.

	Loading margin	Eigenvalue analysis	Total CPU
Contingencies analyzed	35	35	–
Average CPU [s] (per contingency)	0.2290	0.0696	0.2986
Total CPU [s] (35 contingencies)	8.0150	2.4360	10.4510

SSSC-OPF problem. Eigenvalue analysis is performed for each of the seven stressed operating conditions obtained after solving the SSSC-OPF problem.

Sensitivities of the critical eigenvalue real part with respect to each generator power output are computed by means of numerical differentiation, as described in Subsection 3.3.3. Computing sensitivities implies additional eigenvalue analysis and the evaluation of expression (3.69) for each generator and for each small-signal unstable stressed operating condition. Once sensitivities have been computed, the corresponding sets of constraints (3.50) and (3.63)-(3.64) are included in the SSSC-OPF problem. Tables 3.10 and 3.11 list the average and the total CPU times of each one of these steps for $\lambda^{\mathrm{SM}} = 0.07$ and $\lambda^{\mathrm{SM}} = 0.09$, respectively. These tables also list the number of times per iteration that eigenvalue analysis is performed, eigenvalue sensitivity is computed, and the SSSC-OPF problem is solved, along with the number of iterations that the procedure requires.

Table 3.10: Small-signal stability case study. New England 39-bus, 10-machine system: Computational requirements of the procedure iterations for $\lambda^{\mathrm{SM}} = 0.07$.

	Eigenvalue analysis	Sensitivity computation	SSSC-OPF problem	Total CPU
NTPI	7	20	1	-
NI	11	10	11	-
Average CPU [s]	0.0696	0.2393	0.4864	-
Total CPU [s]	5.3592	47.8650	5.3500	58.5742

NTPI: number of times per iteration; NI: number of iterations.

The procedure takes a total CPU time of 58.5742 s when $\lambda^{\mathrm{SM}} = 0.07$, and 216.7200 s when $\lambda^{\mathrm{SM}} = 0.09$. Observe that the sensitivity computation is the step with the highest computational burden. This phenomenon occurs because eigenvalue sensitivities are computed by means of numerical differentiation. If closed-form sensitivity formulas are used, the computational burden of this step can be considerably reduced.

Table 3.11: Small-signal stability case study. New England 39-bus, 10-machine system: Computational requirements of the procedure iterations for $\lambda^{\mathrm{SM}} = 0.09$.

	Eigenvalue analysis	Sensitivity computation	SSSC-OPF problem	Total CPU
NTPI	7	60	1	-
NI	15	14	15	-
Average CPU [s]	0.0696	0.2393	0.5600	-
Total CPU [s]	7.3080	201.0120	8.4000	216.7200

NTPI: number of times per iteration; NI: number of iterations.

3.5.2 IEEE 145-Bus, 50-Machine System

In this subsection, the proposed security redispatching procedure is applied to a slightly modified version of the IEEE 145-bus, 50-machine benchmark system [101], which is provided in the software package Power System Toolbox (PST) [29]. This system consists of 145 buses, 453 line/transformers, and 50 machines. Machines connected to buses 93, 102, 104, 105, 106, 110, and 111, are modeled through a 6^{th}-order model [114]. These machines are equipped with IEEE ST1a exciters including PSS devices [29]. The classical model is used for the remaining machines. In order to force small-signal instability, the PSS device of the machine connected to bus 102 has been removed. Economic data and technical limits for this system are provided in Appendix D, whereas the rest of data can be found in [29].

3.5.2.1 Base Case

The base-case solution is obtained from the OPF problem described in Appendix A.

3.5.2.2 Selection of the Stressed Operating Conditions

For this system, 434 possible line/transformer outages are analyzed. In the contingency filtering procedure, the MLC-OPF problem described in Appendix B is solved and eigenvalue analysis at the maximum loading condition is performed for each contingency. The desired security margin is $\lambda^{\text{SM}} = 0.05$ and the time period is $\Delta t = 5$ minutes. According to the contingency analysis, five contingencies must be considered in the stressed operating conditions. Table 3.12 provides the system loading margin and the critical eigenvalues for these five contingencies. Since the system loading margins λ^* for the outages

Table 3.12: Small-signal stability case study. IEEE 145-bus, 50-machine system: Loading margin and critical eigenvalues for the selected contingencies.

Contingency	λ^*	$\alpha \pm j\beta$
67 - 124	0.0659	0.2165 ± j9.7872
102 - 117	0.0671	0.0702 ± j6.4852
119 - 130	0.0415	-0.0454 ± j9.4041
119 - 131	0.0392	-0.1010 ± j0
121 - 125	0.0521	0.2882 ± j9.5961

of lines 110-130 and 119-131 are smaller than the required security margin $\lambda^{\text{SM}} = 0.05$, these contingencies can potentially lead to voltage stability issues. On the other hand, the outages of lines 67-124, 102-117 and 121-125 show positive eigenvalues at the maximum loading condition. Thus, these contingencies are selected due to the risk of small-signal instability at the loading condition that corresponds to $\lambda^{\text{SM}} = 0.05$. Finally, the probability of occurrence of each selected contingency is 0.01.

3.5.2.3 Solution for $\lambda^{\text{SM}} = 0.05$

For this case study, the SSSC-OPF problem includes variables and constraints for the adjusted operating condition and for five stressed operating conditions. The proposed procedure requires nine iterations to reach the solution using

$\overline{\delta P} = 1$ p.u. and considering a minimal damping ratio of 0.05 ($\zeta^{\min} = 0.05$) for the small-signal stability constraints. Table 3.13 provides the critical eigenvalues of the considered stressed operating conditions for both the initial and final iteration of the proposed procedure. The solution of the SSSC-OPF prob-

Table 3.13: Small-signal stability case study. IEEE 145-bus, 50-machine system: Critical eigenvalues of the stressed operating conditions before and after applying the proposed procedure for $\lambda^{\text{SM}} = 0.05$.

	Iteration 1	Iteration 4
Contingency	$\alpha^s \pm j\beta^s$	$\alpha^s \pm j\beta^s$
67 - 124	**0.2740 ± j9.7602**	**-0.5177 ± j9.3964**
102 - 117	-0.1009 ± j0	-0.1009 ± j0
119 - 130	-0.1009 ± j0	-0.1009 ± j0
119 - 131	-0.1010 ± j0	-0.1010 ± j0
121 - 125	-0.1010 ± j0	-0.1010 ± j0

lem without small-signal stability constraints (first iteration of the proposed procedure) shows generation redispatching and load curtailment. This result is mainly due to the stabilization of the stressed operating conditions that correspond to the outages of lines 110-130 and 119-131. Note that, for these contingencies, $\lambda^* < \lambda^{\text{SM}}$. The load curtailment affects all stressed operating conditions in such that the stressed conditions that correspond to the outages of lines 102-117 and 121-125 do not present unstable eigenvalues. However, the stressed operating condition that corresponds to the outage of line 67-124 shows small-signal instability. This stressed operating condition is stabilized in the fourth iteration using $\delta\overline{P} = 1$ p.u. The final solution shows a total load curtailment of 2.4078 p.u.

Figure 3.9 depicts two time-domain simulations of the 145-bus system at the stressed operating condition that corresponds to the outage of line 64-124 when subjected to a small disturbance. In particular, Figure 3.9 shows the unstable rotor speed trajectories for the solution of the first iteration and the stable transient for the final solution of the proposed method. Time-domain

simulations confirm eigenvalue analysis.

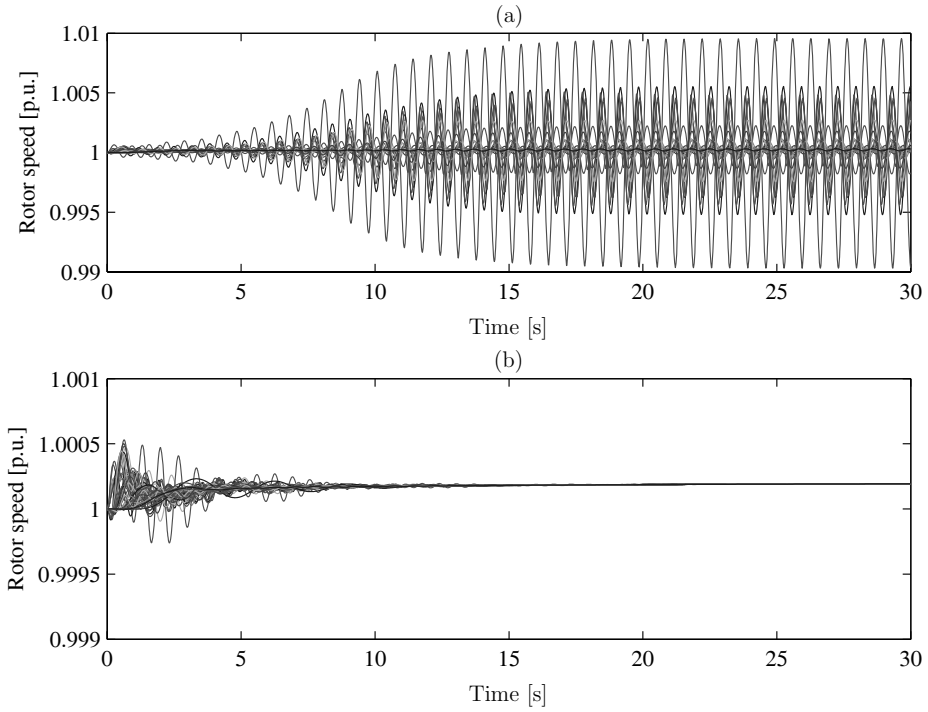

Figure 3.9: Small-signal stability case study. IEEE 145-bus 50-machine system: Time-domain simulation of the stressed operating condition that correspond to the outage of line 64-124. Plot (a) corresponds to the first solution and plot (b) to the final solution.

3.5.2.4 Simulation Times

This subsection discusses the computational requirements of the proposed procedure for the IEEE 145-bus, 50-machine system. The starting point of the procedure is the base-case operating condition obtained from the OPF problem described in Appendix A. This step takes 4.17 s. In the contingency filtering procedure, 434 contingencies are analyzed. This step involves loading margin computation and eigenvalue analysis at the maximum loading condition for each considered contingency. Table 3.14 shows the CPU times for this step. The selection of stressed operating conditions requires 3326.7836 s

($\simeq$ 55.45 minutes). This computing time can be reduced by applying parallel computation techniques.

Table 3.14: Small-signal stability case study. IEEE 145-bus, 50-machine system: Computational requirements of the contingency filtering procedure.

	Loading margin	Eigenvalue analysis	Total CPU
Contingencies analyzed	434	434	–
Average CPU [s] (per contingency)	7.3600	0.3054	7.6654
Total CPU [s] (35 contingencies)	3194.2400	132.5436	3326.7836

Constraints and variables related to five stressed operating conditions are included in the SSSC-OPF problem. The initial solution to this problem (i.e., without small-signal stability constraints) takes 162.09 s.

The procedure requires nine iterations to reach the solution. Each iteration involves eigenvalue analysis, computing sensitivities and solving the SSSC-OPF problem. Eigenvalue analysis is performed for each one of the five stressed operating conditions obtained after solving the SSSC-OPF problem. In this case, only one stressed operating condition shows small-signal instability in the first iteration. For this stressed condition, sensitivities of the critical eigenvalue real part with respect to each generator power output are computed by means of numerical differentiation, as described in Subsection 3.3.3. Once sensitivities have been computed, the corresponding set of constraints (3.50) and (3.63)-(3.64) is included in the SSSC-OPF problem. Table 3.15 lists the average and the total CPU times of each one of these steps. This table also lists the number of times per iteration that eigenvalue analysis is performed, eigenvalue sensitivity is computed, and the SSSC-OPF problem is solved, along with the number of iterations that the procedure requires.

Table 3.15: Small-signal stability case study. IEEE 145-bus, 50-machine system: Computational requirements of the procedure iterations for $\lambda^{\mathrm{SM}} = 0.05$.

	Eigenvalue analysis	Sensitivity computation	SSSC-OPF problem	Total CPU
NTPI	5	50	1	-
NI	9	8	9	-
Average CPU [s]	0.3054	0.8916	99.6822	-
Total CPU [s]	13.7430	356.6400	897.1398	1267.5228

NTPI: number of times per iteration; NI: number of iterations.

The procedure takes a total CPU time of 1267.5228 s ($\simeq$ 21.13 minutes). In this case, the solution to the SSSC-OPF problem is the step with the highest computational burden. This step can be a concern for large-scale power systems if an important number of stressed operating conditions are to be considered. The development of an *ad hoc* solution algorithm for this problem (e.g., based on decomposition techniques) may significantly reduce computing times.

3.6 Summary and Conclusions

This chapter has presented a security redispatching procedure able to resolve security issues that pertain to both voltage and small-signal instability. The proposed procedure is intended to help system operators guarantee an appropriate level of security.

Once a base-case solution is available, contingency analysis is carried out to identify the harmful contingencies pertaining to voltage and small-signal instability. For each one of the pre-specified set of contingencies, the system loading margin is computed. At the maximum loading condition, modal analysis is carried out, and the critical contingencies are identified in terms of the desired security margin along with the eigenvalues obtained from the modal analysis. Then, the procedure solves an OPF problem that includes

both voltage and small-signal stability constraints.

This OPF problem explicitly considers security limits through stressed operating conditions. These stressed operating conditions are defined by both a contingency and a pre-defined loading condition that is higher than that of the base case. Small-signal stability constraints are imposed on the stressed operating conditions. These constraints are formulated based on the first-order Taylor series expansion of the critical eigenvalue real part. Thus, first-order sensitivities of the critical eigenvalue real part with respect to generator powers are used. Provided that the stressed operating conditions are stable, the adjusted operating condition is considered to be stable as well, and it has at least a given security margin even if a contingency occurs.

The performance of the proposed procedure has been illustrated and tested on the WECC 9-bus, 3-machine system, the New England 39-bus, 10-machine system, and the IEEE 145-bus, 50-machine system. The results have been analyzed and discussed in detail.

Simulation results show that redispatching power generation is an effective way to improve the small-signal stability of the system. Moreover, the proposed procedure identifies the minimum-cost preventive redispatching actions for the base-case solution that ensure the required security margin with respect to both voltage and small-signal stability. Simulations also confirm the ability of the proposed procedure to address multi-contingency cases.

The proposed procedure comprises certain steps that are time consuming, which potentially makes their implementation impractical for large-scale power systems. This is the case of eigenvalue analysis and sensitivity computation. The computational burden of the eigenvalue analysis can be reduced by computing only those eigenvalues that have the largest real part. For simplicity, the sensitivities have been computed using numerical differentiation. However, closed-form sensitivity formulas are available in the literature. These formulas considerably reduce (with respect to numerical differentiation) the time required to compute eigenvalue sensitivities.

Solving the proposed SSSC-OPF problem can be also a concern for large-scale power systems if an important number of stressed operating conditions are to be considered. The development of an *ad hoc* algorithm for this problem

(e.g., based on decomposition techniques) may significantly reduce computing times. Since this chapter focuses on the design of an effective procedure, these computational issues have not been specifically addressed.

Chapter 4

Optimal Power Flow with Transient Stability Constraints

This chapter describes a redispatching procedure to restore transient stability. It relies on a transient stability constrained optimal power flow (TSC-OPF) model. In addition to power flow constraints and limits, the resulting optimal power flow model includes discrete time equations that describe the time evolution of all the machines in the system. Transient stability constraints are formulated by reducing the initial multi-machine model to a one-machine infinite-bus equivalent. This equivalent allows imposing angle bounds that ensure transient stability.

This chapter is organized as follows. Section 4.1 presents an overview of transient stability, including the system model and the transient stability assessment method used in this chapter. Section 4.2 describes the contingency filtering procedure used to identify the harmful contingencies from the transient stability point of view. In Section 4.3, the TSC-OPF problem is formulated and the steps of the redispatching procedure are described. In Sections 4.4 and 4.5, this procedure is tested and analyzed using the WECC 9-bus, 3-machine system, the New England 39-bus, 10-Machine system, and a real-world 1228-bus, 292-machine system. Finally, Section 4.6 summarizes and offers some conclusions.

4.1 Transient Stability

Transient stability is concerned with the ability of a power system to maintain synchronism after a large disturbance, such as a fault on a transmission line [102]. During the fault period, the rotors of the synchronous machines suffer an acceleration or deceleration due to the imbalance between the input mechanical torque and the output electromagnetic torque in the generators. As a consequence, the rotor speed of the machines changes and the kinetic energy stored in the rotating parts of the generators increases or decreases. This causes the angular separation of the machines. If the system cannot absorb the kinetic energy stored during the fault period, synchronism is lost. This kind of instability usually takes the form of aperiodic angular separation of the machines due to lack of synchronizing torque. Transient instability often appears during the first swing of the system transient; thus, the time frame of interest is reduced to one or two seconds after the disturbance. However, in certain systems, transient instability can appear after the first swing because of slow inter-area swing modes [73]. This phenomenon is known as multi-swing instability and its study may involve analysis that extend over time periods greater than ten seconds.

4.1.1 System Model

In transient stability studies, as in small-signal stability studies, the power system is represented by a set of differential-algebraic equations (DAE):

$$\begin{bmatrix} \dot{\boldsymbol{x}} \\ \mathbf{0} \end{bmatrix} = \begin{bmatrix} \boldsymbol{f}(\boldsymbol{x}, \boldsymbol{y}, \boldsymbol{p}) \\ \boldsymbol{g}(\boldsymbol{x}, \boldsymbol{y}, \boldsymbol{p}) \end{bmatrix} \tag{4.1}$$

where vector $\boldsymbol{x}$ ($\boldsymbol{x} \in \mathbb{R}^{\mathrm{n_x}}$) contains the state variables (e.g., δ, ω), vector $\boldsymbol{y}$ ($\boldsymbol{y} \in \mathbb{R}^{\mathrm{n_y}}$) includes algebraic variables (e.g., V, θ, Q_G) and $\boldsymbol{p}$ ($\boldsymbol{p} \in \mathbb{R}^{\mathrm{n_p}}$) is the vector of control variables (e.g., P_G, P_D, Q_D). Function $\boldsymbol{f}$ ($\boldsymbol{f} : \mathbb{R}^{\mathrm{n_x}} \times \mathbb{R}^{\mathrm{n_y}} \times \mathbb{R}^{\mathrm{n_p}} \longmapsto \mathbb{R}^{\mathrm{n_x}}$) is a nonlinear vector function associated with the state variables $\boldsymbol{x}$ that usually represents the system differential equations, such as those associated with the synchronous machine dynamics, control devices, etc.;

and vector function $\boldsymbol{g}$ ($\boldsymbol{g} : \mathbb{R}^{\mathrm{n_x}} \times \mathbb{R}^{\mathrm{n_y}} \times \mathbb{R}^{\mathrm{n_p}} \longmapsto \mathbb{R}^{\mathrm{n_y}}$) represents a system of algebraic equations, including the power flow equations, algebraic equations associated with the synchronous machine model, etc.

In this chapter, a classical model is used to represent the power system. This model is based on the following assumptions [5]:

1. The input mechanical power is constant.
2. Damping is neglected.
3. Synchronous machines are represented by a constant electromotive force behind a transient reactance.
4. The mechanical rotor angle of the synchronous machine coincides with the angle of the electromotive force behind the transient reactance.
5. Loads are represented by constant impedances.

Note that this classical model supports sufficient accuracy for moderate computational effort. Within the classical model, the transient behavior of synchronous generators is described by the so-called swing equations:

$$\dot{\delta}_j = \omega_{\mathrm{b}}(\omega_j - 1), \quad \forall j \in \mathcal{G}, \tag{4.2}$$

$$\dot{\omega}_j = \frac{1}{M_j}(P_{\mathrm{m}j} - P_{\mathrm{e}j}), \quad \forall j \in \mathcal{G}, \tag{4.3}$$

where δ_j is the rotor angle, ω_j is the rotor speed, M_j is the inertia coefficient, $P_{\mathrm{m}j}$ is the input mechanical power, and $P_{\mathrm{e}j}$ is the output electrical power of generator j. Finally, ω_{b} in (4.2) represents the base synchronous frequency in rad/s.

Since the loads are approximated as constant impedances, the equivalent load admittance at bus n is

$$\boldsymbol{Y}_{\mathrm{D}n} = \frac{P_{\mathrm{D}n}}{V_n^2} - j\frac{Q_{\mathrm{D}n}}{V_n^2}, \quad \forall n \in \mathcal{N}, \tag{4.4}$$

and the original network can be transformed into an equivalent reduced network whose nodes correspond to the internal generator nodes [5]. The admit-

tance matrix of the reduced network is called the reduced admittance matrix and can be used to define the electrical power of the generators. Thus, the electrical power $P_{\mathrm{e}j}$ in (4.3) can be written as follows:

$$P_{\mathrm{e}j} = E'_j \sum_{\ell} E'_\ell [B_{j\ell} \sin(\delta_j - \delta_\ell) + G_{j\ell} \cos(\delta_j - \delta_\ell)], \quad \forall j, \ell \in \mathcal{G}, \tag{4.5}$$

where E' is the electromotive force of the corresponding generators and $G_{j\ell}$ and $B_{j\ell}$ are the elements of the real and imaginary parts of the reduced admittance matrix $\mathbf{Y}_{\mathrm{bus}}$, respectively. The reduced admittance matrix can also be used with a detailed generator model, as far as the loads are represented as constant impedances and the admittance matrix reduction is stopped at the machine buses and does not extend to the fictitious internal node of the machine model.

4.1.2 Center of Inertia

In transient stability studies, it is convenient to express the generator rotor angles with respect to the system Center Of Inertia (COI) reference to facilitate the visualization of power system dynamics. The position of the COI is defined as

$$\delta_{\mathrm{COI}} = \frac{1}{M_{\mathrm{T}}} \sum_{j \in \mathcal{G}} M_j \delta_j, \tag{4.6}$$

where

$$M_{\mathrm{T}} = \sum_{j \in \mathcal{G}} M_j. \tag{4.7}$$

Then, the rotor angle of the generator j with respect to the COI is expressed as $\delta_j - \delta_{\mathrm{COI}}$.

4.1.3 Transient Stability Assessment: SIME Method

The transient stability assessment is the evaluation of the ability of a power system to withstand sudden large disturbances by surviving the ensuing transient and moving into an acceptable steady-state operating condition [57]. The transient stability assessment can be performed using time-domain simulations, transient energy functions or hybrid methods. Time-domain simulations allow

taking into account the full system dynamic model and consist in checking that inter-machine rotor angle deviations lie within a specific range of values. Unfortunately, this range is system, if not operating-point, dependent and, in general, is not easy to establish. The methods based on the transient energy function greatly reduce the computational burden. However, the main limitation to using these methods lies in the construction of a suitable Lyapunov function and in the definition of the stability domain. Hybrid methods combine the advantages of time-domain simulation and transient energy function methods while avoiding some of their drawbacks.

In this thesis, transient stability is assessed using the SIngle Machine Equivalent (SIME) method [106], which is a hybrid method. A brief summary of its fundamental features is provided in the following subsections.

4.1.3.1 Basis

The SIME method is based on the concept of the One-Machine Infinite Bus (OMIB) equivalent. The OMIB equivalent concept arises out of the observation that a multi-machine power system loses synchronism because of the irrevocable separation of its machines into two groups. These two groups can be replaced by a two-machine system and then by an OMIB equivalent system [105]. Further, the transient stability of the multi-machine system is assessed by applying the Equal-Area Criterion (EAC) to the OMIB equivalent system.

The dynamic model of an OMIB system is represented by the "swing" equation and expressed as

$$M\ddot{\delta} = M\dot{\omega} = P_{\mathrm{m}} - P_{\mathrm{e}} = P_{\mathrm{a}}, \tag{4.8}$$

where δ is the rotor angle, ω is the rotor speed, M is the inertia coefficient, P_{m} is the input mechanical power, P_{e} is the output electrical power, and P_{a} is the acceleration power of the equivalent OMIB system. A detailed definition of the parameters of (4.8) appears in Subsection 4.1.3.3. The main characteristic of the SIME method is that the parameters that define the OMIB equivalent system are obtained from the physical parameters and time varying data of the multi-machine system provided by a time-domain simulation. Thus, de-

tailed dynamic power system models can be considered since equation (4.8) adequately expresses the OMIB system dynamics and the EAC criterion is still valid [106]. Therefore, checking the transient stability of the OMIB equivalent by means of the EAC also evaluates the transient stability properties of the original multi-machine system. Thus, at each time step of a time-domain simulation, the OMIB parameters are updated and the stability of the OMIB equivalent is checked by the EAC.

According to the equivalent OMIB parameters and the EAC, SIME establishes a set of objective stability conditions that allow the time-domain simulation to be stopped as soon as these conditions are met, thereby considerably reducing the computation time.

4.1.3.2 Identification of the system decomposition pattern

SIME uses information of the system evolution from a time-domain simulation of the considered fault. As soon as the system enters the post-fault configuration, SIME constructs a sequence of candidate OMIB equivalents by decomposing the system machines into two candidate groups: (i) the group of machines that are likely to lose synchronism, so-called critical machines, and (ii) all other machines, so-called non-critical machines. The maximum difference (distance) between two adjacent rotor angles, say $\delta_j - \delta_\ell$, indicates the frontier between the two machine groups, as follows. All generators whose rotor angles are greater than δ_j are part of the critical machine group, while all generators whose rotor angles are lower than δ_ℓ are part of the non-critical machine group. These two groups are replaced by an OMIB equivalent system, whose transient stability is determined by means of the EAC. This procedure is carried out for each step of the time-domain simulation until one candidate OMIB equivalent satisfies the instability conditions. This candidate is termed the critical OMIB equivalent or simply the OMIB equivalent.

4.1.3.3 OMIB time-varying parameters

The OMIB equivalent parameters are time-varying since they are refreshed at each time step of the time-domain simulation. The OMIB system parameters,

δ, ω, M, P_{m}, P_{e} and P_{a}, are computed from the corresponding individual parameters of each system machine, as follows. Once the groups of critical machines and non-critical machines are identified, the multi-machine system is reduced to a two-machine system. The group of critical machines and the group of non-critical machines are replaced by two equivalent machines using the concept of partial center of angle. The parameters that define these machines at each time step t of the time-domain simulation are computed as follows:

$$\delta_{\mathrm{C}}^{t} = \frac{1}{M_{\mathrm{C}}} \sum_{j \in \mathcal{G}_{\mathrm{C}}} M_j \delta_j^t, \tag{4.9}$$

$$\delta_{\mathrm{NC}}^{t} = \frac{1}{M_{\mathrm{NC}}} \sum_{j \in \mathcal{G}_{\mathrm{NC}}} M_j \delta_j^t, \tag{4.10}$$

$$\omega_{\mathrm{C}}^{t} = \frac{1}{M_{\mathrm{C}}} \sum_{j \in \mathcal{G}_{\mathrm{C}}} M_j \omega_j^t, \tag{4.11}$$

$$\omega_{\mathrm{NC}}^{t} = \frac{1}{M_{\mathrm{NC}}} \sum_{j \in \mathcal{G}_{\mathrm{NC}}} M_j \omega_j^t, \tag{4.12}$$

where δ_{C}^t and ω_{C}^t are, respectively, the equivalent rotor angle and speed of the critical machine group; and δ_{NC}^t and ω_{NC}^t are, respectively, the equivalent rotor angle and speed of the non-critical machine group. The inertia coefficients of the critical (M_{C}) and non-critical (M_{NC}) equivalents are expressed as follows:

$$M_{\mathrm{C}} = \sum_{j \in \mathcal{G}_{\mathrm{C}}} M_j, \tag{4.13}$$

$$M_{\mathrm{NC}} = \sum_{j \in \mathcal{G}_{\mathrm{NC}}} M_j. \tag{4.14}$$

The OMIB parameters are computed from those of the equivalent two-machine system. The OMIB equivalent rotor angle δ^t and rotor speed ω^t are defined as follows:

$$\delta^t = \delta_{\mathrm{C}}^t - \delta_{\mathrm{NC}}^t, \tag{4.15}$$

$$\omega^t = \omega_{\mathrm{C}}^t - \omega_{\mathrm{NC}}^t. \tag{4.16}$$

Note that ω^t, as defined in (4.16), is a relative value of the OMIB equivalent

rotor speed. The electric power P_{e}^t and the mechanical power P_{m}^t of the OMIB are derived using the following expressions:

$$P_e^t = M\left[\frac{1}{M_{\mathrm{C}}}\sum_{j\in\mathcal{G}_{\mathrm{C}}} P_{ej}^t - \frac{1}{M_{\mathrm{NC}}}\sum_{j\in\mathcal{G}_{\mathrm{NC}}} P_{ej}^t\right], \tag{4.17}$$

$$P_m^t = M\left[\frac{1}{M_{\mathrm{C}}}\sum_{j\in\mathcal{G}_{\mathrm{C}}} P_{mj}^t - \frac{1}{M_{\mathrm{NC}}}\sum_{j\in\mathcal{G}_{\mathrm{NC}}} P_{mj}^t\right], \tag{4.18}$$

where

$$M = \frac{M_{\mathrm{C}}M_{\mathrm{NC}}}{M_{\mathrm{C}} + M_{\mathrm{NC}}}, \tag{4.19}$$

is the inertia coefficient of the OMIB equivalent. Finally, the OMIB accelerating power P_{a}^t is defined by

$$P_{\mathrm{a}}^t = P_{\mathrm{m}}^t - P_{\mathrm{e}}^t. \tag{4.20}$$

4.1.3.4 Stability conditions

The EAC establishes that an OMIB system is transient unstable if the kinetic energy stored during the fault-on period is greater than the maximum potential energy that the power system can dissipate during the post-fault period.

Figures 4.1 and 4.2 depict the OMIB trajectory for an unstable scenario. Figure 4.1 shows the $P-\delta$ curves and Figure 4.2 depicts the phase plane. The kinetic energy stored in the system corresponds to the accelerating area A_{acc}, whereas the potential energy dissipated by the system corresponds to the decelerating area A_{dec}. In this case, the electric power P_{e}^t crosses the mechanical power P_{m}^t or, in other words, the accelerating power P_{a} passes zero and continues to increase. From a physical point of view, $P_{\mathrm{a}}^t = 0$ marks the OMIB loss of synchronism. Moreover, it is observed in the phase plane that $\omega^t > 0$ at the very instant at which P_{e}^t crosses P_{m}^t. Hence, the conditions for an unstable OMIB trajectory are as follows:

$$P_{\mathrm{a}}^{t_{\mathrm{u}}} = 0, \tag{4.21}$$

$$\dot{P}_{\mathrm{a}}^{t_{\mathrm{u}}} = \left.\frac{dP_{\mathrm{a}}^{t}}{dt}\right|_{t=t_{\mathrm{u}}} > 0, \tag{4.22}$$

$$\omega^{t_{\mathrm{u}}} = \omega_{\mathrm{u}} > 0, \tag{4.23}$$

where subscript "u" stands for unstable. The unstable OMIB rotor angle δ_{u} corresponds to the angle at which the instability conditions (4.21)-(4.23) are met.

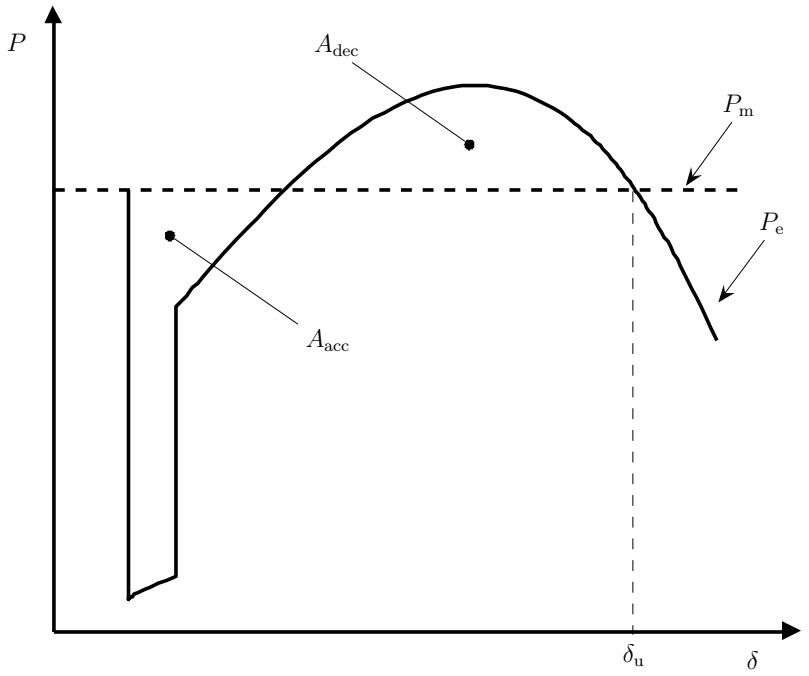

Figure 4.1: Unstable OMIB trajectory. $P - \delta$ curve.

Figures 4.3 and 4.4 depict the OMIB trajectory for a stable scenario. Figure 4.3 shows the $P-\delta$ curves and Figure 4.4 depicts the phase plane. The kinetic energy stored in the system corresponds to the accelerating area A_{acc} ,whereas the potential energy dissipated by the system corresponds to the decelerating area A_{dec}. In this case, the electric power P_{e}^{t} stops increasing before crossing the mechanical power P_{m}^{t} line. Moreover, it is apparent in the phase plane that $\omega^{t} = 0$ at the very instant at which P_{e}^{t} "comes back". Hence, the conditions

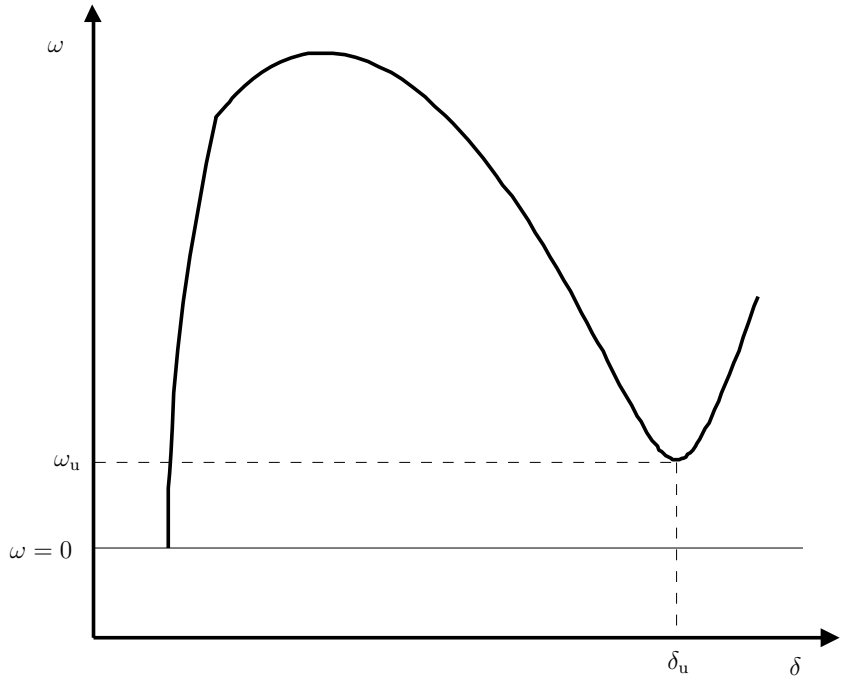

Figure 4.2: Unstable OMIB trajectory. Phase plane.

for a first-swing stable OMIB trajectory are as follows:

$$\omega^{t_r} = \omega_{\mathrm{r}} = 0, \tag{4.24}$$

$$P_a^{t_r} < 0, \tag{4.25}$$

where subscript "r" stands for return. The OMIB rotor angle δ_{r} corresponds to the return angle at which the first-swing stability conditions (4.24)-(4.25) are met.

It should be noted that the instability conditions (4.21)-(4.23) determine the early termination conditions of the time-domain simulation. However, when the stability conditions (4.24)-(4.25) are met, the system is first-swing stable, and the time-domain simulation can be stopped only if multi-swing instability phenomena are not of interest [106].

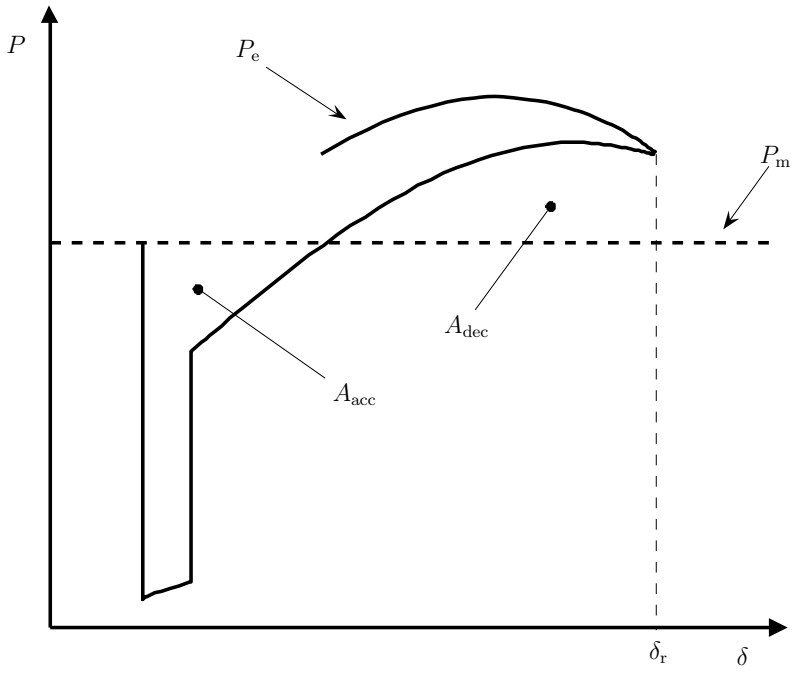

Figure 4.3: Stable OMIB trajectory. $P - \delta$ curve.

4.2 Security Assessment: Contingency Filtering

Contingency analysis selects those contingencies that may lead to system instability from a set of credible contingencies. As in previous chapters, the initial set of contingencies is defined based on the $N - 1$ security criterion. This initial set is reduced with a contingency filtering procedure to identify the most harmful (i.e., critical) contingencies.

Regarding transient stability, the analyzed contingencies consist of a three-phase-to-ground symmetrical fault and the subsequent fault clearing by tripping the corresponding line. Critical contingencies are identify with a time-domain simulation complemented by the SIME method. The contingencies of interest are those that cause the system to lose synchronism, i.e., the contingencies that cause the system OMIB equivalent to met instability conditions (4.21)-(4.23).

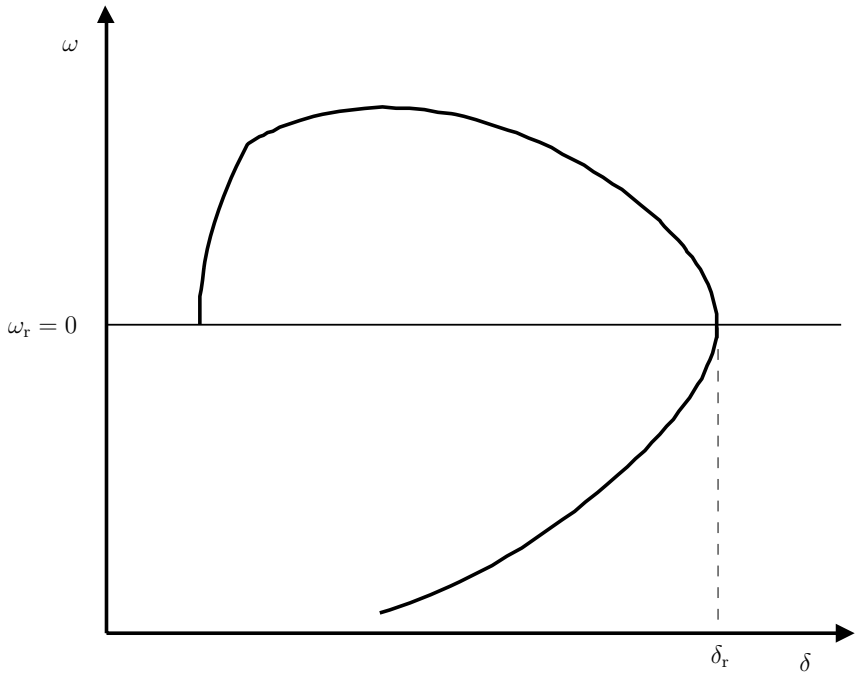

Figure 4.4: Stable OMIB trajectory. Phase plane.

For first-swing unstable contingencies, the SIME method identifies the critical and non non-critical machines, the time t_u and the OMIB equivalent rotor unstable angle δ_u for which instability conditions (4.21)-(4.23) are met. In addition to this information, for multi-swing unstable contingencies, SIME also provides the time t_r and the OMIB equivalent rotor return angle δ_r for which the first-swing stability conditions (4.24)-(4.25) are reached.

Note that the time-domain simulation of one contingency is independent of those of other contingencies. This fact can be exploited to reduce the computation time by using parallel computation.

4.3 Security Redispatching

This section presents a security redispatching procedure based on a Transient Stability Constrained Optimal Power Flow (TSC-OPF) problem to assist the system operator in ensuring transient stability. The proposed TSC-OPF prob-

lem includes, among others, the pre-contingency power flow equations; technical bounds on generators, buses and lines; discrete time swing equations for all the machines of the system (reproducing the actual time-domain simulation); and a transient stability bound on the rotor angle of the system OMIB equivalent. This OMIB equivalent is computed using the SIME method.

The solution of the proposed procedure provides the preventive control adjustments for the base-case solution needed to guarantee transient stability with respect to a set of contingencies. It is assumed that the system operator has access to the technical information of the generators and that the generators provide the ISO with cost offers for redispatching.

4.3.1 TSC-OPF Problem Description

This subsection describes the objective function and all constraints pertaining to the TSC-OPF problem in detail.

4.3.1.1 Objective function

The objective function is aimed at minimizing the variations with respect to the base-case solution. In particular, the objective function is composed of several terms that represent adjustment costs and penalty functions. The adjustment costs correspond to changes in the generation and load powers, while the penalty functions concern voltage magnitudes at generator buses. Thus, the total cost function of generation power adjustments is

$$z_{\mathrm{G}}(\Delta P_{\mathrm{G}j}^{\mathrm{up}}, \Delta P_{\mathrm{G}j}^{\mathrm{down}}) = \sum_{j \in \mathcal{G}} c_{\mathrm{G}j}^{\mathrm{up}} \Delta P_{\mathrm{G}j}^{\mathrm{up}} + c_{\mathrm{G}j}^{\mathrm{down}} \Delta P_{\mathrm{G}j}^{\mathrm{down}}, \tag{4.26}$$

where $c_{\mathrm{G}j}^{\mathrm{up}}$ and $c_{\mathrm{G}j}^{\mathrm{down}}$ are, respectively, the offering cost of generator j to increase and decrease its power dispatch for security purposes. The total penalty function of voltage magnitude adjustments at generator buses is

$$z_{\mathrm{V}}(\Delta V_{n}^{\mathrm{up}}, \Delta V_{n}^{\mathrm{down}}) = \sum_{n \in \mathcal{N}_{\mathrm{G}}} c_{\mathrm{V}n}^{\mathrm{up}} \Delta V_{n}^{\mathrm{up}} + c_{\mathrm{V}n}^{\mathrm{down}} \Delta V_{n}^{\mathrm{down}}. \tag{4.27}$$

The term (4.27) is included to penalize any changes in the base-case voltage magnitudes at generator buses since the voltage profile of the base case is considered to be the most suitable. Furthermore, a term is included to take into account the cost of adjustments to demand powers. These adjustments involve only demand power decrements. The total cost function of demand power adjustments is

$$z_{\mathrm{D}}(\Delta P_{\mathrm{D}i}^{\mathrm{down}}) = \sum_{i \in \mathcal{D}} c_{\mathrm{D}i}^{\mathrm{down}} \Delta P_{\mathrm{D}i}^{\mathrm{down}}, \tag{4.28}$$

where $c_{\mathrm{D}i}^{\mathrm{down}}$ are the cost of demand curtailment. In summary, the resulting objective function is as follows:

$$z = z_{\mathrm{G}}(\Delta P_{\mathrm{G}j}^{\mathrm{up}}, \Delta P_{\mathrm{G}j}^{\mathrm{down}}) + z_{\mathrm{V}}(\Delta V_n^{\mathrm{up}}, \Delta V_n^{\mathrm{down}}) + z_{\mathrm{D}}(\Delta P_{\mathrm{D}i}^{\mathrm{down}}). \tag{4.29}$$

4.3.1.2 Pre-contingency power flow equations

The operating condition of the system is established by the active and reactive power balance at all buses:

$$P_{\mathrm{G}n} - P_{\mathrm{D}n} = \sum_{m \in \Theta_n} P_{nm}(\cdot), \quad \forall n \in \mathcal{N}, \tag{4.30}$$

$$Q_{\mathrm{G}n} - Q_{\mathrm{D}n} = \sum_{m \in \Theta_n} Q_{nm}(\cdot), \quad \forall n \in \mathcal{N}, \tag{4.31}$$

where the powers on the left-hand side of each equation are

$$P_{\mathrm{G}n} = \sum_{j \in \mathcal{G}_n} P_{\mathrm{G}j}, \quad \forall n \in \mathcal{N}, \tag{4.32}$$

$$P_{\mathrm{D}n} = \sum_{i \in \mathcal{D}_n} P_{\mathrm{D}i}, \quad \forall n \in \mathcal{N}, \tag{4.33}$$

$$Q_{\mathrm{G}n} = \sum_{j \in \mathcal{G}_n} Q_{\mathrm{G}j}, \quad \forall n \in \mathcal{N}, \tag{4.34}$$

$$Q_{\mathrm{D}n} = \sum_{i \in \mathcal{D}_n} P_{\mathrm{D}i} \tan(\psi_{\mathrm{D}i}), \quad \forall n \in \mathcal{N}, \tag{4.35}$$

with

$$P_{\mathrm{G}j} = P_{\mathrm{G}j}^{\mathrm{A}} + \Delta P_{\mathrm{G}j}^{\mathrm{up}} - \Delta P_{\mathrm{G}j}^{\mathrm{down}}, \quad \forall j \in \mathcal{G}, \tag{4.36}$$

$$P_{\mathrm{D}i} = P_{\mathrm{D}i}^{\mathrm{A}} - \Delta P_{\mathrm{D}i}^{\mathrm{down}}, \quad \forall i \in \mathcal{D}, \tag{4.37}$$

and

$$\Delta P_{\mathrm{G}j}^{\mathrm{up}} \geq 0, \quad \forall j \in \mathcal{G}, \tag{4.38}$$

$$\Delta P_{\mathrm{G}j}^{\mathrm{down}} \geq 0, \quad \forall j \in \mathcal{G}, \tag{4.39}$$

$$\Delta P_{\mathrm{D}i}^{\mathrm{down}} \geq 0, \quad \forall i \in \mathcal{D}. \tag{4.40}$$

Equation (4.35) implies that constant power factor loads are considered. The functions on the right-hand side of (4.30) and (4.31) are the power flow equations and depend on the device connected between buses n and m. Appendix C describes these equations in detail. In this chapter and for the sake of simplicity, no control devices are considered. Therefore, the power flow equations (4.30) and (4.31) only depend on bus voltage magnitudes and angles. The voltage magnitudes at the generation buses are defined as

$$V_n = V_n^{\mathrm{A}} + \Delta V_n^{\mathrm{up}} - \Delta V_n^{\mathrm{down}}, \quad \forall n \in \mathcal{N}_{\mathrm{G}}, \tag{4.41}$$

with

$$\Delta V_n^{\mathrm{up}} \geq 0, \quad \forall n \in \mathcal{N}_{\mathrm{G}}, \tag{4.42}$$

$$\Delta V_n^{\mathrm{down}} \geq 0, \quad \forall n \in \mathcal{N}_{\mathrm{G}}. \tag{4.43}$$

Finally, note that superscript "A" in (4.36), (4.37) and (4.41) indicates base-case solution.

4.3.1.3 Technical limits

The power production is limited by the capacity of the generators.

$$P_{\mathrm{G}j}^{\min} \leq P_{\mathrm{G}j} \leq P_{\mathrm{G}j}^{\max}, \quad \forall j \in \mathcal{G}, \tag{4.44}$$

$$Q_{\mathrm{G}j}^{\min} \leq Q_{\mathrm{G}j} \leq Q_{\mathrm{G}j}^{\max}, \quad \forall j \in \mathcal{G}. \tag{4.45}$$

Voltages magnitudes throughout the system should be within operating limits,

$$V_n^{\min} \leq V_n \leq V_n^{\max}, \quad \forall n \in \mathcal{N}. \tag{4.46}$$

The current flow through all branches of the network should be below thermal limits,

$$I_k(\cdot) \leq I_k^{\max}, \quad \forall k = (n, m) \in \Omega, \tag{4.47}$$

where functions $I_k(\cdot)$ depend on the device k connected between buses n and m. The expressions of these functions are provided in Appendix C.

4.3.1.4 Initial values of machine rotor angles, rotor speeds and electromotive forces

The initial values of generator rotor angles δ_j^0 and electromotive forces E'_j are obtained from the system pre-fault steady-state conditions as follows,

$$\frac{E'_j V_n \sin(\delta_j^0 - \theta_n)}{x'_{\mathrm{d}j}} - P_{\mathrm{G}j} = 0, \quad \forall j \in \mathcal{G}_n, \tag{4.48}$$

$$\frac{E'_j V_n \cos(\delta_j^0 - \theta_n) - V_n^2}{x'_{\mathrm{d}j}} - Q_{\mathrm{G}j} = 0, \quad \forall j \in \mathcal{G}_n, \tag{4.49}$$

where $x'_{\mathrm{d}j}$ is the transient reactance of generator j and, as defined by (4.41), V_n is the voltage magnitude at the bus to which generator j is connected. Furthermore, since the pre-fault is a steady-state synchronous condition,

$$\omega_j^0 = 1, \quad \forall j \in \mathcal{G}. \tag{4.50}$$

4.3.1.5 Discrete swing equations

The swing equations (4.2) and (4.3) are discretized using the trapezoidal rule. Thus, generator rotor angles and speeds for a generic time step $(t + 1)$ are

defined by the following equations:

$$\delta_j^{t+1} - \delta_j^t - \frac{t_{\text{step}}}{2}\omega_{\text{b}}(\omega_j^{t+1} - 1 + \omega_j^t - 1) = 0, \quad \forall t \in \mathcal{T}, \forall j \in \mathcal{G}, \tag{4.51}$$

$$\omega_j^{t+1} - \omega_j^t - \frac{t_{\text{step}}}{2}\frac{1}{M_j}(P_{\text{m}j} - P_{\text{e}j}^{t+1} + P_{\text{m}j} - P_{\text{e}j}^t) = 0, \quad \forall t \in \mathcal{T}, \forall j \in \mathcal{G}, \tag{4.52}$$

where

$$P_{\text{e}j}^t = E_j' \sum_{\ell} E_\ell'[B_{j\ell}^t \sin(\delta_j^t - \delta_\ell^t) + G_{j\ell}^t \cos(\delta_j^t - \delta_\ell^t)], \tag{4.53}$$

and $P_{\text{m}j} = P_{\text{G}j}$. In (4.51) and (4.52), t_{step} represents the integration time step used in the trapezoidal rule.

Note that the reduced admittance matrix depends on the network topology; therefore in (4.53), the values of $B_{j\ell}^t$ and $G_{j\ell}^t$ are different for the during-fault and post-fault states and consequently depend on time.

4.3.1.6 Transient stability limit

As stated in Subsection 4.1.3, if a time-domain simulation proves to be unstable, the SIME method identifies the critical machines, the time t_{u} and the OMIB rotor unstable angle δ_{u} for which the instability conditions are reached. Similarly, if a time-domain simulation show first-swing stability, the SIME method provides the time t_{r} and the OMIB rotor return angle δ_{r} for which the OMIB equivalent meets the first-swing stability conditions. The SIME criterion is used to define transient stability limits in the OPF problem as follows. For each time step, the equivalent OMIB rotor angle must be below the instability limit provided by SIME.

$$\delta^t \leq \delta^{\max}, \quad \forall t \in \mathcal{T}, \tag{4.54}$$

where $\mathcal{T}$ is as small as possible to reduce computing time but larger than the first swing of the system. The equivalent OMIB rotor angle is computed as

$$\delta^t = \frac{1}{M_{\text{C}}} \sum_{j \in \mathcal{G}_{\text{C}}} M_j \delta_j^t - \frac{1}{M_{\text{NC}}} \sum_{j \in \mathcal{G}_{\text{NC}}} M_j \delta_j^t, \tag{4.55}$$

where

$$M_{\mathrm{C}} = \sum_{j \in \mathcal{G}_{\mathrm{C}}} M_j \quad \text{and} \quad M_{\mathrm{NC}} = \sum_{j \in \mathcal{G}_{\mathrm{NC}}} M_j. \tag{4.56}$$

4.3.1.7 Other constraints

The proposed TSC-OPF problem includes the following additional constraints:

$$-\pi \leq \theta_n \leq \pi, \quad \forall n \in \mathcal{N}, \tag{4.57}$$

$$\theta_{\mathrm{ref}} = 0. \tag{4.58}$$

Equation (4.57) is included to reduce the feasibility region, thereby causing the OPF problem to converge more rapidly in general.

4.3.1.8 TSC-OPF problem formulation

The formulation of the TSC-OPF problem is summarized below:

$$\text{Minimize} \quad (4.29)$$

subject to

1. Pre-contingency power flow equations (4.30)-(4.31).
2. Technical limits (4.44)-(4.47).
3. Initial values of machine rotor angles, rotor speeds and electromotive forces (4.48)-(4.50).
4. Discrete swing equations (4.51)-(4.52).
5. Transient stability limit (4.54).
6. Other constraints (4.57)-(4.58).

The above formulation can be easily extended to the multi-contingency case by including constraints (4.51)-(4.52) and (4.54) for each contingency considered.

4.3.2 Security Redispatching Description

Converting the whole time domain simulation of the system transient stability model into a set of algebraic equations results in a very large number of equations to be included in an OPF. Solving this non-linear OPF problem may require prohibitive computational times and memory burdens, and may lead to convergence issues. To reduce the number of constraints, the reduced admittance matrix is used, and the OMIB equivalent trajectory is constrained only during the first swing of the system. The latter allows the inclusion of discretized transient stability equations (4.51)-(4.52) and (4.54) for only a few seconds after the fault occurs.

The proposed procedure is as follows.

1. *Base-Case Solution.* The base-case solution corresponds to the solution of a dispatching procedure (e.g., a market clearing procedure) adjusted by losses. Specifically, the base-case solution is obtained from the OPF problem described in Appendix A.

2. *Contingency Analysis.* The critical contingencies are identified by applying the procedure described in Section 4.2, i.e., carrying out a time-domain simulation complemented by SIME. For unstable contingencies, SIME outputs the sets of critical and non-critical machines. Equation (4.55) incorporates this information. The system can become unstable in two ways:

   (a) First-swing instability. In this case, the instability angle δ_{u} provided by SIME is used to define the transient stability limit $\delta^{\max}$ in equation (4.54).

   (b) Multi-swing instability. In this case, the OMIB equivalent has a return angle δ_{r} in the first swing. However, after some cycles, the system loses synchronism. The return angle value δ_{r} is used to define the transient stability limit $\delta^{\max}$ in equation (4.54). To avoid multi-swing phenomena, $\delta^{\max}$ is set to $\delta_{\mathrm{r}} - \Delta\delta$, i.e., $\delta^{\max}$ is fixed to a value smaller than δ_{r}. In this way, the system is forced to reach the first-swing stability conditions for a smaller value of the OMIB rotor

angle. This implies a reduction in the energy of the OMIB system and, hence, a reduction in the risk of multi-swing instability. The value of the decrement $\Delta\delta$ is defined based on a heuristic criterion.

3. *Solve the TSC-OPF Problem.* The TSC-OPF problem described in Subsection 4.3.1.8 is solved, and the new operating condition is obtained.

4. *Solution Checking.* A time-domain simulation that includes SIME is solved for the new operating condition obtained in step 3. This simulation is necessary to determine the transient stability of the new operating condition. Three different cases can be encountered:

   (a) The system is stable, and the procedure stops.

   (b) The system is first-swing unstable. This result is due to the fact that the reduced admittance $\mathbf{Y}^t_{\text{bus}}$ used in the optimization problem was calculated for the previous operating condition, which exhibits different voltage values than the solution obtained in step 3 (see equation (4.4)). Thus, the reduced admittance matrix is updated and the transient stability limit $\delta^{\max}$ is fixed to the new value of δ_{u}. The procedure continues at step 3.

   (c) The system is multi-swing unstable. In this case, the OMIB equivalent has a return angle δ_{r} in the first swing. However, after some cycles, the system loses synchronism. The return angle value δ_{r} is used to define the new transient stability limit $\delta^{\max}$. To avoid multi-swing phenomena, $\delta^{\max}$ is set to $\delta_{\text{r}} - \Delta\delta$. Finally, the reduced admittance matrix $\mathbf{Y}^t_{\text{bus}}$ is updated. The procedure continues in step 3.

The flowchart depicted in Fig. 4.5 illustrates the proposed procedure.

Note that, in the first iteration, the TSC-OPF problem is initialized with the base-case solution, while in the following iterations the TSC-OPF problem is initialized with the solution from the previous iteration. In the simulations, convexity problems have not been observed, mainly due to the fact that the initial solution is generally close to the optimum.

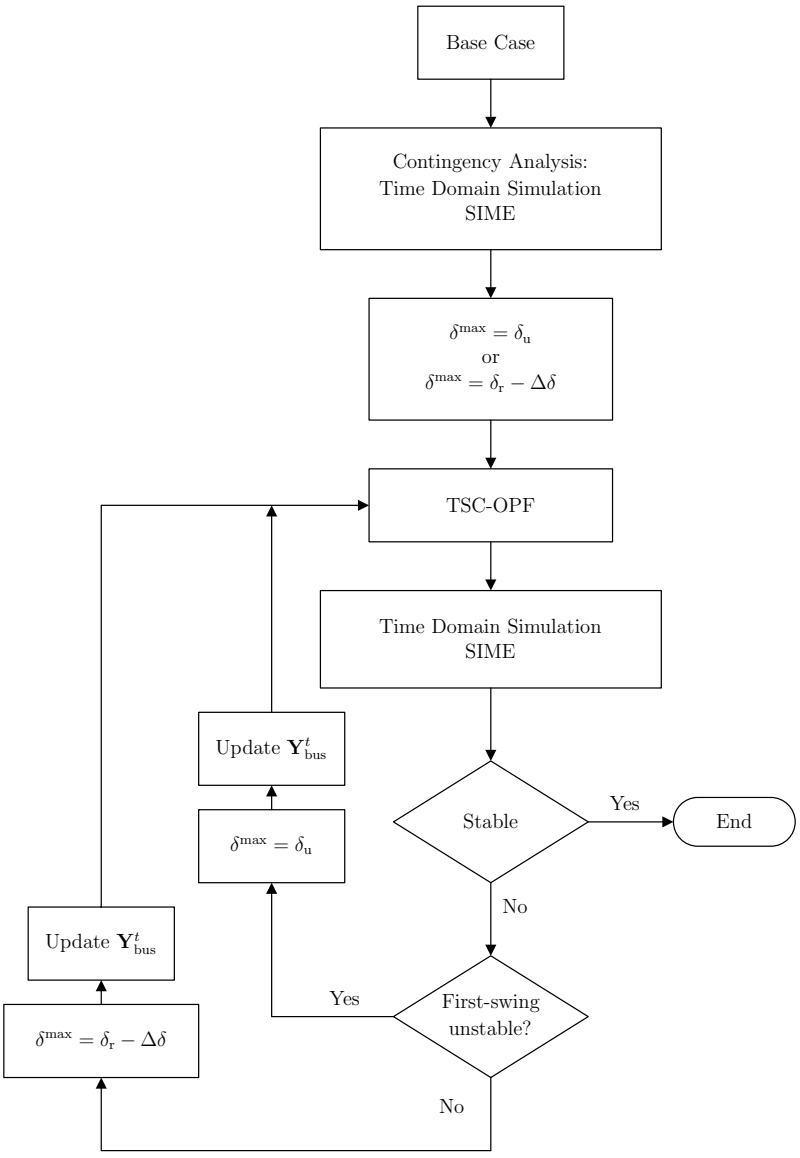

Figure 4.5: Transient stability. Flow chart of the proposed procedure.

For simplicity, it is assumed that a single harmful contingency is identified at step 2. However, as discussed in Subsection 4.3.1.8, multiple contingencies can readily be taken into account by including equations (4.51)-(4.52) and (4.54) for each contingency in the TSC-OPF problem.

There may be situations in which the power adjustments determined by

the proposed procedure modify the instability mode, i.e., they change the set of critical/non-critical machines. This requires including equations (4.54) and (4.55) for both the previous and the new instability mode.

4.4 Transient Stability - Illustrative Example

For illustration purposes, the proposed redispatching procedure is applied to the WECC 9-bus, 3-machine system. The main goal of this example is to clarify the behavior of the transient stability constraints based on SIME in the TSC-OPF problem. To this end, each iteration of the proposed procedure is described in detail.

The generators of the system are represented using a classical model and the loads are modeled as constant impedances. These models are described in Appendix C. Moreover, the one-line diagram and the data for this system are provided in Appendix D.

4.4.1 Base Case

The base-case solution is obtained from the OPF problem described in Appendix A. This base-case solution is identical to the base-case solution provided in Table 4.1 of Chapter 3, which is repeated here for clarity.

4.4.2 Contingency Analysis

A time-domain simulation that includes SIME is solved for the base-case operating condition. The considered contingency is a three-phase-to-ground symmetrical fault that takes place at bus 7 and is cleared after 0.3 s by tripping line 7-5. The clearing time was chosen to force transient instability. The whole simulation time is 5 s.

The base-case operating condition is first-swing unstable for the contingency considered. The OMIB equivalent for the base case is unstable since the OMIB rotor angle δ increases beyond the admissible angle $\delta_{\mathrm{u}} = 155.01$ degrees after $t_{\mathrm{u}} = 0.45$ s. Generators 2 and 3 compose the set of critical machines,

Table 4.1: Transient stability illustrative example. WECC 9-bus, 3-machine system: Base-case solution.

Bus #	Gen. #	Dem. #	$P^{\mathrm{A}}_{\mathrm{G}j}$ [p.u.]	$Q^{\mathrm{A}}_{\mathrm{G}j}$ [p.u.]	$P^{\mathrm{A}}_{\mathrm{D}i}$ [p.u.]	$Q^{\mathrm{A}}_{\mathrm{D}i}$ [p.u.]	V^{A}_{n} [p.u.]	θ^{A}_{n} [rad.]
1	1	-	1.2633	0.2510	0	0	1.1000	0
2	2	-	1.3642	0.0856	0	0	1.1000	0.0514
3	3	-	1.1955	-0.0592	0	0	1.1000	0.0476
4	-	-	0	0	0	0	1.0889	-0.0608
5	-	1	0	0	1.5000	0.6000	1.0595	-0.1164
6	-	2	0	0	1.0800	0.3600	1.0767	-0.0970
7	-	-	0	0	0	0	1.0979	-0.0193
8	-	3	0	0	1.2000	0.4200	1.0863	-0.0567
9	-	-	0	0	0	0	1.1050	-0.0101

whereas generator 1 is the non-critical machine. Figure 4.6 shows the unstable behavior of the base-case OMIB equivalent and the rotor angle trajectories after the occurrence of the contingency and the subsequent fault clearing. Rotor angle trajectories are depicted using the Center Of Inertia (COI) of the system as a reference.

4.4.3 Procedure Iterations

Once the sets of critical and non-critical machines have been identified and the OMIB rotor unstable angle has been calculated, the TSC-OPF problem described in Subsection 4.3.1.8 is solved. The discretized dynamic equations (4.51)-(4.52) are included for the first two seconds. Setting $\mathcal{T} = [0, 2]$ s is sufficient to reveal transient instabilities and considerably reduces the computational burden of the proposed OPF problem. The integration time step t_{step} is set to 0.05 s, and $\delta^{\max}$ is set to the value of δ_{u} provided by SIME, i.e., $\delta^{\max} = 155.01$ degrees. Finally, the reduced admittance matrix $\mathbf{Y}^{t}_{\mathrm{bus}}$ that

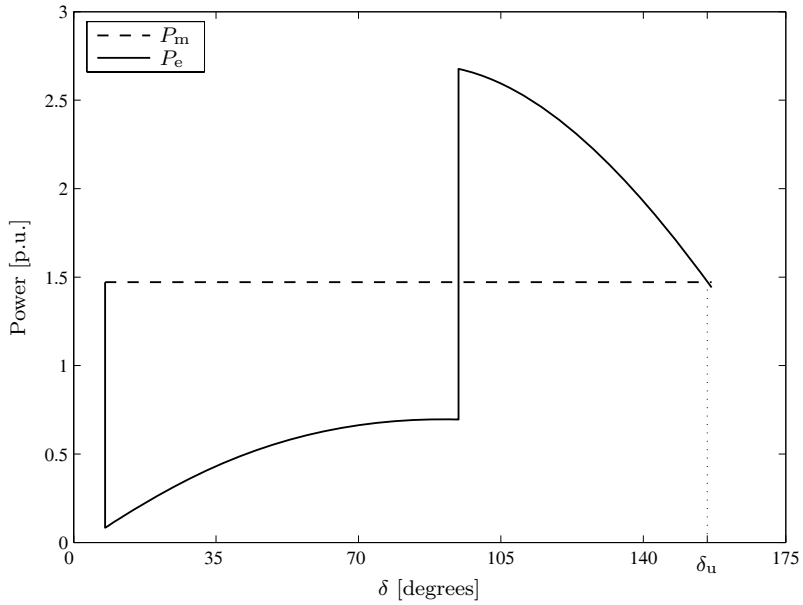

(a)

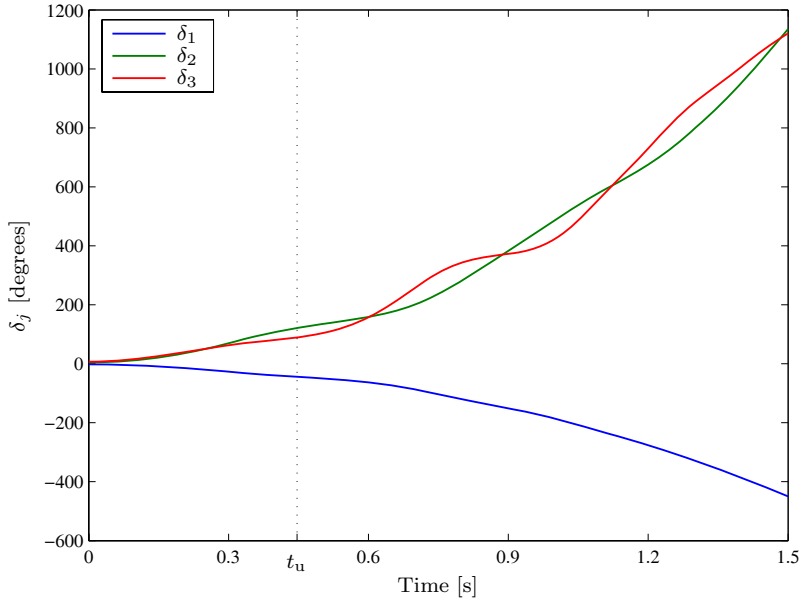

(b)

Figure 4.6: Transient stability illustrative example. WECC 9-bus, 3-machine system: (a) OMIB plot and (b) rotor angle trajectories. Unstable base case.

corresponds to the base-case operating condition is computed. Table 4.2 provides the operating condition corresponding to the solution of the TSC-OPF

problem.

Table 4.2: Transient stability illustrative example. WECC 9-bus, 3-machine system: Solution for the first iteration of the proposed procedure.

Bus #	Gen. #	Dem. #	$P_{\mathrm{G}j}$ [p.u.]	$Q_{\mathrm{G}j}$ [p.u.]	$P_{\mathrm{D}i}$ [p.u.]	$Q_{\mathrm{D}i}$ [p.u.]	V_n [p.u.]	θ_n [rad.]
1	1	-	1.4312	0.2498	0	0	1.1000	0
2	2	-	1.1925	0.0733	0	0	1.1000	0.0112
3	3	-	1.1955	-0.0593	0	0	1.1000	0.0254
4	-	-	0	0	0	0	1.0895	-0.0688
5	-	1	0	0	1.5000	0.6000	1.0606	-0.1323
6	-	2	0	0	1.0800	0.3600	1.0774	-0.1099
7	-	-	0	0	0	0	1.0979	-0.0506
8	-	3	0	0	1.2000	0.4200	1.0863	-0.0842
9	-	-	0	0	0	0	1.1050	-0.0323

The transient stability of the new operating condition obtained after solving the TSC-OPF is checked. A time-domain simulation that includes SIME is carried out. In this first iteration, the TSC-OPF solution is multi-swing unstable: the trajectory of the OMIB equivalent shows a return angle $\delta_{\mathrm{r}} = 131.11$ degrees in the first swing at $t_{\mathrm{r}} = 0.56$ s but the system loses synchronism at $t_{\mathrm{u}} = 1.81$ s. Figure 4.7 confirms that this is a multi-swing case. The critical machines are generators 2 and 3 again, whereas generator 1 is the non-critical machine.

A new transient stability limit is defined based on the return angle provided by SIME. Specifically, $\delta^{\max}$ is set to $\delta_{\mathrm{r}} - \Delta\delta$ using $\Delta\delta = 1$ degree, i.e., $\delta^{\max} = 130.11$ degrees. The reduced admittance matrix $\mathbf{Y}^{t}_{\mathrm{bus}}$ is computed for the operating condition that results from the solution of the first iteration, and the TSC-OPF problem is solved again to obtain a new operating condition. Table 4.3 shows this operating condition.

The transient stability of this new operating condition is checked using a

Table 4.3: Transient stability illustrative example. WECC 9-bus, 3-machine system: Solution for the second iteration of the proposed procedure.

Bus #	Gen. #	Dem. #	$P_{\mathrm{G}j}$ [p.u.]	$Q_{\mathrm{G}j}$ [p.u.]	$P_{\mathrm{D}i}$ [p.u.]	$Q_{\mathrm{D}i}$ [p.u.]	V_n [p.u.]	θ_n [rad.]
1	1	-	1.4771	0.2500	0	0	1.1000	0
2	2	-	1.1764	0.0724	0	0	1.1000	0.0074
3	3	-	1.1955	-0.0591	0	0	1.1000	0.0233
4	-	-	0	0	0	0	1.0895	-0.0696
5	-	1	0	0	1.5000	0.6000	1.0607	-0.1328
6	-	2	0	0	1.0800	0.3600	1.0775	-0.1112
7	-	-	0	0	0	0	1.0979	-0.0535
8	-	3	0	0	1.2000	0.4200	1.0863	-0.0868
9	-	-	0	0	0	0	1.1050	-0.0343

time-domain simulation that includes SIME. In this second iteration, the TSC-OPF solution is stable. Figure 4.8 shows that the OMIB equivalent and rotor angle trajectories remain stable throughout the time-domain simulation. The OMIB return angle is $\delta_{\mathrm{r}} = 126.19$ degrees in the first-swing at $t_{\mathrm{r}} = 0.54$ s.

Table 4.4 provides the generator active powers for the base case and the redispatching actions that correspond to the solution after each iteration of the proposed TSC-OPF-based procedure. Observe that the redispatching actions consist in transferring active power generation from the critical machines, i.e., the "advanced" ones, to the non-critical machines. Specifically, the active power production is transferred from generator 2 to generator 1, whereas the load powers remain unaltered.

4.5 Transient Stability - Case Studies

In this section the results of two case studies based on the New England 39-bus, 10-machine system and a real-world 1228-bus, 292-machine system are

Table 4.4: Transient stability illustrative example. WECC 9-bus, 3-machine system: Generator active powers for the base case and redispatching actions for each iteration of the procedure.

	Base Case	Iteration 1		Iteration 2	
Generator #	$P_{\mathrm{G}j}^{\mathrm{A}}$ [p.u.]	$\Delta P_{\mathrm{G}j}^{\mathrm{up}}$ [p.u.]	$\Delta P_{\mathrm{G}j}^{\mathrm{down}}$ [p.u.]	$\Delta P_{\mathrm{G}j}^{\mathrm{up}}$ [p.u.]	$\Delta P_{\mathrm{G}j}^{\mathrm{down}}$ [p.u.]
1	1.2633	0.1679	0	0.1838	0
2	1.3642	0	0.1716	0	0.1878
3	1.1955	0	0	0	0

presented.

4.5.1 New England 39-Bus, 10-Machine System

As in the illustrative example of Section 4.4, the generators are represented with a classical model, and the loads are modeled as constant impedances. These models are described in Appendix C, whereas the one-line diagram and data for this system are provided in Appendix D.

4.5.1.1 Base Case

The base-case solution is obtained from the OPF problem described in Appendix A. The result from this problem is provided in Appendix D.

4.5.1.2 Contingency Analysis

For this system, 35 possible contingencies are analyzed. Tables D.20 and D.21 in Appendix D contains the network configuration of this system. The contingencies analyzed affect the first 35 branches described in these tables. Each contingency consists of a three-phase-to-ground symmetrical fault at the first bus of each line (bus "From"), which is cleared after 0.08 s ($\simeq$ 5 cycles) by tripping the line. None of these contingencies leads to generator islanding. For each of these contingencies, a time-domain simulation including SIME is

performed. The whole simulation spans 5 s, and an integration time step of 0.01 s is used. Six contingencies lead the system to transient instability. Table 4.5 lists the instability type, the critical machines, the OMIB rotor unstable angle and the time to instability for these six contingencies. Table 4.5 also provides the OMIB rotor return angle in the first swing in the case of multi-swing instability.

Table 4.5: Transient stability case study. New England 39-bus, 10-machine system: Results of the contingency analysis.

Fault at bus	Line tripped	Instability type	Critical machines	δ_u [degrees]	t_u [s]	δ_r [degrees]
21	16 - 21	multi-swing	1,2,3,4,5,6,7,8,9	95.89	3.49	109.14
22	21 - 22	first-swing	6,7	127.62	0.70	-
25	2 - 25	first-swing	1,2,3,4,5,6,7,8,9	89.21	0.77	-
26	26 - 29	first-swing	9	112.50	0.51	-
28	26 - 28	first-swing	9	105.86	0.43	-
28	28 - 29	first-swing	9	107.03	0.44	-

Figures 4.9-4.14 show the unstable behavior of the OMIB equivalent and of the rotor angle trajectories for the base case after the occurrence of the contingencies listed in Table 4.5 and the subsequent fault clearing. Note that the time-domain simulations were stopped at the very instant that synchronism was lost, i.e., when instability conditions (4.21)-(4.23) were met. Rotor angle trajectories are depicted using the COI of the system as a reference. For these contingencies, the system suffers first-swing instability, except for the fault at bus 21 cleared by tripping the line 16-21, which causes the system to experience multi-swing instability. In this latter case, as Figure 4.9 shows, the system remains stable in the first swing but loses synchronism in the second swing due to the separation of generators 1-9 from generator 10. Note that, in this system, generator 10 is the equivalent of a big external network that is represented by a machine with large inertia.

The fault at bus 22 cleared by tripping the line 21-22 results in the separation of generators 6 and 7 from the rest of the system, as shown in Figure 4.10. Observe that the bus and the line affected by the contingency are close to these generators, which leads to their loss of synchronism.

The fault at bus 25 cleared by tripping the line 2-25 results in the loss of synchronism of generators 1-9 with respect to generator 10. This is shown in Figure 4.11.

Figures 4.12, 4.13 and 4.14 depict the power system response to the fault at bus 26 cleared by tripping the line 26-29, fault at bus 28 cleared by tripping the line 26-28, and fault at bus 28 cleared by tripping the line 28-29, respectively. In these three cases, generator 9 loses synchronism with respect to the rest of the system mainly due to the proximity of generator 9 to the buses and lines affected by these contingencies.

4.5.1.3 Procedure Iterations

For each of the contingencies listed in Table 4.5, a set of equations (4.51)-(4.52) and (4.54) is included in the TSC-OPF problem. To properly reproduce the characteristics of the contingencies (all faults are cleared after 0.08 s), these equations are included in the TSC-OPF problem for $\mathcal{T} = [0, 1.98]$ using $t_{\text{step}} = 0.04$ s for the during-fault period and $t_{\text{step}} = 0.05$ s for the post-fault period. The transient stability limit for each contingency is initially set to the corresponding value of δ_{u}, as listed in Table 4.5, except for the contingency at bus 21 (multi-swing case), that is set to $\delta_{\text{r}} - \Delta\delta$ using $\Delta\delta = 1$ degrees. These values are updated in each iteration, as explained in Subsection 4.3.2. Similarly, the reduced admittance matrix $\mathbf{Y}^{t}_{\text{bus}}$ is evaluated for the base case and updated in each iteration.

The procedure requires three iterations to obtain the solution. This solution corresponds to a stable operating condition with respect to the six contingencies considered. Table 4.6 provides the generator active powers for the base case together with the redispatching actions obtained as solution. No load curtailment is needed to stabilize the system. The adjustments correspond to active power transfers from generators 6 and 9 to generators 3 and 10. These

Table 4.6: Transient stability case study. New England 39-bus, 10-machine system: Generator active powers for the base case and redispatching actions.

Generator #	$P_{\mathrm{G}j}^{\mathrm{A}}$ [p.u.]	$\Delta P_{\mathrm{G}j}^{\mathrm{up}}$ [p.u.]	$\Delta P_{\mathrm{G}j}^{\mathrm{down}}$ [p.u.]
1	2.9134	0	0
2	5.9783	0	0
3	7.8748	1.3252	0
4	7.3089	0	0
5	5.7801	0	0
6	7.4560	0	1.1063
7	6.4704	0	0
8	6.1246	0	0
9	9.4772	0	0.8795
10	11.2828	0.6011	0

are the most economical redispatching actions over the base case that stabilize the system with respect to the contingencies considered. Figures 4.15-4.20 depict the behavior of the OMIB equivalent and the rotor angle trajectories after the occurrence of each contingency and the subsequent fault clearing, for the final iteration of the proposed procedure. From the rotor angle trajectories shown in Figures 4.15-4.20, it follows that, for the operating condition obtained after redispatching, the power system remains stable if any of the considered contingencies occurs. All cases exhibit similar stable behavior.

It is noteworthy to mention that the operating condition obtained after applying the proposed redispatching procedure is stable if any of the initial set of contingencies (35 contingencies) occurs. This case study illustrates the ability of the proposed redispatching procedure to tackle multi-contingency cases.

4.5.2 Simulation Times

This subsection analyzes the computational requirements of the proposed procedure for the New England 39-bus, 10-machine system. The starting point of the procedure is the base-case operating condition obtained from the OPF problem described in Appendix A. This step takes 0.14 s.

In the contingency filtering procedure, 35 contingencies are analyzed. This step involves a time-domain simulation of each contingency. If the SIME method identifies an unstable behavior, the time-domain simulation stops. If the system remains stable, the time-domain simulation is performed for a total simulation time of 5 s. Table 4.7 lists the CPU times of the time-domain simulations for the six unstable contingencies. All the other contingencies are stable, and their time-domain simulations take an average CPU time of 5.81 s. The contingency analysis requires a total CPU time of 176.49 s. This computing time can be reduced by applying parallel computation techniques.

Table 4.7: Transient stability case study. New England 39-bus, 10-machine system: Computational requirements for the time-domain simulation of the contingency analysis for unstable cases.

Fault at bus	Line tripped	CPU [s]
21	16 - 21	4.0398
22	21 - 22	0.9306
25	2 - 25	1.0448
26	26 - 29	0.7075
28	26 - 28	0.6357
28	28 - 29	0.6335
Total		7.9921

Each iteration of the proposed procedure involves solving the TSC-OPF problem and checking the solution. The TSC-OPF problem includes transient

stability constraints for six contingencies. Solution checking implies the time-domain simulation of these six contingencies. Table 4.8 provides the CPU times per iteration and the total CPU times of these steps. The total CPU time of the proposed procedure is 120.82 s.

Table 4.8: Transient stability case study. New England 39-bus, 10-machine system: Computational requirements for the procedure iterations.

	Iteration 1 CPU [s]	Iteration 2 CPU [s]	Iteration 3 CPU [s]	Total CPU [s]
TSC-OPF problem	12.8900	3.1300	3.3900	19.4100
Time-domain simulations	33.0136	33.5337	34.8602	101.4075
Total	45.9036	36.6637	38.2502	120.8175

Solution checking by means of time-domain simulations is the step with the highest computational burden. Table 4.9 shows the CPU times of the time-domain simulation of each contingency for each iteration. The computing times of this step can be reduced by using parallel computation techniques. For example, if six processors are available, the computation time for the solution checking is reduced to a CPU time of less than 6 s.

4.5.3 Real-World 1228-Bus, 292-Machine System

A real-world 1228-bus, 1903-branch and 292-machine system is considered in this subsection to show that the proposed technique can be applied to a real-world power system. All machines are modeled using a classical model. The initial power flow solution is assumed to be the result of a market clearing procedure that does not include transient stability constraints.

Figure 4.21 depicts the generator rotor angle trajectories of the system following a three-phase-to-ground symmetrical bus fault cleared after 0.2 s. The time-domain simulation stops at the instant that correspond to the loss of synchronism. The critical machine group comprises 11 machines that suffer loss of synchronism. The base-case OMIB equivalent is unstable since the rotor

Table 4.9: Transient stability case study. New England 39-bus, 10-machine system: Computational requirements related to the time-domain simulations of the procedure iterations.

Fault at bus	Line tripped	Iteration 1 CPU [s]	Iteration 2 CPU [s]	Iteration 3 CPU [s]
21	21 - 16	5.7456	5.8868	5.8746
22	22 - 21	4.0141	3.9214	5.7940
25	25 - 2	5.9785	6.1502	5.9669
26	26 - 29	5.8770	5.9813	5.8352
28	28 - 26	5.6799	5.7777	5.6874
28	28 - 29	5.7186	5.8163	5.7020
Total		33.0136	33.5337	34.8602

angle δ increases beyond the admissible angle $\delta_{\mathrm{u}} = 157.75$ degrees, which is reached at $t_{\mathrm{u}} = 0.4375$ s.

Therefore, a set of equations (4.51)-(4.52) and (4.54) is included in the TSC-OPF problem for the time interval $\mathcal{T} = [0, 2]$ s. The time step used in this case is $\Delta t = 0.1$ s. The whole procedure converges in one iteration, no multi-swing instability appears in this case. The resulting trajectories of the generator rotor angles after redispatching are shown in Figure 4.22.

4.5.3.1 Simulation Times

In this case study, the base-case solution is obtained by solving a power flow of the system. Furthermore, a pre-specified single contingency is considered; therefore, contingency analysis is not performed. The time-domain simulation of the considered contingency for the base-case operating condition takes 8.04 s. To stabilize the system, only one iteration of the proposed procedure is needed. In this single iteration, the CPU time required to solve the TSC-OPF problem is about 57.62 minutes. If the OPF is solved without transient stability constraints, the computational time is 4.76 minutes. Thus, the solution

of the TSC-OPF requires 12.01 times the duration required to solve the OPF without transient stability constraints. The solution obtained is checked with a time-domain simulation of 5 s, which confirms the stable behavior of the system. This time-domain simulation takes 19.31 s. The total CPU time is thus 57.94 minutes.

In this case study, the highest computational burden corresponds to solving the TSC-OPF problem mainly due to its large size.

4.6 Summary and Conclusions

This chapter has presented a redispatching procedure to ensure transient stability. It relies on an OPF model with embedded transient stability constraints. These constraints include a transient stability limit that is established using the information provided by the SIME method. The proposed redispatching procedure ensures transient stability of the system against major disturbances, e.g., faults and/or line outages, which may cause the system to suffer first-swing or multi-swing instability phenomena.

In addition to power flow constraints and bounds, the resulting TSC-OPF model includes discrete time equations that describe the time evolution of all machines in the system and a stability constraint involving the OMIB equivalent defined by the SIME method. The time-domain integration is solved only for a limited time interval, which reduces the size of the optimization problem.

The proposed procedure has been illustrated and tested on the WECC 9-bus, 3-machine system, the New England 39-bus, 10-Machine system, and a real-world 1228-bus, 292-machine system.

The proposed redispatching procedure outputs the minimum-cost preventive redispatching actions for the base-case solution that restore transient stability with respect to the considered contingencies. Simulation results confirm that the proposed procedure can successfully restore transient stability if the system is affected by both first-swing and multi-swing instability phenomena.

An important characteristic of the proposed procedure is its transient stability limit. This limit is established through the SIME method, which provides an objective stability criterion. This fact makes the proposed procedure more

transparent to market participants than other existing approaches based on heuristic criteria.

The stability criterion used in the proposed procedure is independent of the power system model. Therefore, more detailed models can be used, other devices can be considered (e.g., FACTS devices), and other transient stability constraints (e.g., limits on bus voltage magnitudes during transients) can be included in the TSC-OPF problem. However, this can lead to an OPF problem of intractable size.

The simulation carried out for the 1228-bus, 292-machine system shows the applicability of the proposed procedure to real-world large-scale systems. The solution requires a computation time that is probably unacceptable for real-time operation requirements. However, it should be noted that the TSC-OPF problem is solved using a general-purpose solver. The development of an *ad hoc* solution algorithm and the use of more powerful computers may reduce computation times significantly.

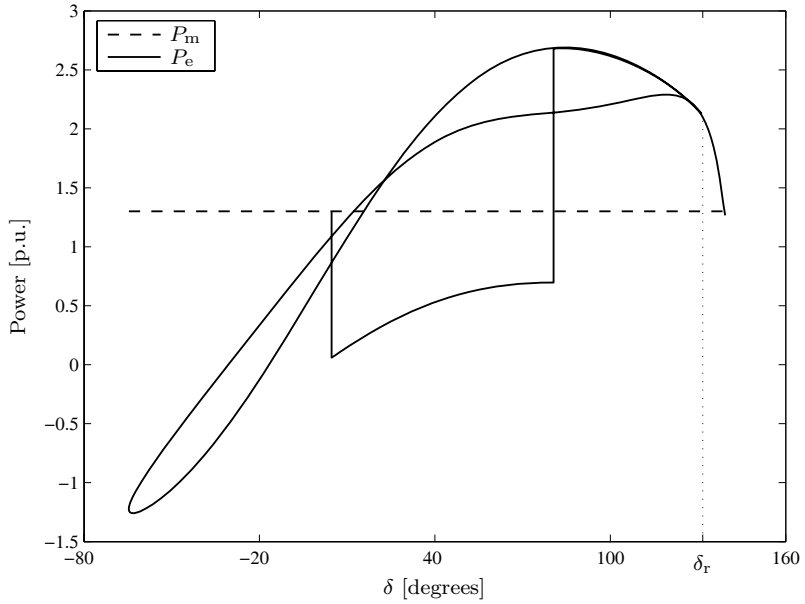

(a)

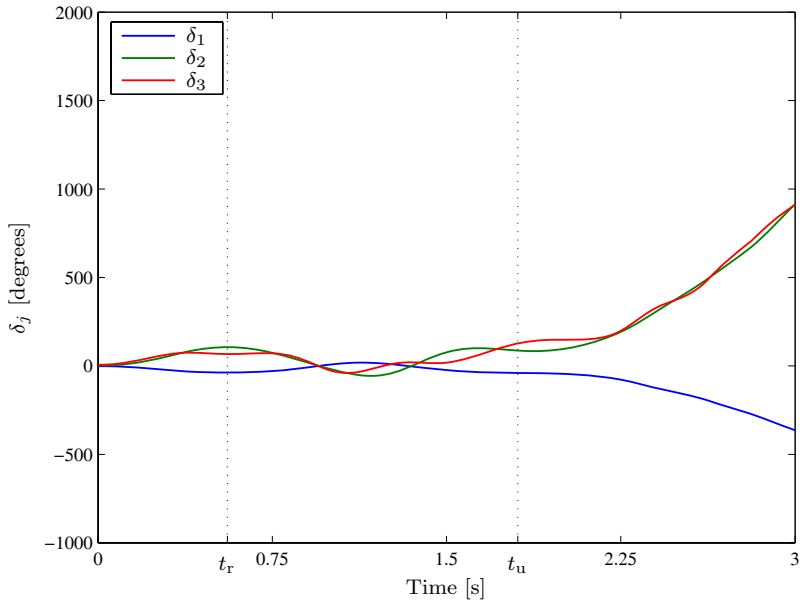

(b)

Figure 4.7: Transient stability illustrative example. WECC 9-bus, 3-machine system: (a) OMIB plot and (b) rotor angle trajectories. First iteration of the proposed procedure. The system exhibits multi-swing instability.

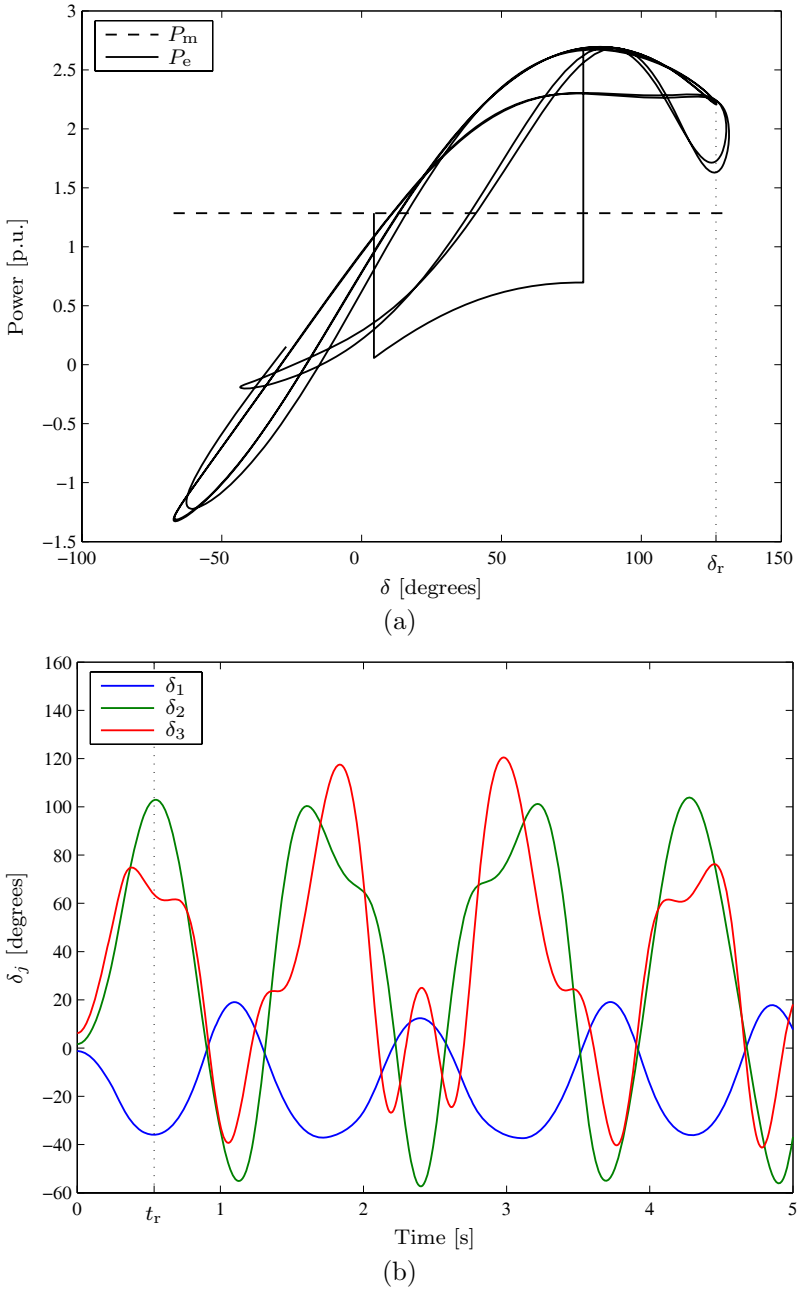

Figure 4.8: Transient stability illustrative example. WECC 9-bus, 3-machine system: (a) OMIB plot and (b) rotor angle trajectories. Second and final iteration of the proposed procedure. The system is stable.

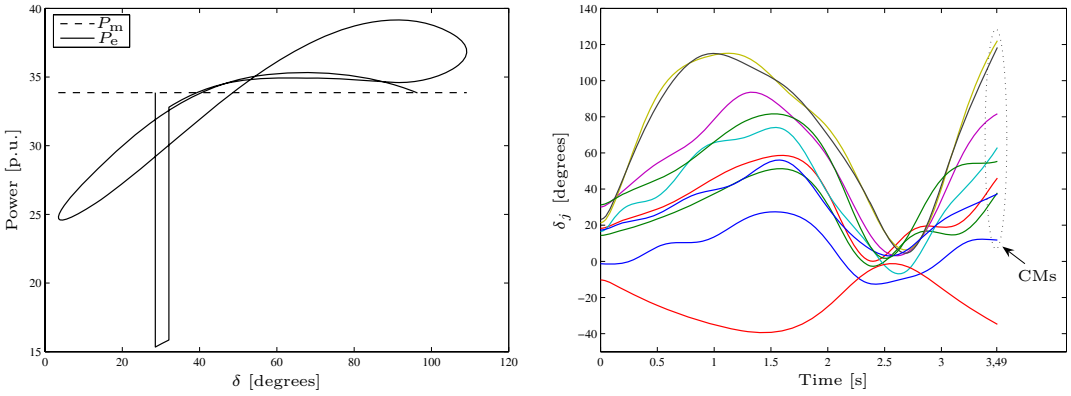

(a) (b)

Figure 4.9: Transient stability case study. New England 39-bus, 10-machine system: (a) OMIB plot and (b) rotor angle trajectories for the base case. Fault at bus 21 cleared by tripping the line 16-21.

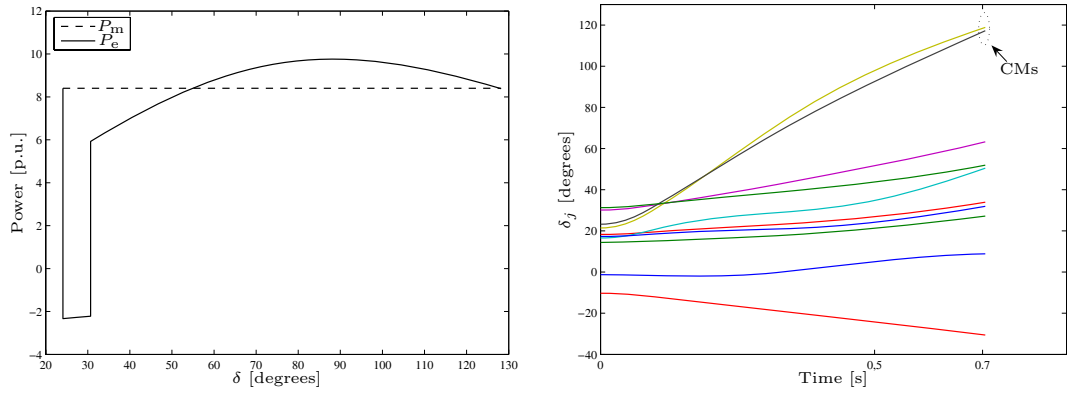

(a) (b)

Figure 4.10: Transient stability case study. New England 39-bus, 10-machine system: (a) OMIB plot and (b) rotor angle trajectories for the base case. Fault at bus 22 cleared by tripping the line 21-22.

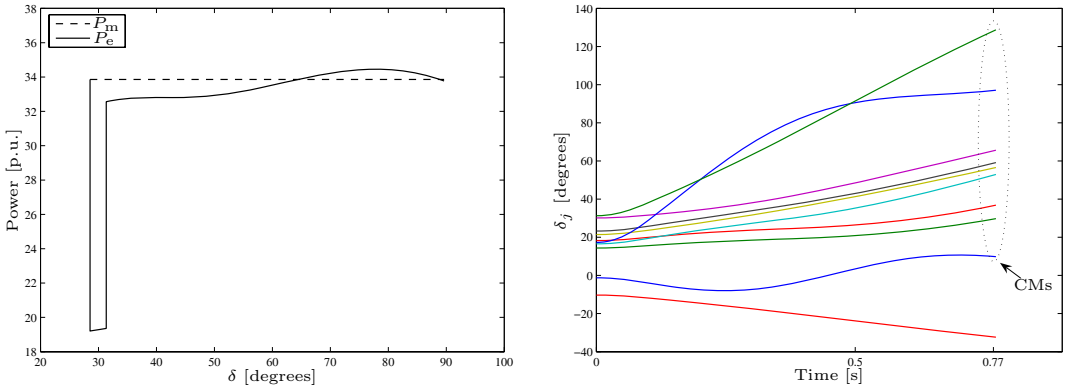

(a) (b)

Figure 4.11: Transient stability case study. New England 39-bus, 10-machine system: (a) OMIB plot and (b) rotor angle trajectories for the base case. Fault at bus 25 cleared by tripping the line 2-25.

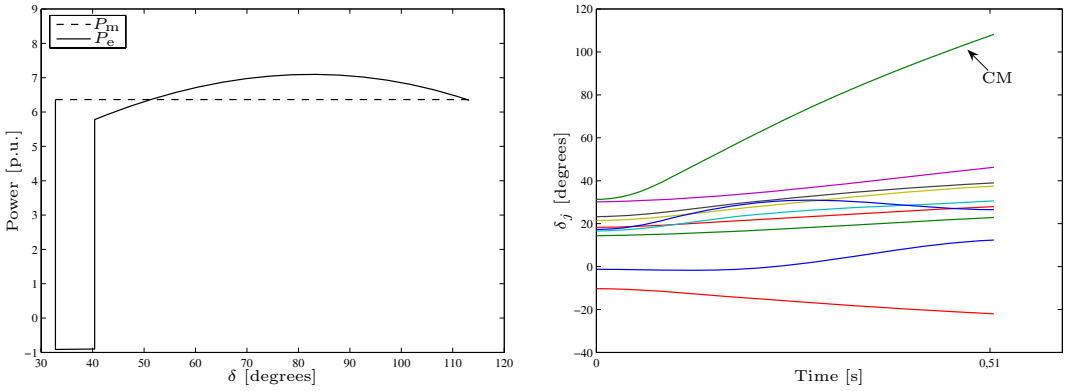

(a) (b)

Figure 4.12: Transient stability case study. New England 39-bus, 10-machine system: (a) OMIB plot and (b) rotor angle trajectories for the base case. Fault at bus 26 cleared by tripping the line 26-29.

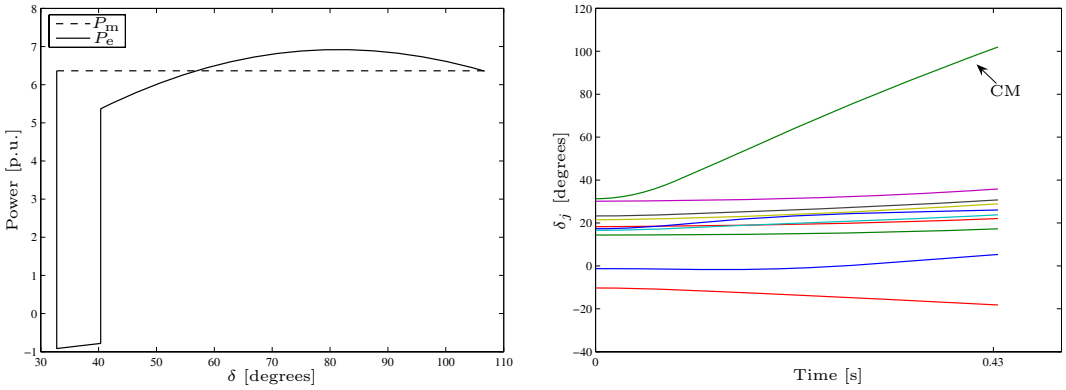

(a) (b)

Figure 4.13: Transient stability case study. New England 39-bus, 10-machine system: (a) OMIB plot and (b) rotor angle trajectories for the base case. Fault at bus 28 cleared by tripping the line 26-28.

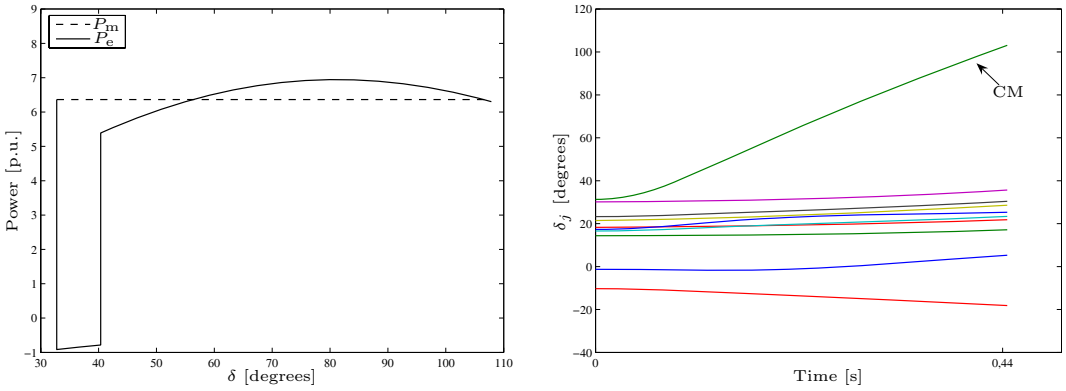

(a) (b)

Figure 4.14: Transient stability case study. New England 39-bus, 10-machine system: (a) OMIB plot and (b) rotor angle trajectories for the base case. Fault at bus 28 cleared by tripping the line 28-29.

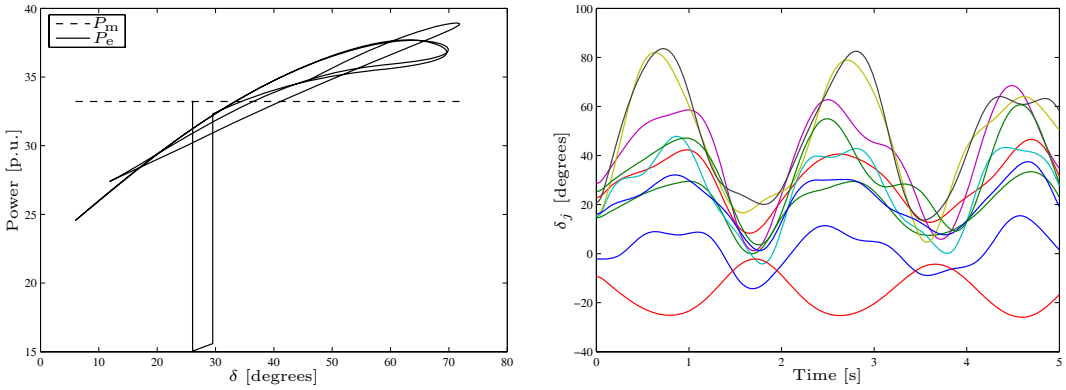

(a) (b)

Figure 4.15: Transient stability case study. New England 39-bus, 10-machine system: (a) OMIB plot and (b) rotor angle trajectories after redispatching. Fault at bus 21 cleared by tripping the line 16-21.

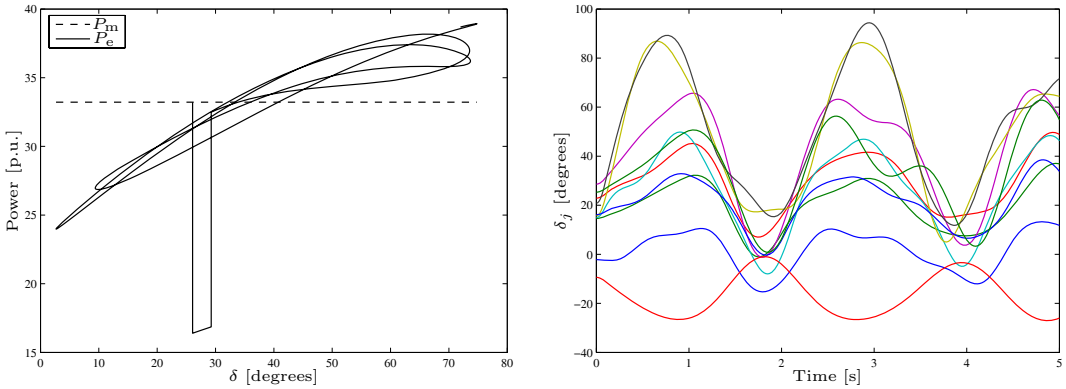

(a) (b)

Figure 4.16: Transient stability case study. New England 39-bus, 10-machine system: (a) OMIB plot and (b) rotor angle trajectories after redispatching. Fault at bus 22 cleared by tripping the line 21-22.

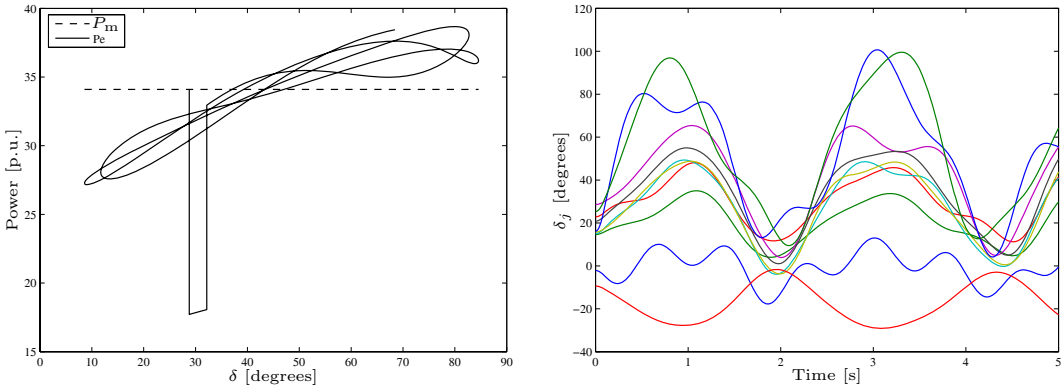

(a) (b)

Figure 4.17: Transient stability case study. New England 39-bus, 10-machine system: (a) OMIB plot and (b) rotor angle trajectories after redispatching. Fault at bus 25 cleared by tripping the line 2-25.

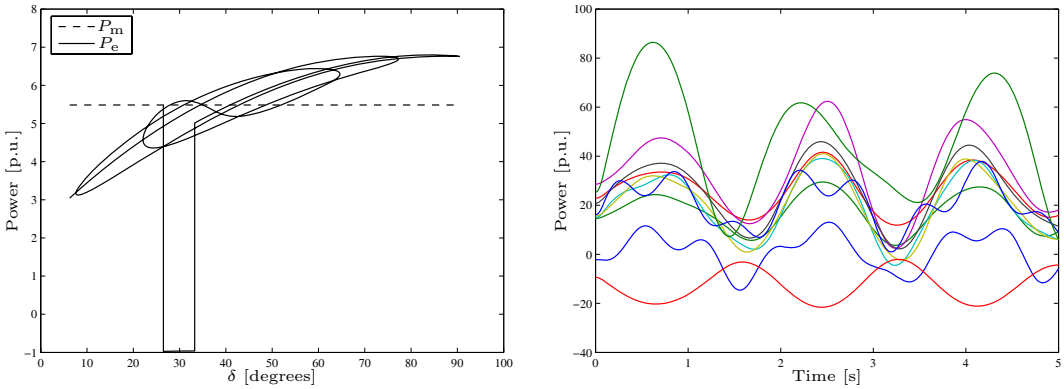

(a) (b)

Figure 4.18: Transient stability case study. New England 39-bus, 10-machine system: (a) OMIB plot and (b) rotor angle trajectories after redispatching. Fault at bus 26 cleared by tripping the line 26-29.

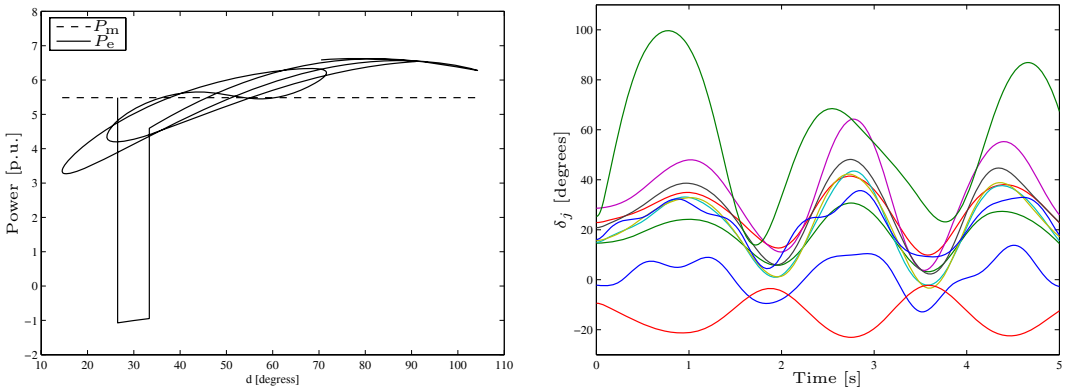

(a) (b)

Figure 4.19: Transient stability case study. New England 39-bus, 10-machine system: (a) OMIB plot and (b) rotor angle trajectories after redispatching. Fault at bus 28 cleared by tripping the line 26-28.

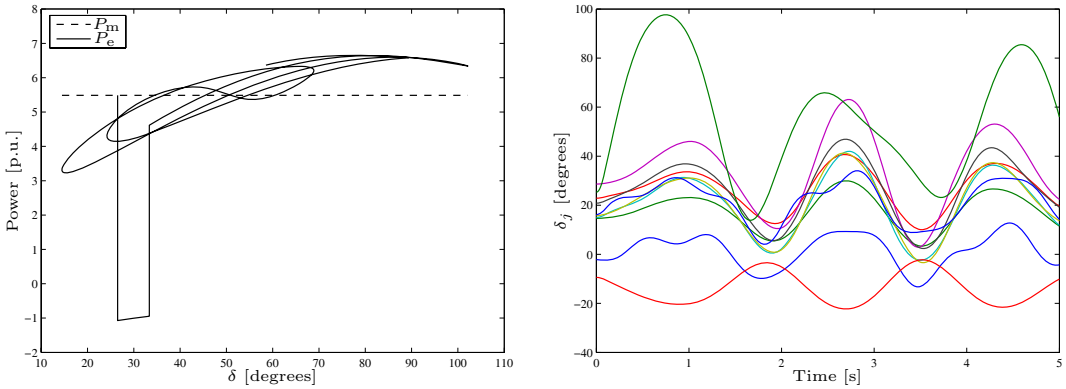

(a) (b)

Figure 4.20: Transient stability case study. New England 39-bus, 10-machine system: (a) OMIB plot and (b) rotor angle trajectories after redispatching. Fault at bus 28 cleared by tripping the line 28-29.

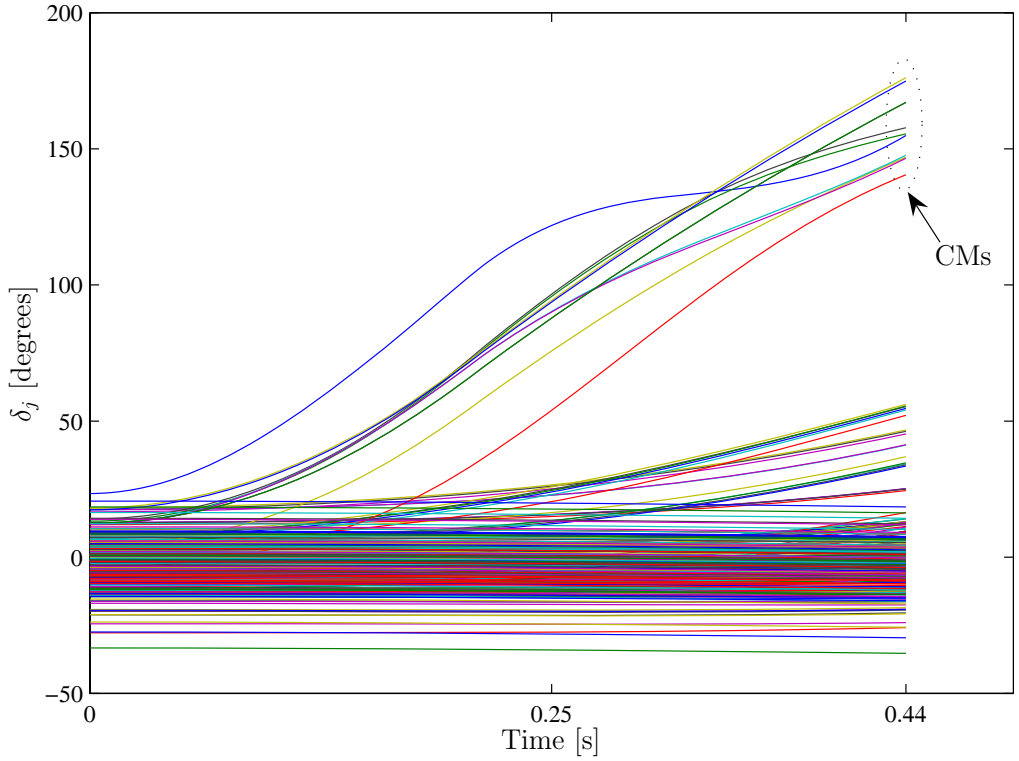

Figure 4.21: Transient stability case study. Real-world 1228-bus 292-machine system: Unstable trajectories of generator rotor angles.

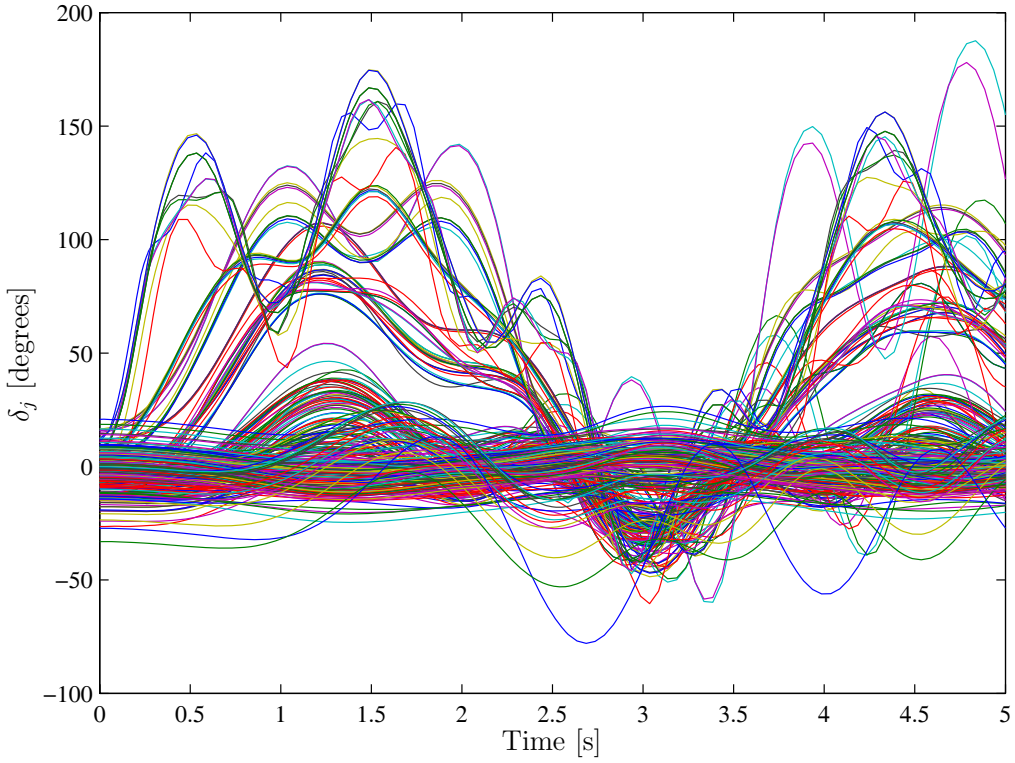

Figure 4.22: Transient stability case study. Real-world 1228-bus 292-machine system: Stable trajectories of generator rotor angles.

Chapter 5

Summary, Conclusions, Contributions and Future Research

This chapter summarizes this dissertation and its main conclusions. Finally, the most important contributions of this work are stated and future research directions are suggested.

5.1 Thesis Summary

In this thesis procedures to assist system operators in avoiding problems related to voltage, small-signal and transient stability in the context of real-time operation are developed, illustrated and analyzed. The proposed procedures include security assessment, contingency filtering, and security control procedures. The characteristics of the security assessment and contingency filtering procedures depend on the instability phenomenon of interest. The contingencies analyzed in the security assessment procedures are those of the $N-1$ security criterion. The security control procedures are essentially redispatching techniques based on OPF problems whose formulation includes constraints related to the stability phenomena that limit the system operation. The proposed procedures should be applied once a market dispatching solution is avail-

able.

It is assumed that the considered market dispatching solution does not take into account any estimate of transmission losses. Thus, the market dispatching solution is first adjusted by solving an OPF problem that minimizes the cost of generating the system losses. Along with a power balanced operating condition, the solution of this OPF problem provides the optimal voltage profile and the optimal set points for transmission control devices. This solution, so-called base-case operating condition, is the starting point of the subsequent analysis.

The proposed procedures are outlined below.

1. Procedures related to voltage stability:

   1.1. Security assessment and contingency filtering procedures. The voltage stability of the base-case operating condition is assessed by computing the loading margin for the post-contingency system configurations. These loading margins are obtained by solving OPF problems that provide the maximum loading condition of each post-contingency system configuration. The initial set of contingencies is filtered by comparing each post-contingency loading margin with a pre-specified value. This value is fixed by the system operator and represents the required security margin. If the post-contingency loading margin is lower than the required security margin, the contingency is included in the security control procedure due to the risk of voltage instability.

   1.2. Security redispatching procedure. The security redispatching procedure uses an OPF problem whose objective is to minimize the cost of the adjustments on the base-case operating condition needed to achieve a secure operation. The constraints for this problem represent several operating conditions. The basic constraints are related to the operating condition that results from adjusting the base case (adjusted operating condition), whereas voltage stability constraints are included in the form of stressed operating conditions. Each stressed operating condition is a post-contingency operating

condition in which the system load is increased with respect to the base-case load. This load increase represents the security margin imposed by the system operator. The contingencies used to define the stressed conditions are those selected in the contingency filtering procedure described in item 1.1. The OPF problem also includes ramping constraints. These are coupling constraints that model the capacity of different system components to adjust their set points in a given period of time. Ramping constraints guarantee that the system is able to reach the considered stressed operating conditions, thus ensuring the security margin.

These procedures are illustrated using a 6-bus system. Furthermore, the performance of several control devices in the security control procedure is analyzed using a 24-bus system.

2. Procedures related to small-signal stability.

   2.1. Security assessment and contingency filtering procedures. First, the maximum loading condition of each post-contingency system configuration is computed using an OPF problem. For each post-contingency maximum loading condition, eigenvalue analysis is performed. The system state matrix is evaluated and its eigenvalues are computed. The initial set of contingencies is filtered by inspecting the eigenvalues that correspond to each post-contingency maximum loading condition. If a post-contingency maximum loading condition presents one or more eigenvalues with positive real part, the contingency is included in the security control procedure due to the risk of small-signal instability.

   2.2. Security redispatching procedure. The security redispatching procedure uses an OPF problem with a similar structure to that in the case of voltage stability, i.e., the OPF includes constraints that represent both the adjusted operating condition and stressed operating conditions. Ramping constraints are also included. The stressed operating conditions are post-contingency operating condi-

tions in which the system load is increased by the security margin imposed by the system operator. The contingencies used to define the stressed conditions are those selected in the contingency filtering procedure described in item 2.1. In addition, each stressed operating condition includes linear small-signal stability constraints that are calculated as follows. For each stressed operating condition, eigenvalue analysis is carried out and critical eigenvalues are identified. Small-signal stability constraints are formulated based on the first-order Taylor series expansion of the critical eigenvalue real part. To this end, first-order sensitivities of the critical eigenvalue real part with respect to generator powers are used.

The performance of these procedures is tested on the WECC 9-bus, 3-machine system and the New England 39-bus, 10-machine system.

3. Procedures related to transient stability:

   3.1. Security assessment and contingency filtering procedures. From the base-case operating condition, a time-domain simulation is carried out for each contingency in the initial set. In this case, the contingency is composed of a fault and the subsequent line tripping. During time-domain simulations, the SIME method is used to check transient stability. This method reduces the multi-machine system to an equivalent one-machine infinite bus system whose transient stability is assessed using the equal area criterion. The initial set of contingencies is then reduced to those contingencies that present transient instability. If the system experiences first-swing instability or multi-swing instability, the contingency is included in the security control procedure due to potential transient instability.

   3.2. Security redispatching procedure. The security redispatching procedure uses an OPF problem that includes constraints that represent the adjusted operating condition. In the context of dynamic analysis, this adjusted operating condition constitutes the pre-contingency operating condition. Security constraints related

to transient stability are modeled using discrete-time equations that describe the multi-machine system. For each contingency selected in the contingency filtering procedure described in item 3.1, a set of these equations is added along with the equation of the OMIB equivalent that characterizes the contingency. Transient stability limits are introduced in the form of bounds on the OMIB equivalent rotor angle. These bounds, together with the OMIB equivalent, are established using the information provided by the analysis carried out in item 3.1.

The performance of these procedures is tested on the WECC 9-bus, 3-machine system, the New England 39-bus, 10-machine system, and a real-world 1228-bus, 292-machine system.

5.2 Conclusions

The most relevant conclusions of the work reported in this dissertation are enumerated below.

1. The security assessment, along with contingency filtering procedures, identifies harmful contingencies, i.e., the contingencies that should be taken into account in OPF-based control tools. These are important tasks in the context of real-time operation because they reduce the size of OPF problems and, therefore, reduce the time required to solve them.

2. Redispatching is an effective control action to avoid problems related to voltage, small-signal, and transient instabilities. The proposed procedures use OPF-based control tools that identify efficacious preventive redispatching actions at minimum cost.

3. Since more than one contingency can endanger the stability of the system, the proposed procedures can address multi-contingency cases.

4. Parallel computation techniques can improve the computational efficiency of the proposed procedures. Security assessment and contingency filtering methods are candidates for parallel computation.

5. The applicability of some of the proposed procedures to large-scale power systems may result in computational intractability, especially in the case of the OPF problem with transient stability constraints. Thus, it is necessary to develop more effective algorithms to solve large-scale OPF problems.

6. Although the proposed OPF problems are non-linear and non-convex and a global optimum cannot be guaranteed, the resulting solutions are reasonable.

7. Finally, the proposed procedures are useful tools for system operators since they ensure the secure operation of current power systems.

5.3 Contributions

The main contributions of this thesis are summarized below:

1. The formulation of an OPF problem that computes the system loading margin.

2. Criteria for contingency filtering for both voltage stability and small-signal stability.

3. The formulation of a security-redispatching OPF-based control tool that explicitly considers voltage stability constraints through a set of stressed post-contingency operating conditions, including coupling constraints that represent the capacity of system control devices to adjust their set points to reach the stressed conditions. This formulation guarantees a security margin with respect to voltage instability.

4. The formulation of simple yet effective small-signal stability constraints that can be included in a OPF problem.

5. The formulation of a security-redispatching OPF-based control tool that includes small-signal stability constraints. This tool guarantees a security margin with respect to small-signal instability.

6. The formulation of a security-redispatching OPF-based control tool that explicitly considers transient stability constraints through a discretized dynamic model of the power system. Transient stability limits are imposed based on the SIME method. This tool can address both first-swing and multi-swing transient instability phenomena.

7. The publication of four papers in relevant SCI journals. Note that the third and fourth papers are directly related to this thesis, while the first and second papers are the result of collateral work.

   (a) F. Milano, A. J. Conejo and R. Zárate-Miñano, "General sensitivity formulas for maximum loading conditions in power systems", *IET Generation Transmission & Distribution*, 1(3):516–526, May 2007.

   (b) R. Mínguez, F. Milano, R. Zárate-Miñano and A. J. Conejo, "Optimal network placement of SVC devices", *IEEE Transactions on Power Systems*, 22(4):1851–1860, November 2007.

   (c) R. Zárate-Miñano, A. J. Conejo and F. Milano, "OPF-based security redispatching including FACTS devices", *IET Generation Transmission & Distribution*, 2(6):821–833, November, 2008.

   (d) R. Zárate-Miñano, T. Van Cutsem, F. Milano and A. J. Conejo, "Securing transient stability using time-domain simulations within and optimal power flow", *IEEE Transactions on Power Systems*, 25(2):243-253, February 2010.

5.4 Future Work

Suggestions for future research are listed below.

1. Application of efficient techniques to reduce the computational burden of the proposed procedures. These techniques include parallel computation, powerful methods for eigenvalue analysis, and closed-form sensitivity formulas.

2. Development of dynamic models for FACTS devices to investigate the effect of these devices on both the small-signal and transient stability of a power system.

3. Investigation of the use of detailed dynamic models and additional stability constraints in the TSC-OPF problem.

4. Investigation of the impact of non-dispatchable plants on power system security.

5. Exploring the effect of alternative objective functions in the considered OPF models.

6. Analysis of alternative OPF formulations (e.g., rectangular coordinates) to improve the computational performance.

7. Exploration of procedures for security-redispatching cost allocation to market participants.

8. Analysis of real-world case studies in direct collaboration with an actual system operator.

Appendix A

Base-Case Operating Condition

This appendix describes the Optimal Power Flow (OPF) problem used throughout this thesis to obtain the base-case operating condition of the power system. The goal of this OPF problem is to correct the system power imbalance due to transmission losses from the solution of a dispatching procedure. The solution provided by the proposed OPF problem corresponds to the generation power adjustments required to achieve the system power balance in an economically optimal manner.

A.1 Introduction

Most electricity markets provide a dispatching solution only based purely on economics, in which the total generation equals the total demand. This solution does not correspond to a power balanced operating condition due to transmission losses that should be supplied. As a consequence, one generator (or a group of generators) should adjust its power output to balance the system. In some electricity markets, the dispatching solution includes an estimate of transmission losses. In this case, the power imbalance corresponds to the error in the estimation of transmission losses, [52], [68] and [144]. Once the power balance has been obtained, the resulting operating condition is the so-called base-case operating condition, which is used as the reference operating condition for security analysis.

The procedure traditionally employed to solve the system power imbalance due to losses is the well-known Power Flow (PF) algorithm. Two different approaches can be used: the single slack bus and the distributed slack bus. In the former approach, one generator (the slack) is selected to compensate for the system power imbalance. The selection of the slack generator is usually arbitrary, e.g., the generator with the largest capacity or a generator of the bus with the largest number of connected lines [59]. In the distributed slack approach, a set of generators contributes to balance the system according to pre-specified participation factors. These coefficients can be determined based on a variety of criteria, e.g., machine inertias, governor droop characteristics, frequency control participation factors, or economic dispatch, [68], [69] and [144].

Regardless of whether the single or distributed slack bus approach is adopted, the voltage magnitude at generator buses and the set point of control devices, such as FACTS devices, must be specified to solve the PF problem. These values are usually fixed to those provided by the state estimator that correspond to the operation of the system with a similar demand profile [85].

In this thesis, the base-case operating condition is obtained by solving an Optimal Power Flow (OPF) problem based on the one proposed in [52]. In the proposed OPF problem, no assumption is made a priori about whether the slack bus is single or distributed. Furthermore, voltage magnitudes at generator buses and the set point of control devices are treated as variables instead of being fixed at a predefined value. These values are provided by the solution of the proposed OPF problem. The considered objective function involves minimizing cost and is explained in Subsection A.2.1 below.

The objective of the proposed OPF problem is to minimize the cost associated with the system power imbalance. One assumption of the proposed OPF problem is that the dispatching solution does not take into account any estimation of transmission losses; thus, minimizing the cost associated with the system power imbalance directly implies minimizing the cost of generating the energy dissipated in system losses.

A.2 Problem Description

This subsection describes the objective function and all constraints used in the proposed OPF problem to identify the base-case operating condition in detail.

A.2.1 Objective Function

The objective of the proposed OPF problem is to minimize the cost of generating the system losses. Since the dispatching procedure does not include an estimate of system losses, losses are equivalent to the additional active power that the generators have to supply with respect to the power assigned in the dispatching procedure. Then, the system losses can be expressed as

$$P_{\text{loss}} = \sum_{j \in \mathcal{G}} \Delta P_{\text{G}j}^{\text{loss}}, \tag{A.1}$$

where $\Delta P_{\text{G}j}^{\text{loss}}$ is the change in the power production of generator j needed to supply the system losses.

The objective function represents the total cost of the additional active power that the generators have to supply to match the system losses

$$z = \sum_{j \in \mathcal{G}} c_j \Delta P_{\text{G}j}^{\text{loss}}, \tag{A.2}$$

where c_j is the cost associated with the power production of generator j. Observe that when all c_j equal one, the objective of the OPF problem is equivalent to minimizing the system losses. In this thesis, the price offered by generator j to increase its power dispatch for security purposes is used as the cost in (A.2), that is, $c_j = c_{\text{G}j}^{\text{up}}$.

A.2.2 Power Flow Equations

The operating condition of the system is established by the active and reactive power balance at all buses:

$$P_{\mathrm{G}n} - P_{\mathrm{D}n} = \sum_{m \in \Theta_n} P_{nm}(\cdot), \quad \forall n \in \mathcal{N}, \tag{A.3}$$

$$Q_{\mathrm{G}n} - Q_{\mathrm{D}n} = \sum_{m \in \Theta_n} Q_{nm}(\cdot), \quad \forall n \in \mathcal{N}, \tag{A.4}$$

where the powers on the left-hand side of each equation are

$$P_{\mathrm{G}n} = \sum_{j \in \mathcal{G}_n} P_{\mathrm{G}j}, \quad \forall n \in \mathcal{N}, \tag{A.5}$$

$$P_{\mathrm{D}n} = \sum_{i \in \mathcal{D}_n} P_{\mathrm{D}i}, \quad \forall n \in \mathcal{N}, \tag{A.6}$$

$$Q_{\mathrm{G}n} = \sum_{j \in \mathcal{G}_n} Q_{\mathrm{G}j}, \quad \forall n \in \mathcal{N}, \tag{A.7}$$

$$Q_{\mathrm{D}n} = \sum_{i \in \mathcal{D}_n} P_{\mathrm{D}i} \tan(\psi_{\mathrm{D}i}), \quad \forall n \in \mathcal{N}, \tag{A.8}$$

with

$$P_{\mathrm{G}j} = P_{\mathrm{G}j}^{\mathrm{M}} + \Delta P_{\mathrm{G}j}^{\mathrm{loss}}, \quad \forall j \in \mathcal{G}, \tag{A.9}$$

$$P_{\mathrm{D}i} = P_{\mathrm{D}i}^{\mathrm{M}}, \quad \forall i \in \mathcal{D}, \tag{A.10}$$

and

$$\Delta P_{\mathrm{G}j}^{\mathrm{loss}} \geq 0, \quad \forall j \in \mathcal{G}. \tag{A.11}$$

Equation (A.8) implies that constant power factor loads are considered. The functions on the right-hand side of (A.3) and (A.4) are the power flow equations and depend on the device connected between buses n and m. Appendix C describes these equations in detail.

Finally, note that superscript "M", in (A.9) and (A.10), indicates dispatching (market) solution.

A.2.3 Technical Limits

The power production is limited by the capacity of the generators.

$$P_{\mathrm{G}j}^{\min} \leq P_{\mathrm{G}j} \leq P_{\mathrm{G}j}^{\max}, \quad \forall j \in \mathcal{G}, \tag{A.12}$$

$$Q_{\mathrm{G}j}^{\min} \leq Q_{\mathrm{G}j} \leq Q_{\mathrm{G}j}^{\max}, \quad \forall j \in \mathcal{G}. \tag{A.13}$$

Voltage magnitudes at generator buses should be within operating limits,

$$V_n^{\min} \leq V_n \leq V_n^{\max}, \quad \forall n \in \mathcal{N}_{\mathrm{G}}. \tag{A.14}$$

Any control device connected to the system is allowed to vary within its rating values. The control devices considered in this thesis are the following regulating transformers and FACTS devices: the on-Load Tap-Changer (LTC), the Phase-Shifting (PHS) transformer, the Static Var Compensator (SVC), and the Thyristor-Controlled Series Compensator (TCSC). Thus, for LTC transformers:

$$T_k^{\min} \leq T_k \leq T_k^{\max}, \quad \forall k = (n, m) \in \Omega_{\mathrm{LTC}}, \tag{A.15}$$

for PHS transformers:

$$\phi_k^{\min} \leq \phi_k \leq \phi_k^{\max}, \quad \forall k = (n, m) \in \Omega_{\mathrm{PHS}}, \tag{A.16}$$

for TCSC devices:

$$x_{\mathrm{TCSC},k}^{\min} \leq x_{\mathrm{TCSC},k} \leq x_{\mathrm{TCSC},k}^{\max}, \quad \forall k = (n, m) \in \Omega_{\mathrm{TCSC}}, \tag{A.17}$$

and for SVC devices:

$$b_{\mathrm{SVC},n}^{\min} \leq b_{\mathrm{SVC},n} \leq b_{\mathrm{SVC},n}^{\max}, \quad \forall n \in \mathcal{N}_{\mathrm{SVC}}. \tag{A.18}$$

There are two kind of limits in the case of regulating transformers and FACTS devices: (i) technical operating limits, such as tap ratio and phase limits (A.15) and (A.16), and (ii) capacity limits, such as the reactance sizes of the TCSC

devices (A.17) and susceptance sizes of the SVC devices (A.18).

Other technical limits, such as the voltage magnitude limits at load buses or the current flow limits of the elements of the network are not included to obtain the base-case solution. These limits are incorporated into the security redispatching procedures described throughout this thesis.

A.2.4 Other Constraints

The OPF problem includes the following additional constraints:

$$-\pi \leq \theta_n \leq \pi, \quad \forall n \in \mathcal{N}, \tag{A.19}$$

$$\theta_{\text{ref}} = 0. \tag{A.20}$$

Equation (A.19) is included to reduce the feasibility region, thereby causing the OPF problem to converge more rapidly in general.

A.2.5 OPF Formulation

The formulation of the OPF problem is summarized below:

$$\text{Minimize} \quad \text{(A.2)}$$

subject to

1. Power flow equations (A.3)-(A.4).
2. Technical limits (A.12)-(A.18).
3. Other constraints (A.19)-(A.20).

Appendix B

Maximum Loading Condition Problem

This appendix describes the Optimal Power Flow (OPF) problem used throughout this thesis to compute the loading margin of a power system working under a given load condition. From the actual system load, the OPF problem maximizes the amount of load increase that complies with system limits. Together with the loading margin, the solution to the proposed OPF problem provides the value of system variables that define the maximum loading condition.

B.1 Introduction

The loading margin is an index that is widely used in static voltage stability analysis [118]. For a particular power system operating condition, the loading margin is defined as the maximum amount of additional load that the system can provide without exceeding a voltage stability limit. As stated in Chapter 2, voltage stability limits lead to system collapse and correspond to a Saddle-Node Bifurcation (SNB) or to a critical Limit-Induced Bifurcation (LIB). In loading margin computations, it is assumed that the load increases slowly such that the dynamics of the system can restore the equilibrium. Thus, the system moves smoothly from one equilibrium point to another as the load increases. This assumption justifies the use of static models in loading margin

computations.

In this thesis, the definition of loading margin is extended to take into account technical limits, such as bus voltage limits and transmission line/transformer thermal limits. These limits do not directly cause collapse but should be avoided since they can initiate cascade line tripping phenomena. In addition, generator ramping limits are taken into account. These ramps represent the capacity of the generators to increase or decrease its active power output within a given period of time (Δt). The generator ramping limits model the fact that the primary frequency control is able to restore the system power balance at a certain rate when the load increases. Similarly, ramping constraints are used to model the capacity of some control devices, such as on-load tap-changing and phase-shifting transformers, to adjust their set points.

Therefore, for a particular operating condition, the loading margin (λ^*) stands for the maximum additional load that the system can provide while satisfying all technical limits and avoiding the occurrence of a voltage collapse within a time interval Δt.

B.2 Maximum Loading Condition Problem

The loading margin λ^* is determined by solving an OPF problem, the Maximum Loading Condition (MLC) problem. This problem is described in the following.

B.2.1 Objective Function

The objective function used in this problem is as follows:

$$z = -\lambda \; . \tag{B.1}$$

Variable λ increases the load of the system (see (B.8)); therefore, minimizing $-\lambda$ corresponds to finding the maximum loading condition of the power system. Then, the maximum value of λ is denoted λ^*.

B.2.2 Power Flow Equations

The maximum loading condition is defined by the active and reactive power balance at all buses:

$$P_{\mathrm{G}n} - P_{\mathrm{D}n} = \sum_{m \in \Theta_n} P_{nm}(\cdot), \quad \forall n \in \mathcal{N}, \tag{B.2}$$

$$Q_{\mathrm{G}n} - Q_{\mathrm{D}n} = \sum_{m \in \Theta_n} Q_{nm}(\cdot), \quad \forall n \in \mathcal{N}, \tag{B.3}$$

where the powers on the left-hand side of each equation are defined as

$$P_{\mathrm{G}n} = \sum_{j \in \mathcal{G}_n} P_{\mathrm{G}j}, \quad \forall n \in \mathcal{N}, \tag{B.4}$$

$$P_{\mathrm{D}n} = \sum_{i \in \mathcal{D}_n} P_{\mathrm{D}i}, \quad \forall n \in \mathcal{N}, \tag{B.5}$$

$$Q_{\mathrm{G}n} = \sum_{j \in \mathcal{G}_n} Q_{\mathrm{G}j}, \quad \forall n \in \mathcal{N}, \tag{B.6}$$

$$Q_{\mathrm{D}n} = \sum_{i \in \mathcal{D}_n} P_{\mathrm{D}i} \tan(\psi_{\mathrm{D}i}), \quad \forall n \in \mathcal{N}, \tag{B.7}$$

and

$$P_{\mathrm{D}i} = (1 + \lambda) P^{\mathrm{A}}_{\mathrm{D}i}, \quad \forall i \in \mathcal{D}. \tag{B.8}$$

Equation (B.7) implies that constant power factor loads are considered. Superscript "A" in (B.8) indicates base-case operating condition. The functions on the right-hand side of (B.2) and (B.3) are the power flow equations and depend on the device connected between buses n and m. Appendix C describes these equations in detail.

B.2.3 Technical Limits

The power production is limited by the capacity of the generators. Hence, at the maximum loading condition,

$$P^{\min}_{\mathrm{G}j} \leq P_{\mathrm{G}j} \leq P^{\max}_{\mathrm{G}j}, \quad \forall j \in \mathcal{G}, \tag{B.9}$$

$$Q_{\mathrm{G}j}^{\min} \leq Q_{\mathrm{G}j} \leq Q_{\mathrm{G}j}^{\max}, \quad \forall j \in \mathcal{G}. \tag{B.10}$$

Voltages magnitudes throughout the system should be within operating limits,

$$V_n^{\min} \leq V_n \leq V_n^{\max}, \quad \forall n \in \mathcal{N}. \tag{B.11}$$

The current flow through all branches of the network must be below thermal limits,

$$I_k(\cdot) \leq I_k^{\max}, \quad \forall k = (n, m) \in \Omega, \tag{B.12}$$

where the functions $I_k(\cdot)$ depend on the device k connected between buses n and m. The expressions of these functions are defined in Appendix C.

The power production of generators is also limited by ramping constraints

$$P_{\mathrm{G}j} - P_{\mathrm{G}j}^{\mathrm{A}} \leq R_{\mathrm{G}j}^{\mathrm{up}} \Delta t, \quad \forall j \in \mathcal{G}, \tag{B.13}$$

$$P_{\mathrm{G}j}^{\mathrm{A}} - P_{\mathrm{G}j} \leq R_{\mathrm{G}j}^{\mathrm{down}} \Delta t, \quad \forall j \in \mathcal{G}, \tag{B.14}$$

where superscript "A" indicates base-case operating condition. The time interval Δt is the time period within which generators should be able to adjust their power productions to reach the maximum loading condition.

If the power system includes control devices, these should be taken into account in the MLC problem. The control devices considered in this thesis are two regulating transformers: the on-Load Tap-Changing (LTC) transformer and the Phase-Shifting (PHS) transformer; and two FACTS devices: the Static Var Compensator (SVC) and the Thyristor-Controlled Series Compensator (TCSC). While the response of SVC and TCSC devices may be considered instantaneous for the considered time period Δt, the response of the LTC and PHS transformers are conditioned by mechanically driven operations and they are not instantaneous. As for generators, these physical constraints relate to ramping limits, i.e.,

$$T_k - T_k^{\mathrm{A}} \leq R_T^{\mathrm{up}} \Delta t, \quad \forall k = (n, m) \in \Omega_{\mathrm{LTC}}, \tag{B.15}$$

$$T_k^{\mathrm{A}} - T_k \leq R_T^{\mathrm{down}} \Delta t, \quad \forall k = (n, m) \in \Omega_{\mathrm{LTC}}, \tag{B.16}$$

and

$$\phi_k - \phi_k^{\mathrm{A}} \leq R_\phi^{\mathrm{up}} \Delta t, \quad \forall k = (n,m) \in \Omega_{\mathrm{PHS}}, \tag{B.17}$$

$$\phi_k^{\mathrm{A}} - \phi_k \leq R_\phi^{\mathrm{down}} \Delta t, \quad \forall k = (n,m) \in \Omega_{\mathrm{PHS}}. \tag{B.18}$$

Finally, any device connected to the system is allowed to vary within design rating values. Therefore, for LTC transformers:

$$T_k^{\min} \leq T_k \leq T_k^{\max}, \quad \forall k = (n,m) \in \Omega_{\mathrm{LTC}}, \tag{B.19}$$

for PHS transformers:

$$\phi_k^{\min} \leq \phi_k \leq \phi_k^{\max}, \quad \forall k = (n,m) \in \Omega_{\mathrm{PHS}}, \tag{B.20}$$

for TCSC devices:

$$x_{\mathrm{TCSC},k}^{\min} \leq x_{\mathrm{TCSC},k} \leq x_{\mathrm{TCSC},k}^{\max}, \quad \forall k = (n,m) \in \Omega_{\mathrm{TCSC}}, \tag{B.21}$$

and for SVC devices:

$$b_{\mathrm{SVC},n}^{\min} \leq b_{\mathrm{SVC},n} \leq b_{\mathrm{SVC},n}^{\max}, \quad \forall n \in \mathcal{N}_{\mathrm{SVC}}. \tag{B.22}$$

There are two kind of limits in the case of regulating transformers and FACTS devices: (i) technical operating limits, such as tap ratio limits (B.19) and phase limits (B.20), and (ii) capacity limits, such as the reactance sizes of the TCSC devices (B.21) and susceptance sizes of the SVC devices (B.22).

B.2.4 Other Constraints

The proposed MLC problem is completed with the following additional constraints:

$$-\pi \leq \theta_n \leq \pi, \quad \forall n \in \mathcal{N}, \tag{B.23}$$

$$\theta_{\text{ref}} = 0. \tag{B.24}$$

Equation (B.23) is included to reduce the feasibility region, thereby causing the OPF problem to converge more rapidly in general.

B.2.5 MLC-OPF Formulation

The formulation of the MLC problem is summarized below:

$$\text{Minimize} \quad \text{(B.1)}$$

subject to

1. Power flow equations (B.2)-(B.3).
2. Technical limits (B.9)-(B.22).
3. Other constraints (B.23)-(B.24).

Appendix C

Modeling of Components

This appendix describes the models of the power system components used throughout the thesis.

C.1 Transmission Line Model

Transmission lines are modeled by the well-known equivalent π-circuit shown in Figure C.1.

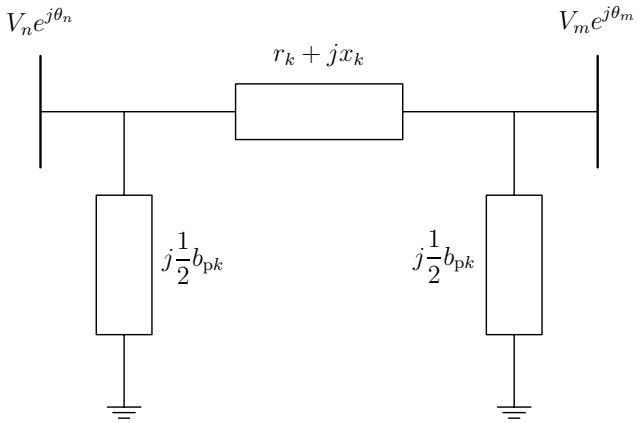

Figure C.1: Transmission line model.

The series admittance of the line is

$$\boldsymbol{Y}_k = \frac{1}{\boldsymbol{Z}_k} = \frac{1}{r_k + jx_k} = g_k + jb_k, \tag{C.1}$$

and the resulting conductance and susceptance are, respectively,

$$g_k = \frac{r_k}{r_k^2 + x_k^2}, \tag{C.2}$$

$$b_k = \frac{-x_k}{r_k^2 + x_k^2}. \tag{C.3}$$

The active and reactive power flows from bus n to bus m are, respectively

$$\begin{aligned} P_{nm}(\cdot) =& V_n^2 g_k - V_n V_m (g_k \cos(\theta_n - \theta_m) \\ &+ b_k \sin(\theta_n - \theta_m)), \quad \forall k = (n,m) \in \Omega_{\mathrm{L}}, \end{aligned} \tag{C.4}$$

$$\begin{aligned} Q_{nm}(\cdot) =& - V_n^2 (b_k + \frac{1}{2} b_{\mathrm{pk}}) - V_n V_m (g_k \sin(\theta_n - \theta_m) \\ &- b_k \cos(\theta_n - \theta_m)), \quad \forall k = (n,m) \in \Omega_{\mathrm{L}}, \end{aligned} \tag{C.5}$$

and the current flow through the transmission line from n to m is

$$\begin{aligned} I_{nm}(\cdot) = \Big(\big(& - V_n \frac{1}{2} b_{\mathrm{pk}} \sin\theta_n + V_n (g_k \cos\theta_n - b_k sin\theta_n) \\ & - V_m (g_k \cos\theta_m - b_k sin\theta_m) \big)^2 + \\ & \big(V_n \frac{1}{2} b_{\mathrm{pk}} \cos\theta_n + V_n (g_k \sin\theta_n + b_k cos\theta_n) \\ & - V_m (g_k \sin\theta_m + b_k cos\theta_m) \big)^2 \Big)^{1/2}, \\ & \forall k = (n,m) \in \Omega_{\mathrm{L}}. \end{aligned} \tag{C.6}$$

C.2 Transformer Models

The models of the on-Load Tap-Changing (LTC) and the PHase-Shifting (PHS) transformers are based on [1]. Figure C.2 depicts a LTC/PHS transformer that connects buses n and m and regulates the voltage/phase at bus m. This model is also used for fixed-tap transformers. The nodal transfer admittance for this

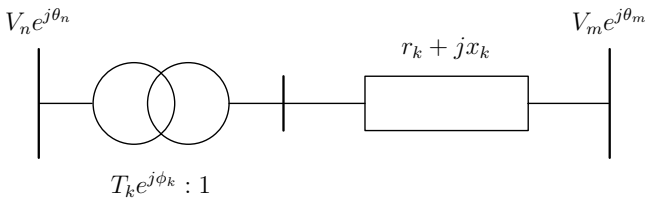

Figure C.2: On-load tap-changing and phase-shifting transformer model.

model is

$$\begin{pmatrix} \boldsymbol{I}_{nm} \\ \boldsymbol{I}_{mn} \end{pmatrix} = (g_k + jb_k) \begin{pmatrix} \frac{1}{T_k^2} & -\frac{1}{T_k} e^{j\phi_k} \\ -\frac{1}{T_k} e^{-j\phi_k} & 1 \end{pmatrix} \begin{pmatrix} V_n e^{j\theta_n} \\ V_m e^{j\theta_m} \end{pmatrix}.$$

Then, the active and reactive power flows from bus n to bus m are, respectively,

$$\begin{aligned} P_{nm}(\cdot) =& \frac{1}{T_k^2} V_n^2 g_k - \frac{1}{T_k} V_n V_m (g_k \cos(\theta_n - \theta_m - \phi_k) \\ &+ b_k \sin(\theta_n - \theta_m - \phi_k)), \end{aligned} \tag{C.7}$$

$$\begin{aligned} Q_{nm}(\cdot) =& -\frac{1}{T_k^2} V_n^2 b_k - \frac{1}{T_k} V_n V_m (g_k \sin(\theta_n - \theta_m - \phi_k) \\ &- b_k \cos(\theta_n - \theta_m - \phi_k)), \end{aligned} \tag{C.8}$$

where the sub-index k identifies the component in between buses n and m, and g_k and b_k have equivalent expressions to those in (C.2) and (C.3), respectively. The active and reactive power flows from bus m to bus n are, respectively,

$$\begin{aligned} P_{mn}(\cdot) =& V_m^2 g_k - \frac{1}{T_k} V_m V_n (g_k \cos(\theta_n - \theta_m - \phi_k) \\ &- b_k \sin(\theta_n - \theta_m - \phi_k)), \end{aligned} \tag{C.9}$$

$$\begin{aligned} Q_{mn}(\cdot) =& -V_m^2 b_k + \frac{1}{T_k} V_m V_n (g_k \sin(\theta_n - \theta_m - \phi_k) \\ &+ b_k \cos(\theta_n - \theta_m - \phi_k)). \end{aligned} \tag{C.10}$$

The current flow through a LTC/PHS/fixed-tap transformer from bus n to bus m is

$$\begin{aligned} I_{nm}(\cdot) = \Big(& \big(\frac{1}{T_k^2} V_n (g_k \cos\theta_n - b_k \sin\theta_n) \\ & - \frac{1}{T_k} V_m (g_k(\cos\theta_m + \phi) - b_k \sin(\theta_m + \phi))\big)^2 + \\ & \big(\frac{1}{T_k^2} V_n (g_k \sin\theta_n + b_k \cos\theta_n) \\ & - \frac{1}{T_k} V_m (g_k \sin(\theta_m + \phi) + b_k \cos(\theta_m + \phi))\big)^2 \Big)^{1/2}, \end{aligned} \tag{C.11}$$

and the current flow through a LTC/PHS/fixed-tap transformer from bus m to bus n is

$$\begin{aligned} I_{mn}(\cdot) = \Big(& \big(V_m (g_k \cos\theta_m - b_k \sin\theta_m) \\ & - \frac{1}{T_k} V_n (g_k \cos(\theta_n - \phi_k) - b_k \sin(\theta_n - \phi_k))\big)^2 + \\ & \big(V_m (g_k \sin\theta_m + b_k \cos\theta_m) \\ & - \frac{1}{T_k} V_n (g_k \sin(\theta_n - \phi_k) + b_k \cos(\theta_n - \phi_k))\big)^2 \Big)^{1/2}. \end{aligned} \tag{C.12}$$

Equations (C.7)-(C.12) are valid for LTC, PHS and fixed-tap transformers as follows:

1. LTC transformer: $k = (n, m) \in \Omega_{\text{LTC}}$, T_k is a variable, and $\phi_k = 0$.

2. PHS transformer: $k = (n, m) \in \Omega_{\text{PHS}}$, ϕ_k is a variable, and T_k is a constant.

3. Fixed-tap transformer: $k = (n, m) \in \Omega_{\text{FT}}$, T_k is a constant, and $\phi_k = 0$.

C.3 Static Var Compensator Model

The Static Var Compensator (SVC) device is modeled as a variable shunt susceptance [4], as shown in Figure C.3. Thus, the reactive power injected by

the SVC at bus n is

$$Q_{\mathrm{SVC},n} = -b_{\mathrm{SVC},n} V_n^2, \quad \forall n \in \mathcal{N}_{\mathrm{SVC}}. \tag{C.13}$$

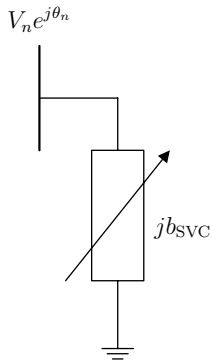

Figure C.3: Static var compensator model.

C.4 Thyristor-Controlled Series Compensator Model

The model of the Thyristor-Controlled Series Compensator (TCSC) used in this thesis is a variable reactance connected in series with a transmission line [60], as depicted in Figure C.4.

The total impedance is

$$\boldsymbol{Z}_k = r_k + j(x_k + x_{\mathrm{TCSC}}), \quad \forall k = (n,m) \in \Omega_{\mathrm{TCSC}}, \tag{C.14}$$

and the resulting conductance and susceptance are, respectively,

$$g_k = \frac{r_k}{r_k^2 + (x_k + x_{\mathrm{TCSC}})^2}, \quad \forall k = (n,m) \in \Omega_{\mathrm{TCSC}}, \tag{C.15}$$

$$b_k = \frac{-(x_k + x_{\mathrm{TCSC}})}{r_k^2 + (x_k + x_{\mathrm{TCSC}})^2}, \quad \forall k = (n,m) \in \Omega_{\mathrm{TCSC}}. \tag{C.16}$$

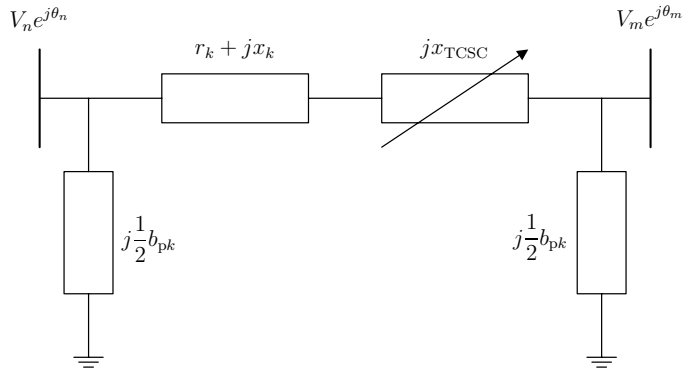

Figure C.4: Thyristor-controlled series compensator model.

Therefore, the active and reactive power flows through a transmission line that incorporates a TCSC device are represented, respectively, by equations (C.4) and (C.5), where parameters g_k and b_k are defined by (C.15) and (C.16), respectively. Similarly, the current flow through a transmission line that incorporates a TCSC device is represented by equation C.6 including (C.15) and (C.16).

C.5 Load Models

Loads are represented by two static models, a constant power model and a constant impedance model. Figure C.5(a) depicts the constant power model. This model is used in the power flow equations. The constant impedance model shown in Figure C.5(b) is used in the time-domain simulations performed throughout the thesis.

C.6 Generator Models

This section describes the generator models used throughout this thesis; one static model and two dynamic models. The dynamic models are the classical model and a two-axis model that incorporates an automatic voltage regulator.

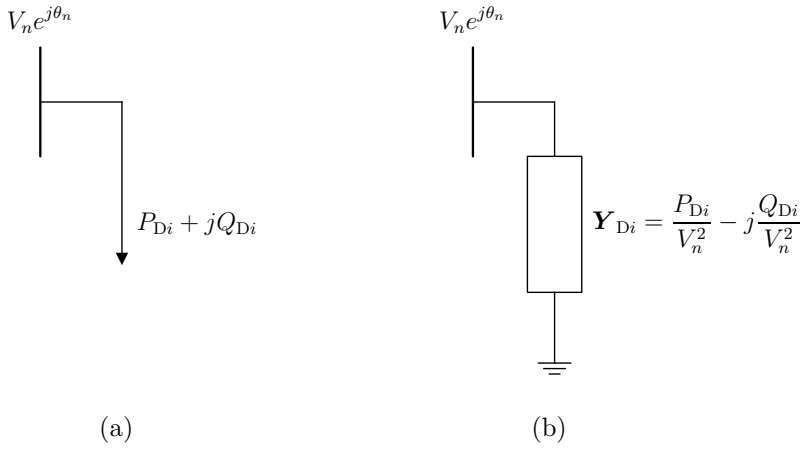

Figure C.5: Load models: (a) constant power; (b) constant impedance.

C.6.1 Static Model

Figure C.6 depicts the generator static model. This model is used in the power flow equations.

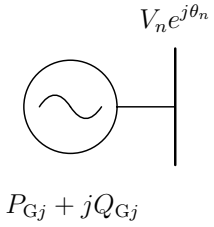

Figure C.6: Generator constant power model.

C.6.2 Classical Model

In the classical model, the synchronous machine is represented by a constant electromotive force behind a transient reactance, as shown in Figure C.7. This model is used in the time-domain simulations of Chapter 4.

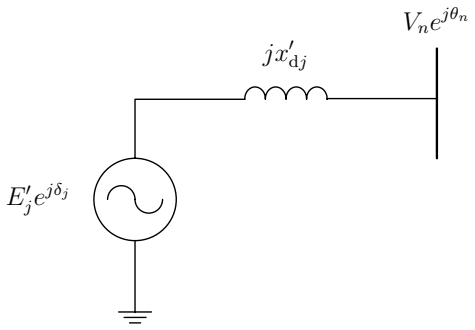

Figure C.7: Generator classical model.

The dynamic equations of this model are as follows:

$$\dot{\delta}_j = \omega_{\mathrm{b}}(\omega_j - 1), \tag{C.17}$$

$$\dot{\omega}_j = \frac{1}{M}(P_{\mathrm{m}j} - P_{\mathrm{e}j}), \tag{C.18}$$

where the electrical power $P_{\mathrm{e}j}$ is defined as

$$P_{\mathrm{e}j} = \frac{E'_j V_n \sin(\delta_j - \theta_n)}{x'_{\mathrm{d}j}}, \tag{C.19}$$

and the reactive power output is

$$Q_{\mathrm{G}j} = \frac{E'_j V_n \cos(\delta_j - \theta_n) - V_n^2}{x'_{\mathrm{d}j}}. \tag{C.20}$$

C.6.3 Two-Axis Model

The two-axis model is shown in Figure C.8 and it is used for the modal analysis in Chapter 3.

This generator model incorporates an Automatic Voltage Regulator (AVR). Neglecting the armature resistance $r_{\mathrm{a}j}$ and the damping coefficient, the dynamic equations of the generator are as follows:

$$\dot{\delta}_j = \omega_{\mathrm{b}}(\omega_j - 1), \tag{C.21}$$

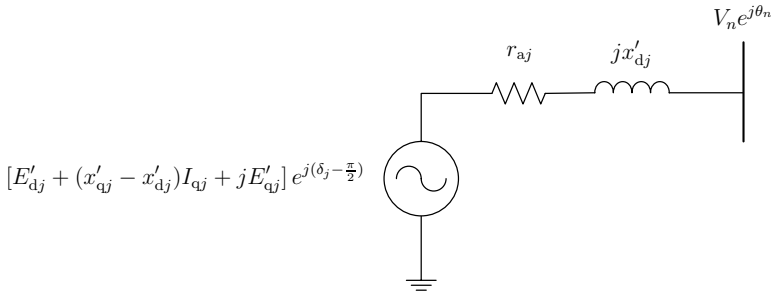

Figure C.8: Generator two-axis model

$$\dot{\omega}_j = \frac{1}{M_j}(P_{mj} - P_{ej}), \tag{C.22}$$

$$\dot{E}'_{qj} = \frac{1}{T'_{d0j}}\big(- E'_{qj} - (x_{dj} - x'_{dj})I_{dj} + V_{fj}\big), \tag{C.23}$$

$$\dot{E}'_{dj} = \frac{1}{T'_{q0j}}\big(- E'_{dj} + (x_{qj} - x'_{qj})I_{qj}\big), \tag{C.24}$$

where the electrical power P_{ej} is defined as

$$P_{ej} = V_{qj}I_{qj} + V_{dj}I_{dj}. \tag{C.25}$$

Finally, the stator algebraic equations are

$$0 = V_{qj} - E'_{qj} + x'_{dj}I_{dj}, \tag{C.26}$$

$$0 = V_{dj} - E'_{dj} - x'_{qj}I_{qj}, \tag{C.27}$$

with

$$V_{dj} = V_n \sin(\delta_j - \theta_n), \tag{C.28}$$

$$V_{qj} = V_n \cos(\delta_j - \theta_n). \tag{C.29}$$

Figure C.9 depicts the AVR model. The dynamic equations of this model are as follows.

$$\dot{V}_{mj} = \frac{1}{T_{rj}}(V_n - V_{mj}),$$

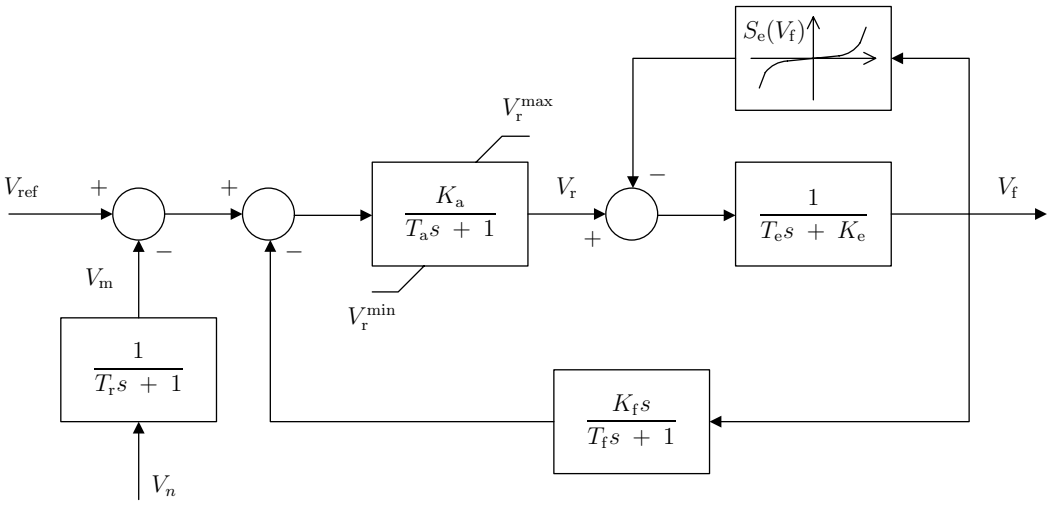

Figure C.9: Automatic voltage regulator model.

$$
\begin{aligned}
\dot{V}_{\mathrm{r}1j} &= \frac{1}{T_{\mathrm{a}j}}\Big(K_{\mathrm{a}j}(V_{\mathrm{ref}j} - V_{\mathrm{m}j} - V_{\mathrm{r}2j} - \frac{K_{\mathrm{f}j}}{T_{\mathrm{f}j}}V_{\mathrm{f}j}) - V_{\mathrm{r}1j}\Big),\\
V_{\mathrm{r}j} &= \begin{cases} V_{\mathrm{r}1j} & \text{if } V_{\mathrm{r}j}^{\min} \le V_{\mathrm{r}1j} \le V_{\mathrm{r}j}^{\max},\\ V_{\mathrm{r}j}^{\max} & \text{if } V_{\mathrm{r}1j} > V_{\mathrm{r}j}^{\max},\\ V_{\mathrm{r}j}^{\min} & \text{if } V_{\mathrm{r}1j} < V_{\mathrm{r}j}^{\min}, \end{cases}\\
\dot{V}_{\mathrm{r}2j} &= -\frac{1}{T_{\mathrm{f}j}}(\frac{K_{\mathrm{f}j}}{T_{\mathrm{f}j}}V_{\mathrm{f}j} + V_{\mathrm{r}2j}),\\
\dot{V}_{\mathrm{f}j} &= -\frac{1}{T_{\mathrm{e}j}}\Big(V_{\mathrm{f}j}\big(K_{\mathrm{e}j} + S_{\mathrm{e}j}(V_{\mathrm{f}j})\big) - V_{\mathrm{r}j}\Big),
\end{aligned}
\tag{C.30}
$$

where

$$
S_{\mathrm{e}j}(V_{\mathrm{f}j}) = A_{\mathrm{e}j}\, e^{B_{\mathrm{e}j}V_{\mathrm{f}j}}. \tag{C.31}
$$

Appendix D

Data

This appendix contains the data for the power systems used in the simulations reported throughout this thesis.

D.1 W&W 6-Bus System

This section provides the data for the W&W 6-bus system used in the illustrative example of Section 2.4 of Chapter 2. This system is based on the 6-bus system reported in [133].

D.1.1 Network Data

Figure D.1 depicts the W&W 6-bus system. There is an unique voltage level of 400 kV. Table D.1 provides the network data and the maximum current magnitudes for branches of this system. The bus voltage magnitude limits are $V_n^{\min} = 0.90$ p.u. and $V_n^{\max} = 1.10$ p.u. for all buses.

D.1.2 Technical Limits for Generators

Table D.2 lists the maximum and minimum power output and ramping limits of the system generators.

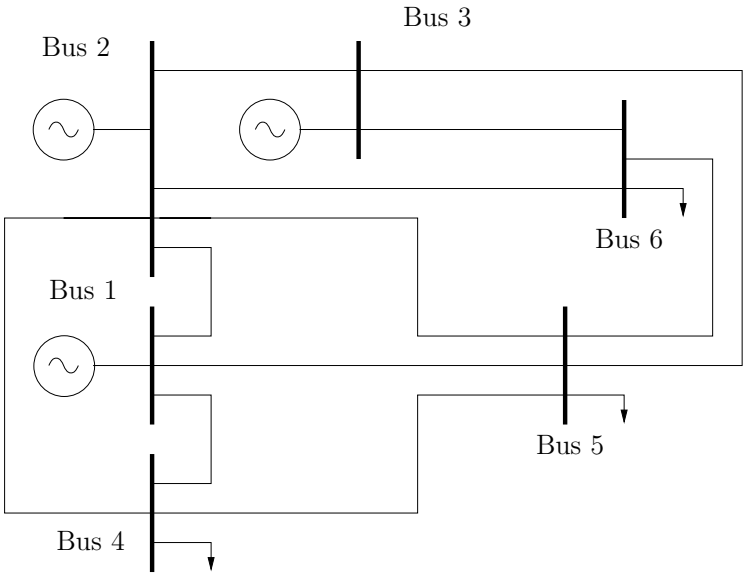

Figure D.1: One-line diagram of the 6-bus system.

D.1.3 Market Solution and Cost Data

Table D.3 shows the generator powers that correspond to the market dispatching solution for the W&W 6-bus system. Table D.3 also provides the offering costs for the generators to increase or decrease their power outputs for security purposes. Table D.4 lists the demand powers that correspond to the market dispatching solution for the 6-bus system. Constant power factor loads are assumed. Table D.4 also provides the value of $\tan(\psi_{\mathrm{D}i})$ and the cost of load curtailment for each demand. Finally, the penalties for voltage magnitude adjustments are $c_{\mathrm{V}n}^{\mathrm{up}} = c_{\mathrm{V}n}^{\mathrm{down}} = \$100/\text{p.u.h}$ for all generator buses. The units of penalty factors are introduced only for compatibility with costs.

D.1.4 Base-Case Operating Condition

Table D.5 shows the base-case operating condition for the W&W 6-bus system. This base case corresponds to the solution of the OPF problem described in Appendix A.

Table D.1: Network data and branch current limits for the W&W 6-bus system.

Branch #	From #	To #	r_k [p.u.]	x_k [p.u.]	$b_{\mathrm{p}k}$ [p.u.]	T_k [p.u.]	ϕ_k [p.u.]	$I_k^{\max}$ [p.u.]
1	1	2	0.1000	0.2000	0.0400	-	-	0.2591
2	1	4	0.0500	0.2000	0.0400	-	-	0.9193
3	1	5	0.0800	0.3000	0.0600	-	-	0.8478
4	2	3	0.0500	0.2500	0.0600	-	-	0.3082
5	2	4	0.0500	0.1000	0.0200	-	-	1.3740
6	2	5	0.1000	0.3000	0.0400	-	-	0.7114
7	2	6	0.0700	0.2000	0.0500	-	-	0.9147
8	3	5	0.1200	0.2600	0.0500	-	-	0.6585
9	3	6	0.0200	0.1000	0.0200	-	-	1.3973
10	4	5	0.2000	0.4000	0.0800	-	-	0.1796
11	5	6	0.1000	0.3000	0.0600	-	-	0.2000

Table D.2: Technical limits of the generators for the W&W 6-bus system.

Generator #	$P_{\mathrm{G}j}^{\min}$ [p.u.]	$P_{\mathrm{G}j}^{\max}$ [p.u.]	$Q_{\mathrm{G}j}^{\min}$ [p.u.]	$Q_{\mathrm{G}j}^{\max}$ [p.u.]	$R_{\mathrm{G}j}^{\mathrm{up}}$ [p.u./min]	$R_{\mathrm{G}j}^{\mathrm{down}}$ [p.u./min]
1	0.1	2.0	-1.5	1.5	0.0333	0.0333
2	0.1	1.8	-1.5	1.5	0.0300	0.0300
3	0.1	1.8	-1.5	1.5	0.0300	0.0300

D.2 IEEE 24-Bus System

This section provides the data of the IEEE 24-bus system used in the case study of Section 2.5 of Chapter 2. This system is based on the IEEE Reliability Test System [100].

Table D.3: The market solution and offering costs for the generators of the W&W 6-bus system.

Generator #	Bus #	$P^{\mathrm{M}}_{\mathrm{G}j}$ [p.u.]	$c^{\mathrm{up}}_{\mathrm{G}j}$ [$/p.u.h]	$c^{\mathrm{down}}_{\mathrm{G}j}$ [$/p.u.h]
1	1	0.4575	12.0	12.0
2	2	1.1694	10.0	10.0
3	3	0.9231	11.0	11.0

Table D.4: The market solution, $\tan(\psi_{\mathrm{D}i})$, and cost of load curtailment for the demands of the W&W 6-bus system.

Demand #	Bus #	$P^{\mathrm{M}}_{\mathrm{D}i}$ [p.u.]	$\tan(\psi_{\mathrm{D}i})$ [p.u/p.u]	$c^{\mathrm{down}}_{\mathrm{D}i}$ [$/p.u.h]
1	4	0.7000	0.7857	1000
2	5	1.0500	0.6667	1000
3	6	0.8000	0.7500	1000

Table D.5: Base-case operating condition for the W&W 6-bus system.

Bus #	Gen. #	Dem. #	$P^{\mathrm{A}}_{\mathrm{G}n}$ [p.u.]	$Q^{\mathrm{A}}_{\mathrm{G}n}$ [p.u.]	$P^{\mathrm{A}}_{\mathrm{D}n}$ [p.u.]	$Q^{\mathrm{A}}_{\mathrm{D}n}$ [p.u.]	V^{A}_{n} [p.u.]	θ^{A}_{n} [rad.]
1	1	-	0.4575	0.3876	0	0	1.1000	-0.0077
2	2	-	1.2441	0.5284	0	0	1.1000	0
3	3	-	0.9231	0.5640	0	0	1.1000	-0.0018
4	-	1	0	0	0.7000	0.5500	1.0466	-0.0368
5	-	2	0	0	1.0500	0.7000	1.0238	-0.0638
6	-	3	0	0	0.8000	0.6000	1.0476	-0.0444

D.2.1 Network Data

Figure D.2 depicts the IEEE 24-bus system. The transmission lines include two voltage levels, 138 and 230 kV. There are 230/138 kV transformers connected

to buses 11-9, 11-10, 12-9, 12-10 and 24-3. Tables D.6 and D.7 provide the

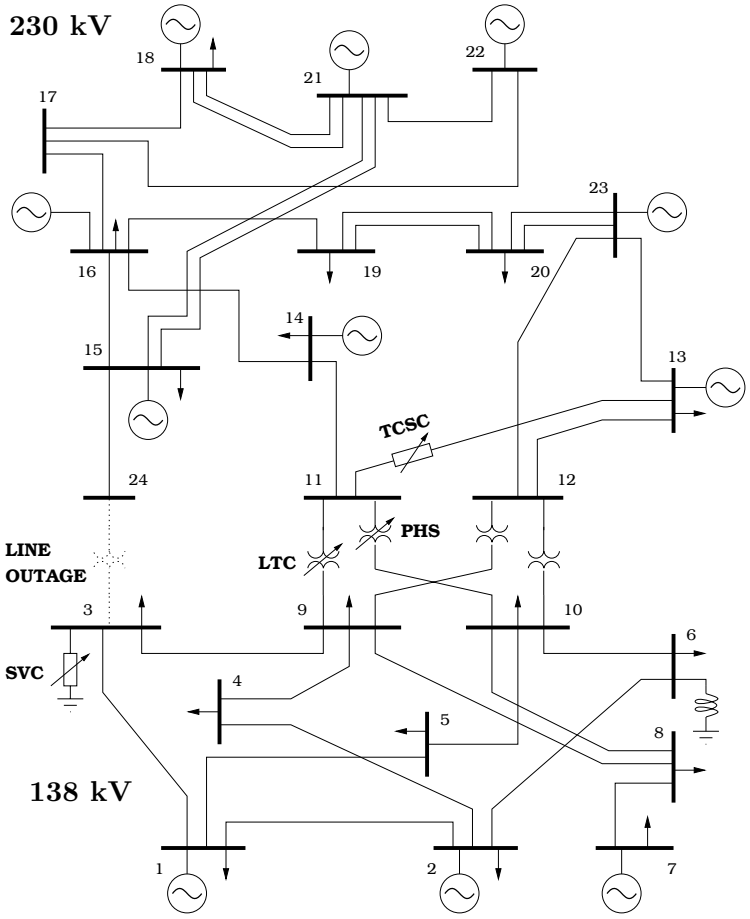

Figure D.2: One-line diagram of the IEEE 24-bus system.

network data and the branch current limits for this system. In addition, a shunt admittance of $-j1$ p.u. is connected to bus 6. The bus voltage magnitude limits are $V_n^{\min} = 0.95$ p.u. and $V_n^{\max} = 1.05$ p.u. for all buses.

Ramping limit values are chosen based on typical response times of LTC and PHS regulators. Positions and data of regulating transformers and FACTS devices are as follows.

- The LTC connects buses 11 and 9. The maximum and minimum tap limits are $T_k^{\max} = 1.05$ p.u./p.u. and $T_k^{\min} = 0.95$ p.u./p.u., respectively,

Table D.6: Network data and branch current limits for the IEEE 24-bus system.

Branch #	From #	To #	r_k [p.u.]	x_k [p.u.]	$b_{\mathrm{p}k}$ [p.u.]	T_k [p.u.]	ϕ_k [p.u.]	$I_k^{\max}$ [p.u.]
1	1	2	0.0026	0.0139	0.4611	-	-	1.75
2	1	3	0.0546	0.2112	0.0572	-	-	1.75
3	1	5	0.0218	0.0845	0.0229	-	-	1.75
4	2	4	0.0328	0.1267	0.0343	-	-	1.75
5	2	6	0.0497	0.1920	0.0520	-	-	1.75
6	3	9	0.0308	0.1190	0.0322	-	-	1.75
7	3	24	0.0023	0.0839	0	1.015	0	4.00
8	4	9	0.0268	0.1037	0.0281	-	-	1.75
9	5	10	0.0228	0.0883	0.0239	-	-	1.75
10	6	10	0.0139	0.0605	2.4590	-	-	1.75
11	7	8	0.0159	0.0614	0.0166	-	-	1.75
12	8	9	0.0427	0.1651	0.0447	-	-	1.75
13	8	10	0.0427	0.1651	0.0447	-	-	1.75
14	9	11	0.0023	0.0839	0	1.030	0	4.00
15	9	12	0.0023	0.0839	0	1.030	0	4.00
16	10	11	0.0023	0.0839	0	1.015	0	4.00
17	10	12	0.0023	0.0839	0	1.015	0	4.00

while the ramp slopes are $R_{\mathrm{T}_k}^{\mathrm{up}} = 0.002$ p.u./p.u.min, and $R_{\mathrm{T}_k}^{\mathrm{down}} = 0.002$ p.u./p.u.min.

- The PHS transformer connects buses 11 and 10. The maximum and minimum phase angle limits are $\phi_k^{\max} = \pi/12$ rad and $\phi_k^{\min} = -\pi/12$ rad, respectively, while the ramp slopes are $R_{\phi_k}^{\mathrm{up}} = \pi/600$ rad/min, and $R_{\phi_k}^{\mathrm{down}} = \pi/600$ rad/min.

- The SVC is placed at bus 3. The maximum and minimum susceptance limits are $b_{\mathrm{SVC},n}^{\max} = 0.5$ p.u., and $b_{\mathrm{SVC},n}^{\min} = -0.5$ p.u., respectively.

Table D.7: Network data and branch current limits for the IEEE 24-bus system (continuation).

Branch #	From #	To #	r_k [p.u.]	x_k [p.u.]	$b_{\mathrm{p}k}$ [p.u.]	T_k [p.u.]	ϕ_k [p.u.]	$I_k^{\max}$ [p.u.]
18	11	13	0.0060	0.0480	0.1000	-	-	1.75
19	11	14	0.0054	0.0418	0.0879	-	-	5.00
20	12	13	0.0060	0.0480	0.1000	-	-	5.00
21	12	23	0.0124	0.0966	0.2030	-	-	5.00
22	13	23	0.0111	0.0865	0.1818	-	-	5.00
23	14	16	0.0050	0.0589	0.0818	-	-	5.00
24	15	16	0.0022	0.0173	0.0364	-	-	5.00
25	15	21	0.0063	0.0490	0.1030	-	-	5.00
26	15	21	0.0063	0.0490	0.1030	-	-	5.00
27	15	24	0.0067	0.0519	0.1091	-	-	5.00
28	16	17	0.0030	0.0259	0.0545	-	-	5.00
29	16	19	0.0030	0.0231	0.0485	-	-	5.00
30	17	18	0.0018	0.0144	0.0303	-	-	5.00
31	17	22	0.0135	0.1053	0.2212	-	-	5.00
32	18	21	0.0033	0.0269	0.0545	-	-	5.00
33	18	21	0.0033	0.0269	0.0545	-	-	5.00
34	19	20	0.0051	0.0396	0.0833	-	-	5.00
35	19	20	0.0051	0.0396	0.0833	-	-	5.00
36	20	23	0.0028	0.0216	0.0455	-	-	5.00
37	20	23	0.0028	0.0216	0.0455	-	-	5.00
38	21	22	0.0087	0.0678	0.1424	-	-	5.00

- The TCSC is placed on the transmission line 11-13. The reactance maximum and minimum limits are $x^{\max}_{\mathrm{TCSC},k} = 0.01$ p.u., and $x^{\min}_{\mathrm{TCSC},k} = -0.01$ p.u., respectively.

D.2.2 Technical Limits for Generators

Tables D.8 and D.9 list the maximum and minimum power outputs, and specify ramping limits for the system generators.

Table D.8: Technical limits for the generators of the IEEE 24-bus system.

Gen. #	$P_{\mathrm{G}j}^{\min}$ [p.u.]	$P_{\mathrm{G}j}^{\max}$ [p.u.]	$Q_{\mathrm{G}j}^{\min}$ [p.u.]	$Q_{\mathrm{G}j}^{\max}$ [p.u.]	$R_{\mathrm{G}j}^{\mathrm{up}}$ [p.u./min]	$R_{\mathrm{G}j}^{\mathrm{down}}$ [p.u./min]
1	0.1000	0.20	0	0.10	0.03	0.03
2	0.1000	0.20	0	0.10	0.03	0.03
3	0.1520	0.76	-0.25	0.30	0.02	0.02
4	0.1520	0.76	-0.25	0.30	0.02	0.02
5	0.1000	0.20	0	0.10	0.03	0.03
6	0.1000	0.20	0	0.10	0.03	0.03
7	0.1520	0.76	-0.25	0.30	0.02	0.02
8	0.1520	0.76	-0.25	0.30	0.02	0.02
9	0.2500	1.00	0	0.60	0.07	0.07
10	0.2500	1.00	0	0.60	0.07	0.07
11	0.2500	1.00	0	0.60	0.07	0.07
12	0.6253	1.97	0	0.80	0.03	0.03
13	0.6253	1.97	0	0.80	0.03	0.03
14	0.6253	1.97	0	0.80	0.03	0.03
15	0	0	-0.50	2.00	0	0
16	0.0240	0.12	0	0.06	0.01	0.01
17	0.0240	0.12	0	0.06	0.01	0.01

D.2.3 Market Solution and Cost Data

Table D.10 shows the generator powers that correspond to the market dispatching solution for the IEEE 24-bus system. Table D.10 also provides the offering costs of the generators to increase or decrease their power outputs for security purposes. Table D.11 shows the demand powers that correspond to

Table D.9: Technical limits for the generators of the IEEE 24-bus system (continuation).

Gen. #	$P_{\mathrm{G}j}^{\min}$ [p.u.]	$P_{\mathrm{G}j}^{\max}$ [p.u.]	$Q_{\mathrm{G}j}^{\min}$ [p.u.]	$Q_{\mathrm{G}j}^{\max}$ [p.u.]	$R_{\mathrm{G}j}^{\mathrm{up}}$ [p.u./min]	$R_{\mathrm{G}j}^{\mathrm{down}}$ [p.u./min]
18	0.0240	0.12	0	0.06	0.01	0.01
19	0.0240	0.12	0	0.06	0.01	0.01
20	0.0240	0.12	0	0.06	0.01	0.01
21	0.5425	1.55	-0.50	0.80	0.03	0.03
22	0.5425	1.55	-0.50	0.80	0.03	0.03
23	1.0000	4.00	-0.50	2.00	0.20	0.20
24	1.0000	4.00	-0.50	2.00	0.20	0.20
25	0	0.50	-0.10	0.16	10.00	10.00
26	0	0.50	-0.10	0.16	10.00	10.00
27	0	0.50	-0.10	0.16	10.00	10.00
28	0	0.50	-0.10	0.16	10.00	10.00
29	0	0.50	-0.10	0.16	10.00	10.00
30	0	0.50	-0.10	0.16	10.00	10.00
31	0.5425	1.55	-0.50	0.80	0.03	0.03
32	0.5425	1.55	-0.50	0.80	0.03	0.03
33	1.4000	3.50	-0.25	1.50	0.04	0.04

the market dispatching solution for the 24-bus system. Constant power factor loads are assumed. Table D.11 also provides the value of $\tan(\psi_{\mathrm{D}i})$ and the cost of load curtailment for each demand. Finally, the penalties for voltage magnitude adjustments at generator buses ($c_{\mathrm{V}n}^{\mathrm{up}}$, $c_{\mathrm{V}n}^{\mathrm{down}}$) and the penalties for set point adjustments of control devices ($c_{\mathrm{LTC}n}^{\mathrm{up}}$, $c_{\mathrm{LTC}n}^{\mathrm{down}}$, $c_{\mathrm{PHS}k}^{\mathrm{up}}$, $c_{\mathrm{PHS}k}^{\mathrm{down}}$, $c_{\mathrm{SVC}n}^{\mathrm{up}}$, $c_{\mathrm{SVC}n}^{\mathrm{down}}$, $c_{\mathrm{TCSC}k}^{\mathrm{up}}$, $c_{\mathrm{TCSC}k}^{\mathrm{down}}$) are all set to \$100/p.u.h The units of penalty factors are introduced only for compatibility with costs.

Table D.10: The market solution and offering costs for the generators of the IEEE 24-bus system.

Gen. #	Bus #	$P_{\mathrm{G}j}^{\mathrm{M}}$ [p.u.]	$c_{\mathrm{G}j}^{\mathrm{up}}$ [$/p.u.h]	$c_{\mathrm{G}j}^{\mathrm{down}}$ [$/p.u.h]	Gen. #	Bus #	$P_{\mathrm{G}j}^{\mathrm{M}}$ [p.u.]	$c_{\mathrm{G}j}^{\mathrm{up}}$ [$/p.u.h]	$c_{\mathrm{G}j}^{\mathrm{down}}$ [$/p.u.h]
1	1	0.1000	26.01	24.01	18	15	0.1200	22.02	21.02
2	1	0.1000	26.00	24.00	19	15	0.1200	22.01	21.01
3	1	0.7600	12.01	10.01	20	15	0.1200	22.00	21.00
4	1	0.7600	12.00	10.00	21	15	1.5500	11.00	9.00
5	2	0.1000	26.01	24.01	22	16	1.5500	11.00	9.00
6	2	0.1000	26.00	24.00	23	18	4.0000	7.00	5.00
7	2	0.7600	12.01	10.01	24	21	4.0000	7.00	5.00
8	2	0.7600	12.00	10.00	25	22	0.5000	3.00	1.00
9	7	0.8000	19.00	17.00	26	22	0.5000	3.01	1.01
10	7	0.8000	19.01	17.01	27	22	0.5000	3.02	1.02
11	7	0.8000	19.02	17.02	28	22	0.5000	3.03	1.03
12	13	0.4543	20.00	18.00	29	22	0.5000	3.04	1.04
13	13	0.4543	20.01	18.01	30	22	0.5000	3.05	1.05
14	13	0.4543	20.02	18.02	31	23	1.5500	11.00	9.00
15	14	0	0	0	32	23	1.5500	11.01	9.01
16	15	0.1200	22.04	21.04	33	23	3.5000	11.02	9.02
17	15	0.1200	22.03	21.03					

D.2.4 Base-Case Operating Condition

Table D.12 shows the base-case operating condition for the IEEE 24-bus system. This base case corresponds to the solution of the OPF problem described in Appendix A. Regulating transformers and FACTS devices are not considered. Note that if control devices are considered, the base-case operating condition differs from the one provided in Table D.12.

Table D.11: The market solution, $\tan(\psi_{\mathrm{D}i})$, and cost of load curtailment for the demands of the IEEE 24-bus system.

Dem. #	Bus #	$P_{\mathrm{D}i}^{\mathrm{M}}$ [p.u.]	$\tan(\psi_{\mathrm{D}i})$ [p.u./p.u.]	$c_{\mathrm{D}i}^{\mathrm{down}}$ [$/p.u.h]	Dem. #	Bus #	$P_{\mathrm{D}i}^{\mathrm{M}}$ [p.u.]	$\tan(\psi_{\mathrm{D}i})$ [p.u./p.u.]	$c_{\mathrm{D}i}^{\mathrm{down}}$ [$/p.u.h]
1	1	1.0800	0.2037	2200	10	10	1.9500	0.2051	2300
2	2	0.9700	0.2062	2200	11	13	2.6500	0.2038	2200
3	3	1.8000	0.2056	2200	12	14	1.9400	0.2010	2200
4	4	0.7400	0.2027	2300	13	15	3.1700	0.2019	2100
5	5	0.7100	0.1972	2300	14	16	1.0000	0.2000	2100
6	6	1.3600	0.2059	2300	15	18	3.3300	0.2042	2100
7	7	1.2500	0.2000	2400	16	19	1.8100	0.2044	2200
8	8	1.7100	0.2047	2400	17	20	1.2800	0.2031	2100
9	9	1.7500	0.2057	2300					

D.3 WECC 9-Bus 3-Machine System

This section provides the data of the WECC 9-bus 3-machine system used in the illustrative example of Section 3.4 of Chapter 3 and in the illustrative example of Section 4.4 of Chapter 4. This system is based on the one reported in [114]. The difference with respect to the data provided in [114] is that the load has been increased by 20%.

D.3.1 Network Data

Figure D.3 depicts the WECC 9-bus, 3-machine system. The transmission lines include four voltage levels, 13.8, 16.5, 18 and 230 kV. A 16.5/230 kV transformer connects buses 1-4, a 18/230 kV transformer connects buses 2-7, and a 13.8/230 kV transformer connects buses 3-9. Table D.13 lists the network data for this system. Observe that current limits are not considered. The bus voltage magnitude limits are $V_n^{\min} = 0.90$ p.u. and $V_n^{\max} = 1.10$ p.u. for the generator buses, whereas $V_n^{\min} = 0.80$ p.u. and $V_n^{\max} = 1.20$ p.u. for the remaining buses.

Table D.12: Base-case operating condition for the IEEE 24-bus system.

Bus #	Gen. #	Dem. #	$P_{\mathrm{G}n}^{\mathrm{A}}$ [p.u.]	$Q_{\mathrm{G}n}^{\mathrm{A}}$ [p.u.]	$P_{\mathrm{D}n}^{\mathrm{A}}$ [p.u.]	$Q_{\mathrm{D}n}^{\mathrm{A}}$ [p.u.]	V_n^{A} [p.u.]	θ_n^{A} [rad.]
1	1-4	1	1.7200	0.0500	1.0800	0.2200	1.0021	-0.1260
2	5-8	2	1.7200	0.0500	0.9700	0.2000	1.0025	-0.1279
3	-	3	0	0	1.8000	0.3700	0.9688	-0.0935
4	-	4	0	0	0.7400	0.1500	0.9762	-0.1739
5	-	5	0	0	0.7100	0.1400	0.9931	-0.1788
6	-	6	0	0	1.3600	0.2800	0.9909	-0.2252
7	9-11	7	2.4000	0.6000	1.2500	0.2500	1.0219	-0.1388
8	-	8	0	0	1.7100	0.3500	0.9845	-0.2033
9	-	9	0	0	1.7500	0.3600	0.9894	-0.1360
10	-	10	0	0	1.9500	0.4000	1.0118	-0.1737
11	-	-	0	0	0	0	0.9978	-0.0500
12	-	-	0	0	0	0	0.9855	-0.0276
13	12-14	11	1.8759	0	2.6500	0.5400	0.9907	0
14	15	12	0	2.0000	1.9400	0.3900	1.0377	0.0056
15	16-21	13	2.1500	0.0004	3.1700	0.6400	1.0098	0.2201
16	22	14	1.5500	0.8000	1.0000	0.2000	1.0246	0.2005
17	-	-	0	0	0	0	1.0331	0.2802
18	23	15	4.0000	1.4368	3.3300	0.6800	1.0373	0.3051
19	-	16	0	0	1.8100	0.3700	1.0276	0.1703
20	-	17	0	0	1.2800	0.2600	1.0401	0.1776
21	24	-	4.0000	-0.5000	0	0	1.0297	0.3213
22	25-30	-	3.0000	0.0712	0	0	1.0500	0.4184
23	31-33	-	6.6000	1.7776	0	0	1.0500	0.1941
24	-	-	0	0	0	0	0.9717	0.1057

D.3.2 Technical Limits for Generators

Table D.14 provides the maximum and minimum power output, and the ramping limits of the system generators.

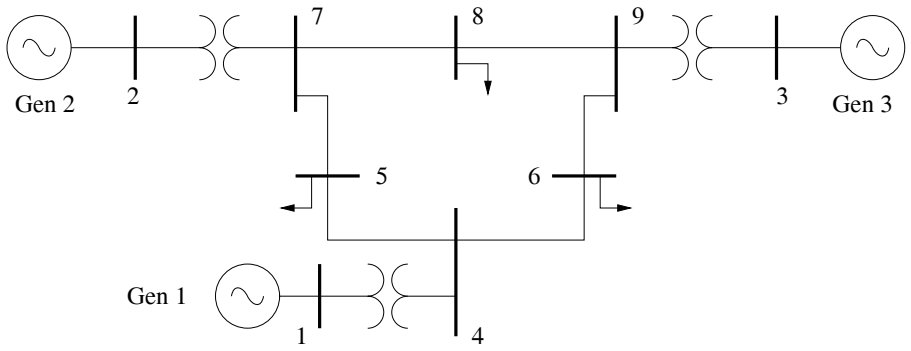

Figure D.3: One-line diagram of the WECC 9-bus, 3-machine system.

Table D.13: Network data for the WECC 9-bus, 3-machine system.

Branch #	From #	To #	r_k [p.u.]	x_k [p.u.]	$b_{\mathrm{p}k}$ [p.u.]	T_k [p.u.]	ϕ_k [p.u.]	$I_k^{\max}$ [p.u.]
1	6	4	0.0170	0.0920	0.1580	-	-	-
2	5	4	0.0100	0.0850	0.1760	-	-	-
3	7	5	0.0320	0.1610	0.3060	-	-	-
4	9	6	0.0390	0.1700	0.3580	-	-	-
5	7	8	0.0085	0.0720	0.1490	-	-	-
6	9	8	0.0119	0.1008	0.2090	-	-	-
7	1	4	0	0.0576	0	1	0	-
8	2	7	0	0.0625	0	1	0	-
9	3	9	0	0.0586	0	1	0	-

D.3.3 Machine Data

Table D.15 shows the dynamic data of the machines for the WECC 9-bus, 3-machine system.

D.3.4 Automatic Voltage Regulator Data

Table D.16 lists the data for the excitation control system of the machines for the WECC 9-bus, 3-machine system.

Table D.14: Technical limits for the generators of the WECC 9-bus, 3-machine system.

Gen. #	$P_{\mathrm{G}j}^{\min}$ [p.u.]	$P_{\mathrm{G}j}^{\max}$ [p.u.]	$Q_{\mathrm{G}j}^{\min}$ [p.u.]	$Q_{\mathrm{G}j}^{\max}$ [p.u.]	$R_{\mathrm{G}j}^{\mathrm{up}}$ [p.u./min]	$R_{\mathrm{G}j}^{\mathrm{down}}$ [p.u./min]
1	0	2.4	-1.5	1.5	0.0720	0.0720
2	0	1.8	-1.5	1.5	0.0540	0.0540
3	0	1.2	-1.5	1.5	0.0360	0.0360

Table D.15: Machine data for the WECC 9-bus, 3-machine system.

Gen. #	M_j [s]	$x_{\mathrm{d}j}$ [p.u.]	$x'_{\mathrm{d}j}$ [p.u.]	$x_{\mathrm{q}j}$ [p.u.]	$x'_{\mathrm{q}j}$ [p.u.]	$T'_{\mathrm{d0}j}$ [s]	$T'_{\mathrm{q0}j}$ [s]
1	47.28	0.1460	0.0608	0.0969	0.0969	8.960	0.310
2	12.80	0.8958	0.1198	0.8645	0.1969	6.000	0.535
3	6.02	1.3125	0.1813	1.2578	0.2500	5.890	0.600

Table D.16: Automatic voltage regulator data for the WECC 9-bus, 3-machine system.

Gen. #	$V_{\mathrm{r}j}^{\max}$ [p.u.]	$V_{\mathrm{r}j}^{\min}$ [p.u.]	$K_{\mathrm{a}j}$ -	$T_{\mathrm{a}j}$ [s]	$K_{\mathrm{f}j}$ -	$T_{\mathrm{f}j}$ [s]	$K_{\mathrm{e}j}$ -	$T_{\mathrm{e}j}$ [s]	$T_{\mathrm{r}j}$ [s]	$A_{\mathrm{e}j}$ -	$B_{\mathrm{e}j}$ -
1	5	-5	20	0.2	0.063	0.35	1	0.314	0.001	0.0039	1.555
2	5	-5	20	0.2	0.063	0.35	1	0.314	0.001	0.0039	1.555
3	5	-5	20	0.2	0.063	0.35	1	0.314	0.001	0.0039	1.555

D.3.5 Market Solution and Cost Data

Table D.17 shows the generator powers that correspond to the market dispatching solution for the WECC 9-bus, 3-machine system. Table D.17 also provides the offering costs of the generators to increase or decrease their power outputs for security purposes. Table D.18 shows the demand powers that correspond to the market dispatching solution for the WECC 9-bus, 3-machine system.

Table D.17: The market solution and offering cost for the generators of the WECC 9-bus, 3-machine system.

Generator #	Bus #	$P^{\mathrm{M}}_{\mathrm{G}j}$ [p.u.]	$c^{\mathrm{up}}_{\mathrm{G}j}$ [\$/p.u.h]	$c^{\mathrm{down}}_{\mathrm{G}j}$ [\$/p.u.h]
1	1	1.2633	2.0	2.0
2	2	1.3212	1.5	1.5
3	3	1.1955	1.8	1.8

Constant power factor loads are assumed. Table D.18 also provides the value of $\tan(\psi_{\mathrm{D}i})$ and the cost of load curtailment for each demand. Finally, the

Table D.18: The market solution, $\tan(\psi_{\mathrm{D}i})$, and cost of load curtailment for the demands of the WECC 9-bus, 3-machine system.

Demand #	Bus #	$P^{\mathrm{M}}_{\mathrm{D}i}$ [p.u.]	$\tan(\psi_{\mathrm{D}i})$ [p.u/p.u]	$c^{\mathrm{down}}_{\mathrm{D}i}$ [\$/p.u.h]
1	5	1.5000	0.4000	1000
2	6	1.0800	0.3333	1000
3	8	1.2000	0.3500	1000

penalties for voltage magnitude adjustments at generator buses ($c^{\mathrm{up}}_{\mathrm{V}n}$, $c^{\mathrm{down}}_{\mathrm{V}n}$) are all set to \$100/p.u.h The units of penalty factors are introduced only for compatibility with costs.

D.3.6 Base-Case Operating Condition

Table D.19 lists the base-case operating condition for the WECC 9-bus, 3-machine system. This base case corresponds to the solution of the OPF problem described in Appendix A.

Table D.19: Base-case operating condition for the WECC 9-bus, 3-machine system.

Bus #	Gen. #	Dem. #	$P_{\mathrm{G}j}^{\mathrm{A}}$ [p.u.]	$Q_{\mathrm{G}j}^{\mathrm{A}}$ [p.u.]	$P_{\mathrm{D}i}^{\mathrm{A}}$ [p.u.]	$Q_{\mathrm{D}i}^{\mathrm{A}}$ [p.u.]	V_n^{A} [p.u.]	θ_n^{A} [rad.]
1	1	-	1.2633	0.2510	0	0	1.1000	0
2	2	-	1.3642	0.0856	0	0	1.1000	0.0514
3	3	-	1.1955	-0.0592	0	0	1.1000	0.0476
4	-	-	0	0	0	0	1.0889	-0.0608
5	-	1	0	0	1.5000	0.6000	1.0595	-0.1164
6	-	2	0	0	1.0800	0.3600	1.0767	-0.0970
7	-	-	0	0	0	0	1.0979	-0.0193
8	-	3	0	0	1.2000	0.4200	1.0863	-0.0567
9	-	-	0	0	0	0	1.1050	-0.0101

D.4 New England 39-Bus 10-Machine System

This section provides the data for the New England 39-bus 10-machine system used in the case study of Subsection 3.5.1 of Chapter 3 and in the case study of Subsection 4.5.1 of Chapter 4. This system is based on the one described in [104]. The difference with respect to the data provided in [104] for this system is that the load has been increased by 15%.

D.4.1 Network Data

Figure D.4 depicts the New England 39-bus, 10-machine system. Tables D.20 and D.21 provide the network data. Observe that current limits are not considered. The bus voltage magnitude limits are $V_n^{\min} = 0.95$ p.u. and $V_n^{\max} = 1.05$ p.u. for the generator buses, whereas $V_n^{\min} = 0.90$ p.u. and $V_n^{\max} = 1.10$ p.u. for the rest of the buses.

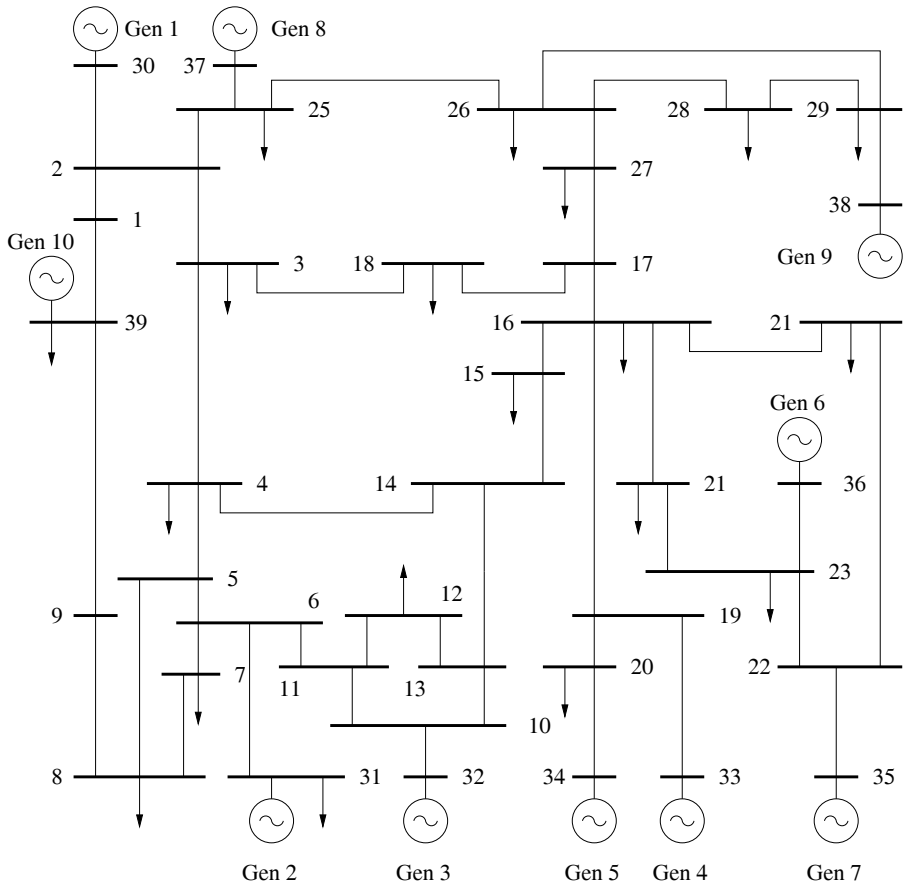

Figure D.4: One-line diagram of the New England 39-bus, 10-machine system.

D.4.2 Technical Limits for Generators

Table D.22 lists the maximum and minimum power outputs, and ramping limits of the system generators.

D.4.3 Machine Data

Table D.23 provides the dynamic data of the machines for the New England 39-bus, 10-machine system.

Table D.20: Network data for the New England 39-bus, 10-machine system.

Branch #	From #	To #	r_k [p.u.]	x_k [p.u.]	b_{pk} [p.u.]	T_k [p.u.]	ϕ_k [p.u.]	I_k^{max} [p.u.]
1	1	2	0.0035	0.0411	0.6987	-	-	-
2	1	39	0.0010	0.0250	0.7500	-	-	-
3	2	3	0.0013	0.0151	0.2572	-	-	-
4	25	2	0.0070	0.0086	0.1460	-	-	-
5	3	4	0.0013	0.0213	0.2214	-	-	-
6	3	18	0.0011	0.0133	0.2138	-	-	-
7	4	5	0.0008	0.0128	0.1342	-	-	-
8	4	14	0.0008	0.0129	0.1382	-	-	-
9	5	6	0.0002	0.0026	0.0434	-	-	-
10	5	8	0.0008	0.0112	0.1476	-	-	-
11	6	7	0.0006	0.0092	0.1130	-	-	-
12	6	11	0.0007	0.0082	0.1389	-	-	-
13	7	8	0.0004	0.0046	0.0780	-	-	-
14	8	9	0.0023	0.0363	0.3804	-	-	-
15	9	39	0.0010	0.0250	1.2000	-	-	-
16	10	11	0.0004	0.0043	0.0729	-	-	-
17	10	13	0.0004	0.0043	0.0729	-	-	-
18	13	14	0.0009	0.0101	0.1723	-	-	-
19	14	15	0.0018	0.0217	0.3660	-	-	-
20	15	16	0.0009	0.0094	0.1710	-	-	-
21	16	17	0.0007	0.0089	0.1342	-	-	-
22	21	16	0.0008	0.0135	0.2548	-	-	-
23	16	24	0.0003	0.0059	0.0680	-	-	-

D.4.4 Automatic Voltage Regulator Data

Table D.24 shows the data for the excitation control system of the machines for the New England 39-bus, 10-machine system.

Table D.21: Network data for the New England 39-bus, 10-machine system (continuation).

Branch #	From #	To #	r_k [p.u.]	x_k [p.u.]	$b_{\mathrm{p}k}$ [p.u.]	T_k [p.u.]	ϕ_k [p.u.]	$I_k^{\max}$ [p.u.]
24	17	18	0.0007	0.0082	0.1319	-	-	-
25	17	27	0.0013	0.0173	0.3216	-	-	-
26	21	22	0.0008	0.0140	0.2565	-	-	-
27	22	23	0.0006	0.0096	0.1846	-	-	-
28	23	24	0.0022	0.0350	0.3610	-	-	-
29	25	26	0.0032	0.0323	0.5130	-	-	-
30	26	27	0.0014	0.0147	0.2396	-	-	-
31	28	26	0.0043	0.0474	0.7802	-	-	-
32	26	29	0.0057	0.0625	1.0290	-	-	-
33	28	29	0.0014	0.0151	0.2490	-	-	-
34	12	11	0.0016	0.0435	0	1.006	0	-
35	12	13	0.0016	0.0435	0	1.006	0	-
36	16	19	0.0016	0.0195	0.3040	-	-	-
37	6	31	0	0.0250	0	1.070	0	-
38	10	32	0	0.0200	0	1.070	0	-
39	19	33	0.0007	0.0142	0	1.070	0	-
40	20	34	0.0009	0.0180	0	1.009	0	-
41	22	35	0	0.0143	0	1.025	0	-
42	23	36	0.0005	0.0272	0	1	0	-
43	25	37	0.0006	0.0232	0	1.025	0	-
44	2	30	0	0.0181	0	1.025	0	-
45	29	38	0.0008	0.0156	0	1.025	0	-
46	19	20	0.0007	0.0138	0	1.060	0	-

D.4.5 Market Solution and Cost Data

Table D.25 lists the generator powers that correspond to the market dispatching solution for the New England 39-bus, 10-machine system. Table D.25 also

Table D.22: Technical limits for the generators of the New England 39-bus, 10-machine system.

Gen. #	$P_{\mathrm{G}j}^{\min}$ [p.u.]	$P_{\mathrm{G}j}^{\max}$ [p.u.]	$Q_{\mathrm{G}j}^{\min}$ [p.u.]	$Q_{\mathrm{G}j}^{\max}$ [p.u.]	$R_{\mathrm{G}j}^{\mathrm{up}}$ [p.u./min]	$R_{\mathrm{G}j}^{\mathrm{down}}$ [p.u./min]
1	0	4.0250	-2.4945	2.4945	0.0671	0.0671
2	0	7.4750	-4.6326	4.6326	0.1246	0.1246
3	0	9.2000	-5.7016	5.7016	0.1533	0.1533
4	0	8.6250	-5.3453	5.3453	0.1437	0.1437
5	0	7.4750	-4.6326	4.6326	0.1246	0.1246
6	0	8.6250	-5.3453	5.3453	0.1437	0.1437
7	0	8.6250	-5.3453	5.3453	0.1437	0.1437
8	0	8.0500	-4.9889	4.9889	0.1342	0.1342
9	0	10.3500	-6.4144	6.4144	0.1725	0.1725
10	0	13.8000	-8.5525	8.5525	0.2300	0.2300

provides the offering costs of the generators to increase or decrease their power outputs for security purposes. Table D.26 shows the demand powers that correspond to the market dispatching solution for the New England 39-bus, 10-machine system. Constant power factor loads are assumed. Table D.26 also provides the value of $\tan(\psi_{\mathrm{D}i})$ and the cost of load curtailment for each demand. Finally, the penalties for voltage magnitude adjustments at generator buses ($c_{\mathrm{V}n}^{\mathrm{up}}$, $c_{\mathrm{V}n}^{\mathrm{down}}$) are all set to \$100/p.u.h. The units of penalty factors are introduced only for compatibility with costs.

D.4.6 Base-Case Operating Condition

Tables D.27 and D.28 list the base-case operating condition for the New England 39-bus, 10-machine system. This base case corresponds to the solution of the OPF problem described in Appendix A.

Table D.23: Machine data for the New England 39-bus, 10-machine system.

Gen. #	M_j [s]	$x_{\mathrm{d}j}$ [p.u.]	$x'_{\mathrm{d}j}$ [p.u.]	$x_{\mathrm{q}j}$ [p.u.]	$x'_{\mathrm{q}j}$ [p.u.]	$T'_{\mathrm{d0}j}$ [s]	$T'_{\mathrm{q0}j}$ [s]
1	84.0	0.1000	0.0310	0.0690	0.0080	10.20	0.10
2	60.6	0.2950	0.0697	0.2820	0.1700	6.56	1.50
3	71.6	0.2495	0.0531	0.2370	0.0876	5.70	1.50
4	57.2	0.2620	0.0436	0.2580	0.1660	5.69	1.50
5	52.0	0.6700	0.1320	0.6200	0.1660	5.40	0.44
6	69.6	0.2540	0.0500	0.2410	0.0814	7.30	0.40
7	52.8	0.2950	0.0490	0.2920	0.1860	5.66	1.50
8	48.6	0.2900	0.0570	0.2800	0.0911	6.70	0.41
9	69.0	0.2106	0.0570	0.2050	0.0587	4.79	1.96
10	1000.0	0.0200	0.0060	0.0190	0.0080	7.00	0.70

Table D.24: Automatic voltage regulator data for the New England 39-bus, 10-machine system.

Gen. #	$V_{\mathrm{r}j}^{\max}$ [p.u.]	$V_{\mathrm{r}j}^{\min}$ [p.u.]	$K_{\mathrm{a}j}$ -	$T_{\mathrm{a}j}$ [s]	$K_{\mathrm{f}j}$ -	$T_{\mathrm{f}j}$ [s]	$K_{\mathrm{e}j}$ -	$T_{\mathrm{e}j}$ [s]	$T_{\mathrm{r}j}$ [s]	$A_{\mathrm{e}j}$ -	$B_{\mathrm{e}j}$ -
1	1.0	-1.0	5.0	0.06	0.0400	1.0000	-0.0485	0.250	0.001	0.0023	0.9971
2	1.0	-1.0	6.2	0.05	0.0570	0.5000	-0.6330	0.405	0.001	0.2784	0.2842
3	1.0	-1.0	5.0	0.06	0.0800	1.0000	-0.0198	0.500	0.001	0.0073	1.2314
4	1.0	-1.0	5.0	0.06	0.0800	1.0000	-0.0525	0.500	0.001	0.0013	1.4303
5	10.0	-10.0	40.0	0.02	0.0300	1.0000	1.0000	0.785	0.001	0	1.9596
6	1.0	-1.0	5.0	0.02	0.0754	1.2460	-0.0419	0.471	0.001	0.0011	1.1430
7	6.5	-6.5	40.0	0.02	0.0300	1.0000	1.0000	0.730	0.001	0.1947	0.3574
8	1.0	-1.0	5.0	0.02	0.0854	1.2600	-0.0470	0.528	0.001	0.0012	1.2833
9	10.5	-10.5	40.0	0.02	0.0300	1.0000	1.0000	1.400	0.001	0.2406	0.2224

D.5 IEEE 145-Bus 50-Machine System

This section provides the technical limits, offering costs and penalty factors for the IEEE 145-bus, 50-machine system used in the case study of Subsection 3.5.2 of Chapter 3. The IEEE 145-bus, 50-machine system was originally

Table D.25: The market solution and offering cost for the generators of the New England 39-bus, 10-machine system.

Gen. #	Bus #	$P_{\mathrm{G}j}^{\mathrm{M}}$ [p.u.]	$c_{\mathrm{G}j}^{\mathrm{up}}$ [$/p.u.h]	$c_{\mathrm{G}j}^{\mathrm{down}}$ [$/p.u.h]
1	30	2.9134	6.9	6.9
2	31	5.9783	3.7	3.7
3	32	7.3250	2.8	2.8
4	33	7.3089	4.7	4.7
5	34	5.7801	2.8	2.8
6	35	7.4560	3.7	3.7
7	36	6.4704	4.8	4.8
8	37	6.1246	3.6	3.6
9	38	9.4772	3.7	3.7
10	39	11.2828	3.9	3.9

reported in [101]. The data used in this thesis correspond to the slightly modified version of this system, which can be found in the software package Power System Toolbox (PST) [29].

It is assumed that the generator and load powers provided in [29] correspond to the solution of a market clearing procedure. Thus, from this market solution, the base-case operating condition is obtained by solving the OPF problem described in Appendix A.

Technical limits, offering costs and penalty factors for the IEEE 145-bus, 50-machine system are as follows. Bus voltage magnitude limits are $V_n^{\max} = 1.1$ p.u. and $V_n^{\min} = 0.9$ p.u. for all generator buses, and $V_n^{\max} = 1.2$ p.u. and $V_n^{\min} = 0.8$ p.u. for the remaining buses. $P_{\mathrm{G}j}^{\min} = 0$ is used for all generators, whereas $P_{\mathrm{G}j}^{\max}$ is set to the value that results from increasing a 10% the active power output of each generator. Ramping limits are $R_{\mathrm{G}j}^{\mathrm{up}} = R_{\mathrm{G}j}^{\mathrm{down}} = (P_{\mathrm{G}j}^{\max} - P_{\mathrm{G}j}^{\min})/60$ p.u./min. Generator reactive power limits are provided in [101]. With regard to the offering costs and penalty factors, $c_{\mathrm{G}j}^{\mathrm{up}} = c_{\mathrm{G}j}^{\mathrm{down}} =$ \$10/p.u.h for all generators, $c_{\mathrm{D}i}^{\mathrm{down}} =$ \$1000/p.u.h for all loads, and $c_{\mathrm{V}n}^{\mathrm{up}} =$

Table D.26: Market solution, $\tan(\psi_{\mathrm{D}i})$, and cost of load curtailment for the demands of the New England 39-bus, 10-machine system.

Dem. #	Bus #	$P_{\mathrm{D}i}^{\mathrm{M}}$ [p.u.]	$\tan(\psi_{\mathrm{D}i})$ [p.u./p.u.]	$c_{\mathrm{D}i}^{\mathrm{down}}$ [$/p.u.h]	Dem. #	Bus #	$P_{\mathrm{D}i}^{\mathrm{M}}$ [p.u.]	$\tan(\psi_{\mathrm{D}i})$ [p.u./p.u.]	$c_{\mathrm{D}i}^{\mathrm{down}}$ [$/p.u.h]
1	3	3.7030	0.0075	1000	11	23	2.8462	0.3418	1000
2	4	5.7500	0.3680	1000	12	24	3.5489	-0.2988	1000
3	7	2.6887	0.3593	1000	13	25	2.5760	0.2107	1000
4	9	6.0030	0.3372	1000	14	26	1.5985	0.1223	1000
5	12	0.0862	11.7333	1000	15	27	3.2315	0.2687	1000
6	15	3.6800	0.4781	1000	16	28	2.3690	0.1340	1000
7	16	3.7835	0.0982	1000	17	29	3.2603	0.0949	1000
8	18	1.8170	0.1899	1000	18	31	0.1058	0.5000	1000
9	20	7.2220	0.1640	1000	19	39	12.6960	0.2264	1000
10	21	3.1510	0.4197	1000					

$c_{\mathrm{V}n}^{\mathrm{down}}$ = \$100/p.u.h for all generator buses, are used. The units of penalty factors are introduced only for compatibility with costs.

Table D.27: Base-case operating condition for the New England 39-bus, 10-machine system.

Bus #	Gen. #	Dem. #	$P^{\mathrm{A}}_{\mathrm{G}j}$ [p.u.]	$Q^{\mathrm{A}}_{\mathrm{G}j}$ [p.u.]	$P^{\mathrm{A}}_{\mathrm{D}i}$ [p.u.]	$Q^{\mathrm{A}}_{\mathrm{D}i}$ [p.u.]	V^{A}_{n} [p.u.]	θ^{A}_{n} [rad.]
1	-	-	0	0	0	0	1.0637	-0.1572
2	-	-	0	0	0	0	1.0598	-0.1018
3	-	1	0	0	3.7030	0.0276	1.0482	-0.1567
4	-	2	0	0	5.7500	2.1160	1.0345	-0.1744
5	-	-	0	0	0	0	1.0442	-0.1556
6	-	-	0	0	0	0	1.0489	-0.1431
7	-	3	0	0	2.6887	0.9660	1.0346	-0.1841
8	-	4	0	0	6.0030	2.0240	1.0324	-0.1935
9	-	-	0	0	0	0	1.0552	-0.1922
10	-	-	0	0	0	0	1.0618	-0.0941
11	-	-	0	0	0	0	1.0559	-0.1107
12	-	5	0	0	0.0862	1.0120	1.0405	-0.1098
13	-	-	0	0	0	0	1.0554	-0.1069
14	-	-	0	0	0	0	1.0449	-0.1370
15	-	6	0	0	3.6800	1.7595	1.0362	-0.1395
16	-	7	0	0	3.7835	0.3714	1.0494	-0.1099
17	-	-	0	0	0	0	1.0504	-0.1320
18	-	8	0	0	1.8170	0.3450	1.0479	-0.1497
19	-	-	0	0	0	0	1.0878	-0.0134
20	-	9	0	0	7.2220	1.1845	1.0265	-0.0328

Table D.28: Base-case operating condition for the New England 39-bus, 10-machine system (continuation).

Bus #	Gen. #	Dem. #	$P^{\mathrm{A}}_{\mathrm{G}j}$ [p.u.]	$Q^{\mathrm{A}}_{\mathrm{G}j}$ [p.u.]	$P^{\mathrm{A}}_{\mathrm{D}i}$ [p.u.]	$Q^{\mathrm{A}}_{\mathrm{D}i}$ [p.u.]	V^{A}_{n} [p.u.]	θ^{A}_{n} [rad.]
21	-	10	0	0	3.1510	1.3225	1.0397	-0.0622
22	-	-	0	0	0	0	1.0514	0.0269
23	-	11	0	0	2.8462	0.9729	1.0436	0.0232
24	-	12	0	0	3.5489	-1.0603	1.0524	-0.1074
25	-	13	0	0	2.5760	0.5428	1.0722	-0.0773
26	-	14	0	0	1.5985	0.1955	1.0672	-0.0997
27	-	15	0	0	3.2315	0.8682	1.0526	-0.1370
28	-	16	0	0	2.3690	0.3174	1.0670	-0.0330
29	-	17	0	0	3.2603	0.3093	1.0685	0.0199
30	1	-	2.9134	0.6096	0	0	1.0433	-0.0529
31	2	18	5.9783	3.4014	0.1058	0.0529	1.0500	0
32	3	-	7.8748	3.6284	0	0	1.0500	0.0576
33	4	-	7.3089	2.4490	0	0	1.0500	0.0823
34	5	-	5.7801	1.8918	0	0	1.0500	0.0632
35	6	-	7.4560	2.1510	0	0	1.0500	0.1260
36	7	-	6.4704	0.6494	0	0	1.0500	0.1842
37	8	-	6.1246	0.4172	0	0	1.0500	0.0522
38	9	-	9.4772	0.6580	0	0	1.0500	0.1549
39	10	19	11.2828	1.0864	12.6960	2.8750	1.0500	-0.1902

Bibliography

[1] E. Acha, H. Ambriz-Pérez, and C. R. Fuerte-Esquivel. Advanced transformer control modeling in an optimal power flow using newton's method. *IEEE Transactions on Power Systems*, 15(1):290–298, February 2000.

[2] V. Ajjarapu and C. Christy. The continuation power flow: A tool for steady state voltage stability analysis. *IEEE Transactions on Power Systems*, 7(1):416–423, February 1992.

[3] O. Alsaç and B. Stott. Optimal load flow with steady-state security. *IEEE Transactions on Power Apparatus and Systems*, PAS-93(3):745–751, May 1974.

[4] H. Ambriz-Pérez, E. Acha, and C. R. Fuerte-Esquivel. Advanced svc models for newton-raphson load flow and newton optimal power flow studies. *IEEE Transactions on Power Systems*, 15(1):129–136, February 2000.

[5] P. M. Anderson and A. A. Fouad. *Power System Control and Stability*. The Iowa State University Press, Ames, Iowa, 1977.

[6] J. Arrillaga and C. P. Arnold. *Computer Analysis of Power Systems*. John Wiley & Sons, Englewood Cliffs, NJ, 1990.

[7] T. Athay, R. Podmore, and S. Virmani. A practical method for the direct analysis of transient stability. *IEEE Transactions on Power Apparatus and Systems*, PAS-98(2):573–584, March 1979.

[8] R. J. Avalos, C. A. Cañizares, F. Milano, and A. J. Conejo. Equivalency of continuation and optimization methods to determine saddle-node and

limit-induced bifurcations in power systems. *IEEE Transactions on Circuits and Systems - I: Regular Papers*, 56(1):210–223, January 2009.

[9] N. Balu, T. Bertram, A. Bose, V. Brandwajn, J. Cauley, D. Curtice, A. A. Fouad, L. Fink, M. G. Lauby, B. F. Wollenberg, and J. N. Wrubel. On-line power system security analysis. *Proceedings of the IEEE*, 80(2):262–280, February 1992.

[10] M. S. Bazaraa, H. O. Sherali, and C. M. Shetty. *Nonlinear Programming: Theory and Algorithms*. John Wiley & Sons, New York, NY, 1993.

[11] M. Begovic and A. Phadke. Control of voltage stability using sensitivity analysis. *IEEE Transactions on Power Systems*, 7(1):114–123, February 1992.

[12] A. Berizzi, P. Finazzi, D. Dosi, P. Marannino, and S. Corsi. First and second order methods for voltage collapse assessment and security enhancement. *IEEE Transactions on Power Systems*, 13(2):543–551, May 1998.

[13] J. H. Bian and P. Rastgoufard. Power system voltage stability and security assessment. *Electric Power Systems Research*, 30(3):197–201, November 1994.

[14] E. Bompard, P. Correia, G. Gross, and M. Amalin. Congestion management schemes: A comparative analysis under a unified framework. *IEEE Transactions on Power Systems*, 18(1):346–352, February 2003.

[15] H. J. Bremermann. *Optimization through Evolution and Recombination*. Self Organization Systems. Spartan Books, Wasington D. C., 1962.

[16] A. Brooke, D. Kendrick, A. Meeraus, R. Raman, and R. E. Rosenthal. *GAMS, a User's Guide*. GAMS Development Corporation, 1217 Potomac Street, NW, Washington, DC 20007, USA, December 1998. available at http://www.gams.com/.

[17] H. R. Cai, C. Y. Chung, and K. P. Wong. Application of differential evolution algorithm for transient stability constrained optimal power flow. *IEEE Transactions on Power Systems*, 23(2):719–728, May 2008.

[18] C. A. Cañizares. Calculating optimal system parameters to maximize the distance to saddle-node bifurcations. *IEEE Transactions on Circuits and Systems - I: Regular Papers*, 45(3):225–237, March 1998.

[19] C. A. Cañizares and F. L. Alvarado. Point of collapse and continuation methods for large AC/DC systems. *IEEE Transactions on Power Systems*, 8(1):1–8, February 1993.

[20] C. A. Cañizares, A. Z. de Souza, and V. H. Quintana. Comparison of performance indices for detection of proximity to voltage collapse. *IEEE Transactions on Power Systems*, 11(3):1441–1450, August 1996.

[21] C. A. Cañizares, N. Mithulananthan, F. Milano, and J. Reeve. Linear performance indices to predict oscillatory stability problems in power systems. *IEEE Transactions on Power Systems*, 18(2):1104–1114, May 2004.

[22] F. Capitanescu and T. Van Cutsem. Preventive control of voltage security margins: a multicontingency sensitivity-based approach. *IEEE Transactions on Power Systems*, 17(2):358–364, May 2002.

[23] F. Capitanescu and T. Van Cutsem. Unified sensitivity analysis of unstable or low voltages caused by load increases or contingencies. *IEEE Transactions on Power Systems*, 20(1):321–329, February 2005.

[24] F. Capitanescu, M. Glavic, D. Ernst, and L. Wehenkel. Contingency filtering techniques for preventive security-constrained optimal power flow. *IEEE Transactions on Power Systems*, 22(4):1690–1697, November 2007.

[25] F. Capitanescu and L. Wehenkel. A new iterative approach to the corrective security-constrained optimal power flow problem. *IEEE Transactions on Power Systems*, 23(4):1533–1541, November 2008.

[26] J. Carpentier. Contribution à l'étude du dispatching économique. *Bulletin de la Société Française des Électriciens*, 3:431–447, August 1962.

[27] D. Chattopadhyay and D. Gan. Market dispatch incorporating stability constraints. *International Journal on Electric Power & Energy Systems*, 23(6):459–469, August 2001.

[28] L. Chen, Y. Tada, H. Okamoto, R. Tanabe, and A. Ono. Optimal operation solutions of power systems with transient stability constraints. *IEEE Transactions on Circuits and Systems - I: Fundamental Theory and Applications*, 48(3):327–339, March 2001.

[29] Cherry Tree Scientific Software, Colborne, ON, Canada. *Power System Toolbox Ver. 2.0: Dynamic Tutorial and Functions*, 1999.

[30] H. D. Chiang and R. Jean-Jumeau. Toward a practical performance index for predicting voltage collapse in electric power systems. *IEEE Transactions on Power Systems*, 10(2):584–592, May 1995.

[31] H. D. Chiang, F. F. Wu, and P. P. Varaiya. A BCU method for direct analysis of power system transient stability. *IEEE Transactions on Power Systems*, 9(3):1194–1200, August 1994.

[32] C. Y. Chung, L. Wang, F. Howell, and P. Kundur. Generation rescheduling methods to improve power transfer capability constrained by small-signal stability. *IEEE Transactions on Power Systems*, 19(1):524–530, February 2004.

[33] J. Condren and T. W. Gedra. Expected-security cost optimal power flow with small-signal stability constraints. *IEEE Transactions on Power Systems*, 21(4):1736–1743, November 2006.

[34] J. Condren, T. W. Gedra, and P. Damrongkulkamjorn. Optimal power flow with expected-security costs. *IEEE Transactions on Power Systems*, 21(2):541–547, May 2006.

[35] A. J. Conejo, E. Castillo, R. Mínguez, and R. García-Bertrand. *Decomposition Techniques in Mathematical Programming*. Springer, Berlin; New York, 2006.

[36] A. J. Conejo, F. Milano, and R. García-Bertrand. Congestion management ensuring voltage stability. *IEEE Transactions on Power Systems*, 21(1):357–364, April 2006.

[37] A. J. A. S. Costa, F. D. Freitas, and H. E. Peña. Power system stabilizer design via structurally constrained optimal control. *Electric Power System Research*, 33(1):33–40, April 1995.

[38] T. Van Cutsem. A method to compute reactive power margins with respect to voltage collapse. *IEEE Transactions on Power Systems*, 6(1):145–156, February 1991.

[39] T. Van Cutsem. An approach to corrective control of voltage instability using simulation and sensitivities. *IEEE Transactions on Power Systems*, 10(2):616–622, May 1995.

[40] T. Van Cutsem. Voltage instability: Phenomena, countermeasures, and analysis methods. *Proceedings of the IEEE*, 88(2):208–227, February 2000.

[41] T. Van Cutsem, Y. Jacquemart, J. N. Marquet, and P. Pruvot. A comprehensive analysis of mid-term voltage stability. *IEEE Transactions on Power Systems*, 10(3):1173–1182, August 1995.

[42] T. Van Cutsem and R. Mailhot. Validation of a fast voltage stability analysis method on the hydro-quebec system. *IEEE Transactions on Power Systems*, 12(1):282–292, February 1997.

[43] T. Van Cutsem, C. Moisse, and R. Mailhot. Determination of secure operating limits with respect to voltage collapse. *IEEE Transactions on Power Systems*, 14(1):327–335, February 1999.

[44] T. Van Cutsem and C. Vournas. *Voltage Stability of Electric Power Systems*. Springer, New York, NY, 1998.

[45] A. C. Z. de Souza, C. A. Cañizares, and V. H. Quintana. New techniques to speed up voltage collapse computations using tangent vectors. *IEEE Transactions on Power Systems*, 12(3):1380–1387, August 1997.

[46] C. L. DeMarco and C. A. Cañizares. A vector energy function apprach for security analysis of AC/DC systems. *IEEE Transactions on Power Systems*, 7(3):1001–1011, August 1992.

[47] I. Dobson and H. D. Chiang. Towards a theory of voltage collapse in electric power systems. *Systems & Control Letters*, 13(3):253–262, September 1989.

[48] I. Dobson and L. Lu. Voltage collapse precipitated by the immediate change of stability when generator reactive power limits are encountered. *IEEE Transactions on Circuits and Systems - I: Regular Papers*, 39(2):762–766, September 1992.

[49] H. W. Dommel and W. F. Tinney. Optimal power flow solutions. *IEEE Transactions on Power Apparatus and Systems*, PAS-87(10):1866–1876, October 1968.

[50] A. S. Drud. *GAMS/CONOPT*. ARKI Consulting and Development, Bagsvaerdvej 246A, DK-2880 Bagsvaerd, Denmark, 1996. Available at http://www.gams.com/.

[51] H. M. Zein El-Din and R. T. H. Alden. Second order eigenvalue sensitivities applied to power system dynamics. *IEEE Transactions on Power Apparatus and Systems*, 96(6):1928–1936, November 1977.

[52] A. G. Expósito, J. L. M. Ramos, and J. R. Santos. Slack bus selection to minimize the system power imbalance in load-flow studies. *IEEE Transactions on Power Systems*, 19(2):987–995, May 2004.

[53] D. Z. Fang, Y. Xiaodong, S. Jingqiang, Y. Shiqiang, and Z. Yao. An optimal generation rescheduling approach for transient stability enhancement. *IEEE Transactions on Power Systems*, 22(1):386–394, February 2007.

[54] M. M. Farsangi, Y. H. Song, and K. Y. Lee. Choice of FACTS device control inputs for damping interarea oscillations. *IEEE Transactions on Power Systems*, 19(2):1135–1143, May 2004.

[55] Z. H. Feng, V. Ajjarpu, and D. J. Maratukulam. A comprehensive approach for preventive can corrective control to mitigate voltage collapse. *IEEE Transactions on Power Systems*, 15(2):791–797, May 2000.

[56] N. Flatabø, O. B. Fosso, R. Ognedal, T. Carlsen, and K. R. Heggland. A method for calculation of margins to voltage instability applied on the norwegian system for maintaining required security level. *IEEE Transactions on Power Systems*, 8(3):920–928, August 1993.

[57] A. A. Fouad and V. Vittal. *Power System Transient Stability Analysis Using the Transient Energy Function Method*. Prentice-Hall, Englewood Cliffs, NJ, 1992.

[58] F. D. Freitas and A. S. Costa. Computationally efficient optimal control methods applied to power systems. *IEEE Transactions on Power Systems*, 14(3):1036–1045, August 1999.

[59] L. L. Freris and A. M. Sasson. Investigation of the load-flow problem. *Proceedings of the Institution of Electrical Engineers*, 115(10):1459–1470, October 1968.

[60] C. R. Fuerte-Esquivel, E. Acha, and H. Ambriz-Pérez. A thyristor controlled series compensator model for the power flow solution of practical power networks. *IEEE Transactions on Power Systems*, 15(1):58–64, February 2000.

[61] D. Gan, R. J. Thomas, and R. D. Zimmerman. Stability-constrained optimal power flow. *IEEE Transactions on Power Systems*, 15(2):535–540, May 2000.

[62] B. Gao, G. K. Morison, and P. Kundur. Voltage stability evaluation using modal analysis. *IEEE Transactions on Power Systems*, 7(4):1529–1542, November 1992.

[63] B. Gao, G. K. Morison, and P. Kundur. Toward the development of a systematic approach for voltage stability assessment of large-scale power systems. *IEEE Transactions on Power Systems*, 11(3):1314–1324, August 1996.

[64] T. W. Gedra. On transmission congestion and pricing. *IEEE Transactions on Power Systems*, 14(1):241–248, February 1999.

[65] A. Gómez-Expósito, A. J. Conejo, and C. Cañizares Editors. *Electric Energy Systems: Analysis and Operation*. CRC Press, Boca Raton, FL, 2009.

[66] S. Greene, I. Dobson, and F. L. Alvarado. Sensitivity of the loading margin to voltage collapse with respect to arbitrary parameters. *IEEE Transactions on Power Systems*, 12(1):262–268, February 1997.

[67] L. T. Grujic, A. A. Martynyuk, and M. Ribbens-Pavella. *Large Scale Systems Stability Under Structural and Singular Perturbations*. Springer-Verlag, New York, NY, 1987.

[68] X. Guoyu, F. D. Galiana, and S. Low. Decoupled economic dispatch using the participation factors load flow. *IEEE Transactions on Power Apparatus and Systems*, 104(6):1377–1384, June 1985.

[69] P. H. Haley and M. Ayres. Super decoupled loadflow with distributed slack bus. *IEEE Transactions on Power Apparatus and Systems*, 104(1):104–113, January 1985.

[70] D. J. Hill. Nonlinear dynamic load models with recovery for voltage stability studies. *IEEE Transactions on Power Systems*, 8(1):166–176, February 1993.

[71] M. Huneault and F. D. Galiana. A survey of the optimal power flow literature. *IEEE Transactions on Power Systems*, 6(2):762–770, May 1991.

[72] M. Klein, G. J. Rogers, S. Moorty, and P. Kundur. Analytical investigation of factors influencing power system stabilizers performance. *IEEE Transactions on Energy Conversion*, 7(3):382–390, September 1992.

[73] P. Kundur. *Power System Stability and Control*. McGraw-Hill, New York, NY, 1994.

[74] P. Kundur, M. Klein, G. J. Rogers, and M. S. Zywno. Application of power system stabilizers for enhancement of overall system stability. *IEEE Transactions on Power Systems*, 4(2):614–626, May 1989.

[75] P. Kundur, M. G. Rogers, D. Y. Wong, L. Wang, and M. G. Lauby. A comprehensive computer program package for small signal stability of power systems. *IEEE Transactions on Power Systems*, 5(4):1076–1083, November 1990.

[76] A. Kurita, H. Okubo, K. Oki, S. Agematsu, D. B. Klapper, N. W. Miller, W. W. Price, J. J. Sánchez-Gasca, K. A. Wirgau, and T. D. Younkins. Multiple time-scale power system dynamic simulation. *IEEE Transactions on Power Systems*, 8(1):216–223, February 1993.

[77] H. G. Kwatny and G. E. Piper. Frequency domain analysis of hopf bifurcations in electric power systems. *IEEE Transaction on Circuits and Systems*, 37(10):1317–1321, October 1990.

[78] D. Layden and B. Jeyasurya. Integrating security constraints in optimal power flow studies. *Proceedings of the IEEE PES General Meeting*, 1:125–129, June 2004.

[79] C. W. Liu and J. S. Thorp. A novel method to compute the closest unstable equilibrium point for transient stability region estimate in power systems. *IEEE Transactions on Power Systems*, 44(7):630–635, July 1997.

[80] P. A. Löf, T. Smed, G. Andersson, and D. J. Hill. Fast calculation of a voltage stability index. *IEEE Transactions on Power Systems*, 7(1):54–64, February 1992.

[81] D. G. Luenberger and Y. Ye. *Linear and nonlinear programming*. Springer, Spring Street, NY, third edition, 2008.

[82] A. M. Lyapunov. *Stability of Motion*. Academic Press, New York, NY, 1966.

[83] G. A. Maria, C. Tang, and J. Kim. Hybrid transient stability analysis. *IEEE Transactions on Power Systems*, 5(2):384–393, May 1990.

[84] N. Martins. The dominant pole spectrum eigensolver. *IEEE Transactions on Power Systems*, 12(1):245–254, February 1997.

[85] E. L. Miguélez, L. R. Rodríguez, T. G. San Román, F. M. E. Cerezo, M. I. N. Fernández, R. C. Lafarga, and G. L. Camino. A practical approach to solve power system constraints with application to the Spanish electricity market. *IEEE Transactions on Power Systems*, 19(4):2029–2037, November 2004.

[86] F. Milano. An open source power system analysis toolbox. *IEEE Transactions on Power Systems*, 20(3):1199–1206, August 2005.

[87] F. Milano, C. A. Cañizares, and A. J. Conejo. Sensitivity-based security-constrained opf market clearing model. *IEEE Transactions on Power Systems*, 20(4):2051–2060, November 2005.

[88] F. Milano, C. A. Cañizares, and M. Invernizzi. Multiobjective optimization for pricing system security in electricity markets. *IEEE Transactions on Power Systems*, 18(2):596–604, May 2003.

[89] F. Milano, C. A. Cañizares, and M. Invernizzi. Voltage stability constrained opf market models considering N-1 contingency criteria. *Electric Power Systems Research*, 74(1):27–36, April 2005.

[90] F. Milano, A. J. Conejo, and R. Zárate-Miñano. General sensitivity formulas for maximum loading conditions in power systems. *IET Generation Transmission & Distribution*, 1(3):516–526, May 2007.

[91] R. Mínguez, F. Milano, R. Zárate-Miñano, and A. J. Conejo. Optimal network placement of SVC devices. *IEEE Transactions on Power Systems*, 22(4):1851–1860, November 2007.

[92] N. Mithulananthan, C. A. Cañizares, J. Reeve, and G. J. Rogers. Comparison of pss, svc, and statcom controllers for damping power system oscillations. *IEEE Transactions on Power Systems*, 18(2):786–792, May 2003.

[93] A. J. Monticelli, M. V. F. Pereira, and S. Granville. Security-constrained optimal power flow with post-contingency corrective rescheduling. *IEEE Transactions on Power Systems*, 2(1):175–182, February 1987.

[94] G. K. Morison, B. Gao, and P. Kundur. Voltage stability analysis using static and dynamic approaches. *IEEE Transactions on Power Systems*, 8(3):1159–1171, August 1993.

[95] B. A. Murtagh, M. A. Saunders, W. Murray, P. E. Gill, R. Raman, and E. Kalvelagen. *GAMS/MINOS: A Solver for Large-Scale Nonlinear Optimization Problems*, 2002. Available at http://www.gams.com/.

[96] H. K. Nam, Y. K. Kim, K. S. Shim, and K. Y. Lee. A new eigen-sensitivity theory of augmented matrix and its applications to power system stability analysis. *IEEE Transactions on Power Systems*, 15(1):363–369, February 2000.

[97] J. E. Van Ness, J. M. Boyle, and F. P. Imad. Sensitivities of large, multiple-loop control systems. *IEEE Transactions on Automatic Control*, 10(3):308–315, July 1965.

[98] T. B. Nguyen and M. A. Pai. Dynamic security-constrained rescheduling of power systems using trajectory sensitivities. *IEEE Transactions on Power Systems*, 18(2):848–854, May 2003.

[99] O. O. Obadina and G. J. Berg. Determination of voltage stability limit in multimachine power systems. *IEEE Transactions on Power Systems*, 3(4):1545–1554, November 1988.

[100] Reliability Test System Task Force of the Application of Probability Methods Subcommittee. The IEEE reliability test system - 1996. *IEEE Transactions on Power Systems*, 14(3):1010–1020, August 1999.

[101] IEEE Stability Test Systems Task Force of the Dynamic System Performance Subcommittee. Transient stability test systems for direct stability methods. *IEEE Transactions on Power Systems*, 7(1):37–43, February 1992.

[102] IEEE/CIGRE Joint Task Force on Stability Terms and Definitions. Definition and classification of power system stabiliy. *IEEE Transactions on Power Systems*, 19(2):1387–1401, May 2004.

[103] T. J. Overbye and C. L. DeMarco. Voltage security enhancement using energy based sensitivities. *IEEE Transactions on Power Systems*, 6(3):1196–1202, August 1991.

[104] M. A. Pai. *Energy Function Analysis for Power System Stability*. Kluwer, Norwell, MA, 1989.

[105] M. Pavella. Generalized one-machine equivalents in transient stability studies. *IEEE Power Engineering Review*, 18(1):50–52, January 1998.

[106] M. Pavella, D. Ernst, and D. Ruiz-Vega. *Transient Stability of Power Systems: A Unified Approach to Assessment and Control*. Kluwer, Norwell, MA, 2000.

[107] M. Pavella and P. G. Murthy. *Transient Stability of Power Systems, Theory and Practice*. John Wiley & Sons, New York, NY, 1993.

[108] I. J. Pérez-Arriaga, G. C. Verghese, and F. C. Schweppe. Selective modal analysis with applications to electric power systems, part I: Heuristic introduction. *IEEE Transactions on Power Apparatus and Systems*, (9):3117–3125, September 1982.

[109] G. Rogers. *Power System Oscillations*. Kluwer, Norwell, MA, 2000.

[110] W. Rosehart, C. A. Cañizares, and V. H. Quintana. Multiobjective optimal power flows to evaluate voltage security costs in power networks. *IEEE Transactions on Power Systems*, 18(2):578–587, May 2003.

[111] L. Rouco and I. J. Pérez-Arriaga. Multi-area analysis of small signal stability in large electric power systems by sma. *IEEE Transactions on Power Systems*, 8(3):1257–1265, August 1993.

[112] D. Ruiz-Vega and M. Pavella. A comprehensive approach to transient stability control: Part I - near optimal preventive control. *IEEE Transactions on Power Systems*, 18(4):1446–1453, November 2003.

[113] Y. Saad. Variations on Arnoldi's method for computing eigenelements of large unsymmetric matrices. *Linear Algebra and its Applications*, 34, 1981.

[114] P. W. Sauer and M. A. Pai. *Power System Dynamics and Stability*. Prentice-Hall, Upper Saddle River, NJ, 1998.

[115] M. La Scala, M. Trovato, and C. Antonelli. On-line dynamic preventive control: An algorithm for transient security dispatch. *IEEE Transactions on Power Systems*, 13(2):601–609, May 1998.

[116] R. Seydel. *Practical Bifurcation and Stability Analysis: From Equilibrium to Chaos*. Springer-Verlag, New York, NY, 1994.

[117] T. Smed. Feasible eigenvalue sensitivity for large power systems. *IEEE Transactions on Power Systems*, 8(2):555–563, May 1993.

[118] IEEE/PES Power System Stability Subcommittee. Voltage stability assessment: Concepts, practices and tools. *IEEE Special Publication*, Technical Report SP101PSS, August 2002. Available from IEEE.

[119] Y. Sun, Y. Xinlin, and H. F. Wang. Approach for optimal power flow with transient stability constraints. *IEE Proceedings - Generation, Transmission and Distribution*, 151(1):8–18, January 2004.

[120] Y. Tamura, H. Mori, and S. Iwamoto. Relationship between voltage instability and multiple load flow solutions in electric power systems. *IEEE Transactions on Power Apparatus and Systems*, 102(5):1115–1125, May 1983.

[121] C. W. Taylor. Concepts of undervoltage load shedding for voltage stability. *IEEE Transactions on Power Delivery*, 7(2):480–488, April 1992.

[122] C. W. Taylor. *Power System Voltage Stability*. McGraw-Hill, New York, NY, 1994.

[123] The MathWorks, Inc. *Matlab Programming*. Natick, MA, USA, 2005. Available at http://www.mathworks.com.

[124] E. Vaahedi, Y. Mansour, C. Fuchs, S. Granville, M. de Lujan Lastore, and H. Hamadanizadeh. Dynamic security constrained optimal power flow/var planning. *IEEE Transactions on Power Systems*, 16(1):38–43, February 2001.

[125] L. S. Vargas and C. A. Cañizares. Time dependence of controls to avoid voltage collapse. *IEEE Transactions on Power Systems*, 15(4):1367–1375, November 2000.

[126] V. Venkatasubramanian, H. Schättler, and J. Zaborszky. Dynamics of large constrained nonlinear systems - a taxonomy theory. *Proceedings of the IEEE*, 83(11):1530–1560, November 1995.

[127] G. C. Verghese, I. J. Pérez-Arriaga, and F. C. Schweppe. Selective modal analysis with applications to electric power systems, part II: The dynamic stability problem. *IEEE Transactions on Power Apparatus and Systems*, (9):3126–3134, September 1982.

[128] C. D. Vournas, M. A. Pai, and P. W. Sauer. The effect of automatic voltage regulation on the bifurcation evolution in power systems. *IEEE Transactions on Power Systems*, 11(4):1683–1688, November 1996.

[129] L. Wang, F. Howell, P. Kundur, C. Y. Chung, and W. Xu. A tool for small-signal security assessment of power systems. *Proceedings of the IEEE PES International Conference on Power Industry Computer Applications*, Australia, 2001.

[130] X. Wang, G. C. Ejebe, J. Tong, and J. G. Waight. Preventive/corrective control for voltage stability using direct interior point method. *IEEE Transactions on Power Systems*, 13(3):878–883, August 1998.

[131] L. Wehenkel. *Automatic Learning Techniques in Power Systems*. Kluwer, Norwell, MA, 1998.

[132] X. Wen and V. Ajjarapu. Application of a novel eigenvalue trajectory tracing method to identify both ocillatory stability margin and damping margin. *IEEE Transactions on Power Systems*, 21(2):817–824, May 2006.

[133] A. J. Wood and B. F. Wollenberg. *Power Generation, Operation and Control*. John Wiley & Sons, New York, NY, second edition, 1996.

[134] S. J. Wright. *Primal-Dual Interior Point Methods*. Siam, PA, 1997.

[135] Y. Xia, K. W. Chan, and M. Liu. Direct nonlinear primal-dual interior-point method for transient stability constrained optimal power flow. *IEE Proceedings - Generation, Transmission and Distribution*, 152(1):11–16, January 2005.

[136] K. Xie, Y. H. Song, J. Stonham, E. Yu, and G. Liu. Decomposition model and interior point methods for optimal spot pricing of electricity in deregulation environments. *IEEE Transactions on Power Systems*, 15(1):39–50, February 2000.

[137] H. Xin, D. Gan, Y. Li, T. S. Chung, and J. Qiu. Transient stability preventive control and optimization via power system stability region analysis. *Proceedings of the IEEE PES General Meeting*, 1:74–81, June 2006.

[138] Y. Yuan, J. Kubokawa, and H. Sasaki. A solution of optimal power flow with multicontingency transient stability constraints. *IEEE Transactions on Power Systems*, 18(3):1094–1102, August 2003.

[139] J. Yuryevich and K. P. Wong. Evolutionary programming based optimal power flow algorithm. *IEEE Transactions on Power Systems*, 14(4):1245–1250, November 1999.

[140] M. A. B. Zammit, D. J. Hill, and R. J. Kaye. Designing ancillary services markets for power system security. *IEEE Transactions on Power Systems*, 15(2):675–680, May 2000.

[141] R. Zárate-Miñano, A. J. Conejo, and F. Milano. OPF-based security redispatching including FACTS devices. *IET Generation, Transmission & Distribution*, 2(6):821–833, November 2008.

[142] X. Zhang, R. W. Dunn, and F. Li. Stability constrained optimal power flow in a practical balancing market. *Proceedings of the IEEE/PES General Meeting*, 1, 2007.

[143] E. Z. Zhout, O. P. Malik, and G. S. Hope. Theory and method for selection of power system stabilizer location. *IEEE Transactions on Energy Conversion*, 6(1):170–176, March 1991.

[144] A. Zobian and M. D. Ilić. Unbundling of transmission and ancillary services. Part I: Technical issues. *IEEE Transactions on Power Systems*, 12(2):539–548, May 1997.

Index